Dual energy X-ray absorptiometry derived bone quantity in an ovine model of osteoporosis.

Dr Nick Mahony

MB BCh BA.O MSc MICGP FFSEM

Thesis submitted to the Department of Mechanical and Manufacturing Engineering, Trinity College Dublin in fulfilment of the requirement for a Doctoral degree.

March 2013

DECLARATION

I declare, that apart from work credited in the text to co-researchers, that this thesis is all my own work and has / will not be submitted to this or any other university as part of any other post graduate programme. I grant permission to the Trinity College librarian to lend or copy this thesis in part on request.

Signature:_____ March 2013.

TABLE OF CONTENTS

CHAPTER 1

CHAPTER 1 (continued)

CHAPTER 2

CHAPTER 3

CHAPTER 4

CHAPTER 5

CHAPTER 6

CHAPTER 7

ACKNOWLEDGMENTS

I wish to thank the following people without whose assistance these studies would not have been possible; Terry Mooney and the staff of Irish Country Meats, Athboy, Navan, Co. Meath, for kindly providing me with sheep bones for the Studies 1 and 2; and from the Trinity Centre for Bioengineering, School of Veterinary Science UCD and the Royal College of Surgeons in Ireland; Sue Rackard, Oran Kennedy and Orlaith Brennan for the animal preparation work in the 'Bone for Life' project; and especially Orlaith Brennan and Gerardo Presbitero for providing the mechanical testing, microarchitecture and microdamage data. Lastly, for their constructive criticism and extreme patience I would like to thank my two supervisors, Professors Clive Lee (RCSI) and David Taylor (TCD); Clive Lee for giving me the opportunity to be part of the 'Bone for Life' research project and for review of the transfer report; and, especially David Taylor, Head of the School of Manufacturing and Mechanical Engineering in TCD, for reviewing and advising on content and corrections of the final thesis.

A special mention for two special colleagues, mentors and friends, from the Anatomy Department in Trinity College; firstly to Moira O'Brien for permission to use the DXA scanner but also for her personal support, to me as I progressed from MSc student, demonstrator and then temporary and full time lecturer in Anatomy; secondly to the legendary figure that is Bernard Donne for; his technical support with the DXA scanner, advice on statistical analysis, healthy scepticism of all things engineering and British, and many patient hours, without too much complaint reviewing the manuscript for typos, spelling and grammar mistakes of which there were many! Thanks a million, Moira and Bernard, the best colleagues anyone could wish for.

Special thanks also to my family for all their support; to my late mother Anne Mahony (*nee Blakeley 1935-2005*), my father Michael "Yes, Dad the thesis is now finished you can stop nagging now! ", my brother David; and my sisters Sarah and Katy.

Wreszcie do mojego króliczka miodu, Marta niezależna kobieta z Żory, Śląsk, Polska. Oprócz języka polskiego z jego wymówienia słów ostatnich trzech lat sześć miesięcy były niesamowite, i nie mogę się doczekać, aby spędzać wiele lat razem. Kocham cię bardziej. Torty dla dzieci.

LIST OF ABBREVIATIONS

aBMD	Areal bone mineral density
ANOVA	Analysis of variance
BMAD	Bone mineral apparent density
BMC	Bone mineral content
BMDD	Bone mineral density distribution
BMU	Bone remodelling unit
BV / TV	Bone volume fraction
^{o}C	Degree centigrade
CI	Confidence interval
cm	Centimetre
cm^2	Square centimetre
CM	Carcass mass
CON	Control group
CSA	Cross-sectional area
CSF-1	Macrophage colony stimulating factor 1
CSMI	Cross-sectional moment of inertia (area)
CT	Computerised tomography
CWT	Cortical wall thickness
CV%	Coefficient of variation
d	Cohen's d (effect size)
DA	Degree of anisotropy
D_{app}	Apparent density
D_{mat}	Material density
DXA	Dual energy X-ray absorptiometry
E	Elastic or Young's modulus
ε	Strain (deformation expressed as a ratio / percentage)
EA	Estimated area
EBM	Estimated body mass
EN	Energy to failure
FPS	Farnesyl pyrophosphate synthase
FE	Finite element modelling
FGF	Fibroblast growth factor

LIST OF ABBREVIATIONS

Fmax	Ultimate breaking force
FMR	Femur (right)
g	Gram
$g.cm^{-2}$	Gram per centimetre squared (units of areal density)
$g.cm^{-3}$	Gram per centimetre cubed (units of volumetric density)
HMR	Humerus (right)
HSA	Hip structural analysis (algorithm in modern DXA scanners)
Hz	Hertz (frequency per second)
I	Cross sectional moment of area
ICC	Intraclass coefficient (repeatability)
IGF-1	Insulin like growth factor 1
IL-1	Interleukin 1
IL-6	Interleukin 6
IQR	Inter quartile range (25^{th} to 75^{th} percentile)
kg	Kilogram
kJ	Kilojoule
kN	Kilo Newton
L	Litre
L1	Lumbar vertebra 1
95%LOA	95% Limits of agreement
LS	Lumbar spine
M	Arithmetic mean
m	Metre
mg	Milligram
mL	Millilitre
mm	Millimetre
m^2	Square metre
µm	Micrometre
µCT	Microcomputed tomography
MPa	Mega Pascal
MRI	Magnetic resonance imaging
mRNA	Messenger RNA

LIST OF ABBREVIATIONS

n	number in the sample / sample size
NaCl	Sodium chloride
nm	Nanometre
$N.m^{-2}$	Newton per metre squared (Pascals) units of stress
NMR	Nuclear magnetic resonance
OB	Osteoblast
OC	Osteoclast
OI	Osteogenesis imperfecta
OPG	Osteoprotegrin
OVX	Ovariectomised group
P	Probability (statistical)
%	Percentage / or units of strain
%TEM	Percentage technical error of measurement (relative reliability)
pQCT	Peripheral quantitative computed tomography
PTFE	Polytetrafluoroethylene
PTH	Parathyroid hormone
RANK	Receptor activator for nuclear factor beta
RANKL	RANK ligand
R1	Sub-region 1
r1	Region of interest 1
r	Pearson correlation coefficient
r^2	Coefficient of determination
RDR	Radius (right)
ROI	Region of interest
S1	Initial scan
S2	Repeat scan
SD	Standard deviation
SEM	Standard error of the mean
σ max	Breaking stress
SMI	Structural model index
SPA	Single photon absorptiometry
SRA	Sub-regional analysis

LIST OF ABBREVIATIONS

SXA	Single photon X-ray absorptiometry
Sy.X	Standard error of the estimate (variability in regression analysis)
Tb.N	Trabecular number
Tb.Sp	Trabecular spacing
Tb.Th	Trabecular thickness
TBR	Tibia (right)
TEM	Technical error of measurement (absolute reliability)
TGF	Transforming growth factor
TNAP	Tissue non-specific alkaline phosphatase
TNF-α	Tumour necrosis factor alpha
TS	Thoracic spine
T score	DXA aBMD expressed relative to a normative predicted peak value
UCS	Ultimate compressive strength
vBMD	Volumetric BMD
vs.	Versus
ω	Distance to the centre of mass from the centroid
WB	Whole bone
WHO	World Health Organisation
X	Cross-bred variety
Y1	Year 1 (12 month) time point of sacrifice
Y3	Year 3 (31 month) time point of sacrifice
yr	Year
Z	Section modulus
ZOL	Zoledronic acid treated group in Y3
Z score	DXA aBMD expressed relative to normative predicted value for age

LIST OF FIGURES (short titles)

CHAPTER 1

LIST OF FIGURES (short titles)

CHAPTER 2

CHAPTER 3

CHAPTER 4

LIST OF FIGURES (short titles)

CHAPTER 5

CHAPTER 6

LIST OF FIGURES (short titles)

LIST OF TABLES (short titles)

CHAPTER 2

CHAPTER 3

CHAPTER 5

CHAPTER 6

LIST OF PUBLICATIONS AND PRESENTATIONS

The DXA work in this thesis has been presented in the following publications, international and national conferences and symposia.

Book Chapters

Lee C, McHugh P, O'Brien F, O'Mahony D, Taylor D, Bruzzi M, Rackard S, Kennedy O, **Mahony N**, Harrison N, Lohfield S, Brennan O, Gleeson J, Hazenberg J, Mullins L, Tyndyk M, McNamara L & Prendergast P (2004). 'Bone for life': Osteoporosis, bone remodelling and computer simulation. In: Topics in Bio-Mechanical Engineering, Prendergast P and McHugh P (Eds). Trinity Centre for Bio-Engineering, Dublin and National Centre for Biomedical Engineering Science, Galway, Ireland pp.: 58-93.

Journal Papers

Holland J, Kennedy O, Brennan O, Mahony N**,** Rackard S, O'Brien F, Taylor D & Lee C (2013). Examination of osteoarthritis and subchondral bone alterations within the stifle joint of an ovariectomised ovine model. *J Anat*, accepted for publication March 2013, in press.

Kennedy O, Brennan O, Mahony N**,** Rackard S, O'Brien F, Taylor D & Lee C (2008).Effects of high bone turnover on the biomechanical properties of the l3 vertebra in an ovine model of early stage osteoporosis. *Spine* **33**: 2518–2523.

Keeley B, Heidari B, Mahony N, Rackard S, O'Brien F, Lee C, Brennan O, Kennedy O, FitzPatrick D (2008). Biomechanical comparison of the pull-out properties of external skeletal fixation pins in the tibiae of intact and ovariectomised ewes. *Vet Comp Orthop Trauma* **21**:418-26.

International Conference Abstracts

Brennan O, Kennedy O, Mahony N, Lee C, Rackard S & O'Brien F (2007). Bone quality, in addition to bone mineral density measurements, is necessary to accurately predict bone strength in osteoporosis. 2nd International Conference of Mechanics of Biomaterials and Tissues, Kaui, Hawaii.

Brennan O, Kennedy O, Mahony N, Lee C, Rackard S & O'Brien F (2007). BMD measurements do not predict bone fracture risk in an ovine model of osteoporosis. Transactions of 53rd meeting of the Orthopaedic Research Society, San Diego, California.

LIST OF PUBLICATIONS AND PRESENTATIONS

Brennan O, Kennedy O, Mahony N, Lee C, Rackard S & O'Brien F (2006). Mechanical and histomorphometric variations in osteoporotic trabecular bone. In: Proceedings of the 5th World Congress of Biomechanics, Munich, Germany.

Brennan O, Kennedy O, Mahony N, Lee C, Rackard S & O'Brien F (2006) BMD measurements do not adequately assess the onset of osteoporosis. In: Transactions of 52nd Meeting of the Orthopaedic Research Society, Chicago, Illinois: 1795.

National Conferences and Symposia / Abstracts

Mahony N, Donne B, Taylor D, Lee C (2008). Effect of ovariectomy on bone quantity in the ovine skeleton. In: Proceedings of the 14th Annual Conference of the Section of Bioengineering of the Royal Academy of Medicine in Ireland.

Brennan O, Kennedy O, Kelleher D, Mahony N, Lee C, Rackard S & O'Brien F (2007). Bone Architecture and Mineralisation as Determinants of Fracture Risk. In: Proceedings of the 13th Annual Conference of the Section of Bioengineering of the Royal Academy of Medicine in Ireland.

Brennan O, Kennedy O, Mahony N, Lee C, Rackard S & O'Brien F (2006). Mechanical and histomorphometric variations in normal and osteoporotic trabecular bone. In: Proceedings of the 12th Annual Conference of the Section of Bioengineering of the Royal Academy of Medicine in Ireland.

Mahony N, Donne B, Taylor D, Lee C, O'Brien M (2005)**.** Reliability, measurement error, and normal database for DXA assessment of bone density at five sites in the ovine skeleton**.** In: Proceedings of the 11th Annual Conference of the Section of Bioengineering of the Royal Academy of Medicine in Ireland.

Mahony N, Donne B, Taylor D, Lee C, O'Brien M (2004)**.** Reliability and reproducibility of fan beam DXA in global and sub-regional analysis of bone density variables in ovine tibia. In: Proceedings of the 10th Annual Conference of the Section of Bioengineering of the Royal Academy of Medicine in Ireland.

ABSTRACT

Dual energy X-ray absorptiometry (DXA) is the most widely used bone quantity investigation in human osteoporosis; it is so ubiquitous that many clinicians now mistakenly equate DXA derived areal BMD with bone strength. Bone strength partly depends on bone mass and the distribution of this mass in terms of size and shape but also depends on bone quality factors of microarchitecture, material properties, accumulated microdamage and remodelling rate. In osteoporosis research, sheep have emerged as a useful large animal model due to size and physiological similarities to humans; and, as a flock animal, large numbers of sheep can be reared at reasonable costs. The aim of this research, part of the 'Bone for Life' group of studies, was to evaluate; DXA scanner validity in the ovine animal model, DXA derived bone quantity (aBMD) change in an ovine animal model of osteoporosis, and following on from these preliminary studies; to examine the influence of DXA derived aBMD on cortical and trabecular bone mechanical properties.

In initial validation studies of DXA scanner reliability and assessment of natural variation in aBMD in the Irish sheep population *ex-vivo* bone samples were sourced from healthy Irish mixed breed ewes (age>5yr) at routine commercial sacrifice. Further samples were also harvested from control (CON) and ovariectomised (OVX) sheep in a specially reared flock at two time points, 12 and 31 month post-ovariectomy, to determine the short- and long-term effect of ovariectomy on bone quantity (aBMD); and in further collaborative studies, bone quantity and quality relationships to mechanical properties. The DXA scan protocol consisted of standardised alignment of the whole sample (WB) on a holding jig within a tank filled with normal saline, followed by baseline repeat data acquisition scans using a standard algorithm. The same algorithm allowed further analysis (SRA) of six sub-regions down the length of selected long bones femur (FMR), tibia (TBR), humerus (HMR) and radius (RDR); and, the six vertebrae spinal samples (LS); as well as smaller region of interest (ROI) analyses in areas of high trabecular bone content. Statistical analysis was made of initial repeat test data to determine DXA scanner reliability, establish measurement limits; and assess biological variability; and for the specially reared flock, inter-group differences in aBMD were analysed for effect of ovariectomy, and then re-analysed in conjunction with bone quality variables to assess the strength of aBMD and bone quality relationships to mechanical test data.

The results of preliminary studies confirmed an acceptable level of; repeatability (ICC >0.9), reliability (%TEM 3-5%) and measurement limits (95%LOA ± 0.035 $g.cm^{-2}$) of the adapted DXA scanning protocol for large ovine bone samples. In a representative sample of the Irish ewes evaluation of biological variability revealed; an aBMD range of approximately 0.60 to 1.20 $g.cm^{-2}$, minimal inter-breed variation and a small seasonal effect toward lower density in Spring months at some sites. Analysis of inter-group differences between CON and OVX detected no significant difference in aBMD post-ovariectomy at any spinal or long bone site at 12 month; but did detect a significant reduction in aBMD in the proximal humeral region and an unexpected finding of increased aBMD in the mid-region of the tibia, both with large effect size, at the 31 month time point. In follow on studies; aBMD (r^2~0.83) and then structural geometric properties of CSMI (r^2~0.75) and section modulus (r^2~0.65) had the strongest association with breaking strength (Fmax) of ovine radii in three point bending. In microdamage analysis of radii exposed to cyclic loading, and stratified as high, medium or low aBMD, results also suggested significantly higher microcrack numerical and surface density in bones with lower aBMD. Analysis of compressive strength of isolated trabecular cores was less clear, but significant inter-group differences in trabecular thickness of large effect size were detected in the CON vs. OVX comparison at the 31 month time point, and in terms of relationships to strength, trabecular number and spacing (r^2~0.4 to 0.5) were better related to compressive strength and modulus than any DXA or microCT derived bone quantity variable.

In conclusion this work has further validated DXA bone quantity measurement and defined measurement limits for scanning and sub-regional analysis of whole bone samples in this animal model. Bone quantity data for Irish sheep were of a similar range to those seen in human female populations, and exhibited some seasonal variation again similar to human populations living in northern latitudes. In this animal model ovariectomy alone however, did not prove a sufficient enough stimulus in the short-term to produce a significant reduction in bone quantity detectable by DXA in time frames suitable for research; however longer term changes detected in the proximal humerus and tibia require further evaluation. In terms of relationships to strength DXA derived aBMD data was the better predictor of bending strength in a typical long bone mid-shaft site; but in compression of isolated trabecular cores, bone quality factors were more closely associated to mechanical properties.

CHAPTER 1

Introduction: background information and literature review

1.0: INTRODUCTION

"Bone is a highly vascular, living, constantly changing mineralised connective tissue. It is remarkable for its hardness, resilience and regenerative capacity as well as its growth mechanisms," (Soames *et al*., 1995). The ultra-structure and design of bone reflects its main functions; mechanical support and leverage for the musculoskeletal system, protection of vital organ systems, a site of mineral storage and homeostasis, and within its hollow marrow cavities; lipid storage and haematopoiesis. Bone is comprised of cellular elements and an intercellular matrix of mineral and collagen; and with evolution, structural design, composition and bone biology has adapted bone into a material of great strength for its associated mass and metabolic costs.

This introductory chapter outlines; basic bone structure from the macroscopic to the microscopic level, the organisation of basic mineral and organic components and how basic structure and composition contribute to the material properties. Bone is an active living tissue which throughout life has to respond to changing ambient forces as it grows, develops and ages, and as it moves through its gravitational environment. This chapter also outlines biological processes of bone growth, remodelling and repair; and the control process whereby bone remodelling responses to external stress are initiated and controlled at the molecular level.

The research is primarily focussed on bone quantity and its relationship to bone strength, the chapter outlines mechanical and material properties of bone, measurement of bone quantity, and the relationship of bone quantity to bone strength. Osteoporosis results from unbalanced bone remodelling due to ageing, disease, drugs, and causes reduction in bone mass, architectural deterioration, and ultimately decreased bone quality with increased susceptibility to fracture. This chapter reviews osteoporosis and the ovine large animal model used in osteoporosis research.

The chapter concludes with the research aims of a series of dual energy X-ray absorptiometry (DXA) studies on an ovine large animal model including; preliminary DXA validation, effect of natural variation and ovariectomy on bone density in the animal model, and with co-researchers in the "Bone for Life Project" studies relating DXA derived bone quantity data to results of whole bone mechanical tests to further elucidate the relationship of bone quantity and quality to bone strength.

1.1: Bone structure

The human skeleton is comprised of some 206 individual bones adapted in shape and size according to functions of protection, weight bearing and movement. For descriptive purposes the skeleton is divided into the axial skeleton which is comprised of the skull, the vertebral column, ribs and sternum, and the appendicular skeleton comprised of; the limb girdles, scapula and pelvis and the long bones of the limbs (Figure 1.1a).

During evolution the adoption of an upright posture of the vertebral column and bipedal system of locomotion of the lower limbs freed the upper limb for fine manipulative tasks. The non-weight bearing upper limb bones are smaller, lighter and their articulations more mobile but as a consequence less stable. In contrast, bones of the lower vertebral column, pelvic girdle and lower limb, are larger, heavier, and have less mobile but more stable articulations for weight bearing and locomotion. Thus external shape of individual bones of the skeleton are adapted to their mechanical function; the expanded ends of long bones provide a greater surface area for load bearing at major joints, and internal structure such as the lightweight sandwich construction of the skull plates is adapted for protective function. Bone is thus adapted to function and optimised for weight and strength (Currey, 2003a).

1.1.1: Bone macroscopic structural appearances

When cut in cross-section and inspected visually bone is seen to be comprised of an internal porous latticework of struts and plates of cancellous, spongiform or trabecular bone; enclosed by a dense outer shell of cortical bone (Figure 1.1d). Trabecular bone is more evident within the vertebral bodies and at the ends of the long bones where ambient forces are experienced in multiple directions and cortical bone is most prominent at the mid-shafts of the long bones, where forces are usually unidirectional. In engineering terms Gibson and Ashby (1997) consider cortical bone with its high relative density a solid with holes; and trabecular bone, with a low relative density, a cellular solid.

Figure 1.1: (a) The human skeleton, (b) a lumbar vertebra, (c) a femur and (d) cut away section to show inner cancellous or trabecular network surrounded by an outer shell of cortical bone (*adapted from Bone Academy.com accessed online May 2006*).

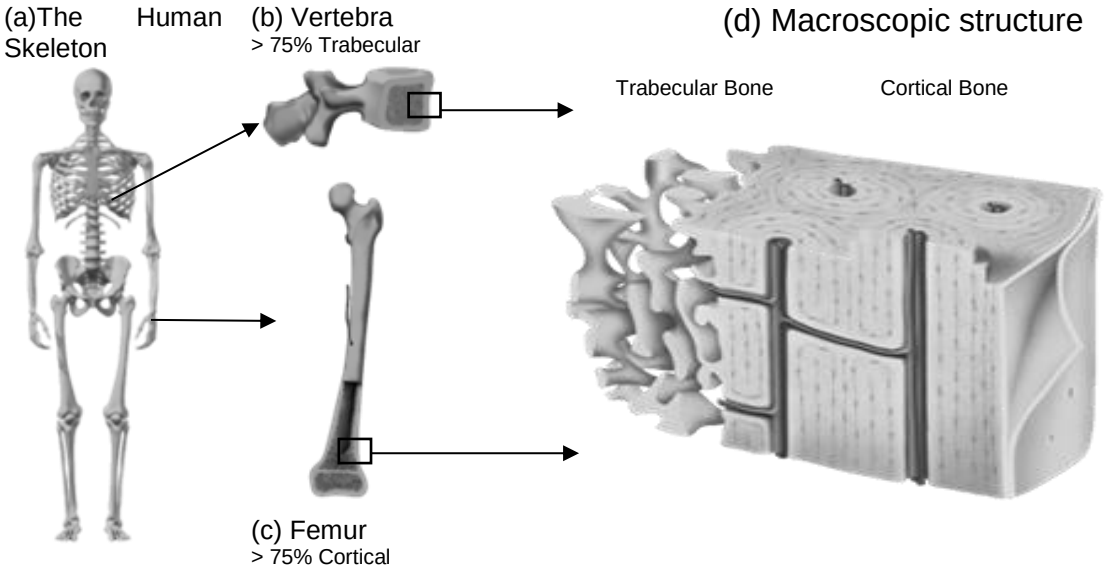

1.1.2: Bone ultra-structural appearances

Histologically, or at higher powers of magnification, bone tissue is of two basic types, woven and lamellar bone. Woven bone is an immature form making up all bone at birth and characterised by randomly arranged collagen fibres, it is replaced by lamellar bone in early childhood and afterward, is only seen in the adult in healing fracture callus or in certain bone diseases. Lamellae bone (Figure 1.2), the adult form, is characterised by layered collagen fibres arranged along lines of force, it gives bone anisotropic properties, that is the ability to better withstand forces in certain directions than others (Khan *et al*., 2001).

In trabecular bone the interconnected rods and plates are formed by two to three layers of flat lamellae. In cortical bone the structure is more complex with lamellae arranged in three ways. The smooth polished outer surfaces of bone are made up of three to four layers of circumferential lamellae; deep to this are parallel tubes of concentrically arranged lamellae called osteons or ‘Haversian’ systems; and, lastly between adjacent osteons and circumferential lamellae are the interstitial lamellae and a thin boundary layer or cement line. The interstitial lamellae are thought to represent older osteons which have been partially removed during the process of bone remodelling (Soames *et al*., 1995).

Figure 1.2: Diagram of the microscopic features of trabecular and cortical bone (adapted from Soames *et al*., 1995).

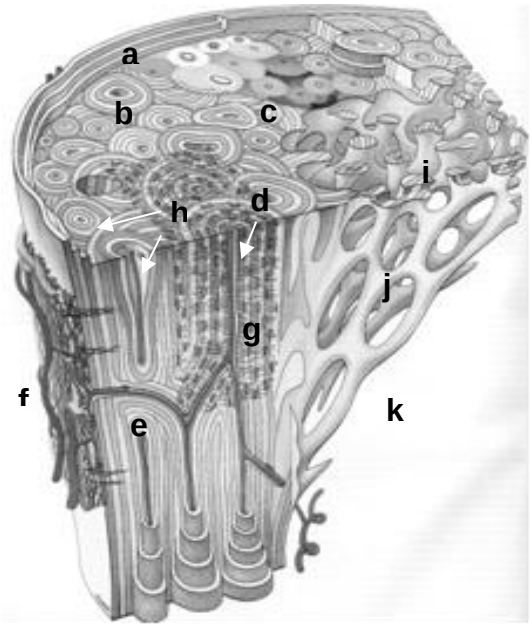

Key
(a) circumferential lamellae
(b) osteons (tubular lamellae)
(c) interstitial lamellae
(d) a central 'Haversian' canal,
(e) 'Volkmann's' canal,
(f) periosteum and periosteal blood vessels,
(g) osteocyte network of cellular processes traversing adjacent lamellae.
(h) resorbtion cavity or basic remodelling unit (BMU),
(i) lamellae forming trabeculae
(j) inter-connecting struts
(k) marrow spaces and cavity

1.1.3: Cortical bone

In cortical bone osteons are arranged in parallel along the long axis of the long bones. They are most numerous or thickest in the mid-shaft of the long bone, where stresses are unidirectional, they support body weight without bending and breaking. However, if forces are placed obliquely or transversely across the line of the osteons they are vulnerable to fracture (Khan *et al*., 2001). In cortical bone the concentric layers of osteonal bone are arranged around a central neurovascular 'Haversian' canal, further transverse or obliquely orientated channels called Volkmann's canals interconnect with the Haversian systems (Figures 1.2 and 1.3). Osteonal bone has a high relative density, low porosity (5 to 30%) and low surface area and is metabolically less active than cancellous bone (Gibson & Ashby, 1997; Einhorn, 1996).

Figure 1.3: High power view of a transverse section of compact bone from a human finger showing: (a) osteons, (b) osteocytes with their fine canalicular connections passing across adjacent lamellae, (c) interstitial lamellae and d) Haversian canals (adapted from Arnett & Boyd, 2006).

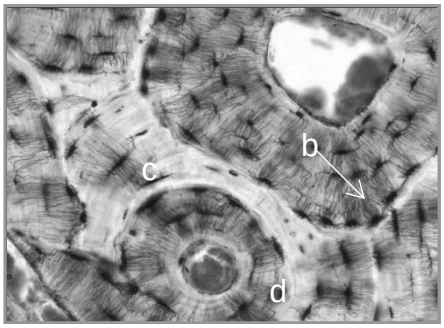

1.1.4: Trabecular bone

Trabecular or cancellous bone is typically found at the proximal and distal ends of the long bones and within vertebral bodies, areas of low mechanical stress but where stresses are applied in more than one direction. The internal struts and plates are comprised of flat lamellae, and form a light interconnected inner scaffolding reducing skeletal weight. Trabeculae rods and plates are orientated along the lines of the predominant mechanical loads and are braced by interconnecting struts.

Figure 1.4: A scanning electron micrograph trabecular bone from (a) a vertebral body; and, (b) the head of femur showing the porous trabecular pattern of interconnected struts and plates (adapted from Arnett & Boyd, 2006).

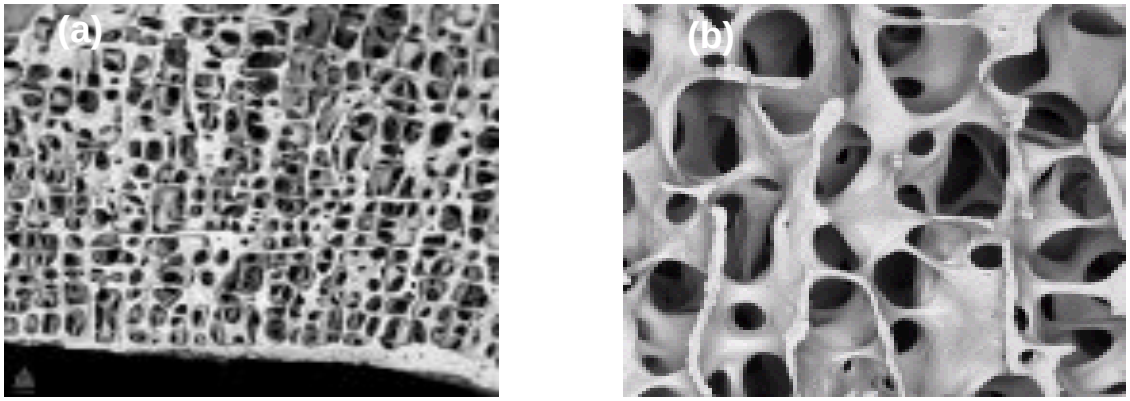

The internal trabecular lattice work provides a higher surface area than compact bone, approximately 7.5 m^2, and is thus the primary site of action of bone forming and re-absorbing cells involved in calcium homeostasis. The trabecular spaces contain red marrow, the site of haematopoiesis, and a variable amount of fatty yellow marrow. Fatty marrow gradually replaces the red marrow in long bones with ageing, and in later life red marrow is only found within the sternum, ribs and iliac bones (Soames *et al*., 1995).

1.1.5: Periosteum and endosteum

The outer cortical surface is covered with membrane the periosteum, which is comprised of an outer fibrous layer, a vascular layer and an inner cellular layer. It isolates bone from surrounding tissues and provides a route for blood vessels and nerves into bone. The inner cellular layer of periosteum contains osteoprogenitor cells and osteoblasts responsible for appositional or circumferential growth which continues throughout life and healing and repair mechanisms following fracture. The

inner trabecular bone surfaces are lined by a single layered membrane, the endosteum; comprised of flattened osteoprogenitor cells. This is the primary source of osteoblasts for new bone formation during remodelling and repair, and is the more metabolically active layer in terms of calcium homeostasis (Soames *et al*., 1995).

1.1.7: Bone cells

The predominant bone cell types are osteoprogenitor cells, osteoblasts, osteocytes and osteoclasts. Osteoblasts and osteocytes are derived from mesenchymal progenitor cells. Osteoclasts have a different lineage being derived from fusion of bone marrow mononuclear cells and have similar precursors to macrophages.

Osteoblasts arise from pluripotent mesenchymal stem cells and lay down the extracellular matrix or osteoid, and regulate its mineralization (Yamaguchi *et al*., 2000). In humans, mature osteoblasts survive about 8 weeks, and are capable of laying down up to 1.5 μm of osteoid per day. Osteoblasts which become fixed in the calcified matrix they produce form osteocytes, become lining cells, or die through apoptosis (Sommerfeldt & Rubin, 2001). They are basophilic cuboidal mononuclear cells which form a single covering layer on the bone matrix they are producing during growth, repair or remodelling. In less active phases they are most numerous on the endosteal surfaces of bone, or deep within resorbtion cavities in osteons undergoing remodelling.

Osteoblastic osteoid synthesis and mineralisation involves alkaline phosphatase, during periods of high bone formation some of alkaline phosphatase enzyme reaches the circulation and measurement is a useful clinical marker of bone turnover (Khan *et al*., 2001). Collagen synthesis occurs in the rough endoplasmic reticulum and then Golgi apparatus before secretion through numerous vesicles from their secretory surface on the bone (Soames *et al*., 1995).

Osteoblast cell surfaces express many receptors, the predominant ones are for parathyroid hormone (PTH), oestrogen and 1, 25-dihydroxy-vitamin D_3, however, glucocorticoids, growth hormone and sex hormones all have effects on their function (Khan *et al*., 2001). Osteoblasts are active during bone growth, remodelling and repair in response to growth factors, micro-damage and mechanical loading. Their actions are controlled at a local level by autocrine and paracrine hormones,

implicated control factors include PTH related protein, transforming growth factor (TGF-beta), fibroblast (FGF) and insulin like growth factors (IGF). Osteoblastic activity is also coordinated through intercellular signalling via contact with other osteoblasts and osteocytes through gap junctions of their cytoplasmic canalicular extensions (Khan *et al*., 2001).

Osteocytes are derived from osteoblasts that have become entrapped within bone matrix during bone formation; located in small lacunae between lamellae they have fine cytoplasmic extensions passing in canaliculi between and across the layers (Khan *et al*., 2001). Their cytoplasmic extensions are in contact via gap junctions with the extracellular fluid space surrounding capillaries and nerve endings within the Volkmann's and Haversian canals. They receive their nutrition directly from the blood as opposed to chondrocytes which are supplied by passive diffusion through a background matrix of cartilage (Soames *et al*., 1995). Osteocytes (Figure 1.5) and their canaliculi form a communicating network through the bone matrix; stretch or damage to this network is thought to modulate repair and remodelling in response to changes in mechanical load and damage, in a process called mechanotransduction (Khan *et al*., 2001; Einhorn, 1996).

Osteoclasts are derived from haematopoietic stem cells of the bone marrow which give rise to myeloid and lymphoid cell lines. Lymphoid precursors develop into T and B cells of the immune system, while the myeloid stem cells give rise to erythroblasts and ultimately red blood cells, and white blood cells such as monocytes and neutrophils.

Figure 1.5: (a) osteocytes trapped embedded within an osteonal system; and, (b) scanning electron micrograph of osteocytes with fine cytoplasmic connections (adapted from Sommerfeldt & Rubin, 2001).

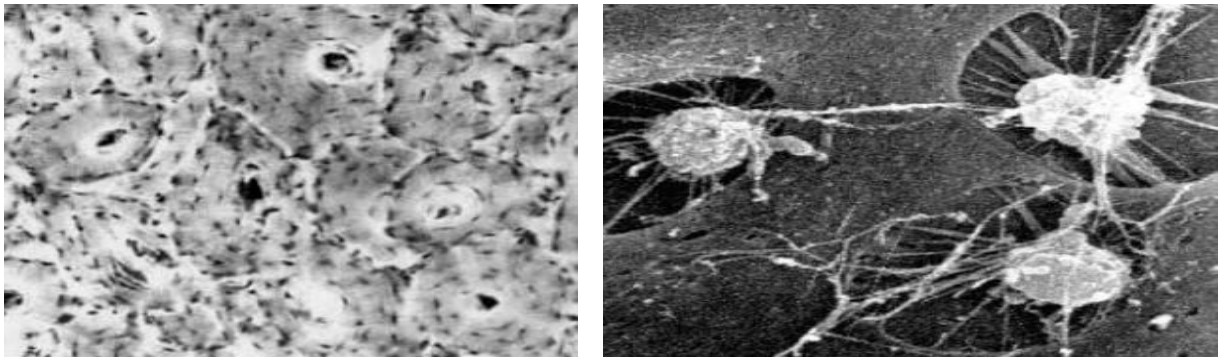

Osteoclasts arise from peripheral mononuclear cells in the blood (Figure 1.6), but undergo subsequent maturation on bone surfaces under the influence of the ligand receptor activator for nuclear factor ß or RANK (Gallagher & Sai 2010).

Figure 1.6: Osteoclast differentiation (adapted from Ritchlin, 2004).

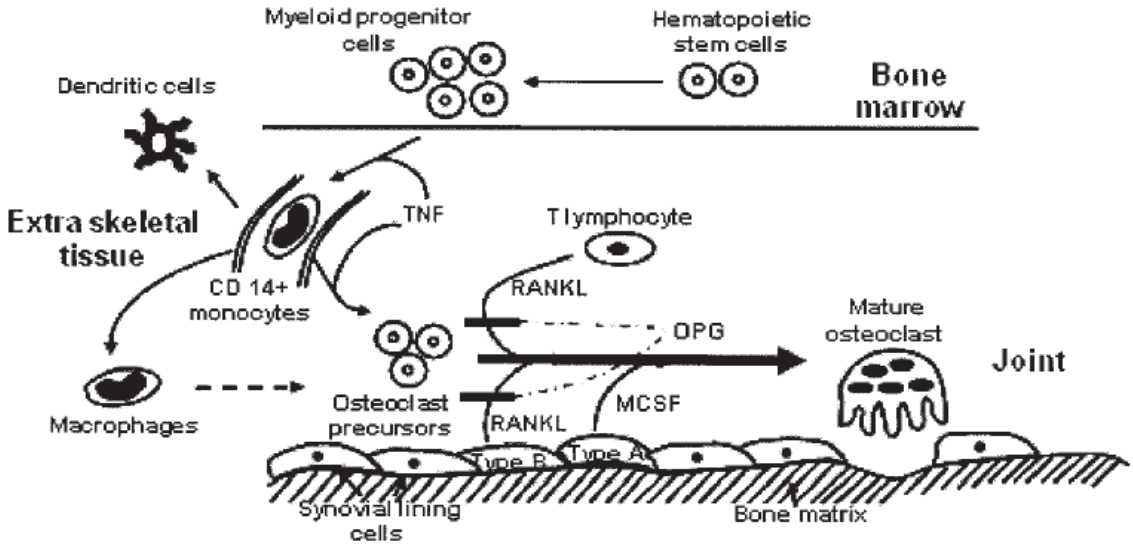

Osteoclasts are large multinucleate cells with a resorptive function to remove bone matrix. They lie on internal and external bone surfaces in Howslip's lacunae, are found in the cutting cones of basic remodelling units, and are capable of migration into areas of damaged bone for repair (Soames *et al*., 1995).

The ruffled sides of their cell membranes attach and enclose a discrete area on the bone surface, forming small sub-osteoclastic bone resorbing compartments. They release osteolytic enzymes into these compartments which break down mineral and protein components of the bone matrix. The acid content breaks collagen linkages with hydroxyapatite crystals and the proteolytic enzymes, collagenase and cathepsin, breakdown the organic elements. In a similar manner to other bone cell types, osteoclasts are under the influence of many local controlling factors and hormones, resorbtion is increased by both progenitor cell proliferation and by increasing activity, and inhibition of these processes reverses their activity (Khan *et al*., 2001).

Figure 1.7: (a) Bone forming osteoblasts OB and large multi-nucleate osteoclasts OC clustered alongside bony spicules in a sample of membranous bone (adapted from Soames *et al.,* 1995); and, (b) an osteoclast gouging out a groove on trabecular strut (adapted from Sommerfeldt & Rubin, 2001).

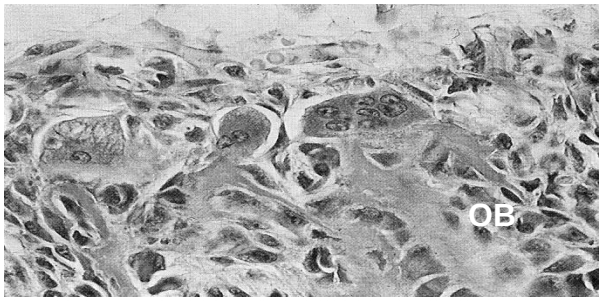

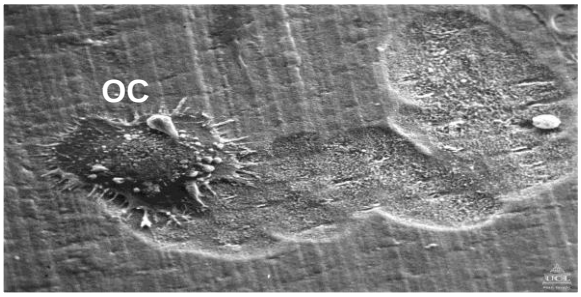

1.1.8: Bone matrix

The cellular elements of bone, like other connective tissues, are embedded within or are closely related to the surfaces of surrounding matrix. Bone is made up of an organic phase of cells (2 to 5%), water (5%), osteoid (25%) collagen fibres, non-collagenous proteoglycans and proteins; and, a mineral phase of inorganic calcium hydroxyapatite salts (70%). The organic phase consists of Type I collagen fibres (94%), a few type IV collagen fibres and non-collagenous proteoglycans, glycoprotein, osteocalcin and osteonectin (6%). If formed *ex-vivo* the non-organic crystalline structure is brittle but when combined with the organic phase, the resultant composite has greater hardness, strength and resilience to mechanical load (Khan *et al*., 2001). Figure 1.8 shows the two phases in isolation after preparation in various chemicals.

Figure 1.8: Mineral and collagen elements of bone; a cortical bone sample treated with bleach (hypochlorite) to digest collagen and with hydrochloric acid to dissolve the mineral (adapted from Arnett & Boyd, 2006).

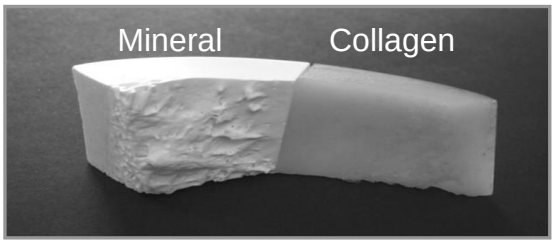

The organic phase conveys both strength and flexibility, parallel Type I collagen fibres and ground substance are laid down during early bone formation as osteoid. The non-collagenous proteins within osteoid seem to be required for growth, cell signalling, and in particular osteopontin, osteonectin, and matrix-gla protein seem to be responsible for deposition and adhesion of bone mineral (Sommerfeldt & Rubin,

2001). In small animal models of bone disease genetic deletions in mice have shown osteocalcin deficiency to cause increased bone formation, and a lack of osteonectin leads to osteopaenia (Ducy *et al*., 1996; Delany *et al*., 2000). Proteoglycans, in bone matrix are now thought to be involved in spatial organization of the extracellular matrix and molecular signalling during growth and development (Aszodi *et al*., 2000).

Bone mineral is mainly comprised of imperfect crystals of calcium and phosphate hydroxides, known as hydroxyapatite, with small amounts of calcium carbonate and other trace elements. The mineral phase is usually referred to as hydroxyapatite [$Ca_{10}(PO_4)_6(OH)_2$], and if constituted *ex-vivo* it forms plate-like crystals approximately 20 to 80 nm long and 2 to 5 nm thick. The crystal structure is smaller and less perfect than naturally occurring apatite crystals, and it is thus more reactive and soluble *in-vivo* which facilitates more rapid chemical turnover. Perfect crystalline structures would be harder to form and reabsorb, and therefore would be unsuitable energetically for biological systems. The amount of mineralisation is correlated with bone strength, and it is important to measure bone quantity clinically. The usual bone mineral quantity variable measured in clinical practice is bone mineral density (BMD), usually by dual-energy X-ray absorptiometry (DXA) giving an areal (2D) density value or in distal limb bones peripheral quantitative computed tomography (pQCT) which can give a true volumetric density (Rizzoli *et al*., 1995).

Figure 1.9: Summary of bone structure (adapted from Rho & Kuhn-Spearing, 1998).

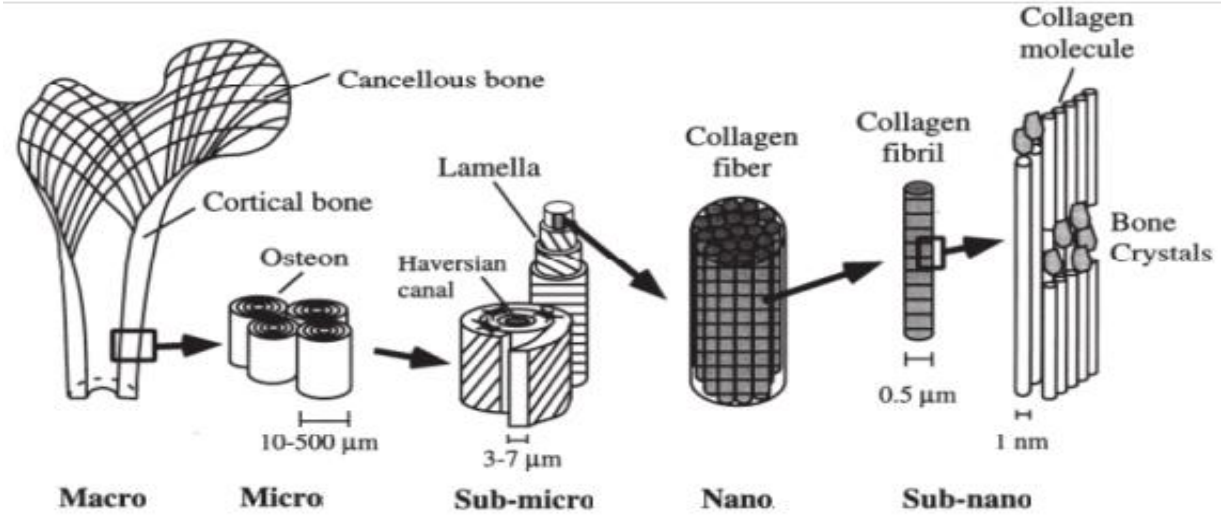

1.2: Bone physiology

1.2.1: Growth, modelling and remodelling

The skeleton begins to develop at 6 weeks of embryonic life, when the foetus is 12 mm long and will continue to develop for another 25 years. Most bone development in the axial and appendicular skeleton is by the gradual ossification of a cartilaginous model; however some of the first bones to form and ossify do so by a process of intra membranous ossification. Bones grow in length at cartilaginous growth plates called epiphyses and in girth by endosteal resorbtion and sub periosteal apposition. Bone also undergoes modelling and remodelling during life.

Modelling is the process in which bones changes its overall shape in response to biological influences or mechanical forces, gradually adapting to the prevailing ambient forces it is exposed to during daily activity. Bones may widen or change axis by removal or addition of bone to the appropriate surfaces by the independent action of osteoblasts and osteoclasts in response to biomechanical forces. Bones also normally widen with aging in response to periosteal apposition of new bone and endosteal resorbtion of old bone.

Bone remodelling is the process by which bone is renewed to maintain bone strength and mineral homeostasis; remodelling involves continuous removal of discrete packets of old bone, and replacement of these packets with newly synthesized osteoid and subsequent mineralisation to form new bone. The remodelling process reabsorbs old bone and forms new bone to prevent accumulation of bone microdamage. Thus bone is an active living tissue capable of adapting to forces in its external environment.

1.2.2: Intra-membranous ossification

In membranous ossification bone is laid down in vascular membranes of primitive mesenchymal cells, bones formed in membrane include the skull plates and the clavicles. Stages of membranous bone formation are summarised in Figure 1.10. Mesenchymal cells differentiate into clusters of osteoprogenitor cells and proliferate to form ossification centres around capillary networks. The osteoprogenitor cells differentiate into osteoblasts which form osteoid on the cell surface away from the blood vessel, which then mineralises.

Figure 1.10: Membranous ossification (adapted from Soames, 1995)

(a) Osteoprogenitor cells differentiate forming a central group cells condenses together in mesenchyme near a small blood vessel.

(b) The cells differentiate into osteoblasts secrete osteoid which subsequently mineralises to form bony spicules away from the blood vessel.

(c) An outer periosteal layer develops, osteo-blasts continue to secrete and mineralise osteoid, surround local blood vessels, become embedded to form osteocytes.

(d) Bone development undergoes consolidation, osteoclasts initiate a remodelling process, and primitive trabeculae are formed creating a primary spongiosa.

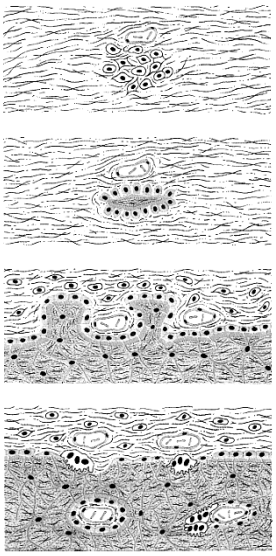

Spicules of bone form and spread outward away from trapped blood vessels within forming a primary spongiosa of trabeculae. As further layers of osteoid are lay down, osteoblasts become enclosed and primary osteons form around the spiral layers of trabeculae, these primary osteons later remodel producing compact bone, and the outer mesenchymal layers differentiate into periosteum. The advantage of woven bone is that it can be can be laid down fairly quickly, and gives protection early in foetal life to the developing brain but it is not as strong as osteonal bone and thus in most species it is usually replaced by a process of Haversian remodelling (Currey, 2003a).

1.2.3: Endochondral ossification

The majority of bone develops from hyaline cartilaginous models formed during embryogenesis (Figure 1.11). At 6 weeks gestation the humerus and femoral bones are present in the foetus. The model of hyaline cartilage is surrounded by a membrane of vascular mesenchyme with inner layers of osteoprogenitor cells. Growth is interstitial from within and appositional on the surface. Initially chondrocytes enlarge in the centre of the model, forming a primary ossification centre. Primary centres enlarge pushing matrix into thin perforated layers, subsequent cells death produces large lacunae which begin to mineralise at their

walls. At the same time on the outer surface of the model, a layer of bone is formed by differentiating osteoblasts on the inner layer of vascular mesenchyme. This layer gets thicker and longer, and eventually encloses the complete shaft of the cartilaginous model with a thin bony collar. Osteogenic buds invade the thin periosteal collar, bringing in capillary buds, osteoclasts and osteoblasts which have differentiated from the osteoprogenitor layer. Thus blood vessels enter the perichondrium and make contact with inner lining cells.

Figure 1.11: Endochondral ossification (adapted from Soames *et al*., 1995)

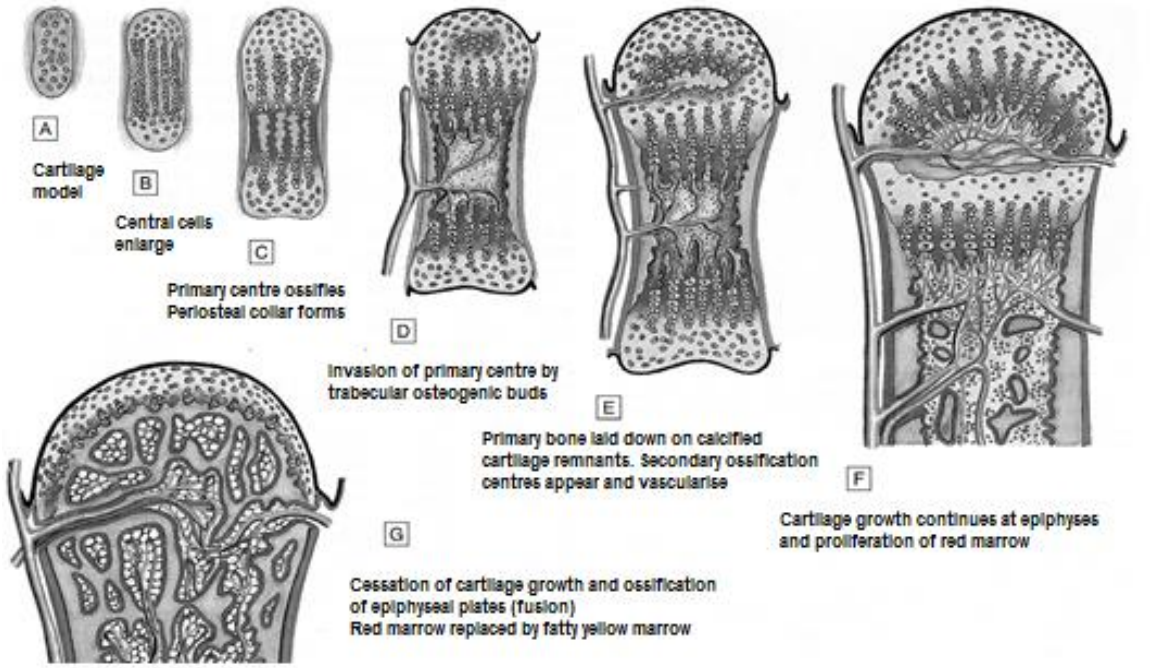

Osteoclasts then erode into the primitive sub periosteal collar and calcified lacunae, forming larger intercommunicating spaces which are in turn invaded again by vascular mesenchyme, osteoblasts and osteoclasts, and haematopoietic stem cells of the future marrow. Osteoblasts then start filling in the spaces from ‘out to in’ with osteoid, and as the osteoid becomes calcified cells become trapped, further layers are added and the vascular spaces are narrowed. The process of ossification spreads longitudinally along the bone; however epiphyses remain cartilaginous, allowing continued growth in length of the bone until the process of secondary ossification begins with puberty.

The earlier timing of puberty and the presence of oestrogen causes faster epiphyseal closure in the female, and as a consequence of earlier termination of growth the female of the species have smaller stature and thinner bones. Material density of

female bone is similar to the male; however, smaller bones are not as strong. During development bone also grows in width or diameter by a process of appositional growth where bone is reabsorbed from the endocortical or endosteal surface and laid down on the outer sub-periosteal surfaces. This importance of having bigger diameter bones is discussed in the section on mechanical properties.

1.2.4: Bone remodelling

In the 17th century 'Galileo' (1638) observed that bone could adapt to new forces, he recognized the significance of trabeculation and observed that hollow cylinders were stronger weight for weight than solid rods (Soames *et al*., 1995). In the 19th century, based on earlier work by Meyer and Roux, Wolff proposed 'The law of bone transformation' (Wolff, 1892); this stated that any change in function of a bone was followed by a change in the internal and external form of the bone (Lee & Taylor, 1999). The process whereby old bone is replaced by new bone is known as remodelling and the process whereby bone adapts to greater than normal stresses is known as modelling. Remodelling is normally a balanced physiological process of removal and accrual; it is sensitive to ambient forces, as well as metabolic requirements to maintain normal calcium levels.

Remodelling increases in perimenopausal and early postmenopausal women and then slows with further aging, but continues at a faster rate than in premenopausal women and is thought to increase mildly in aging men. In un-balanced remodelling due to ageing, drugs and certain diseases there are profound effects on bone strength (Seeman, 2002). Remodelling is broken down into four phases; resting, resorbtion, reversal and formation. In resorbtion, osteoclasts remove mineral and organic components of bone matrix in an external vacuole between the cell and bone surface with acid and proteolytic enzymes. When osteoclasts have resorbed most of the matrix, they die off in the reversal phase and osteoblasts migrate and occupy the resorbed surface. Finally, in the formation phase, osteoblasts deposit new un-mineralised osteoid (collagen matrix) which is subsequently mineralised and new bone is formed (Baron, 2003).

In cortical bone remodelling, osteoclasts form cutting cones of cells coring out small tunnels moving through bone at approximately 50 μm per day (Kanis, 1994). The

space left by the tunnelling osteoclasts or resorbtion cavity is closed in layers by following osteoblasts, from the outer surface to the centre of the space, and as the osteoid mineralises forming new lamellae, entrapped osteoblasts become osteocytes (Figure 1.12). Successive lamellae are formed as osteoblasts add more and more layers in the "closing cone" until the space is filled toward the central capillary. Approximately 10% of bone is replaced each year during the process of remodelling and activity is coupled so no net loss occurs.

Figure 1.12: Cortical bone remodelling (adapted from Kanis, 1994)

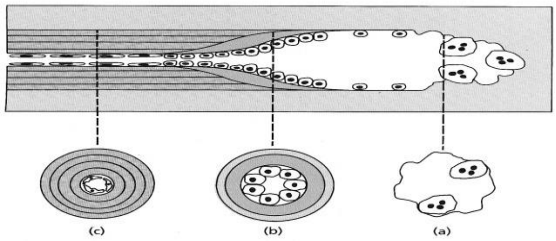

(a) osteoclasts tunnelling a 'cutting cone' followed by smoothing in the reversal zone and (b) laying down of new concentric lamellae filling the cavity inwards to form (c) Haversian canal and embedded osteocytes.

The presence of bone remodelling units moving through cortical bone creates resorbtion cavities that temporarily weaken bone structure where they pass through. Resorbtion cavities can act as "stress risers" localised areas where stresses may be focussed leading to failure. In normal healthy bone the number of resorbtion cavities is usually small and the resorbtion cavities are relatively quickly refilled. The cutting and closing cones moving through bone cortex have the effect of removing excessive amounts of micro-damage, small cracks that form and propagate within bone during every day loading along lines of stress. In osteoporosis greater activation and incomplete refilling of BMU's increases the number and size of resorbtion cavities thereby increasing porosity and ultimately decreasing resistance to bending forces.

A similar process of remodelling occurs on trabecular surfaces, osteoclasts first gouge out grooves on old or damaged trabeculae and in reversal zones the following osteoblasts fill in the grooves and indentations left behind (Figure 1.13). Removal and accrual is again usually matched with resorbtion balanced by refilling. In osteoporosis, trabecular remodelling becomes unmatched, some trabeculae become thinner and some get thicker, and interconnecting struts are lost.

The overall effect weakens trabecular bone making it more susceptible to failure when exposed to loads in unusual directions, such as a fall onto the hip producing an abnormal bending moment at the femoral neck. Thus trabecular thinning and loss of

connectivity plus endocortical loss combine to make the bone fragile enough to produce a fracture (Seeman, 2002).

Figure 1.13: Remodelling on trabeculae surfaces (adapted from Kanis 1994)

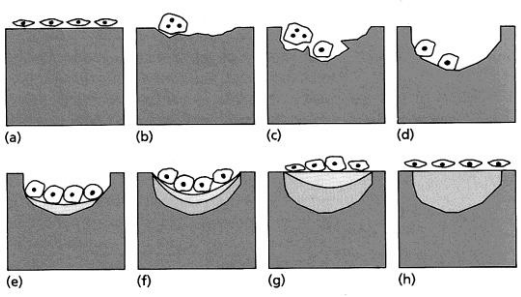

(a) Resting phase (b) Osteoclast activation (c) Formation of resorbtion cavity (d) smoothing by mono-nuclear cells (reversal) (e) Differentiation of osteoblasts in erosion cavity (coupling) (f) matrix formation/mineralization (g) complete matrix mineralization (h) lining osteo-progenitor cells cover new bone.

1.2.5: Control of bone remodelling

At a cellular level the process of bone remodelling is well characterised but what initiates and controls the process? In the 1960's Frost suggested that bone has a mechanostat capable of responding to changes in direction and magnitude of ambient forces. Frost and other researchers have proposed that mechanical strain or localised microdamage initiated a process of adjustment of bone mass and geometry leading to accrual or altered distribution of mass, enabling structure to withstand new forces (Frost, 1994; Einhorn, 1996). The result of mechanotransduction is remodelling and modelling, a dynamic process involving continuous destruction and renewal, the net effect is usually a balanced activity of both osteoblasts and osteoclasts (Khan *et al*., 2001). The process appears to be strain dependent, purported minimum strains to prevent disuse and overload strains required to make bone stronger, are presented in the Figure 1.14.

The anatomical site of the mechanostat appears most likely to be the osteocytic network, and has been postulated that fluid flow induced shearing forces stretch or damage the fine cytoplasmic extensions of the network to initiate the processes at a molecular level through connections to surface osteoblasts (Frost, 1994; Klein-Nulend *et al*., 2005).

Figure 1.14: Mechanical strain and remodelling (adapted from Frost, 1994)

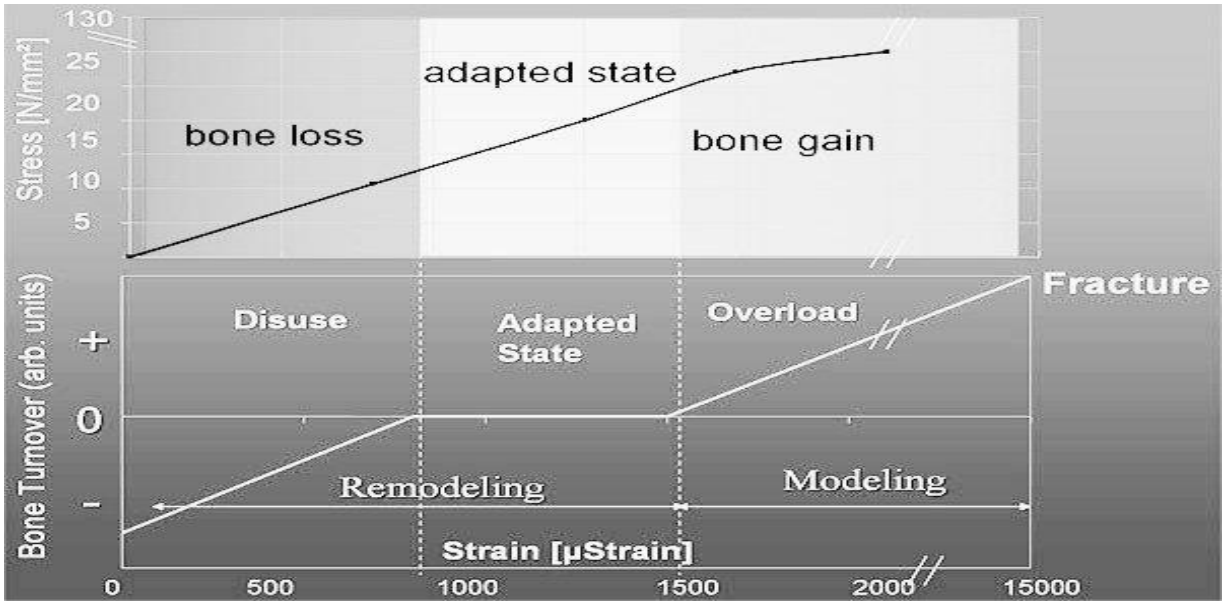

1.2.6: Molecular control of bone remodelling

The discovery of the osteoclast receptor activator for nuclear factor kappa beta (RANK) signalling pathway, and various genetic, hormonal and mechanical factors that affect it, have shed new light on the pathogenesis of bone weakening diseases including osteoporosis (Figure 1.15). The molecular level control of balanced osteoclastic removal and osteoblastic accrual and therefore skeletal health is related to molecular expression and concentrations of 3 factors; RANK, its ligand RANKL and osteoprotegrin (Boyle *et al*., 2003).

Figure 1.15: Recent advances in the molecular biology of bone remodelling.

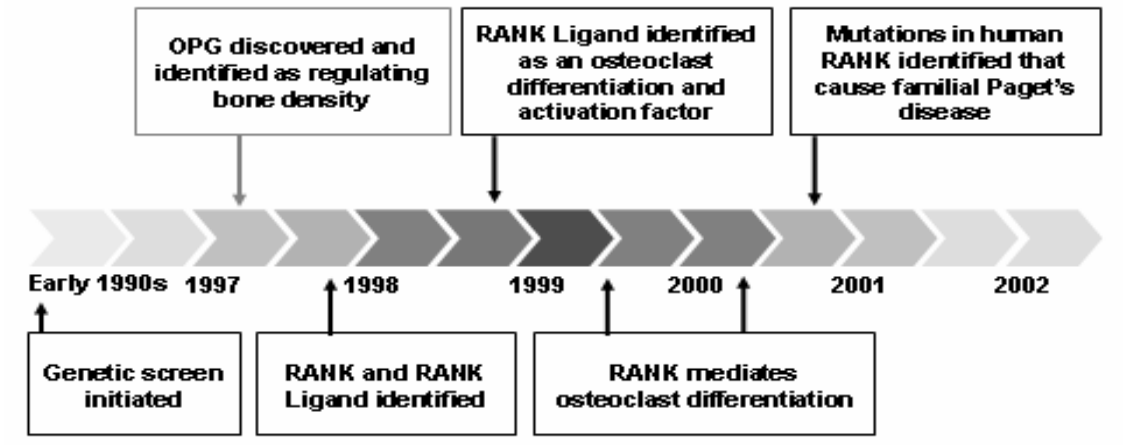

Relative over expression of RANK ligand in relation to osteoprotegrin leads to increased osteoclastic activity and excessive bone removal, whereas inhibition of RANK ligand or increased osteoprotegrin level leads to bone accrual (Boyle *et al*. 2003; Lacey *et al*. 1998; Hofbauer *et al*. 2004). Mechanical stress and strain, certain hormones and cytokines stimulate surface osteoblasts to produce an increase in macrophage colony stimulating factor (CSF-1) and RANKL and then subsequently activate RANK on macrophage precursor cells in the bone marrow. Both factors are necessary for differentiation and expression of genes coding for the osteoclastic cell lineage and the action of osteoclasts on bone surfaces (Boyle *et al*., 2003).

It was the discovery of the inhibitory protein osteoprotegrin that blocks osteoclast differentiation *in vitro* and bone resorbtion in animal models that lead to the initial breakthrough in the osteoclast signalling pathway (Simonet *et al*., 1997). The similarities of osteoprotegrin to other trans-membrane signalling proteins lead to the discovery RANK. Osteoprotegrin is now known to act as a decoy receptor which binds RANKL and decreases osteoclast activation and bone resorbtion. The role of these molecular control factors and their receptors is coupled, so that osteoblasts on bone surfaces initially signal the onset of remodelling by initiating osteoclast differentiation and activation, but then activated osteoclasts in turn signal nearby osteoblasts to initiate the reversal process so the overall process remains in balance. The calcium regulating hormones PTH and Vitamin D3, and other factors various cytokines; TNF-ά, IL-1 and IL-6 and growth factors IGF-1 also affect resorbtion by up-regulation of mRNA for RANKL.

In order to prevent bone resorbtion associated with menopause, metastatic cancer, osteoporosis and side effects of powerful anti-inflammatory drugs, pharmacological research is currently underway on a number of targets in the RANK pathway (Boyle *et al.,* 2003; Hofbauer *et al*., 2004). To date over 60 proteins are known to be involved in the RANK signalling pathway which is still not fully understood, a summary of principle controlling factors are presented in Figure 1.16.

Figure 1.16: Schematic representation of the molecular biology / hormonal control of bone remodelling (adapted from Gallagher & Sai 2010)

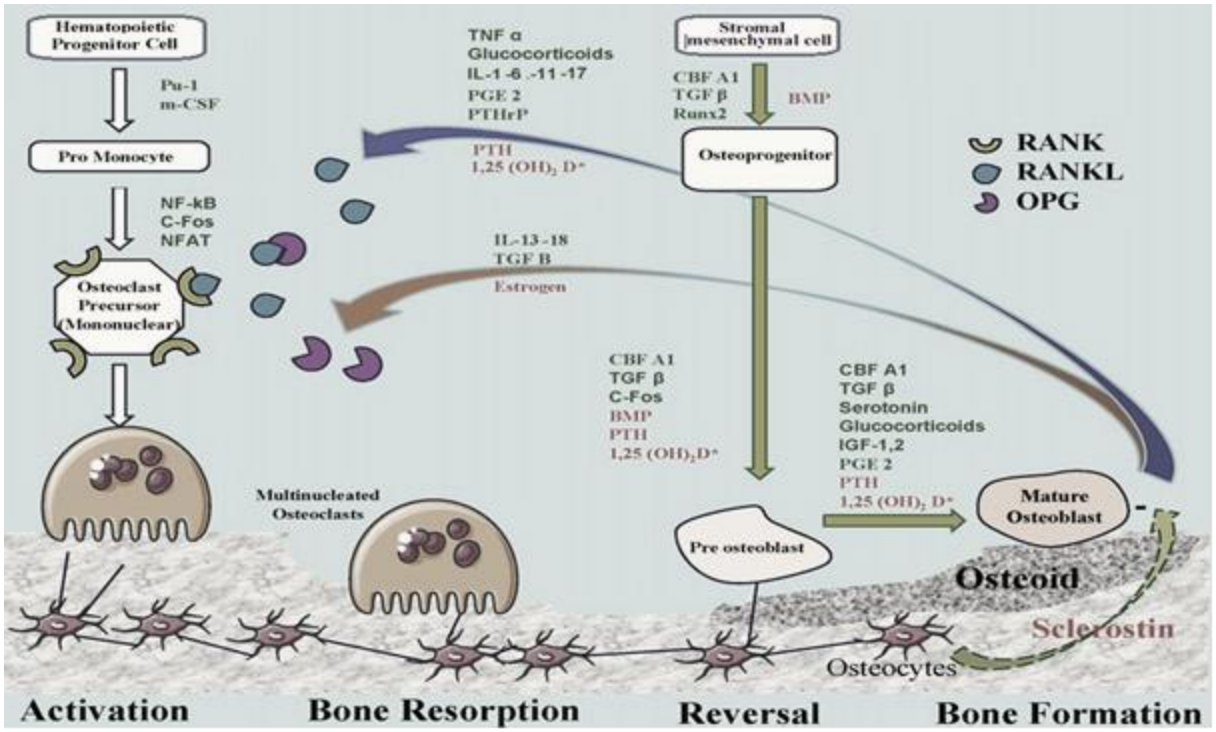

RANKL expression is induced in osteoblasts, activated T cells, synovial fibroblasts and bone marrow stromal cells, and subsequently binds to its specific membrane-bound receptor RANK, triggers a network of kinase cascades that promote osteoclast differentiation, activation and survival. Conversely, OPG expression is induced by factors that block bone catabolism and promotes anabolic effects. OPG binds and neutralizes RANKL, leading to a block in osteoclast proliferation and activity as well as decreased survival of pre-existing osteoclasts.

1.2.7: Bone mineralisation

The mineralisation of extra-cellular matrix is a physiological process in bone and a pathological one in soft tissues. In bone, mineralisation begins 10-15 days after organic matrix has been laid down; mineral content increases rapidly at first (70% of total osteoid) and then continues at a slower rate for several months (30%).

Although still poorly understood, it is thought that hydroxyapatite crystal formation begins with super-saturation in the extra-cellular fluid of bilaminar lipid packets, budded by exocytosis from dividing chondrocytes or from osteoblasts on bone surfaces. Eventually lipid bi-layers break down and mineral components are exposed

to collagen fibres, mineralisation then proceeds rapidly with collagen fibres and glycoproteins controlling orientation and matrix-gla protein and glycosaminoglycans preventing over-mineralisation (Christoffersen *et al*., 1991; Yagami *et al*., 1999).

Control of mineralisation is still poorly understood, but genetic studies have shown that bone mineralisation requires normal extra-cellular phosphate concentration; lower concentrations prevent mineralisation, however, raising phosphate concentration will not in itself cause pathological mineralisation due to the presence in the extracellular matrix of pyrophosphate, an inhibitor of mineralisation. Mineralisation occurs in bone because of co-expression in osteoblasts of Type I collagen and tissue non-specific alkaline phosphatase (TNAP), an enzyme that cleaves pyrophosphate (Murshed *et al*., 2005).

1.3: Bone mechanical properties

Bone is exposed to loading through normal everyday activity as the body moves in its gravitational environment. The ability of bone to bear force is a function of the intrinsic material properties of density, stiffness and strength, allied to geometric properties of shape, size, cortical thickness and cross sectional area and trabecular architecture (Carter & Hayes, 1976; Gibson & Ashby, 1997). Bone mineral imparts stiffness and strength, and the organic phase toughness.

The architectural design of bone makes them well suited for the structural demands placed on them. The flat plates of the skull, with a thin layer of high density trabecular bone are well adapted to resist direct impact forces; and the hollow tubular structure of long bones provides greater strength and resistance than solid rods against bending and axial compression while minimising weight and thus decreasing the energy costs of locomotion.

The ultimate tensile strength of bone is similar to cast iron, bone's capacity to absorb and release energy is double that of oak, and bone density is only one third that of steel (Martin & Burr, 1989). However, fracture can still occur if loading is applied suddenly outside of the normal physiological directions or when repetitive loading causes fatigue damage beyond the capability of natural repair mechanisms. Structural and material properties of bone are affected by; growth and development, bone remodelling, disease and drugs, hormonal changes at the menopause in the

female, and ageing in both genders. A summary of factors affecting bone quality is shown in Figure 1.17.

Figure 1.17: Factors affecting bone quality (Felsenberg & Boonen, 2005).

Structural properties	**Material properties**

• **Geometry**
  ○ Size and shape
  ○ Material distribution
• **Trabecular micro-architecture**
  ○ No.s / thickness / connectivity
• **Cortical micro-architecture**
  ○ porosity / thickness
	• **Mineralisation**
	  ○ Real and apparent density
	  ○ Mineral-to-matrix ratio
	  ○ Crystal size
	• **Collagen**
	  ○ Type / cross-links
	• **Microdamage**
	  ○ crack no's / length / density

Bone remodelling	

1.3.1: Stress and strain

Stress is a measure of applied loading and strain the resulting deformation due to loading and both are used to describe bone mechanical properties (Turner & Burr, 1993). Stress is expressed in units of force per unit area ($N.m^{-2}$) or Pascals (Pa) and may be compressive, tensile, torsional or shear depending on the location within the bone and action of surrounding muscles (Figure 1.18). Strain is expressed as a ratio of starting and finishing dimensions as a fraction, for example, a value of 0.001 or 1000 microstrain represents a 0.1% shortening due to compressive stress or lengthening due to tensile stress (Heinonen, 2001).

Figure 1.18: Tensile and compressive stress over the length of a femur (adapted from Soames *et al*., 1995).

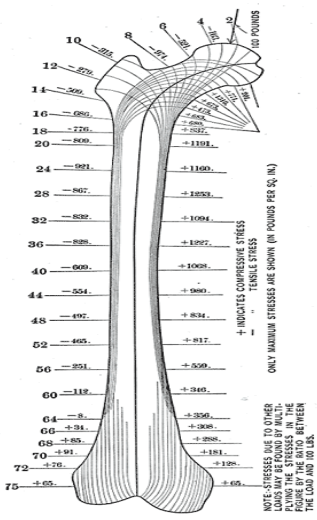

1.3.2: Strength and stiffness

Strength and stiffness are further intrinsic material properties of bone that can be measured during mechanical tests when known loads are applied in a controlled way to a sample of bone. Stiffness is stress divided by strain determined from the elastic portion of the stress / deformation curve, and strength is the force at yield or failure,

both concepts are best illustrated on stress strain curves derived from mechanical tests of bone to failure (Figures 1.19 & 1.20).

Figure 1.19: Schematic stress-strain curve of bone during mechanical test to determine material properties (adapted from Einhorn, 1996). Stiffness is indicated by the slope of the line in the elastic region of the curve and is termed the Elastic or Young's modulus. Strength is indicated by yield and failure points.

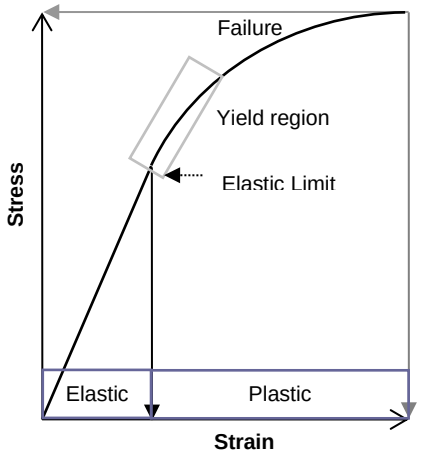

Equation 1.1: Bone Stiffness E = S / ε

E = Young's or Elastic modulus

ε = strain and S = stress

Areas under the curve represent strain energy, in the elastic region this is termed resilience, and the total energy stored at the point of fracture defines the material toughness (Figure 1.20).

Figure 1.20: Resilience and toughness (adapted from Felsenberg & Boonen, 2005). Stiffness or initial reaction to load the maximum slope of the curve is important in bone resistance to bending or buckling. The height of the curve represents the ultimate load the bone can withstand, and toughness the energy required to break the bone; resilience is the energy stored in the elastic region under the curve.

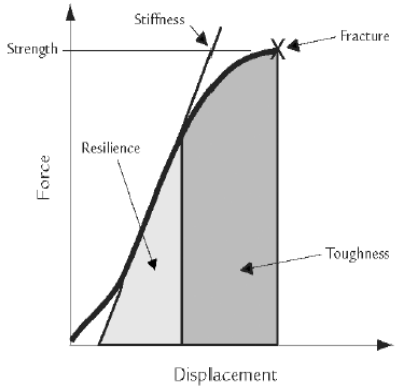

1.3.3: Bone geometry and strength

Mammalian long bones are usually curved longitudinally with thick cortical shells approximately tubular or triangular in cross-section with expanded ends to spread stress at the major load bearing joints. This design allows the bones to bear relatively large loads but remain relatively light. Mechanically, long bones can be considered as beams loaded in bending and the amount of bending or displacement they undergo for any given load can be described by bending or beam formula, such as described in Equation 2 (Rubin & Lanyon, 1982).

Equation 1.2: Beam Displacement = $M L^2 \div 8 E I$	Where: M = bending moment, L = length, E = Elastic modulus, I = Cross sectional moment of inertia.

It follows from Equation 1.2, that for any given value of M, beam deflection or bending can be reduced by decreasing the length of the bone (L), by increasing stiffness (E) making the bone more rigid by addition of extra material; or if mass is to be preserved, by placement of the available mass further away from the central axis by increasing cross-sectional moment of inertia (I). The effect of changing the second moment of inertia is achieved by changes in the outer periosteal radius and or the inner endosteal radius as depicted in Figure 1.21.

Equation 1.3 shows that the contribution of mass to bone strength is proportional to its distance from the axis of bending to the fourth power and thus small changes in external geometry can have a profound effect on bone strength. The formula is true for perfect tubes, but most long bone cross-sections are elliptical or triangular, and more complex mathematical formulae based on the parallel axis theorem are used to describe I for real long bones (Turner & Burr, 1993). In a tubular structure efficient distribution of material thus accounts for some of the resistance to bending loads; and if material density is kept constant the strength of a bone can be increased through simple geometric adaptation by addition of small amounts of bone to the periosteal surface (Turner & Burr, 1993; Sommerfeldt & Rubin, 2001).

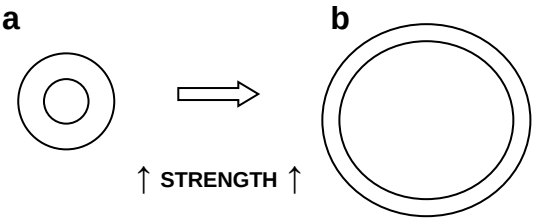

	a	b
Cortical area	**100%**	**100%**
Bone mass	**100%**	**100%**
I	**100%**	**400%**

Figure 1.21: Resistance to bending in long bones; by placing cortical mass further from the central axis. In (a) and (b) cortical mass is the same; however bone (b) has greater bending strength due to its greater cross sectional or moment of area or inertia (I).

Equation 1.3: I = CSMA = $\pi/4\ (r_p^4 - r_e^4)$

Where r_e = inner radius and r_p = outer radius

The bone expansion shown in Figure 1.21, endosteal resorbtion and sub-periosteal deposition also represents a type of homeostatic adaptation maintaining bending strength despite loss of bone mass seen with ageing in humans (Martin & Atkinson, 1977; Bouxsein *et al*., 1994). However, bone is also capable of adaptive structural optimisation by localised periosteal bone formation increasing r_p in areas of high stress or strain. Animal studies involving loaded and unloaded limbs have shown bone accrual on periosteal surfaces at sites with the greatest strain, and then

subsequent increase in I and increased resistance to bending in mechanical tests post-sacrifice (Warden *et al*., 2005; Robling *et al*., 2002).

1.3.4: Section modulus and buckling ratio

Limitations to adaptation shown in Figure 1.21 also exist as ultimately bone will break if the cortical shell becomes too thin in relation to the distance from the centre to the outer periosteal surface. In engineering, section modulus and buckling ratio are two variables relating placement of material from the central axis to structural integrity. Section modulus (Z) is the ratio of the moment of inertia I of the cross-section of a beam undergoing bending to the greatest distance of an element from the neutral axis. Structural strength in bending is proportional to the maximum stress in the cross-section and maximum stress is inversely related to section modulus (Z) and is thus an index of bending strength (Beck, 2003).

Buckling ratio relates the outer periosteal radius r_p to the cortical thickness, for cylindrical structures a ratio of about 10 appears to be the critical limit where structural integrity breaks down (Beck, 2003). In the femoral neck of patients with osteoporosis, loss of bone mass is associated with regional cortical thinning due to endosteal resorbtion; this increases the buckling ratio making the bone more the susceptible to failure (Crabtree *et al*., 2002). Estimation of section modulus and buckling ratio is now possible using Hip Structural Analysis (HSA) software algorithms of newer generation DXA scanners (Beck, 2003), however, some authors have questioned the sensitivity of such algorithms and highlighted limitations of predictions of bone strength based on 2-D measurements (Bouxsein & Seeman, 2009).

1.3.5: Trabecular strength

Trabecular bone is mainly located within the ends of long bones and vertebral bodies where bone is exposed to multidirectional forces. Trabecular bone is anisotropic, that is the major struts and plates are arranged to withstand predominant ambient forces (Figure 1.22) and then distribute them into the cortical shell (Turner, 2006).

The complex inner geometry of trabecular bone was first noted by Ward in 1838 when he described trabecular morphology, suggested functional significance and

performed mechanical tests on trabecular bone (Lee & Taylor, 1999). Vertebral trabeculae are known to increase in size and thickness during adolescence but get thicker and loose connectivity in older age (Mosekilde, 2000).

Similar changes occur in the superior femoral neck (Figure 1.23c) where the trabecular density and orientation is designed to accommodate normal loading experienced during ambulation. Trabecular strength is dependent on bone density, trabecular numbers, size and density distribution of its mass, microarchitecture, anisotropy and porosity.

Figure 1.22: Femoral trabeculae patterns, stress trajectories, and trabecular density. (a) Principal stresses and trajectories (b) macroscopic trabeculae patterns, and (c) Lunar DXA scan image showing bone density distribution at the human femoral neck (adapted from Soames *et al*., 1995; Gibson & Ashby, 1997; Rizzoli, 2004.)

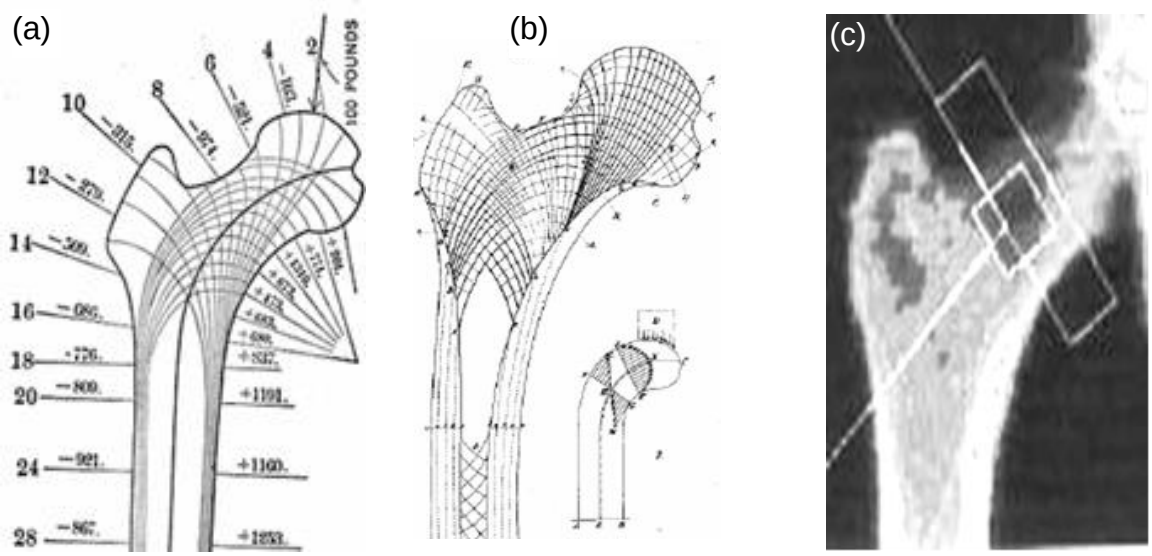

The inter-relationships between these factors to strength is complex; however, studies of trabecular bone strength are important because the internal trabecular network has a high surface area for osteoclastic action and is thus the main site of bone mass loss with ageing, hormonal deficiency post-menopause, drugs and disease; and loss of bone mass has profound effects on bone quality.

Trabecular bone density approximately halves between the ages of 20 and 80 years whereas bone strength is reduced by a factor of 4 to 5 (Mosekilde *et al*., 2000) and trabecular compressive strength has been shown to be approximately related to the square of the apparent density (Carter & Hayes, 1977). Other studies of power relationship of apparent density to strength, across wider density windows or with corrections for material and apparent density, have reported the power relationships

for most trabecular bone between 2 and 3 (Mosekilde *et al.*, 2000; Zioupos *et al*., 2008). The distribution of bone mass or bone density distribution (BMDD) within trabecular networks is along the major stress trajectories, Figure 1.23 shows theoretically predicted volumetric density distributions in the human femur during maturation in three loading conditions. The theoretical modelling closely correlates with the findings in clinical and animal studies and are similar to areal density distributions recorded in the DXA image in Figure 1.22c (Carter *et al.,* 1992) .

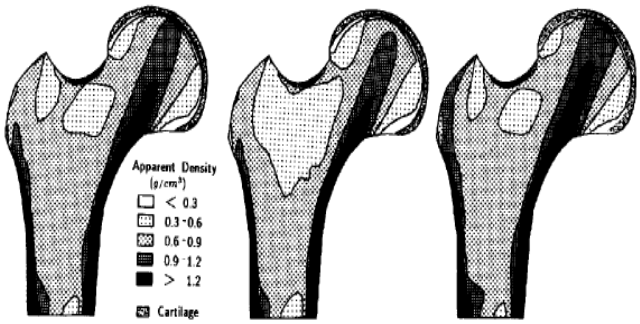

Figure 1.23: Finite element modelling of femoral neck density distributions during simulated maturation in three loading conditions (a) normal loading (b) reduced loading and (c) increased loading due to activity (adapted from Carter *et al.,* 1992)

1.3.6: Trabecular number, size and connectivity

The number and size of trabecular struts affects strength but loss of trabecular numbers has a far greater proportionate effect on strength (Seeman, 2008). The relationship of trabecular numbers and size is shown in Figure 1.24a, for a 10% drop in trabecular density the loss of strength is far greater with loss of trabecular numbers (Van der Linden *et al.,* 2001) than with a drop in size. In ageing vertical load bearing trabecular struts and plates in the vertebrae and femoral neck become thicker in the lines of normal ambient forces but horizontal supporting struts are lost; thus connectivity decreases, anisotropy rises and structural fragility increases (Mosekilde *et al.,* 1993; Seeman, 2008).

The disproportionate loss of strength due to osteoclastic perforation and removal of supporting struts is explained by Euler's theorem (Rubin, 2005) which states that the strength of a column is inversely related to the square of the length of the unsupported part of the column (Figure 1.24b). Thus additional effects of hypo-oestrogenaemia on trabecular structure further reduces strength, as interconnecting supporting struts are lost and the main load bearing trabeculae become thinner and may buckle.

Figure 1.24: (a) relationship of trabecular density, number and thickness to strength (Seeman, 2008) and (b) Euler's theorem; on the right, half of the vertical structure is unsupported due to a disconnected horizontal strut and is 4 times weaker than left structure even though bone mass is the same in both (adapted from Rubin, 2005).

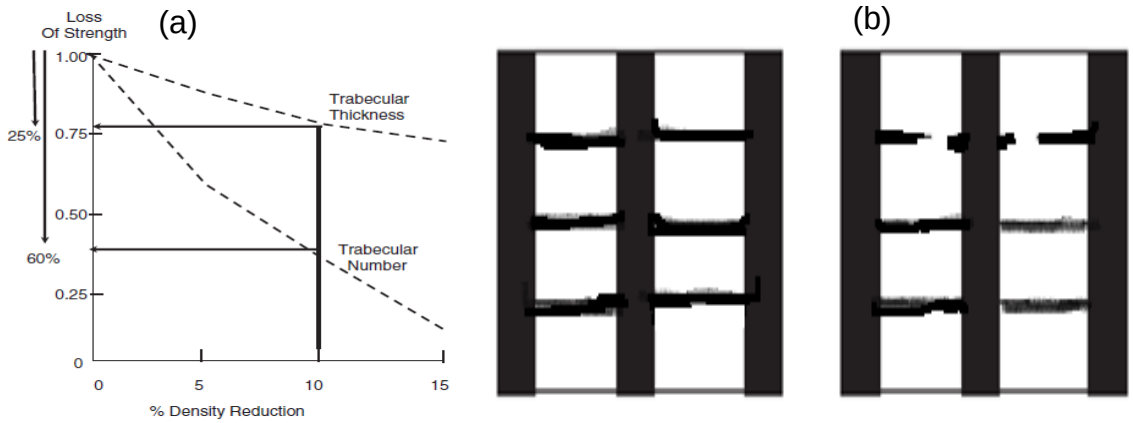

1.3.7: Trabecular microarchitecture and porosity

Gibson and Ashby (1997) have further examined the trabecular microarchitecture and consider trabecular bone as a 'cellular solid' with varying morphologies (Figure 1.25). They describe four predominant cellular structural arrangements of trabecular bone; lower density 'open equiaxed cells,' formed predominantly of rods or struts, cells of low or intermediate density with 'equiaxed' walls and higher density areas with either a 'prismatic cell' or 'parallel plate' like cell structure with solid closed walls.

Figure 1.25: Cellular solid structures found within human trabecular bone. (a) Low density open cell (b) equiaxed cell (c) high density prismatic cell and (d) parallel plate structures (adapted from Gibson & Ashby, 1997).

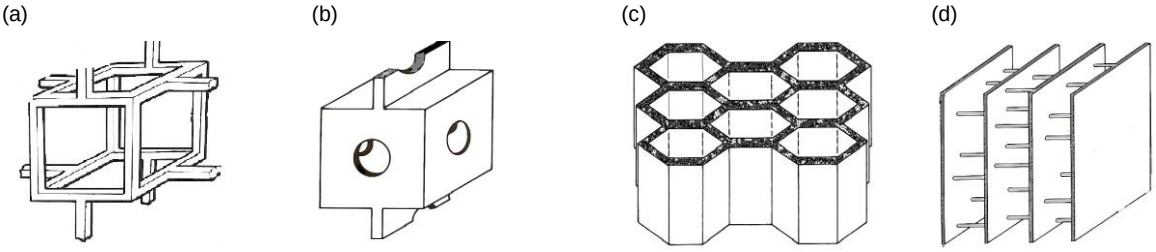

These structures impart different mechanical characteristics; theoretical predictions of the behaviour of these cellular solid structures suggest that higher density parallel plate and hexagonal structures fail by tissue-level yielding whereas in the low-density open celled structures bone failure occurs by excessive bending or buckling; albeit depending on the strength and density characteristics used in experimental studies (Gibson, 1985; Morgan *et al.*, 2003).

In order to quantify and compare effects of structural micro-architecture and spacing or porosity to mechanical strength in research, two often used indices are a structure modular index (SMI) for architecture and tissue volume fraction BV/TV for porosity. SMI values for trabecular bone made up of higher density plates are scored 0 and lower density more open cells score 3.

Porosity of trabecular structures can be defined as, the ratio of bone material volume over tissue volume or BV/TV (Zioupos *et al*., 2008). BV/TV features prominently in experimental studies of cancellous bone mechanics, but also indirectly, in theoretical studies as it relates linearly to the ratio of D_{app} / D_{mat}, or the normalised density of the structure (Gibson & Ashby, 1997).

Bevill *et al.* (2006) examined large-deformation failure mechanisms in trabecular bone from varying sites according to structure (SMI) and porosity (BV/TV). The changes in strength were highly correlated with both SMI and porosity indicating that this type of failure mechanism is dependent on microarchitectural organisation of material and its spacing, see Figure 1.26.

Figure 1.26: (a) change in mechanical strength of trabecular bone moving from plate like micro-architecture (SMI, 0) to rod like structure (SMI, 3) in large deformation failure; and (b) effect of change of a surrogate marker of porosity (BV/TV) on compressive strength (adapted from Bevill *et al.,* 2006).

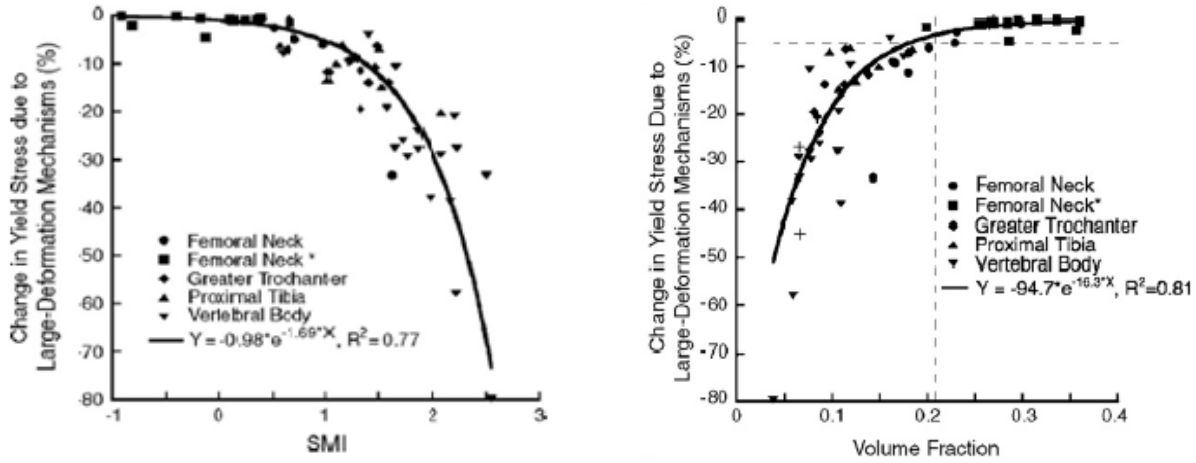

1.3.8: Cortical microarchitecture

In cortical bone the presence of resorbtion cavities and Haversian canals produce a porous bone structure, pore diameters vary and can be very small from 5 to 10 μm or large from 6 to 800 μm (Figure 1.27).

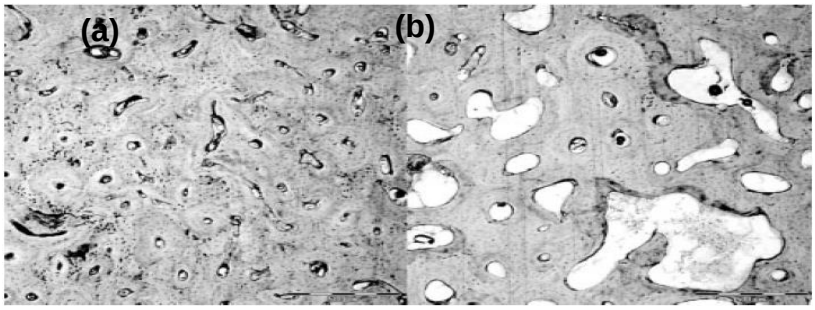

Figure 1.27: Cortical bone from the femoral shaft from an elderly woman (a) dense bone and (b) an example of more porous bone (adapted from Augat & Schorlemmer, 2006)

The greater number and size of pores the greater the intracortical porosity accounting for approximately 70% of elastic modulus and 55% of yield stress (Augat & Schorlemmer, 2006; Dong & Guo, 2004). In conjunction with increased porosity as might be expected there are also corresponding decreases in bone mineral density and fracture toughness possibly due to increased porosity reducing available bone for microcrack propagation (Wachter *et al*., 2002; Yeni *et al*., 1997). In mechanical tests there are strong correlations between intracortical porosity and cortical bone material properties, see Figure 1.28).

Figure 1.28: Porosity of cortical bone with increasing age and associated reduction in ultimate stress and toughness (adapted from Seeman, 2008). [Note in Graph B porosity expressed as a fraction and Graph C as a percentage]

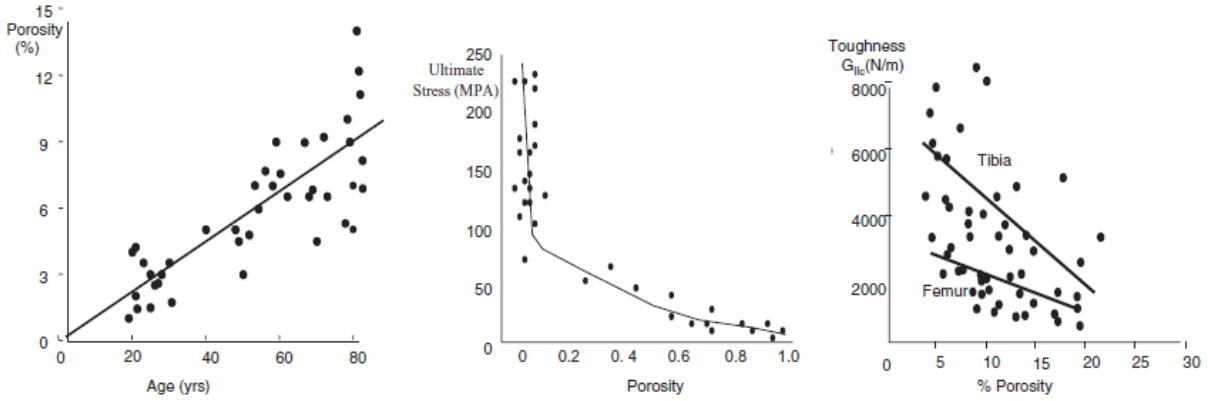

1.3.9: Material properties

Material properties of bone are determined by the absolute quantity of bone and the quality and spatial arrangement of its organic and inorganic parts. The mineral component resists compression and makes bone stiff, without enough mineral bone become more bendable or ductile but if mineralisation is too great, bone becomes more brittle (Currey, 2003a; Seeman, 2008). Resistance to tension or torsion is provided by the organic collagen matrix which makes bone more ductile imparting the ability to bend without breaking or toughness (Wang *et al*., 2002). Abnormal excessive mineralisation as in hyperpetrosis makes bone brittle, and the presence of

abnormal collagen due to genetic disorders such as osteogenesis imperfecta (OI) decreases toughness and ultimate strength. Thus intrinsic material properties have a major role in bone strength.

1.3.9a: Mineral content

Numerous studies have shown how the amount of mineral, measured directly as ash weight (g) or indirectly by X-ray absorptiometry methods DXA and QCT as bone mineral content (BMC, g) or expressed as an areal or volumetric bone mineral density (BMD, $g.cm^{-2}$ or $g.cm^{-3}$) is related to bone strength (Rubin, 2005; Turner, 2006).

The mineral phase imparts strength and stiffness to bone tissue, however with increasing mineralisation, bone becomes brittle and requires less energy to fail (Zioupos & Currey, 1998; Seeman, 2008). The relationship of BMC of bones from various animal species and bending strength are presented in Figure 1.29a; and changing stiffness and ultimate strain with changes in mineralisation in Figure 1.29b.

As well as the absolute quantity of mineral in terms of BMC or BMD, the mechanical properties in cortical and trabecular bone depend on the size and distribution of mineral crystals (Martin & Ishida, 1989). Mineralisation has been studied at an ultra-structural level, initially using back scattered electron microscopy and later infra-red spectroscopy, and results demonstrate non-uniform distribution of mineral within both cortical and trabecular bone (Boskey *et al*., 1999). In young bone, a composition of recently formed small crystals and mature large crystals can be detected. This mixture of small and large crystals may represent and optimal situation for good resistance to load.

In ageing bone, the average crystal size increases and bone becomes more brittle because of the greater number of large crystals. Thus deviation from an idealised mass and composition of a mixture of different sizes of crystal and distribution of mineral within a structure to a more homogenised type is associated with the deterioration of mechanical properties (Augat & Schorlemmer, 2006).

Figure 1.29: (a) increasing mineralisation and bending strength in animal long bones as a function of mineral composition (adapted from Currey, 2002); and, (b) changes in stiffness and ultimate strain of animal bone with differences in mineral volume fraction, as mineralisation increases, stiffness increases but ultimate strain decreases; and in young (1yr) vs. old (9yr) cattle, the older more mineralised bone has become stiffer and more brittle (adapted from Turner, 2006).

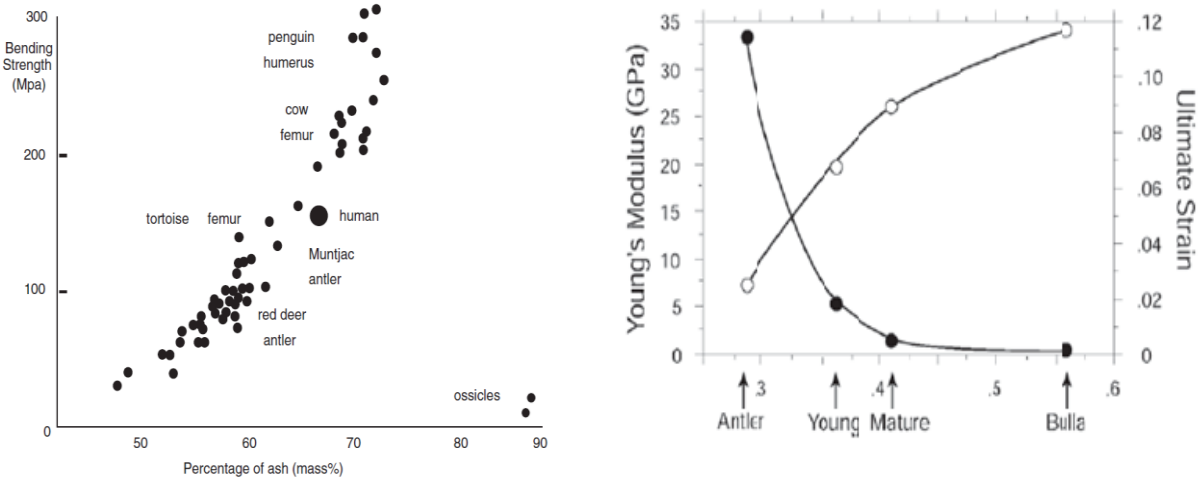

1.3.9b: Collagen

The quality of the main type I collagen fibres, the orientation of fibrils and decay in collagen structure with ageing all play a part in determining the strength of bone tissue. Collagen spacing and orientation determine the nucleation of bone mineral and propagate the mineralisation process parallel to the fibre. Collagen fibre orientation varies within lamellae according to predominant tensile forces within bone which are usually not unidirectional (Augat & Schorlemmer, 2006). If collagen proteins denature or composition is altered genetically, chemically by lathyric agents, or by heat, bone toughness is reduced (Zioupos *et al*., 1999; Boskey, 1999; Viguet-Carrin *et al*., 2006). Collagen quality can be affected by alteration in amino acid composition and interference with crosslinks in the triple helix structure. Clinical abnormalities in amino acid content of collagen have been studied in families of patients with osteogenesis imperfect (OI) and in animal models with genetic deletions expressing the OI bone phenotype (Boskey, 1999). In some forms of OI bone mineral density is not affected although mechanical properties are severely affected. The end overlap structure of collagen fibrils forms spaces for preliminary crystal deposition, in OI spaces are larger and as a consequence hydroxyapatite nucleations are larger than normal, a factor known to make bone more brittle (Boskey, 1999).

The absolute amount of collagen present in bone also partly determines bone strength; studies on the effect of ageing on collagen have shown that collagen concentration is related to ultimate fracture strain (Ding *et al*., 1996). However, given adequate amounts of collagen, fibril arrangement is also important; in woven bone although mineral composition is greater than lamellar bone, fibril organisation is haphazard and strength is almost certainly reduced (Currey, 2003b). The presence of optimally orientated fibrils in lamellar bone approximately doubles ultimate tensile strength and increases elastic modulus tenfold (Martin & Ishida, 1989). A recent animal study has shown that remodelling may optimise collagen fibril orientation; in beagles exposed to endurance exercise bone mechanical properties were maintained despite a significant fall in mineral content and no change in collagen density; these results suggested that strength was maintained due to a re-orientation of collagen fibres (Puustjarvi *et al*., 1999).

1.3.10 Microdamage

Microcracks (Figure 1.30) are short splits in cortical bone tissue approximately 30 to 100 μm in length with a 'linear' morphology which accumulate as a consequence of prolonged loading and result in bone fatigue (Augat & Schorlemmer 2006; Burr *et al*., 1990). Bone microdamage was first studied in detail by Frost in the 1960's (Taylor & Lee, 2003). Initial observations suggested that the presence of microcracks was related to the number of resorbtion cavities; and, subsequently led to research which linked microdamage and the remodelling process (Currey, 2003b). If microcracks are un-repaired and continue to propagate they can lead to fatigue failure in the form of a stress fracture (Burr *et al*., 1990). In ageing cortical bone accumulation of un-repaired microdamage reduces bone quality with reduction in stiffness and strength (Zioupos, 2001).

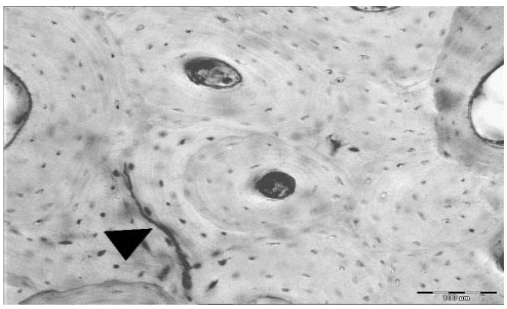

Figure 1.30: Microcrack (black arrow) in human cortical bone propagating partly along a cement line. Light microscopic image x100 magnification, Paragon staining (adapted from Augat & Schorlemmer, 2006).

1.3.11: Summary of factors affecting bone strength

In summary; bone strength is dependent on bone quantity and quality. Primarily strength is related to material density, size and shape in that greater mineralisation and growth builds a bigger more dense bone, and with small additional changes in periosteal deposition or endocortical resorbtion and changes in shape can profoundly affect geometric indices of bone strength through modelling or remodelling (Seeman, 2002; Turner & Burr, 2003; Turner, 2006). The use of increasingly sophisticated technology at a microscopic, nanoscopic and molecular level has allowed elucidation of ultra-structure and intrinsic material factors affecting bone quality in research but radiographic techniques with application to human populations are still lacking (Augat & Schorlemmer, 2006).

Therefore, the proportional contributions of various quantity and quality factors to mechanical strength are difficult to quantify exactly but estimates have been made from multiple regression analyses of data from mechanical tests on whole bone specimens (Augat *et al.,* 1996; Lochmuller *et al*., 2002); computational models of bone strength using qCT derived geometric data (Lang *et al.,* 1997b), and the closest predictions of bone mechanical properties have come from finite element modelling (FE) where BMD, geometric properties, local material properties and altered loading states can all be considered together (Keyak *et al.,* 2003).

A combination of bone quantity and quality factors thus offers the best prediction of bone strength. In the research setting using a rat model, vertebral BMD has been shown to predict 60% of the variance of maximal load, and incorporation of bone quality factors of elastic modulus and hardness improved the prediction to 70 and then 95%, respectively (Ammann, 2009).

In clinical studies on humans, measurement of areal BMD by DXA has been possible, reliable, and cost effective for many years; however, DXA does not predict all fractures, nor does DXA objectively chart increases in strength with drug therapies, and can only provide minimal information on bone quality. Measurement of bone quantity and bone quality together to predict bone strength is only now becoming possible with the advent of CT, pQCT and MRI. However, in a clinical setting MRI scanning for huge numbers of osteoporosis patients would be prohibitively expensive and CT scanning uses huge doses of radiation; a CT estimation of BMD requires a radiation dosage in excess 35 to 40 times a standard

chest X-ray. The next section gives a general overview of the assessment of bone quantity, specifically X-ray absorptiometry; the bone quantity evaluation method used in the research studies presented in later chapters in this thesis.

1.4: Measurement of bone quantity

Bone quantity is the amount of normally calcified bone present; it may be expressed in terms of bone mineral content (BMC) in gram but it is more usually expressed in terms of a density variable. True density being a volumetric term is the BMC per unit volume of bone ($g.cm^{-3}$), can be ascertained directly by measurement of ash weight and volume determinations of the specimen using Archimedes' principle. Volumetric density can now also be measured indirectly using μCT and expressed as a real or apparent density. The predominant method of clinical assessment of bone quantity is DXA scanning which expresses bone quantity as a two dimensional measure BMC per unit area ($g.cm^{-2}$) and is referred to as the area or areal density (aBMD).

Bone density is also defined at a tissue level or material level; the wet mineralised mass of bone at the tissue level over the volume occupied by the tissue defines the 'apparent' density value and the same mass of material over the volume occupied by the material itself defines the 'real' or 'material density' of bone (Zioupos *et al*., 2008). Apparent density D_{app} considers the myriad within bone that is; resorbtion cavities, canalicular systems, Volkman's and Haversian canals in cortical bone and marrow spaces of the trabecular network. Material density D_{mat} considers only the material itself. D_{app} primarily influences whole bone mechanical properties, while D_{mat} determines material behaviour firstly at the trabecular level and then the structural level (Rice *et al*., 1988). DXA can give an estimate of apparent density but only μCT has the resolution to determine real density.

In humans, individual areal BMD measurements at the common sites affected by osteoporosis in the human skeleton are compared to normative data for the same age, ethnicity and gender (arbitrarily termed a Z score) and to normative data representative at the age of peak bone mass in the normal population (arbitrarily termed a T score). If measured data are lower than predicted values (T scores and Z scores) from the human database an accurate diagnosis and grading of low BMD then in part determines future management. The WHO has set descriptive limits for

T score in order to classify patients risk, a T score between +1 and -1 (i.e. within ±1SD of the mean) is normal, between -1 and -2.5 defines osteopaenia, below -2.5 is osteoporosis, and below -2.5 in the presence of a fracture at a typical site as severe osteoporosis. The predictive capacity of this method has been assessed in numerous meta-analyses of fracture risk in relation to T score at the femoral neck, in the lumbar spine and the distal radius (Marshall *et al*., 1996). Overall sensitivity of DXA scanning in fracture prediction is too low to recommend usage for mass population screening and is best employed on a case finding basis in those at risk; and DXA data should only be used in conjunction with other risk factors in clinical decision making (Kanis, 2002).

It is well known that diet, ethnic origin, age, hormonal status and disease all effect human BMD data. In order to improve usefulness of DXA data therefore, several large databases of BMD data for the normal human population have been created allowing more accurate interpretation of data from potentially osteopaenic patients against the normal variation in various standard populations (Kanis, 2002). Large research databases of BMD data also exist for some primate animal models (Havill *et al*., 2003) and some population data exists for the ovine animal model (Turner *et al*., 1995). These animal databases although small have been invaluable in the study of BMD changes in cross sectional and longitudinal studies (Havill *et al*., 2003).

1.4.1: Radiogrammetry and single photon absorptiometry

Radiographic techniques include radiogrammetry, where measurements are made of the thickness of cortical bone at fixed skeletal sites, the mid-shaft of the 2nd metacarpal is the site most commonly used. However, this technique is limited by its low sensitivity and specificity, as it does not measure cancellous bone density or cortical porosity. Other techniques such as single photon absorptiometry (SPA) using a collimated beam from a radioactive Iodine source and scintillation detector, has been used on distal sites in long bones and is an accurate procedure provided positioning and soft tissue thickness are both well controlled (Kanis, 1994). However, both these previous methods were limited clinically due to time constraints and high radiation dosage; and both have now been superseded by low energy X-ray absorptiometry techniques.

1.4.2: X-ray absorptiometry

X-ray absorptiometry developed to measure bone quantity when it was discovered that lower energy X-ray beams could produce similar absorption patterns to SPA using radioisotopes such as Gadolinium and Iodine. Introduced in the late 1980's X-ray absorptiometry has now become the most widely used technique for assessing bone density in both research and clinical practice due to the technical advantages of low radiation dosage, production of high resolution images, good precision and stability of calibration.

Earlier absorptiometry scanners using single photon X-ray sources and pencil beams (SXA) have now been superseded by dual energy devices (DXA) utilising fan beams, which allow quicker scan times and new clinical applications (Genant *et al*., 1991). SXA and DXA photon beam attenuation is compared at 2 sites, the region of interest comprised of bone and soft tissue, and the adjacent non bone soft tissue (Figure 1.31).

Figure 1.31: Schematic diagram of a DXA scan of a long bone sample (adapted from Seeman, 2002). Beam attenuation depends on the following; (1) incident energy of the photons (2) path length to the detector array and (3) the material properties of the specimen. Since path length and incident energies are known, providing accurately repeatable positioning, the areal BMD measurement is dependent on material properties of the specimen within the region of interest.

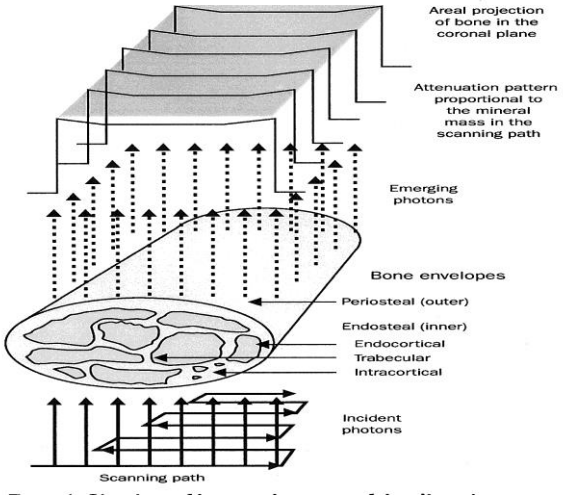

Both SXA and DXA precisely evaluate bone mass in terms of bone mineral content BMC (g), the total amount of bone mineral as hydroxyapatite within the measured region; and when BMC is divided by the projected area of the specimen, SXA and DXA can also derive data for bone areal density in gram of bone mineral per unit of bone area scanned ($g.cm^{-2}$).

The 2-dimensional areal BMD measure is not a true density which is a volumetric term (g.cm^{-3}) and because the relationship of area to volume is non-linear, bone size can affect the apparent density (Figure 1.32).

Figure 1.32: Areal and volumetric BMD (adapted from Khan *et al*., 2001). Bone mineral density measured by DXA is dependent on the size of the measured sample. Block B has twice the areal BMD of block A despite having the same true density.

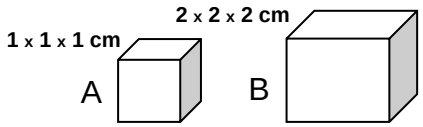

	A	B
Bone Material Density	**1 g.cm^{-3}**	**1 g.cm^{-3}**
Bone Mineral Content	**1 g**	**8 g**
Bone Area projection	**1 cm^{2}**	**4 cm^{2}**
areal Bone Density	**1 g.cm^{-2}**	**2 g.cm^{-2}**

Volumetric BMD can now be measured by computerised tomography (CT), other advantages include the ability to delineate trabecular architecture and it is not affected by bone artefacts like osteophytes. Peripheral quantitative computerised tomography (pQCT) can be used for *in-vivo* long bone studies in patients and smaller *ex-vivo* samples can be scanned using μCT. Unfortunately QCT is limited to peripheral long bone sites due to high radiation dosage and μCT for research on small bone biopsies, which limit usage in the clinical setting. A comparison of DXA data (areal BMD) and CT data (true density) with age, see Figure 1.33, illustrates that nature in general builds a bigger bone not a more dense bone. Note also that areal BMD (Figure 1.32a) peaks in and around the middle of the third decade, this is the peak bone mass data used to derive the 'T' score, and note a certain degree of scatter.

Figure 1.33: Bone density data at the femoral shaft in male and female volunteers from age of 5 to 25 year; (a) DXA derived area BMD in g.cm^{-2}; and, (b) CT derived volumetric BMD in g.cm^{-3} (adapted from Seeman, 2002).

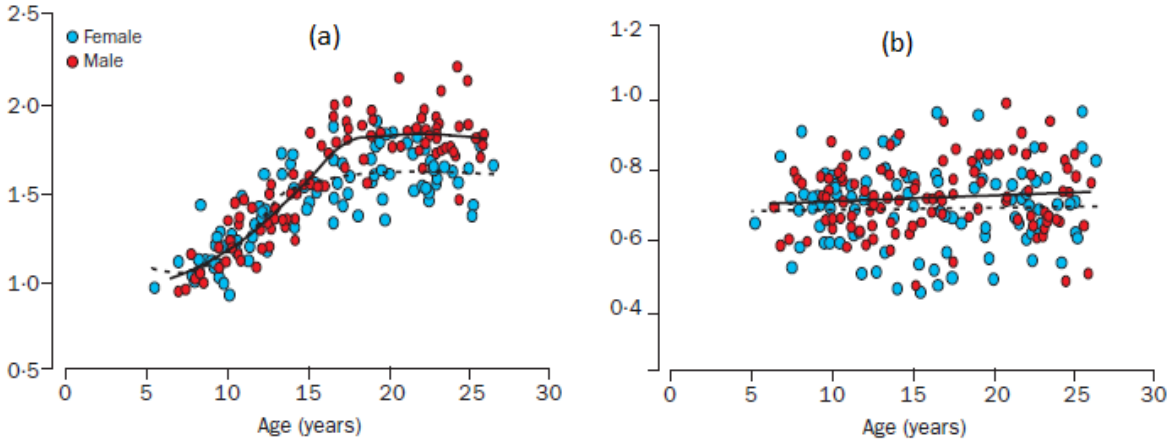

The scatter or distribution of data if represented at standard ages shows a normal Gaussian distribution, and the normal distribution of T scores moves to the left with age, the decline starting after the natural peak in BMD late in the 3rd decade (Kanis, 2002). DXA scanner algorithms allow individual patient data to be compared to a population reference database derived from the normal distributed range of BMD data at standard ages and for different racial groups.

Figure 1.34 presents the DXA scan result for a female athlete with amenorrhoea, an eating disorder and mild osteopaenia at the lumbar spine. Her mean BMD data for L1 to L4 vertebrae was 0.910 $g.cm^{-2}$ and the T score -1.25 which indicated mild osteopaenia, more worryingly the individual data for L4 vertebrae was lower 0.890 $g.cm^{-2}$ and the T score was -2.05 which would be termed clinically as severe osteopaenia. Note also that if her bone density data marked **+** on the reference database follows the normal change with ageing, she would attain the BMD defined osteoporosis criteria of a T score less than -2.5 by the age of 50 year. Fortunately, her rate of decline in BMD from previous scans was not of concern and hip scores were also entirely normal and when her all her risk factors were considered non-pharmacological measures were opted for in her treatment plan to improve her BMD.

Figure 1.34: A DXA scan result for a female athlete aged 25 year diagnosed with female athletic syndrome (eating disorder, amenorrhoea, and osteopaenia). The human lumbar spine reference database is shown on the left and BMD data, T and Z scores on the right.

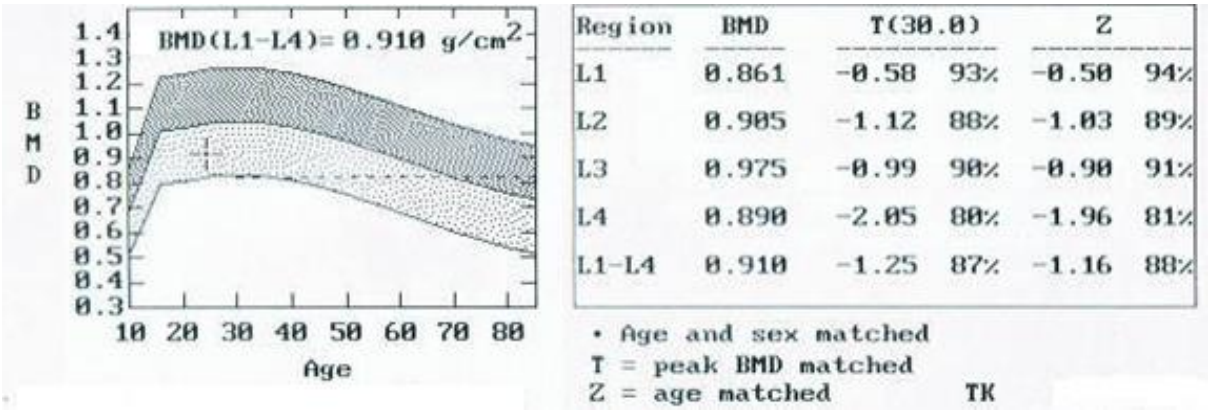

1.4.3: Limitations of DXA

The results of densitometry are a widely used endpoint in clinical practice and research and it is important to state its limitations. DXA can only provide a two dimensional view of a three dimensional property of bone, the last dimension to

quantify volume, depth, is not known. During growth, areal BMD increases, suggesting, incorrectly, that actual volumetric bone density has risen. Increases in BMD are predominantly the result of increase in size, and an overall increase in normally mineralised bone in the cortical shell, in other words volumetric BMD does not change but the bone gets bigger and aBMD has increased giving the false impression that true density has increased.

During ageing, bone resorbtion reduces the amount of bone within the cortical shell and the trabecular network gets thinner and less connected. Geometric adaptation to maintain strength with periosteal bone formation partly offsets bone weakening processes elsewhere; however, adaptations are different in men and women. Unfortunately older generation DXA scanners were insensitive to localised geometric and gender specific changes in both trabecular and cortical bone (Seeman, 2001). Inadequate operating procedures; of calibration, region selection, acquisition mode and positioning have also been cited as possible sources of error in diagnosis of osteoporosis using DXA (Kanis, 2002). In animal or human studies when undertaking DXA the following measurement error must be kept to a minimum, especially in cross sectional or longitudinal studies where only small changes may be apparent due to an intervention. This has limited the use of DXA to sites where positioning and alignment can be controlled for. Correct positioning on a repeatable basis requires a high quality operator performance assured by a prior reliability study (Kanis, 2002; Sievänen *et al*., 1996).

BMC and areal BMD measurements are also prone to misinterpretation in individuals of different size. Larger individuals have more bone mineral but because their bigger bone size and therefore bigger projected bone area, areal BMD is usually lower,. The effect of large and small *ex-vivo* samples from the same site can be controlled for with proper reference standards corrected for size. Further technical issues that have to be accounted for when making DXA measurements are detailed further in Chapter 2, a validation study of DXA methods in *ex-vivo* ovine bone samples, but the main problem with DXA areal BMD measurement is that it is not a true density.

1.4.4: Prediction of fracture risk from DXA data

Despite theoretical problems with areal rather than volumetric density and recent technical advances in CT and MRI, posterior anterior views of the lumbar spine and proximal femur remain the mainstay of clinical assessment due to their greater utility in clinical decision making (Blake & Fogelman, 1997; Kanis 2002). In the clinical setting, fortunately for the continued use of DXA, errors introduced by measuring areal density rather than volumetric density actually overestimate areal BMD measurement as a predictor of fracture, due to the fact that both the attenuation due to mineral in the path length and the area component gives some measure of bone size which is also a determinant of bone strength (Kanis, 2002; Genant & Compston, 2004). The positive predictive ability of DXA in terms of fracture as an outcome is approximately 45 to 50% and fracture risk has been shown to approximately double with every standard deviation below the mean T score (Kanis, 2002).

In a research setting, the amount and distribution of bone mass is also related to material properties of bone stiffness and strength. Power relationships have been proposed for trabecular bone material properties with bone stiffness and strength purportedly related to the cube and to the square of material density respectively (Carter & Hayes, 1977). In some *in vitro* studies BMD has been estimated to explain up to 90% of the breaking strength of excised bone (Martin, 1991).

Technological improvements in DXA scanners have recently allowed estimation, albeit in one plane, of cross sectional moments of inertia and elastic modulus from BMC and bone widths. Computer models have been developed to estimate geometry of the hip from digital DXA data which are then used in hip structural analysis (HSA) to predict failure better than BMD alone in excised femora (Beck *et al*., 1990).

Seivänen *et al*. (1996) reported that computational estimates of apparent density (BMAD), cortical wall thickness (CWT) and various dimensional variables derived from DXA scans could be used to estimate stiffness and strength indices of typical long bones. The derivation of geometrical indices from areal BMD data have been criticised as it is not possible to ascertain the contribution of geometry independent of a bone mineral measure and due to the fact that newer imaging modalities can now measure geometry far more accurately.

1.5: Osteoporosis

The WHO (1994) defined osteoporosis as a systemic skeletal disease characterised by low bone mass and micro-architectural deterioration of bone tissue, with a consequent increase in bone fragility and susceptibility to fracture. Osteoporosis can also be defined clinically in terms of bone quantity measurement as an aBMD of greater than 2.5 standard deviations below the mean data for peak bone mass in young adults (arbitrarily termed a 'T' score). A fragility fracture at any typical site also defines osteoporosis even in the absence of low BMD, although severe osteoporosis is defined as the above plus an osteoporotic related fracture (Kanis, 2002). DXA and osteoporosis terminology is presented in Appendix 1.

1.5.1: Pathogenesis

The causes of osteoporosis are multi-factorial and include genetic and environmental factors; hormonal, nutritional and ageing effects on material properties, the effects of metabolic, bone and systemic diseases; and various drug regimens. Long term failure of bone remodelling and repair processes leads to degradation of bone material properties, and eventually fragile bone of limited strength and stiffness that will fracture even under normal environmental loading conditions. Genetic and environmental factors are responsible for the development of smaller bones, with fewer thinner trabeculae, and thinner cortices and low peak bone mass. Maintenance of bone material properties by remodelling, and focal replacement of older damaged bone becomes mismatched with advancing age.

The result is a net loss of bone mass, thinner less connected trabeculae, and increased porosity in thinner cortical bone. The effect of oestrogen withdrawal at the menopause in the female gender and hypogonadism in 20 to 30% of the male gender accelerates this process in later life. Hyperparathyroidism secondary to calcium malabsorption at any age in either gender can lead to decreased mineralization (Seeman, 2002). Fragility fractures typically occur at the distal radius, the vertebral bodies, and the neck of the femur; areas of the skeleton with a high proportion of trabeculae bone, with high surface area for resorbtion and higher metabolic activity of osteoclasts.

1.5.2 Clinical complications

The clinical complications of the disease depend on the site of the fracture although vertebral and hip fractures result in an excess mortality. In the vertebral column; pain, disability and spinal deformity are the main secondary problems. The most serious complications arise with hip fracture; up to 50% of patients will suffer permanent disability, and between 10 to 20% will die within 3 months to a year (Cummings & Melton, 2002). The usual causes of death after an osteoporotic fracture are due to associated prolonged immobility, especially in the elderly with coincident chronic illnesses and morbidity in other major organ systems; most notably bronchopneumonia, stroke, pulmonary embolism and myocardial infarction (Cummings & Melton, 2002).

Fragility fractures are dependent on both bone quantity and bone quality. DXA assesses areal BMD and still remains the gold standard of clinical diagnosis of osteoporosis (Kanis, 2002). However, DXA data cannot fully explain all fragility fractures, and DXA derived aBMD does not correlate with significant reduction in fracture risk following treatment with anti-resorptive drugs. It is increasingly clear from bone ultra-structure and bone biology that bone quality is also a major determinant of bone fragility, albeit at present with few clinical applications for prediction of fractures.

Figure 1.35: Scanning electron micrographs from the human femur showing (a) normal and (b) osteoporotic trabeculae; and, (c) osteoporotic cortical bone. In (b) note less numerous, thinner and thicker trabeculae, loss of connectivity and increased porosity. In (c) Haversian systems are more heterogeneous and grey areas indicate patchy mineralization (adapted from Rizzoli, 2004).

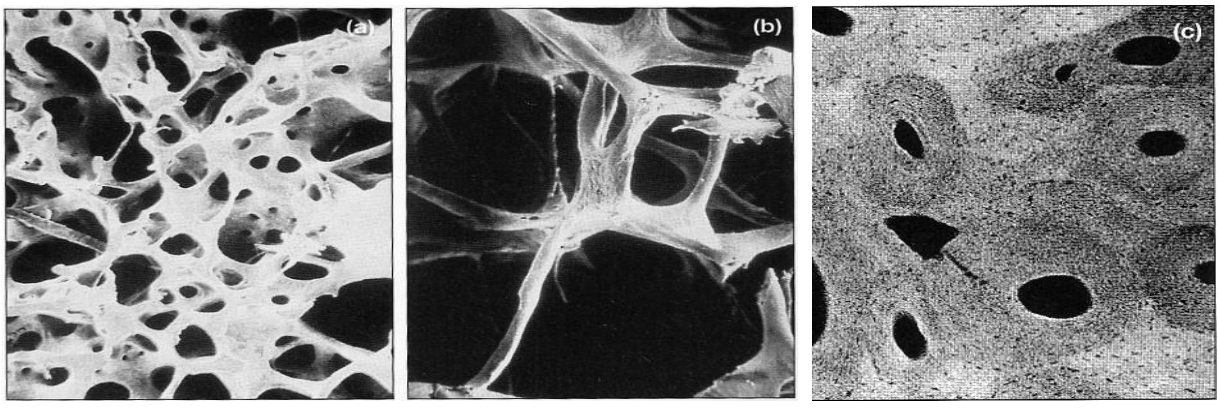

1.6: Animal models of osteoporosis

In 1994, the United States Federal Drug Administration guidelines recognised that animal models provide invaluable information on bone quality and structure not obtainable from clinical trials, and also that no one animal model can truly mimic osteoporosis. They also stated that studies of potential therapeutic agents should be conducted in both small and large animal models prior to human clinical trials (Thompson *et al*., 1995). Suitable animal models of osteoporosis are necessary prerequisites for research studies into bone structure, mechanics, growth, remodelling and repair, and various therapeutic interventions in osteoporosis (Bonjour *et al*., 1999).

1.6.1: Rodent models

The ovariectomised (OVX) rat model is probably the most extensively studied small animal model of osteopaenia (Miller *et al*., 1995). The rat shows transient increases in endochondral growth, periosteal apposition and cancellous bone re-absorption in many of its long bones, however, changes are often offset by increase in body mass and bone size (Miller *et al*., 1995). However, the smaller bones of rats may not be amenable to all bone quantity assessments at all sites, a study by Sato (1995) on an OVX rat model reported *in-vivo* DXA analysis more suited to the axial skeleton and QCT to the appendicular bones.

1.6.2: Non-human primates

Non-human primates, old world monkeys and baboons have also been extensively studied. Jerome *et al*. (1995) developed a model of osteopaenia in cynomologus monkeys and Havill *et al*. (2003) developed BMD reference standards in Baboons. The benefit of non-human primates are similar monthly menstrual cycles, similar hormone patterns to women; and following ovariectomy the development of low spinal mass due to higher bone turnover rates, again similar to humans. However, the advantages of non-human primate models in terms of physiological similarities are outweighed by the many disadvantages which include; trapping of animals from the wild population can introduce disease, skeletal maturity is not reached until 9 years of age, primates are difficult to handle and veterinary legislation requires specific housing requirements making them expensive to rear (Newman *et al*., 1995).

1.6.3: Ovine model

Sheep are ungulate ruminant quadrupeds with all four limbs adapted for support and movement. The proximal limb long bones are shorter than their human homologues and the lower long bones radius and tibia relatively longer in proportion. The other noticeable difference is the elevated ankle joint, elongated carpus and tarsus (cannon bone) and ground contact through the phalanges. A more detailed account is given below and the sheep skeleton is shown in Figure 1.36.

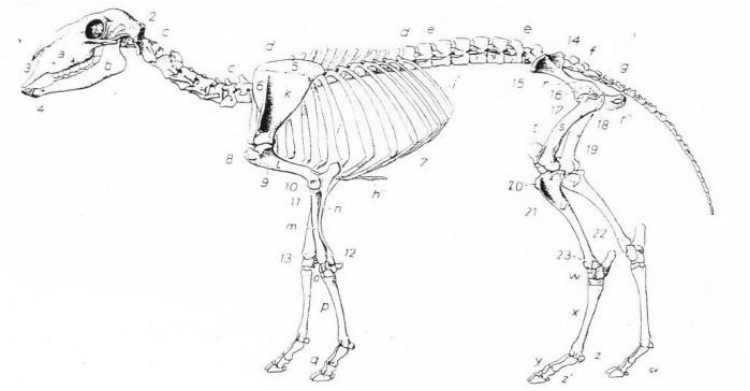

Figure 1.36: The ovine skeleton. In the axial skeleton; skull *a*, mandible *b*, cervical spine *c*, thoracic spine *d*, lumbar spine *e*. In the forelimb, long bones include; humerus *l*, radius *m*, and cannon bone *p*; and hind limb, femur *s*, tibia *u*, and cannon bone *x*.

The sheep skeleton has an approximately 205 to 206 bones depending on breed and individual variability in the number of vertebrae of the spine. A significant difference between the sheep and human is the lack of a collar bone, with the sheep forelimb attached to the axial skeleton by muscles, tendons and ligaments that attach from the scapula to the trunk. Sheep leg bones are proportionately different from the human, the sheep knee is equivalent to the human carpus and the hock is equivalent to the human ankle joint and calcaneus. Lower leg bones of sheep are homologues of the human hand or foot. The fetlock is comprised of the proximal sesamoid bones between the cannon bone, a single large metacarpal or metatarsal, and the proximal phalanges. Sheep also have no muscles in the legs below the knees and hocks, only skin, hair, bone, tendon ligamentous and cartilage and other specialised tissues, equivalent to the human nail making up the hooves.

Ovine bone has anatomical similarities in terms of shape, size and bone mineral content (BMC), however, bone ultra-structure is different, ovine bone is plexiform in structure undergoing a variable amount of Haversian remodelling in later life. Plexiform bone has a sandwich structure of woven and lamellae bone, is anisotropic and is the predominant form of bone found in grazing animals (Currey, 1984). In

some breeds of sheep similar physiological properties to human bone have been noted in terms of effects of hormonal control, response to ovariectomy and response to exogenously administered drugs known to affect bone turnover (Turner A, 2002). The majority of studies using an ovine model of osteoporosis have demonstrated decreased BMD after artificially induced menopause with ovariectomy (Newman *et al*., 1995). Research advantages of an ovine model are; that as flock animals large numbers can be kept together, they are docile, compliant and easy to handle, their disadvantages include lack of a natural menopause, different oestrus cycles, and the plexiform rather than Haversian bone structure (Newman *et al*., 1995).

1.7: Research aims

1.7.1 'Bone for Life'

The research in this thesis was part of wider research project entitled 'Bone for Life' involving collaborative bioscience research groups from the Trinity Centre for Bioengineering (TCBE), the Royal College of Surgeons in Ireland (RCSI), and University College Dublin. The 'Bone for Life' research theme was developed in response to epidemic proportions of skeletal disease in all ages worldwide. The economic cost of osteoporosis in terms of morbidity and mortality is enormous, and is projected to double by the year 2050. In the European Union alone in 2000 there were an estimated 3.79 million osteoporotic fractures with an estimated treatment cost of €32 billion (Reginster & Burlet, 2006).

The wider aim of the overall research project was to establish the contribution of factors effecting bone quality; micro-architecture, material properties, micro-damage and remodelling, to bone strength. In order to investigate this research question, a large animal model of postmenopausal osteoporosis was created using ovariectomised sheep.

At project start up the following broad projects were defined; development of an experimental ovine model of osteoporosis, subsequent harvesting of bone at 12 and 31 month post-ovariectomy; further follow on projects involved; µCT/FE modelling of trabecular bone strength, immunohistochemistry and TUNEL staining, nano-indentation, with associated mechanical testing for whole bone response and theoretical modelling.

1.7.2 DXA studies

The DXA work reported in this thesis was part of two elements within the broad framework of the 'Bone for Life' project described above. Firstly, in the experimental ovine project *ex-vivo* whole bone samples from 5 skeletal sites underwent data acquisition scans for later analysis of the effects of ovariectomy on the experimental flock; and, secondly to compare DXA derived areal BMD and geometric data to whole bone mechanical test data in order to ascertain the contribution of bone quantity and geometry to bone strength. The measurement of bone quantity in research is possible using a variety of techniques but DXA areal BMD measurement, even with its many practical and theoretical limitations remains the only useful bone strength surrogate in clinical practice today.

The thesis presents a series of studies conducted on *ex-vivo* ovine bone samples using DXA; preliminary studies investigated the validity and measurement limits of a DXA protocols and the natural variability in DXA derived bone quantity data. Follow-on studies then examined changes in DXA derived bone quantity post-ovariectomy in bone harvested from animals in the experimental flock sacrificed at 12 and 31 month post-ovariectomy; and, then finally concluding studies assessed the contribution of DXA derived bone quantity and structural analysis to bone strength. A schematic outline of the studies in this thesis is given in Figure 1.37 with rationale and aims of each study in subsequent sub-sections.

Figure 1.37: Outline of DXA research studies in the 'Bone for Life' project

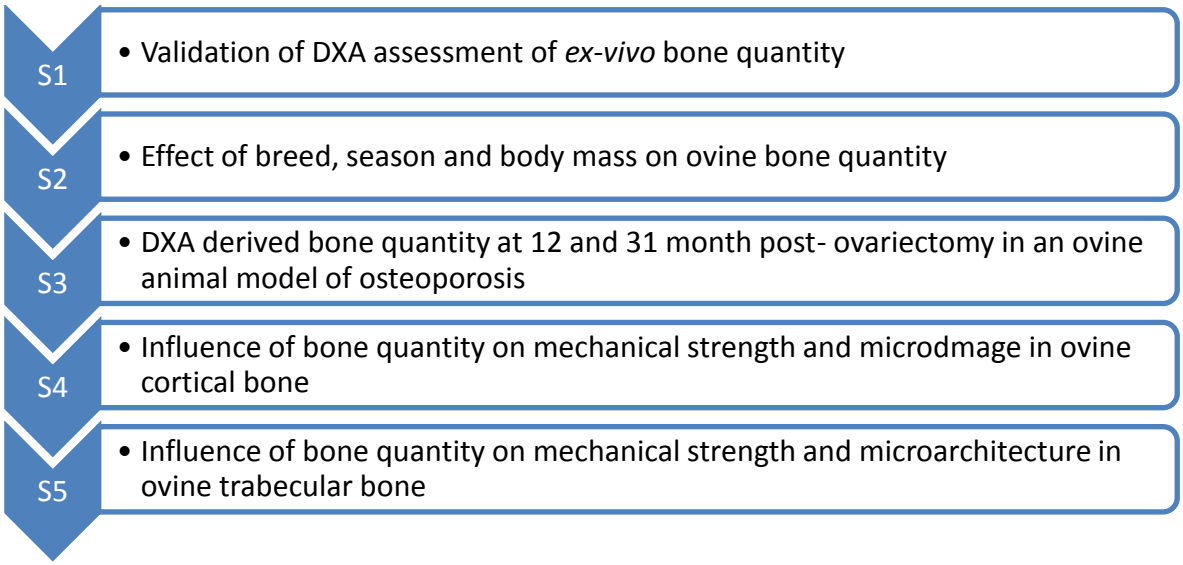

1.7.3 Study 1:

Validation of DXA methods for large ovine bone samples

There are innumerable studies in the literature employing DXA to measure BMC but few validation studies and no study to date has defined all aspects of validation for bone quantification by DXA in an ovine model. The aim of this study, expanding on the work of previous researchers, was to assess the validity of a standardised DXA protocol for measurement of bone quantity in *ex-vivo* ovine bone samples by showing that data was repeatable, reliable and accurate. In so doing the study would also define scanner measurement limits for later interventional studies. Standardisation procedures for human scanning are discussed briefly in Section 1.4 and in more detail in the introduction of Chapter 2.

1.7.4 Study 2:

Effect of breed, season and body mass on ovine bone quantity

Human DXA scanning procedures allow comparison to large reference databases, enabling comparison of data to the general population, standardised for age, body mass and racial group, and at two predominant skeletal sites. The aim of this study was to examine variation of BMD in the normal Irish sheep population in relation to body mass, breed of the animals and seasonal variation in a further validation of the ovine model. The study also aimed to profile BMD down the length of a spinal and four long bone sites and examine BMD in areas in the ovine skeleton with high trabecular bone content reflective of areas in the human skeleton associated with the clinical condition osteoporosis.

1.7.5 Study 3:

Short and long term effect of ovariectomy on ovine bone quantity

This study was part of the ‘Bone for Life’ project, a multidisciplinary project involving evaluation of factors affecting bone strength by examination of qualitative and quantitative changes in bone from an ovariectomised ovine model of osteoporosis. The aim of the DXA arm of this study was to determine bone quantity at 12 and 31 month post-ovariectomy (OVX) at five skeletal sites and three levels of analysis;

whole bone, according to sub-region within individual lumbar vertebrae and along the length of long bones, and also in smaller regions of high trabecular bone content such as the proximal femur, humerus, and distal radius sites typically associated fragility fractures in human populations.

1.7.6 Study 4:

Influence of aBMD on strength and microdamage in ovine cortical bone

The aim of this study was to compare the results of sub-regional DXA BMD data to the results of whole bone mechanical testing and microdamage analysis of radial mid-shaft cortical bone, in normal, low and high density ovine bone from both OVX and control groups. The mechanical testing, three point bending tests on the mid-shaft of the radius and microdamage analysis was performed by co-researchers in the ‘Bone for Life’ project.

1.7.7 Study 5:

Influence of aBMD and microarchitecture on strength in ovine trabecular bone

The aim of this study was to compare the results of sub-regional DXA BMD data to the results of whole bone mechanical testing and microarchitecture analysis of trabecular bone cores from the proximal ovine femur, in normal, low and high density ovine bone from both OVX and control groups. The mechanical testing, compression tests to failure and microarchitectural analysis was performed by co-researchers in the ‘Bone for Life’ project.

CHAPTER 2

Validation of DXA methodology for large ovine bone samples

2.0: Summary / Abstract

Dual energy X-ray absorptiometry (DXA) scanners are now frequently used in bone research to investigate bone quantity in *ex-vivo* bone samples from both animal and human sources; however, despite vigorous evaluation of validity and measurement limits for human *in-vivo* scanning there are only a few systematically conducted studies evaluating the validity of DXA methods for *ex-vivo* animal bones. A test re-test study design was used to assess operator dependent DXA methods measuring bone density variables at 2 spinal and 4 long bone sites in the ovine skeleton. Repeat sample acquisition scans (S1 and S2) and sub-regional analyses were performed to create three discrete levels of measurement, whole bone (WB), sub-regional (SRA) and region of interest (ROI). Statistical analysis of repeat scan data at each level was assessed for repeatability using interclass correlation coefficient (ICC), systematic bias and scedasticity was assessed using Bland Altman plots. Measurement limits or reliability was expressed both as an absolute value; 95% limits of agreement (LOA) and as a relative value; % technical error of measurement (TEM). In final validation procedures accuracy was determined by comparison of BMC to ash weight. aBMD repeatability (ICC) was >0.98 for WB and SRA, and was >0.90 for ROI at most sites. No significant systematic bias was detected and the relationship between difference and mean data was homoscedastic. Measurement limits for aBMD expressed as 95%LOA and %TEM in parentheses; for WB were; ± 0.02g.cm^{-2} (1%), SRA ±0.03g.cm^{-2} (1 to 2%) and for ROI ±0.05 g.cm^{-2} (2 to 3%). In BMC vs. ash weight comparison ICC and %TEM for pooled WB data were 0.99 (1 to 3%) and for pooled SRA data 0.95 (6 to 9%). The results confirm the repeatability, reliability and accuracy of the methodology used for bone quantity assessment of large *ex-vivo* whole bone samples, and has allowed us to define scanner measurement limits of the DXA methodology for later use in development of an ovine model of osteoporosis.

Key words: Ovine Model, Bone Density, DXA, Reliability, Measurement Error.

2.1: Introduction

Modern scientific techniques, as well as making things measurable, must also evaluate the nature of any error within the measurement process. Reliability implies precision or consistency of measurement but for validity, an assessment of accuracy is also required. Despite widespread usage of DXA to determine bone quantity in the ovine animal model there are only a few DXA validity studies, and these studies are restricted by sample size, in addition, reliability data only exist for a narrow range of body mass across the ovine population, and only a few studies have determined accuracy by comparison to ash weight (Turner *et al*., 1995a; Kaymakci & Wark, 1994; Pouilles *et al*., 2000). In addition, DXA assessments of *ex-vivo* ovine samples are confined to a few skeletal sites; usually the proximal femur, distal radius and lumbar spine (Turner *et al*., 1995a). Sites selected for research in the ovine skeleton are typically those sites associated with human osteoporosis, or sites which are easy to reposition accurately in longitudinal studies (Turner *et al*., 1995b).

DXA methodology used in human scanning have been adapted to investigate bone quantity both in small and large animal models of osteoporosis (Newman *et al*., 1995; Thompson *et al*., 1995; Miller *et al*., 1995; Turner *et al*., 1995; Hornby *et al*., 1995; Havill *et al*., 2003). However, bone researchers should be aware of the limitations of DXA, especially machine/operator based scanning error and that DXA methodology for assessment of bone quantity in *ex-vivo* animal and human bone is not fully validated. Measurement error in human DXA occurs due to inadequate calibration procedures, inappropriate acquisition mode and region selection (Kanis *et al*., 1997). The magnitude of any DXA error is critical in longitudinal intervention studies where changes in bone quantity may be very small, similar to natural variation or within the measurement limits of the DXA device (Miller *et al*., 1995; Turner *et al*., 1995b; Hornby *et al*., 1995).

Errors also occur when multiple repeat measures are made without accurate repositioning; alignment procedures have to be repeatable as small changes in orientation affect area projection and consequently areal BMD data. In human studies, repeatable positioning requires high quality operator performance assured by a prior reliability study (Kanis *et al*., 1997; Kanis 2002). In studies on live animals this problem has limited the use of DXA to sites where positioning and alignment can be controlled in a similar manner to human scanning (Turner *et al*., 1995a). DXA

scanner manufacturer algorithms assume homogeneity of all non-bone soft tissues and that lean and fat tissue mass ratios are the same in the two regions scanned, namely bone and non-bone; this assumption may not always be true and differential absorption of photons by surrounding non bone tissue may thus give rise to measurement error (Bolotin, 2007). Artefactual errors in human DXA scanning also occur due to interference of X-ray photons by metal objects, abnormal bone such as osteophytes, and calcification in blood vessels and lymph nodes (Kanis *et al*., 1997; Kanis, 2002). This potential problem for *in-vivo* human and animal studies can be easily controlled for with *ex- vivo* samples by sample selection, soft tissue dissection and by scanning bone in a uniform fluid medium (Grier & Turner, 1996).

Numerous researchers have adapted human DXA methods to facilitate scanning of anaesthetised animals and *ex-vivo* bone samples scanned in a fluid media simulating non-bone soft tissue (Miller *et al*., 1995; Turner *et al*., 1995a; Turner *et al*., 1995b). Kaymakci and Wark (1994) evaluated optimal scanning conditions for *ex-vivo* ovine samples at two skeletal sites, namely, lumbar spine and proximal femur. Lumbar and hip scan algorithms were used for large bone samples and ultra-high resolution scanning algorithms were used for smaller bone samples, optimum depth of fluid immersion was 5 cm, precision improved with usage of holding devices, and DXA accuracy was confirmed in small rib samples. Turner *et al*. (1995) examined pencil beam DXA measurement ovine bone samples both *in-vivo* and *ex-vivo*. Repeatable measurements were only possible *in-vivo* at lumbar spine and proximal long bone sites, at other sites adequate repeatability was only possible with *ex-vivo* material (Turner *et al*., 1995a, 1995b).

Unfortunately, in the latter and numerous other DXA studies repeatability was inferred from simple Pearson product moment correlation analysis. Repeatability should be quantified using interclass correlation coefficients (ICC). Perfect repeatability occurs when data lie along the line of equality on a scatter plot, not the same as perfect correlation which occurs if data lies along any straight line. Correlation analysis is an inappropriate statistical method to analyse repeated data sets and was avoided in this study (Bland & Altman, 1986). Measurement reliability is defined as consistency of measurement and absence of measurement errors, or minimum acceptable error for the effective practical use of a measurement technique (Atkinson & Neville, 1998). In most, if not all previous DXA reliability studies in

animal models, few authors describe systematic bias and the true measurement error of their measurement techniques. Most report reliability as coefficient of variation (CV%); that is the standard deviation divided by the mean assessed from a series of repeated measurements, see Equation 2.1. The use of CV% is convenient but maybe statistically inappropriate without prior examination of repeat data scedasticity. Gluer *et al*. (1995) recommended that all authors report their measurement error as an absolute value and in relative terms as a percentage.

Usage of CV% should be confined to DXA scanner calibration data where CV% is used to describe long and short-term measurement stability assessed using standard reference samples; or to define measurement error proportional to the magnitude of the measured variable.

When the measurement error is unrelated to the magnitude of the measured variable, the statistical variable 'technical error of measurement' (TEM) or its synonym 'standard error of measurement' (SEM), see Equation 2.4 (Dahlberg, 1940; Gore, 2005) is more appropriate. TEM is widely used in human anthropometry and is gaining acceptance in other biological sciences (Harris & Smith, 2009). In agreement with Gluer *et al*. (2005), most authors recommend that the measurement error in any process is stated in absolute terms as TEM and in relative terms as %TEM; calculated by dividing TEM by the combined mean of the repeat measurement data set (Gore, 2005; Goto & Mascie-Taylor, 2007; Harris & Smith, 2009). Bland and Altman (1998) suggested using limits of agreement (LOA) to describe homoscedastic measurement error. LOA is the mean difference in measurement with 95% confidence intervals (Mean ±1.96 standard deviation of difference data) and also yields an indication of systematic bias, see Equation 2.4.

In most studies, DXA remains the preferred method for rapid assessment of bone quantity in large *ex-vivo* bone samples. However, reliability and measurement limits in data analysis of whole bone and sub-regional analysis of *ex-vivo* bone at more than two skeletal sites and across the range of bone size seen in normal populations have yet to be evaluated and stated using appropriate statistical methodology. The aim of this study was to systematically evaluate a DXA methodology for large ovine bone samples that would be potentially applicable to bone quantity assessment in large *ex-vivo* whole bone samples from any species.

2.2: Methods

2.2.1: Sample selection and preparation

Whole bone samples were collected from 77 healthy skeletally mature sheep (>4yr), mean (±SD) body mass 69.9 ± 18.3kg. The lowest 6 vertebrae in thoracic (TS) and lumbar spine (LS) were selected; incisions were made in connective tissue elements, inter-vertebral discs and ligaments to straighten natural curvatures to facilitate later alignment procedures. The selected long bones; femur (FMR), tibia (TBR), humerus (HMR) and radius (RDR), were disarticulated and all soft tissues were removed by dissection.

2.2.2: Alignment procedures

A 60cm long, 40cm wide by 20cm tall clear Perspex tank (Figure 2.1) was filled with 0.9% saline to simulate non-bone soft tissue, to a complete depth of 10cm. Radiolucent screws made of PTFE threaded rod fixed centrally on two movable inner partitions were used to fix bone samples in position. The securing screws were 5cm from the base, the optimum depth for bone sample fluid immersion recommended in a previous study (Kaymakci & Wark, 1995). Holding screws were adjusted to lock the sample in place before alignment in three planes; screws were positioned at either end of the spinal canal in spinal samples and at either end of the long bone sample as close as possible to the central axis. Rotational positioning was then made using a small spirit level placed transversely across anatomical landmarks on long bones; and in spinal samples transverse and spinous processes were visually aligned using horizontal and vertical positioning lines on the end walls of the scanning tank. Longitudinal centre alignment was then made by placing the detector array laser guide along the centre line of the sample; this ensured that the central incident fan beam was directed through the middle of all scanned bone samples. Horizontal positioning was made by visual alignment of upper straight edges to horizontal lines on the front and rear walls of the scanning tank. A schematic showing alignment procedure for a long bone sample is depicted in Figure 2.1.

2.2.3: Scanner stability and short-term precision

DXA scanner quality control (QC) procedures for long term stability of measurement were undertaken as part of daily start-up procedures using a standard lumbar spine

phantom in accordance with the manufacturer's guidelines. Short term precision was evaluated by repeat scans (x40) of block phantoms (#085, Hologic, Waltham, MA, USA) of low (0.605g.cm^{-2}), medium (0.993g.cm^{-2}) and high (1.568g.cm^{-2}) standard densities, and an ovine femur. Measurement stability and short term precision were expressed as CV%, see Equation 2.1.

Equation 2.1: CV% = SD ÷ M	*Where M = mean of all measured data and SD = standard deviation*

2.2.4: Data acquisition scan (WB)

The Perspex tank was placed on the platform of a fan beam DXA scanner (QDR 4500 Elite, Hologic, MA, USA). No alterations were made to manufacturer scan speed or width settings to accommodate *ex-vivo* bone samples. Initial sample acquisition scan (WB) consisted of the entire length of the long bone or 6 vertebrae spinal samples. Scan length limits were re-set according to the length of the sample, and varied from 16 to 18 cm for the humerus, to 23 to 24 cm for the tibia and spinal samples. The human lumbar spine protocol was used for all whole bone (WB) sample acquisition scans.

Following alignment, the acquisition scan took approximately 1 minute over the pre-set area of interest (S1). The 'Analysis' mode was then selected for the bone sample pixel image, and minor adjustment to image intensity was made to allow clear visualisation of the bone edges. Beam attenuation within the area of interest was then analysed and estimated area (EA in cm^2), bone mineral content (BMC in g) and (areal BMD in g.cm^{-2}) data for the sample were generated. Bone samples were removed, replaced in the tank after a 180° change in orientation, realigned and then rescanned (S2).

The initial scan (S1) and re-scan (S2) data generated difference data or measurement error which were statistically analysed for repeatability, scedasticity and reliability. In a pilot study EA data were usually within 1.0 cm^2 of each other, differences in EA > 1 cm^2 usually indicated that the bone had moved on the holding jig and WB samples in these cases were repositioned and re-scanned.

Figure 2.1: Alignment protocol schematic for *ex-vivo* ovine long bone samples in a perspex tank (20 x 40 x 60cm), with screws mounted on vertically and horizontally adjustable inner walls within grooved tank side walls (not shown).

Fixation: the bone was first fixed into the alignment jig with perspex pins, as close to the central longitudinal axis of the shaft at 5 cm from the base of the tank.

Rotational alignment was by positioning easily identifiable land-marks on the upper (anterior) surface of the bone in line with the horizontal plane with use of a level

Horizontal: centre alignment was then made by placing a centre line along the length of bony shaft with the red laser guide of the detector array

Vertical: final alignment was made of the height of the inner walls such that bone ends and shaft were visually within the centre of 2 horizontal guide lines on the front of the scanning tank

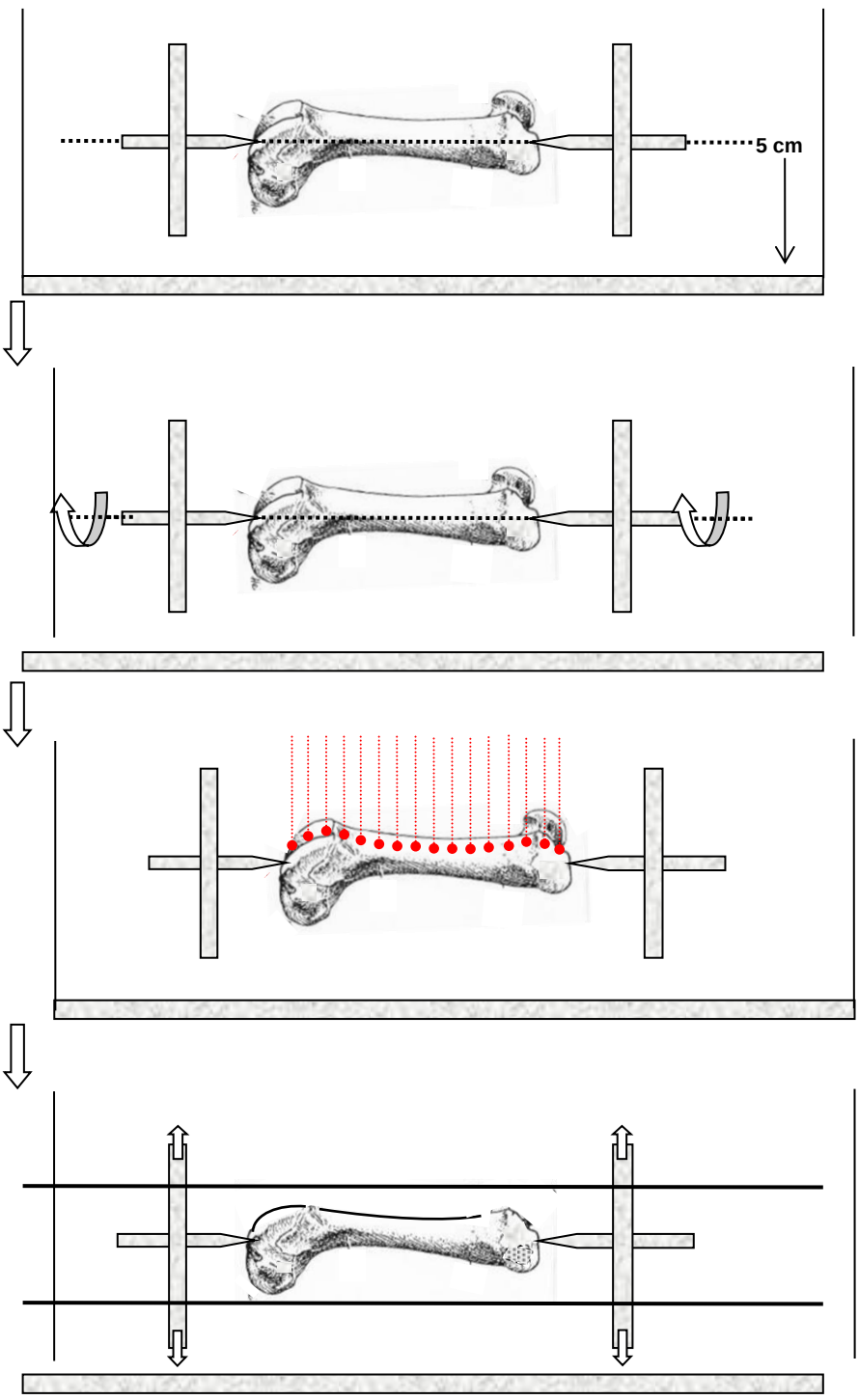

2.2.5: Sub-regional analysis (SRA)

Manufacturer software also allowed analysis of operator selected sub-regions from any previously scanned WB sample; therefore quantification was subsequently

conducted for individual vertebrae and six equal length sub-regions of each long bone (R1-6). In thoracic and lumbar spinal samples, SRA boxes were placed one pixel width outside the cortical edges of the vertebral body, gaps between boxes corresponded to the height of the inter-vertebral discs. Box width was set at 1 pixel width outside the lateral borders of the cortical edges. The sub-regional vertebral scan therefore also included the medial transverse processes and spines as well as vertebral bodies. In the long bones, after measurement of overall length, samples were divided into six equal length regions were placed along the length of the long bone sample, R1 was located proximally, R2 in the proximal metaphysis, R3 and R4 in the mid-shaft, R5 at the distal metaphysis and R6 the most distal (Figure 2.2b). The same region setting protocol was used for both S1 and S2 images, and test re-test data were generated in a similar manner to WB to determine reproducibility and reliability associated with the sub-regional analysis protocol.

Figure 2.2: (a) Whole bone acquisition scan (WB); (b) sub-regional analysis (SRA) of the ovine femur and (c) vertebral sub-regional analysis (not to scale).

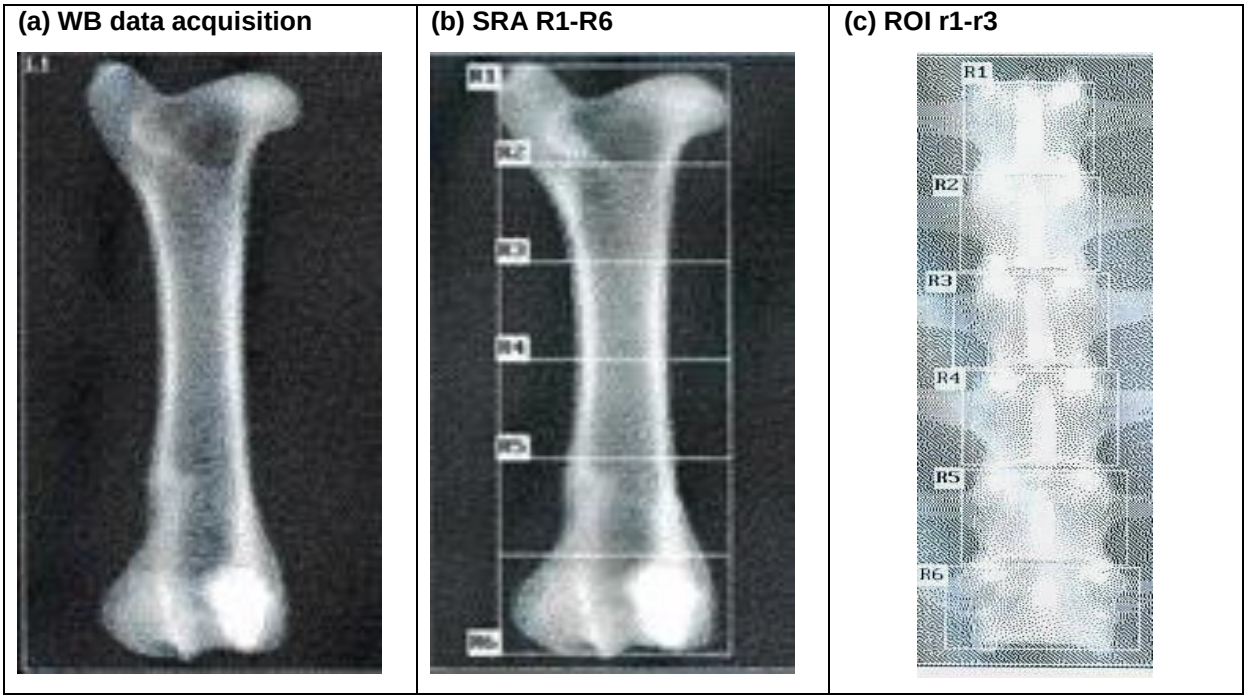

2.2.6: Region of interest analysis (ROI)

In the third level of analysis, three smaller regions of interest (r1-3) were placed in long bone sub-regions with a high proportion of trabecular bone areas of increased bone turnover in osteoporosis, namely; proximal femur, proximal humerus and distal radius. The proximal tibial plateau was scanned to provide bone quantity data close

to an articular surface for a study on articular cartilage. Figure 2.2c shows ROI boxes over the head r1, the neck r2 and inter-trochanteric areas of the proximal femur. ROI box dimensions were set at the same relative size for each bone depending on SRA dimensions; in the humerus and femur 1/3 of the width of R1, in the distal radius 1/3 the length of R6, and in the tibia 1/3 the length and width of R1. In the femur boxes r1-3 were offset using anatomical landmarks to give the best representation of head, neck and inter-trochanteric regions; in the humerus the boxes were set horizontally without an offset; in the distal radius boxes were set sequentially and in the tibia boxes were offset slightly across the tibial plateau depending on anatomical variation, see Figure 2.3.

Figure 2.3: ROI box placements for the proximal and distal limb bones

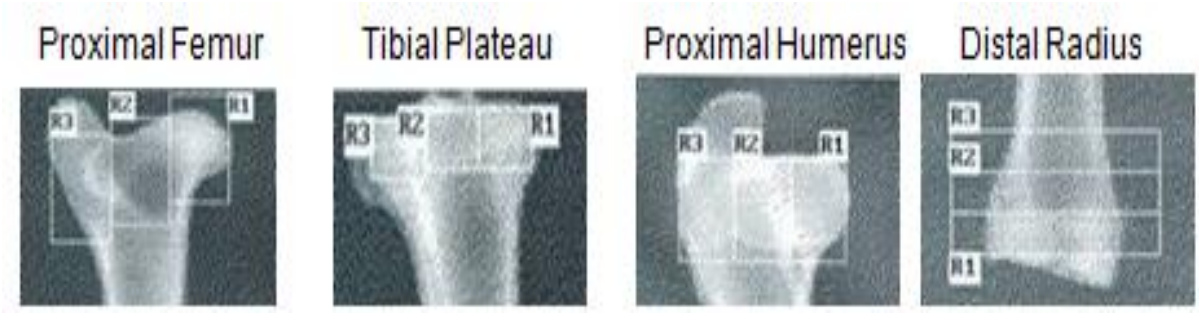

2.2.7: Ash weight

Accuracy was assessed by comparison of DXA derived BMC data to ash weight. Nine samples were selected from LS, and the 4 long bone sites. WB samples were selected from animals of low, medium and high body mass in order to assess accuracy over a range of bone size. Spinal samples (LS) were divided through inter-vertebral discs and transverse processes were removed in line with the lateral edges of the upper and lower borders according to the edge protocol used in the SRA analysis. Long bones were sectioned into 6 equal length sub-regions with a fine bone saw; cuts were placed as close as possible to the division of SRA boxes. Sub-divided bone samples were then placed in a muffled oven (Carbolite, Hope Valley, UK) for 12 hour at 300°C to de-grease, and then a further 12 hour at 600°C until only the mineral fraction remained. Sub-regions were weighed to the nearest 0.01g with digital scales (Scaltec SAC 51, Denver Instruments, CO, USA) and compared to BMC (g) for SRA precision for each sub-region and summated for WB precision.

2.2.8: Data analysis

Repeatability was expressed as interclass correlation coefficient (ICC) according to methods of Bland and Altman (Bland & Altman, 1983; Altman & Bland, 1986). ICC data were derived from the SD of pooled S1 and S2 data and technical error of measurement (TEM) of difference data (S1-S2), see Equation 2.2.

Equation 2.2: $ICC = 1 - [TEM^2 / SD^2]$	*Where SD = standard deviation of pooled S1 and S2 data and* $TEM = [\Sigma (S1-S2)^2 \div 2n]^{0.5}$

Measurement variation, systematic bias and scedasticity was then examined using Bland Altman plots of mean [(S1+S2) **/** 2] vs. difference data (S1-S2) for all variables. Scedasticity, the relationship of the error or variation in measurement to the size of the measured variable, was examined using simple correlation of mean ([S1+S2]/2) and difference data (S1-S2), with r < 0.3 considered homoscedastic and r > 0.5 inferring heteroscedastic. Depending on scedasticity, appropriate statistical expression of precision was then computed in terms of absolute measurement limits as 95% LOA and in relative terms as %TEM for homoscedastic data, or as coefficient of variation (CV%) for heteroscedastic data, see Equations 1, 3 and 4.

Equation 2.3: $95\%\ LOA = M_{diff} \pm 1.96\ SD_{diff}$	*Where* M_{diff} *= mean difference and* SD_{diff} *is SD of difference data for repeat scan data (S1-S2)*

Equation 2.4: $\%TEM = [TEM \div M_{S1\&S2}]$ **x100**	*Where* $TEM = [\Sigma (S1-S2)^2 \div 2n]^{0.5}$ *and* $M_{S1\&S2}$ *is pooled mean [S1+S2] ÷ 2*

Statistical analysis of accuracy, DXA derived BMC (g) vs. ash weight (g), was made by comparison of pooled WB and SRA data. Interclass correlation coefficient, systematic bias and scedasticity were calculated as described previously and overall accuracy was expressed as %TEM.

2.3: Results

2.3.1: Stability and short-term DXA precision

Long term stability of measurement, for the duration of this study scanner block phantom CV% did not exceed 0.3%. Short-term BMD precision (CV%) was < 1% for high density; and <0.5% for medium and low density block phantoms, respectively. CV% of EA, BMC and BMD data for repeat measurements (x40) of a single ovine femur were all <0.4%.

2.3.2: Repeatability

ICC for data acquisition (WB) scans was >0.99 at all spinal and long bone sites. Repeatability of areal BMD for WB sample acquisition, SRA and ROI analyses for the femur are shown in Figure 2.4. Repeatability of more operator dependent sub-regional analyses (R1-6) was more variable. In sub-regional analysis of individual lumbar and thoracic vertebrae, and proximal limb bones, femur and humerus, ICC was >0.99. In distal long bones with more varied morphology repeatability was slightly reduced ICC were; 0.97-0.99 for the tibia (TBR) and 0.94-0.98 for the radius (RDR). At the third level of analysis (ROI) at sites within proximal and distal long bone sub-regions ICC was; >0.96 at the distal radius, >0.97 at the head and neck of the humerus, and in the proximal femoral head, neck and inter-trochanteric areas ICC was 0.99 for all three sub-regions. At the tibial plateau ICC was 0.96 on the medial side, 0.98 in the central zone, but less repeatable on the lateral side where ICC was ~ 0.91.

Figure 2.4: Repeatability of DXA BMD data at three levels of analysis whole bone (WB), sub-regional analysis (SRA) and within region of interest (ROI) for the right ovine femur (n=77). [[Median (bar), IQR (boxes), range (whiskers), mean (+) and S1 clear / S2 shaded]. Graphical mean data for FMR is shown in Appendix 2.

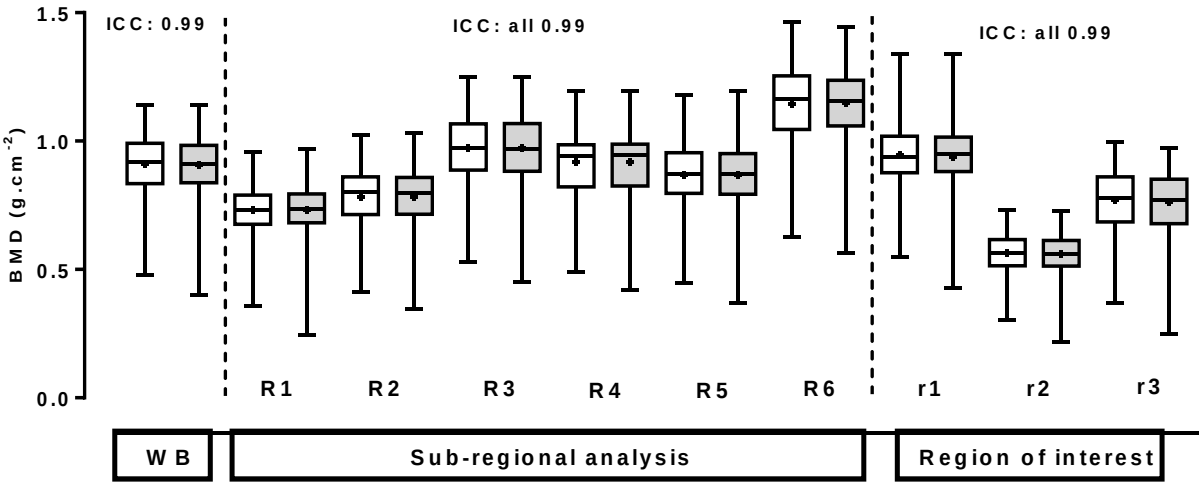

Repeatability of bone mineral content (BMC) and projected area (EA), the determinants of areal BMD are shown in Tables 2.1 and 2.2. ICC for BMC and EA data acquisition scan (WB) was >0.99 at all sites; for SRA BMC was >0.98 and projected area EA ranged from 0.89 to 0.99. At the third level of analysis (ROI), ICC varied between 0.90 to 0.99 for BMC data and 0.85 to 0.98 for EA data.

Table 2.1: Repeatability (ICC) BMC data: for WB, SRA (R1-6) and ROI (r1-3)

Site	n	WB	R1	R2	R3	R4	R5	R6	r1	r2	r3
TS	26	0.99	0.99	0.99	0.99	0.99	0.99	0.99	-	-	-
LS	36	0.99	0.99	0.98	0.99	0.99	0.99	0.98	-	-	-
FMR	76	0.99	0.99	0.99	0.99	0.99	0.99	0.99	0.98	0.96	0.97
TBR	77	0.99	0.99	0.99	0.99	0.99	0.99	0.99	0.95	0.97	0.93
HMR	74	0.99	0.96	0.99	0.99	0.99	0.99	0.99	0.97	0.98	0.97
RDR	74	0.99	0.98	0.96	0.99	0.98	0.99	0.98	0.99	0.97	0.90

Table 2.2: Repeatability (ICC) EA data: for WB, SRA (R1-6) and ROI (r1-3) sites

SITE	n	WB	R1	R2	R3	R4	R5	R6	r1	r2	r3
TS	26	0.99	0.95	0.97	0.95	0.95	0.93	0.96	-	-	-
LS	36	0.99	0.95	0.93	0.94	0.97	0.94	0.94	-	-	-
FMR	76	0.99	0.97	0.99	0.99	0.99	0.97	0.96	0.89	0.93	0.89
TBR	77	0.99	0.98	0.99	0.99	0.98	0.98	0.97	0.85	0.93	0.94
HMR	74	0.99	0.90	0.98	0.99	0.99	0.99	0.97	0.94	0.96	0.91
RDR	74	0.99	0.89	0.95	0.98	0.97	0.98	0.91	0.96	0.97	0.98

2.3.3: Scedasticity

Correlation analysis of BMD mean vs. difference data for lumbar (n=36) and thoracic (n=26) regions revealed r < 0.3 for WB and SRA indicating a strong homoscedastic relationship. In FMR; r values were 0.3 to 0.5 for WB, SRA R1, and ROI r2 (Neck), however, for all other sub-regions (R2-6) and ROI data r was <0.3. In TBR, similar measurement variation was observed, r values for WB and proximal SRA (R1, 2) and medial zone tibial plateau ROI analysis were between 0.3 and 0.5, but in the majority of sub-regions (R3-6) and regions of interest r was <0.3. Sample Bland Altman plots of difference data for the femur are presented in Figure 2.5.

In fore limb bones; HMR and RDR there was a strong homoscedastic relationship at all levels of analysis (r<0.3). Consequently, at most sites and levels of analysis, the relationship of difference to mean BMD data was deemed homoscedastic. Reliability was thus expressed in absolute units as 95% limits of agreement (95%LOA) and in relative terms as % technical error of measurement (%TEM) rather than CV% a more appropriate statistic for heteroscedastic data.

2.3.4: Bias and measurement reliability

At all sites, for WB there was no systematic bias with 95%LOA of the order of ±0.020 g.cm^{-2} and relative reliability (%TEM) of ~1%. In SRA, the second level of analysis, individual vertebrae and long bone sub-regions (R1-6), showed no evidence of systematic bias apart from R1 in the proximal radius. SRA measurement limits were lowest and most consistent for spinal and hind limb samples with 95%LOA in the range of ±0.030 g.cm^{-2} and %TEM <2%. In SRA of fore limb long bones 95%LOA were approximately ±0.040 g.cm^{-2} for mid-shaft and distal sub-regions. However, in more variably shaped proximal sub-regions R1-2 of the radius and R1 in the humerus, 95%LOA were greater. In the tertiary level ROI analyses of proximal femur, humerus, and distal radius measurements again showed little systematic bias and 95%LOA were similar to SRA. Across the tibial plateau measurement showed both negative and positive systematic bias and a higher range of measurement limits. Measurement limits at all levels of analysis are reported in Table 2.3.

Figure 2.5: Mean (S1+S2 /2) vs. Difference (S1- S2) data plots for femur (n=76); (a) WB data acquisition scan; and, (b) SRA sub-region R3 femoral shaft

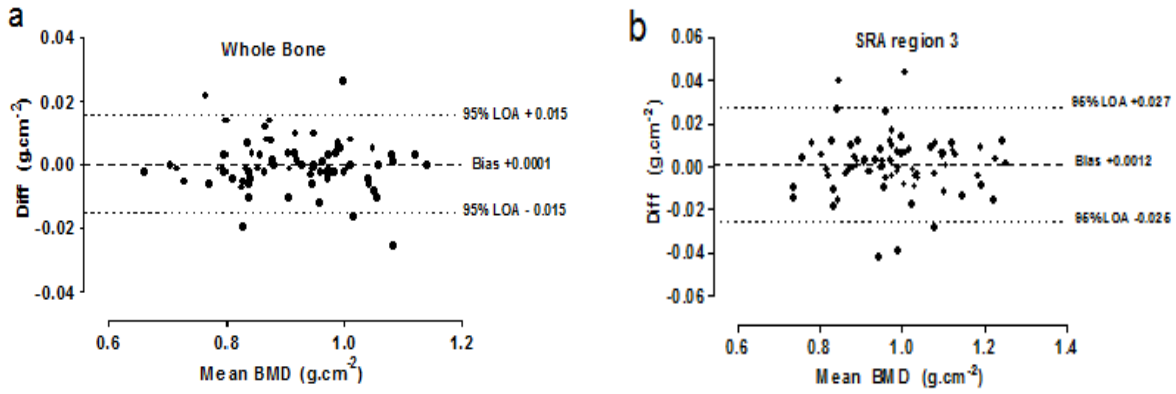

2.3.5: Accuracy

Global analysis of pooled BMC and ash weight data for WB at all sites showed high interclass correlation (ICC=0.99). Systematic bias was <0.1g, the relationship of difference to mean data was homoscedastic (r<0.3) and relative reliability (%TEM) was 1 to 3%. In comparison with pooled SRA data (R1-6), interclass correlation of BMC and ash weight was 0.85 for LS, 0.90 for HMR, 0.93 for RDR and for hind limb sites FMR and TBR, 0.95. Minimal systematic bias was recorded at each site, 0.4g for LS and ~0.3 g for the long bones. At all sites, BMC ash weight difference and mean SRA data were homoscedastic, 'r' ranged from 0.2 to 0.4. Scatter plots of

pooled WB and SRA data comparisons of BMC vs. ash weight are presented in Figure 2.5 and %TEM at each site is reported in Table 2.4.

Table 2.3: Absolute measurement limits 95%LOA ($g.cm^{-2}$) and relative reliability (%TEM) below (in bold) of DXA BMD for data acquisition (WB), sub-regional analysis (SRA) and region of interest (ROI) at six sites in the ovine skeleton.

	DA	Sub Regional Analysis (SRA)						Region of Interest (ROI)		
Site	**WB**	**R1**	**R2**	**R3**	**R4**	**R5**	**R6**	**r1**	**r2**	**r3**
TS (26)	+0.014 - 0.015 **0.6**	+0.036 - 0.039 **1.4**	+0.027 - 0.023 **1.0**	+0.042 - 0.045 **1.8**	+0.017 - 0.023 **0.9**	+0.038 - 0.035 **1.5**	+0.025 - 0.033 **1.2**	-	-	-
LS (36)	+0.020 - 0.018 **0.7**	+0.031 - 0.028 **0.8**	+0.036 - 0.042 **0.7**	+0.018 - 0.019 **0.6**	+0.030 - 0.029 **1.0**	+0.029 - 0.035 **1.1**	+0.037 - 0.033 **1.2**	-	-	-
FMR (76)	+0.015 - 0.015 **0.9**	+0.010 - 0.016 **1.4**	+0.026 - 0.020 **1.3**	+0.028 - 0.025 **1.2**	+0.022 - 0.024 **1.0**	+0.024 - 0.026 **1.3**	+0.022 - 0.029 **0.9**	+0.033 - 0.026 **1.5**	+0.020 - 0.016 **1.7**	+0.030 - 0.019 **1.8**
TBR (77)	+0.023 - 0.018 **0.8**	+0.028 - 0.020 **1.0**	+0.033 - 0.028 **1.2**	+0.030 - 0.032 **1.0**	+0.036 - 0.035 **1.2**	+0.043 - 0.045 **1.7**	+0.035 - 0.025 **1.3**	+0.051 - 0.101 **3.0**	+0.063 - 0.089 **2.7**	+0.195 - 0.112 **5.6**
HMR (74)	+0.013 - 0.018 **0.6**	+0.050 - 0.043 **2.2**	+0.030 - 0.042 **1.5**	+0.030 - 0.032 **1.3**	+0.035 - 0.040 **1.2**	+0.025 - 0.032 **0.9**	+0.030 - 0.025 **0.9**	+0.047 - 0.041 **1.7**	+0.049 - 0.050 **1.7**	+0.070 - 0.065 **2.9**
RDR (74)	+0.027 - 0.020 **1.0**	+0.128 - 0.090 **4.6**	+0.077 - 0.062 **2.4**	+0.033 - 0.029 **1.2**	+0.032 - 0.043 **1.6**	+0.032 - 0.039 **1.9**	+0.038 - 0.032 **1.7**	+0.049 - 0.047 **2.0**	+0.052 - 0.043 **2.7**	+0.034 - 0.034 **1.9**

Table 2.4: %TEM for WB and SRA analysis of accuracy of BMC (g) in comparison to ash weight (g) at five sites in the ovine skeleton in small, medium and large sized animals (n=9).

	WB	SRA	R1	R2	R3	R4	R5	R6
LS	2.73	6.25	7.50	5.39	2.72	8.04	5.67	6.40
FMR	2.16	7.82	7.72	5.66	7.35	6.24	8.78	6.62
TBR	1.67	7.41	7.08	5.68	6.87	7.40	9.26	3.57
HMR	1.49	9.03	2.98	8.84	4.74	10.09	8.54	7.15
RDR	2.73	6.81	2.68	7.81	6.56	5.15	7.71	4.45

Figure 2.5: Scatter plots of pooled WB and SRA data for DXA derived BMC (g) and ash weight. Dashed line indicates the line of equality (y = x).

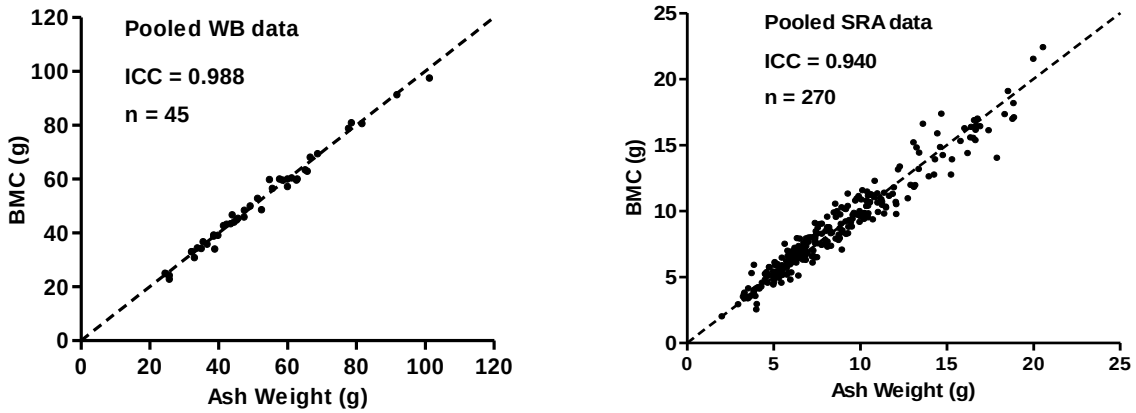

2.4: Discussion

2.4.1: Study design

This study was based on well described methods for examination of measurement variation available in the literature (Altman & Bland 1983; Bland & Altman, 1986; Atkinson & Neville 1998; Gore, 2005; Goto & Mascie, 2007; Harris & Smith, 2009). The ovine bone samples selected were collected from 77 skeletally mature animals, site selection included both spinal and long bone, fore limb and hind limb sites, and animals were selected over a wide range of body mass and breeds representative of the normal Irish sheep population. Long and short-term precision were confirmed with repeat scans of Hologic™ block phantoms and a whole bone specimen; and the scanning protocol was optimised to minimise error previously reported for both *in* and *ex-vivo* bone DXA scanning (Kaymakci & Wark, 1994; Turner *et al*., 1995a; Kanis, 2002; Bolotin, 2007).

2.4.2: Sample selection

In this study sample size (n=77), maturity (4-6yr) and range of body mass (30-100kg), to the authors knowledge, represents the most comprehensive validation of DXA methods for *ex-vivo* ovine bone, to date. The sampling procedures in the few DXA validation studies available in the literature (Kaymakci & Wark, 1994; Turner *et al.,* 1995a; Pouilles *et al*., 2000) show more variable sample size, maturity and range of body mass. In Kaymakci and Wark (1994) sample size was low (n=8), sheep were immature (<2yr) and all had low body mass (32-40kg). In Turner *et al*. (1995a) sample size (n=48) was large, sheep were mature, but body mass was not stated; and in Pouilles *et al*. (2000) two immature low body mass animals and three mature heavier animals underwent repeat scanning. The restricted sampling procedures in these studies were adequate for their needs in determination of scanner precision with variations in scan protocol (Kaymakci & Wark, 1994), reproducibility across anatomical site and type of scanner used (Turner *et al*., 1995a); but scedasticity of data conducted in the latter study (Pouilles *et al*., 2000) with so few animals (n=5) was effected by selection bias and do not agree with the results of this study (n=77). Only Turner *et al.* (1995a) had sufficient numbers to allow a complete statistical evaluation of validity, but unfortunately the statistical analysis reported by these authors was limited.

2.4.3: Sample alignment protocol

In the present study a holding jig consisting of PTFE holding pins enabled the central longitudinal axis of specimen to be held at a depth of immersion previously reported optimal by Kaymakci and Wark (1994) and also allowed alignment of anatomical landmarks in all three planes. The use of holding devices and surrounding the specimen in a uniform saline medium improves edge detection and subsequent repeatability (Grier & Turner, 1996). In Turner *et al.* (1995a) repeatable DXA measurements on live animals were only possible at the distal radius, calcaneus and lumbar spine, sites amenable to repeat positioning, but similar to this study all *ex-vivo* repeat scans were highly repeatable at all sites.

2.4.4: Scan algorithm

The human lumbar spine scanning algorithm was used throughout the study for all analyses, WB, SRA and ROI. The results of this study agree with previous studies in that the use of this standard human protocol was suitable for assessment of larger explanted *ex-vivo* bones of large animals such as sheep (Kaymakci & Wark, 1994; Turner *et al*., 1995b; Grier & Turner 1996). The human lumbar spine software is especially useful, once the whole bone sample has been scanned, the operator can set regions to suit the bone concerned, and providing landmarks are easily seen and dimensions of ROI's follow a strict protocol the results show DXA has an acceptable level of precision in terms of TEM (2 to 3%) in all areas except the proximal tibia. The author agrees with previous studies with regard to very small bone samples in that the only suitable algorithm for very small bones is the ultra-high resolution protocol (Grier & Turner, 1996).

2.4.5: Statistical analysis

Statistical analysis examined all relevant areas; repeatability, scedasticity, bias, and used appropriate expressions of reliability for the homoscedastic repeated data set. Finally, accuracy was confirmed by comparison of DXA derived WB and pooled SRA data vs. ash weight, and as previously recommended, measurement limits and reliability were expressed in both absolute and relative terms (Gluer *et al*., 2005). The relative reliability of DXA methods in this study was 1 to 3% at all sites, similar to that reported in both human (Cummings *et al*., 2002) and animal studies (Libouban *et*

al., 2002; Grier & Turner, 1996); and similar to acceptable levels of reliability reported for measurement in human anthropometry (Gore, 2005).

2.4.6: Accuracy

Accuracy data reported in previous studies are limited due to methods employed; animals selected were immature, very few skeletal sites were used; and due to small sample size accuracy was not examined across a range of bone size seen in the normal ovine population (Newman *et al*., 1995; Turner *et al*., 1995b; Pouilles *et al*., 2000). The %TEM of between 2 to 4% for WB assessing BMC vs. ash weight across a range of small, medium and larger sized bone samples and 6 to 9% for the pooled SRA data are comparable to accuracy reported in human and animal studies (Kaymakci & Wark, 1994; Seeman, 2002). DXA derived BMC data in studies of excised rat bones have been reported to be accurate, precise and highly correlated to ash weight for three types of DXA device; with computed CV% of 1.7 and 3.6% for femur and tibia measurements, respectively (Libouban *et al*., 2002). The higher accuracy for WB analysis was due to the methodology used, WB samples were scanned first and subsequently cut, the resulting pooled R1-6 SRA data were thus a reflection of the accuracy of placement of cuts and small amount of mineral lost during cutting. In the study by Kaymakci and Wark (1994) small ovine rib sections, cut first and subsequently scanned, showed a similar degree of accuracy to that of our WB data.

2.4.7: Implications for future studies

In future longitudinal studies in order for a true change in BMD to have occurred, not only must detected changes achieve statistical significance ($P<0.05$) but they must also exceed the measurement limits of the device at the various sites and different levels of analysis. Both absolute and relative reliability therefore have implications for sample size estimations prior to intervention studies. If BMD alone was to be used as an outcome measure, intergroup differences would have to be greater than the 1 to 3% measurement limits to infer a true change. In sample size calculations based on measurement limits in a previous study, the authors calculated that a sample size of 35+ animals per group would be needed to show a 1% change in BMD at a

significance level of $P<0.05$ (Grier & Turner, 1996). Similar sample size calculations based on measurement limits in this study were made for future studies with unpaired two-tailed designs with two (un-paired Student's T test) or more groups (ANOVA), at an α level of 0.05 (Type I error) and a β level of 0.8 (Type II error); in both cases estimated sample size was greater than 70 animals per group would be required.

Following sample size calculations DXA bone quantity evaluation study design should consider the skeletal site to be examined. In this study, measurement limits for WB and SRA were approximately ±0.03g.cm^{-2} and <1.5% at all sites in absolute and relative terms, respectively. Reliability was similar throughout the skeletal sites selected; however, greater relative reliability of measurement (<1%) was seen in the proximal femur and lumbar vertebrae and lower relative reliability in the proximal radius. This suggests, similar to human scanning, that proximal femoral and vertebral sub-regions might be more suitable skeletal sites for longitudinal examination of BMD; over time, or with drug, hormonal or dietary interventions. Small bone quantity changes occurring at these sites are more likely to exceed the smaller human operator and scanner measurement limits. SRA in the proximal radius and ROI analyses across the tibial plateau showed greater measurement limits and lower relative reliability than the majority of other regions, these regions should either be avoided or alternatively the scan protocol further adapted to improve reliability.

2.4.7: Conclusions

1. This study presents a systematic DXA methodology for measurement of large *ex-vivo* bone samples and presents data analysis techniques to assess reliability (precision) and validity (accuracy) of DXA measurement for large *ex-vivo* bone samples at spinal and long bone sites and at three levels; for whole bones, and for large and small sub-regions in an Irish sheep population.

2. The thorough examination of measurement variation across a wide range of animal size and breed for bias and scedasticity confirmed the initial suspicion that the widespread use of CV% to express relative reliability in animal DXA studies may be questionable. The results suggest that 95% LOA should be used to express absolute measurement limits for DXA derived ovine BMD data, and that future researchers use %TEM to quantify relative reliability rather than CV%.

3. The results of this study have expanded the assessment of measurement variation confirming reliability over a range of bone size and age typical of animals selected from the population to be sampled in future research and the methodology described should be applicable to further studies employing DXA bone quantity measurement of large *ex-vivo* bone either animal or human.

CHAPTER 3

Effect of breed, season and body mass on ovine bone quantity

3.0: Summary / abstract

The aim of this study, following preliminary DXA validation of accuracy, reliability and evaluation of scanner measurement limits, was to examine the natural variation of bone quantity across breed, season of sacrifice and body mass in proximal long bone and spinal sites in the ovine skeleton. *Ex-vivo* bone samples were sourced from 77 healthy skeletally mature ewes that were slaughtered for commercial reasons at a local meat rendering facility. Sourced samples included the lower six thoracic (TS) and lumbar (LS) vertebrae; the femur (FMR), tibia (TBR), humerus (HMR) and radius (RDR). Whole bone samples (WB) were positioned on a holding jig within a Perspex tank containing isotonic saline (0.9% NaCl) on the scanning platform of a Hologic QDR4500 dual energy X-ray (DXA) scanner. Repeat WB data acquisition scans were performed using the human lumbar spine algorithm which allowed further sub-regional analysis (SRA) down the length of the samples and also within regions of interest (ROI) of high trabecular content. At the level of resolution used in human scanning (WB, SRA and ROI), no inter-breed differences in bone quantity were detected; however, in analysis of seasonal effects (W/S vs. S/A) a difference was apparent within the proximal femur ($P<0.05$). The relationship of bone quantity to body mass (r^2) was better for BMD (~0.5) than either component of BMD, namely; EA or BMC (~0.3 to 0.4), however, correlation of BMD was good across all sites ($r>0.7$) and especially within the same limb ($r>0.9$). BMD was evenly distributed down the length of TS, and in LS there was a gradual reduction in density from R1 to R6. In long bones, high density regions were present in all mid-shaft regions (R3 and R4) with additional high density regions in distal femoral and humeral condyles, and in the proximal radius due the presence of the ulnar reinforcing strut. This study was the first systematic evaluation of BMD in the skeleton of Irish sheep; and as such provides a useful template of wider DXA validation beyond technical evaluation procedures. The BMD to body mass relationship has been charted for whole bone samples at six ovine skeletal sites; at a sub-regional level for individual vertebrae and in six long bone sub-regions providing preliminary ovine BMD reference standards across body mass. Preliminary population data generated will allow better interpretation of any changes in *ex-vivo* ovine bone occurring in cross-sectional and longitudinal interventional studies using the sheep model of osteoporosis.

Key words: DXA, bone density, sheep animal model, seasonal variation

3.1: Introduction

The aged ewe as a large animal model of osteoporosis research has several advantages over other large animal models including; commercial availability in large numbers, ease of handling and as a flock animal in interventional studies animals can be reared in similar conditions (Miller *et al*., 1995; Turner *et al*., 1995a, Lee & Taylor, 2003). Ovine bone mass, architecture, and strength are similar to humans and there are physiological similarities to humans in terms of the cyclical hormonal changes during oestrus and in bone remodelling (Newman *et al*., 1995). However, seasonal effects on bone density have recently been documented in sheep and other inter-species differences are also likely and should be considered when using sheep as an animal model for bone research (Aerssens *et al.,* 1998; Turner, 2007).

Rapid efficient accurate and precise measurement of ovine bone quantity became possible in the early 1990's when dual energy x-ray absorptiometry (DXA) scanning technology developed for assessment of human bone density and osteoporosis was adapted for large and small animals (Kaymakci & Wark, 1994; Grier & Turner, 1996; Libouban *et al.,* 2002;). DXA has been used extensively to assess ovine bone mineral quantity in numerous studies both *in-vivo* and in large *ex-vivo* cadaveric bone samples (Turner *et al.,* 1995a).

However, despite widespread use of DXA in animal research, published data on the natural variation of ovine bone quantity in the normal population is scarce; and well established reference ranges which exist for human populations (Kanis, 2002) and in some animal models (Havill *et al*., 2003), are currently unavailable for sheep.

The aim of this observational DXA study was to examine interbreed and seasonal variation in *ex-vivo* ovine bone quantity, profile distribution of bone mass at whole bone and sub-regional levels at spinal and long bone sites in the ovine skeleton; and, in doing so generate preliminary ovine bone quantity reference data to aid further evaluation of results of cross-sectional and longitudinal interventional studies.

3.2: Methods

3.2.1: Sample selection

Large ovine spinal and long bone samples were obtained from 77 mature ewes, mean (±SD) body mass was 69.7 ± 17.8 kg, after processing at a local meat factory (Irish Country Meats, Athboy, Ireland), transported for 1 hour and frozen at -20^{o}C until preparation and scanning. All animals underwent veterinary check prior to slaughter; age was >4yr, and breeds were representative of those in commercial use in the Republic of Ireland. Breed, carcass mass, and date of slaughter were recorded to evaluate; effect of breed, seasonal variation and body mass on bone mineral quantity variables.

3.2.2: Sample preparation and alignment protocol

Skeletal sites selected were; lower six thoracic and lumbar vertebrae, and proximal right side long bones; femur, tibia, humerus and radius, see Figure 3.1. In a previous pilot study no right left limb BMD difference was noted and left sided bones were kept for use in case of damage to right sided samples during preparation. Soft tissues were cleared by dissection and additionally in spinal samples; ligaments and inter-vertebral discs were cut to straighten natural curvatures for optimal scanning. Samples were placed in a holding jig bathed in normal saline, and positioned and scanned using a previously validated protocol.

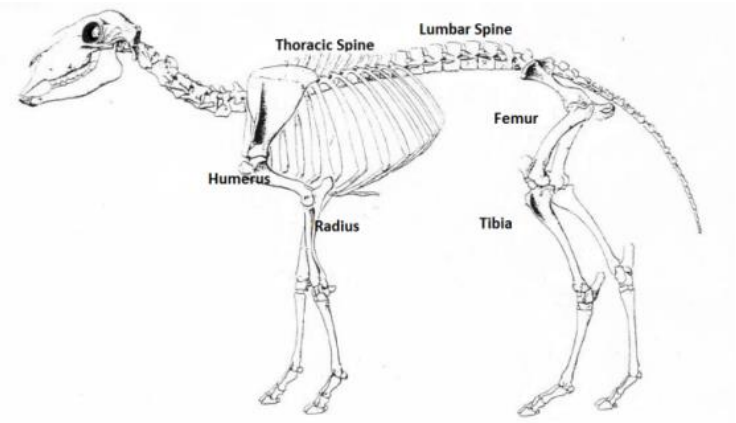

Figure 3.1: Sample selection Bone sample sites selected for DXA analysis; the lower 6 vertebrae from the thoracic (TS) and lumbar spine (LS); and, whole long bone samples; femur (FMR), tibia (TBR), humerus (HMR), radius (RDR).

3.2.3: Data acquisition scans (WB)

The human lumbar spine algorithm of a Hologic QDR4500 (Hologic, Waltham, MA, USA) dual energy X-ray (DXA) scanner measured bone mineral content (BMC in g),

estimated area (EA in cm^2) and areal bone mineral density (BMD in $g.cm^{-2}$). Initial whole bone data acquisition scans (WB) were performed on fully articulated 6 vertebrae spinal samples and individual long bones.

3.2.4: Sub-regional analysis protocols (SRA and ROI)

The human lumbar spine analysis protocol was used to perform SRA and smaller region of interest (ROI) analyses. Vertebral box dimensions were set 1 pixel width from lateral vertebral body margins. In the long bones, data acquisition scan images were divided into 6 equal sub-regions; areas scanned were the proximal epiphysis (R1), metaphysis (R2), mid-shaft diaphysis regions (R3, R4), distal metaphysis (R5) and epiphysis (R6), see Figure 3.2.

Figure 3.2 SRA: Vertebral and long bones SRA box placement (not to scale)

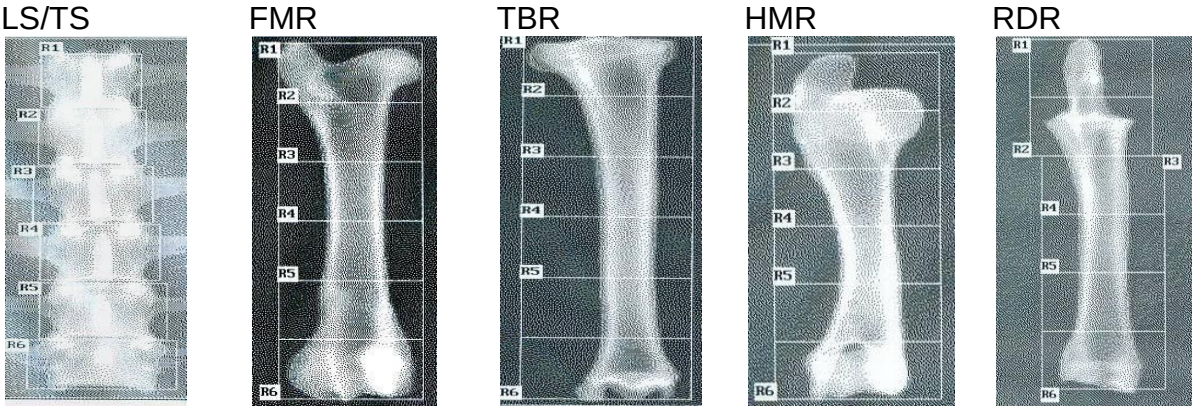

Region of interest analyses (ROI) were performed in areas of high trabecular bone content within selected sub-regions of each long bone. Box dimensions were set at the same relative dimensions for each site analysed. Analyses included; head (r1), neck (r2) and inter-trochanteric regions (r3) of the proximal femur and humerus; medial, intermediate and lateral zones of the tibial plateau; and 3 consecutive sections of similar length in the distal radius. In the proximal femur and tibia slight offsets were made to centre scan boxes with the region of interest, see Figure 3.3.

Figure 3.3: Region of interest protocol

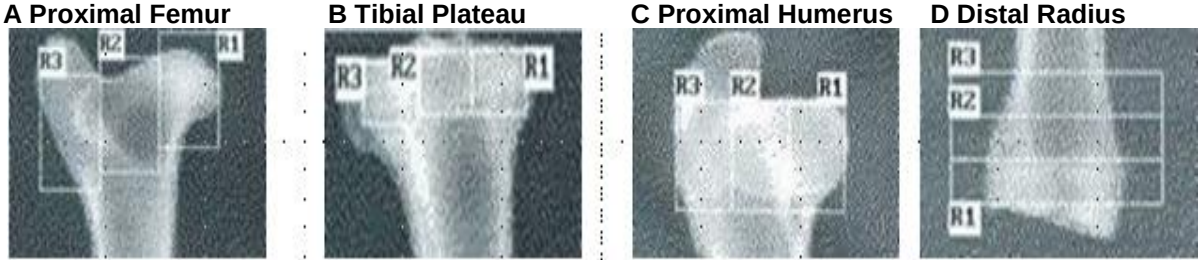

3.2.5: Data handling

BMC, EA and BMD data were grouped and tabulated according to breed, month of sacrifice and body mass for each bone sample on an Excel$^{(TM)}$ spread sheet. Data from damaged or diseased bone samples was excluded; and where possible, data from an unaffected opposite limb was substituted. Outliers were removed from statistical analyses if more than 3 standard deviations from the mean. All grouped data sets were tested for matching of body mass prior to analysis of bone quantity.

3.2.5a: Inter-breed and seasonal effects

Data grouped for breed were assessed for normality (D'Agostino & Pearson) and inter-breed differences using parametric (ANOVA) or non-parametric (Kruskal Wallis) tests as appropriate. In the analysis of seasonal effects comparison of data grouped by month of sacrifice and according to season was made for all whole bone and selected spinal and proximal long bone sub-regions. In all cases $P<0.05$ inferred statistical significance and either Tukey (parametric) or Dunn's (non-parametric) *post-hoc* tests were performed where significant differences were detected.

3.2.5b: Effect of body mass

The relationship of bone quantity was examined in relation to carcass mass, a lean body mass surrogate and for a standardised body mass of 70kg using linear regression analysis. The 95% confidence intervals around the line of best fit were plotted on the linear regression plots to show EA, BMC and BMD across the range of body mass of the sheep sampled.

3.2.5c: Bone density distribution

Variation in BMD ($g.cm^{-2}$) was examined across skeletal site by comparison of WB data. Regional density distributions; R1-6 at all sites and r1-3 in the long bones, were compared for inter-region differences within each site. Correlation analysis was used for associations between skeletal sites and inter-regional differences were compared using one way ANOVA with Tukey *post-hoc* analyses performed in case of significant differences with $P<0.05$ inferring significance.

3.3: Results

3.3.1: Sample size and exclusions

385 bone samples (77 animals by 5 sites) were prepared for scanning; bones samples for two animals with a right /left limb difference and 7 diseased or damaged bone samples (2 thoracic spine, 1 femur, 1 tibia, 1 humerus and 2 radii) were identified during soft tissue clearances, and withdrawn. Data on 75 animals and 378 samples were thus analysed for effect of breed, seasonal variation and body mass.

3.3.2: Variation in bone quantity across breed

Breeds were Suffolk (15), Suffolk X (24), Texel (6), Texel X (5), Kerry (6), Cheviot (5), a small number of less common breeds; Bellclare, Charollais, Grey face, and some horned mountain varieties, were grouped as "others" (14). Pooled data (all breeds; n=75), and individual breeds and 'others', where n>12, were normally distributed at all sites (D'Agostino & Pearson). Analysis of median body mass across group were similar (Kruskal Wallis *P*>0.05) thus groups were well matched for body mass. Non-parametric analyses of bone quantity data showed no inter-breed variation in bone quantity at any spinal or long bone site (Kruskal Wallis; *P*>0.05). Figure 3.4 presents inter-breed variation in BMD data at the two spinal sites TS and LS.

Figure 3.4: Interbreed variation in BMD in 6 vertebrae TS and LS sites
[Median (bar), IQR (boxes), 10-90% (whiskers), mean (+) and outliers (˙), data table in Appendix 3]

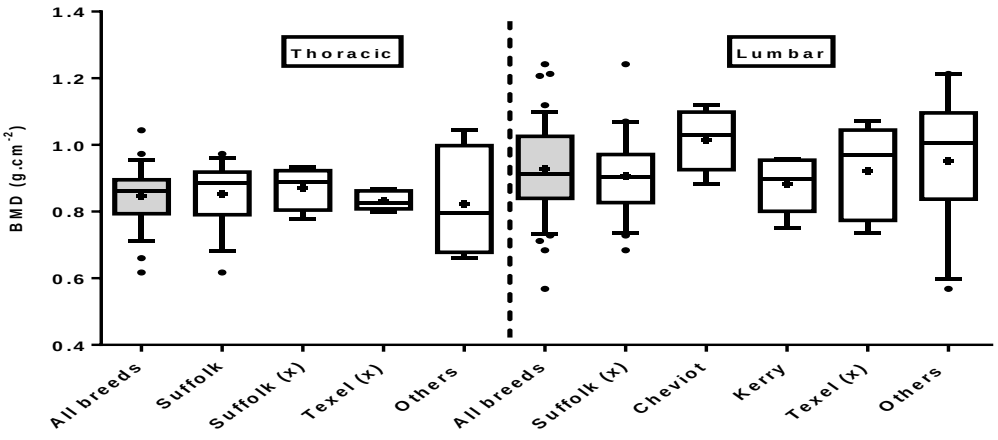

Analysis of sub-regional BMD across breed also showed no significant differences for SRA (R1-6) and ROI (r1-3) at all spinal and long bone sites (Kruskal Wallis; *P*>0.05). Figure 3.5 presents BMD data across breed for the whole femur (WB) and the most proximal sub-region R1.

Figure 3.5: Interbreed variation in BMD in the femur (a) for whole bone (WB) and (b) proximal sub-region R1 [Median (bar), IQR (boxes), 10-90% (whiskers), mean (+) and outliers (·), data table in Appendix 3]

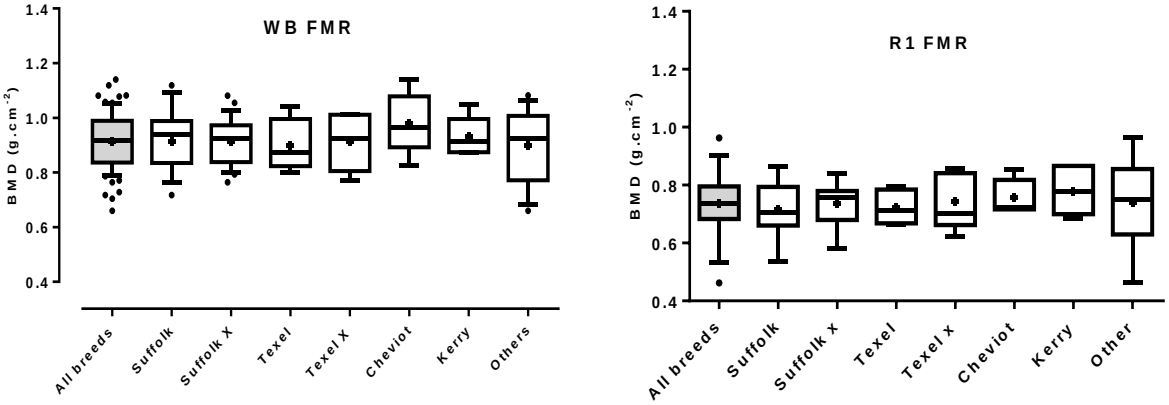

3.3.3: Variation in bone quantity across month and season

Normality testing of data grouped by month of sacrifice (February, March, April, June, September and November) was restricted by sample size in some groups; however, data sets grouped by season (Winter/Spring, Summer/Autumn) were normally distributed (D'Agostino & Pearson). Bone density data were matched for body mass in data grouped by month (Kruskal Wallis; $P>0.05$) and season (ANOVA; $P>0.05$). No significant differences were detected in whole bone sample BMD across month of sacrifice (Kruskal Wallis; $P>0.05$) or across season (ANOVA; $P>0.05$) at any whole bone site. Figure 3.6 presents seasonal variation for pooled spinal and femoral whole bone data.

Figure 3.6: Spinal and femoral pooled aBMD across month and season of sacrifice [Median (bar), IQR (boxes), 10-90% (whiskers), mean (+) and outliers (·), data table in Appendix 3]

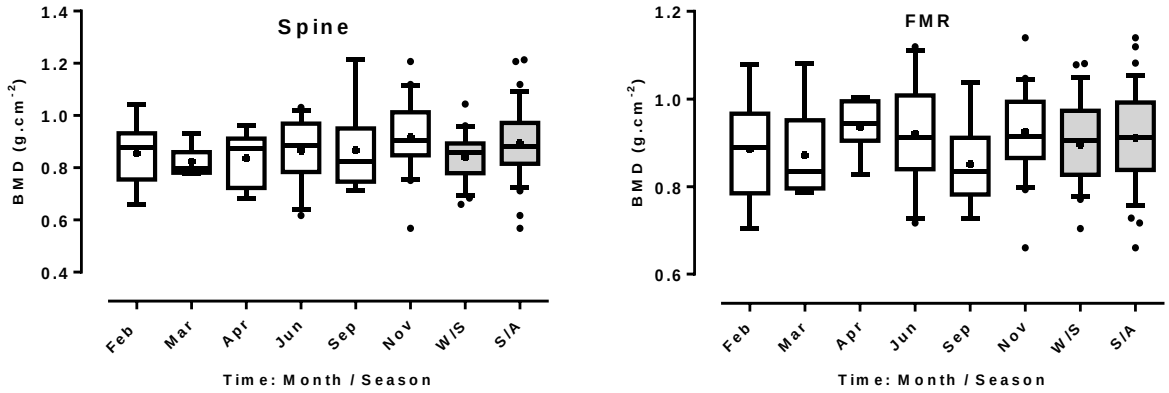

Further analysis of BMD in selected sub-regions; lower 4 thoracic or lumbar vertebrae in the spine, and R1, head (r1), neck (r2) and inter-trochanteric (r3) sub-regions of FMR and HMR; and the distal radius in the majority of cases showed no

significant differences at any site across month or season apart from r2 femoral neck. Figure 3.7 shows seasonal variation within FMR R1 and at r2, the femoral neck.

Figure 3.7: Femoral sub-region R1 / r2 aBMD across month and season of sacrifice [Median (bar), IQR (boxes), 10-90% (whiskers), mean (+) and outliers (˙), data table in Appendix 3]

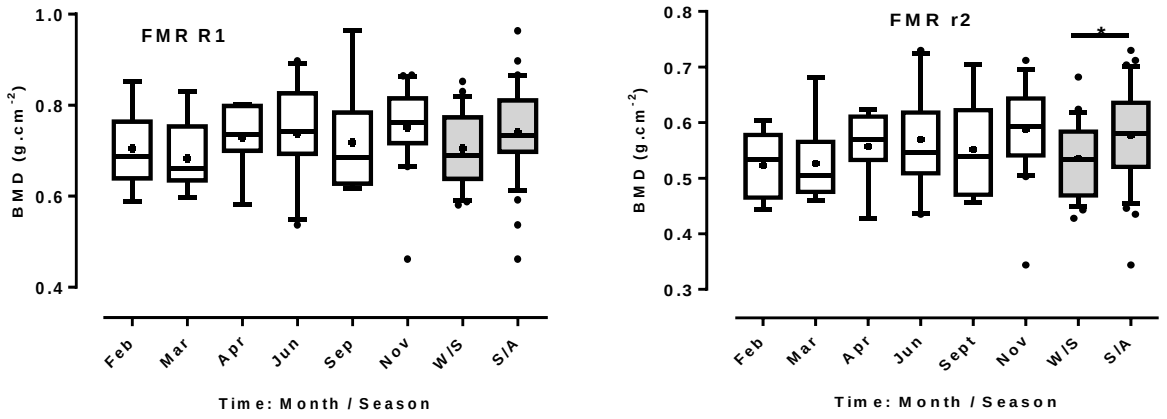

* denotes S/A significantly greater than W/S (*P* = 0.05) @ R2

3.3.4: Relationship of ovine EA / BMC / BMD across site to body mass

Animal body mass was as expected more highly related to bone quantity variables with a component of mass, that is BMC and BMD rather than to EA; the geometric projected area of the scan. Highest r^2 data (0.40 to 0.50) were computed for BMD at all sites apart from TS (r^2=0.38); r^2 data for BMC were similar to BMD, and for EA were much lower. Linear regression plots for EA, BMC and BMD vs. estimated body mass for pooled (lower six vertebrae) spinal and whole long bones are presented in Figure 3.8.

Figure 3.8: Relationship of DXA derived bone density variables EA, BMC, and BMD to estimated body mass (2.1 x CW) for (a) TS (b) LS (c) FMR (d) TBR (e) HMR and (f) RDR [Solid line = line of best fit and dashed lines represent 95% CI].

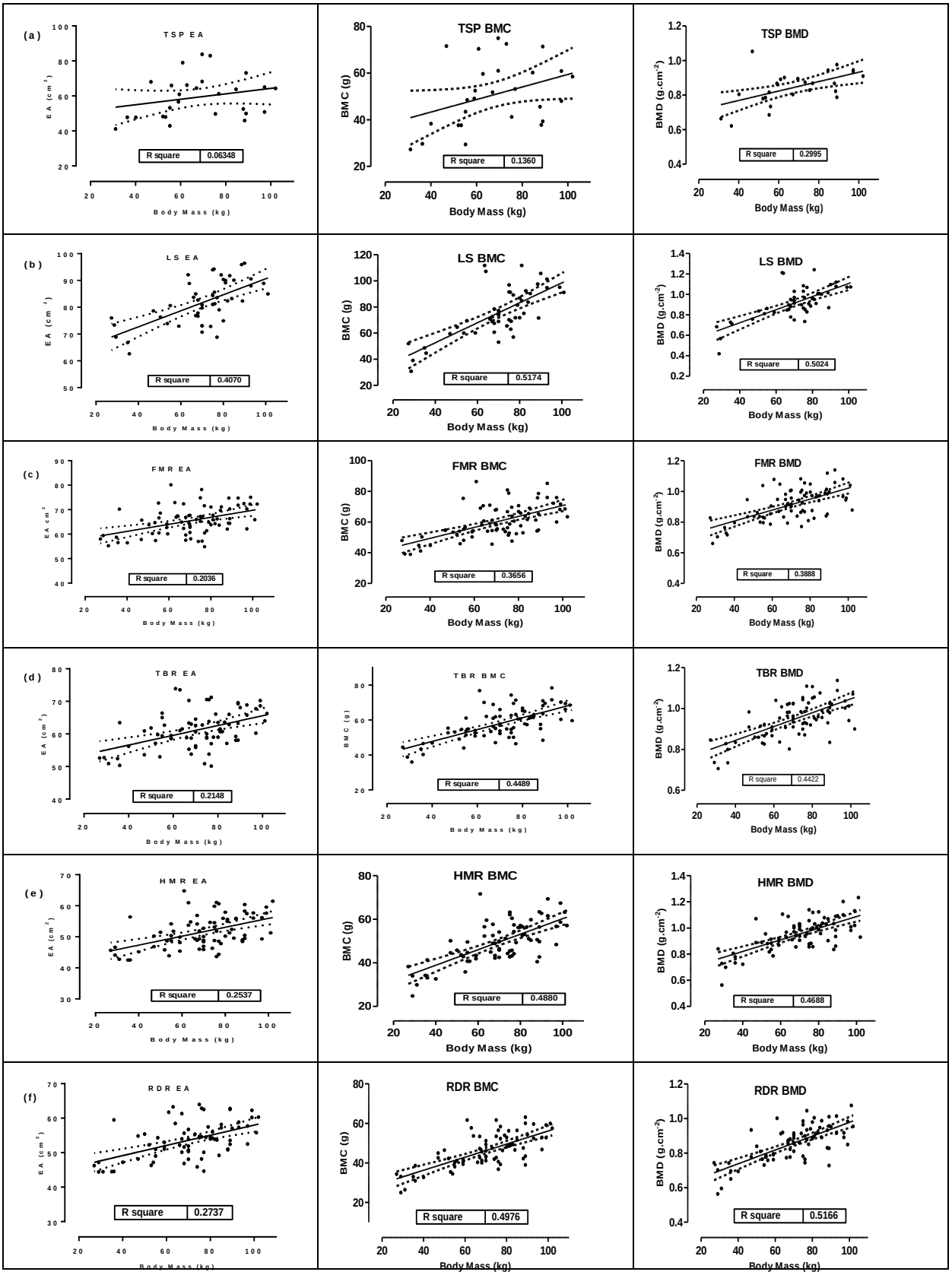

3.3.5: Effect of normalisation of bone quantity data for body mass

Normalisation of data to carcass mass and estimated body mass; or standardisation of data to a mean body mass of 70 kg had minimal effect on BMC and BMD data distributions. Figure 3.9 shows raw data, data normalised for carcass mass (CM) and estimated body mass (2.1 x CM); and data standardised to a mass of 70kg, equivalent to the mean estimated body mass of sheep in the sample population.

BMC data comparisons across site revealed significant differences, especially between spinal and long bone sites, in the majority of cases, however, differences remained similar when normalised or standardised for body mass. In the case of BMD data, bone quantity expressed per unit of projected area ($g.cm^{-2}$), no significant differences were detected across site, with or without normalisation or standardisation for body mass.

Figure 3.9: BMC and aBMD data (a) raw (b) normalised to carcass mass; and (c) for standard mass 70kg [Median (bar), IQR (boxes), range (whiskers), mean (+), data tables in Appendix 3].

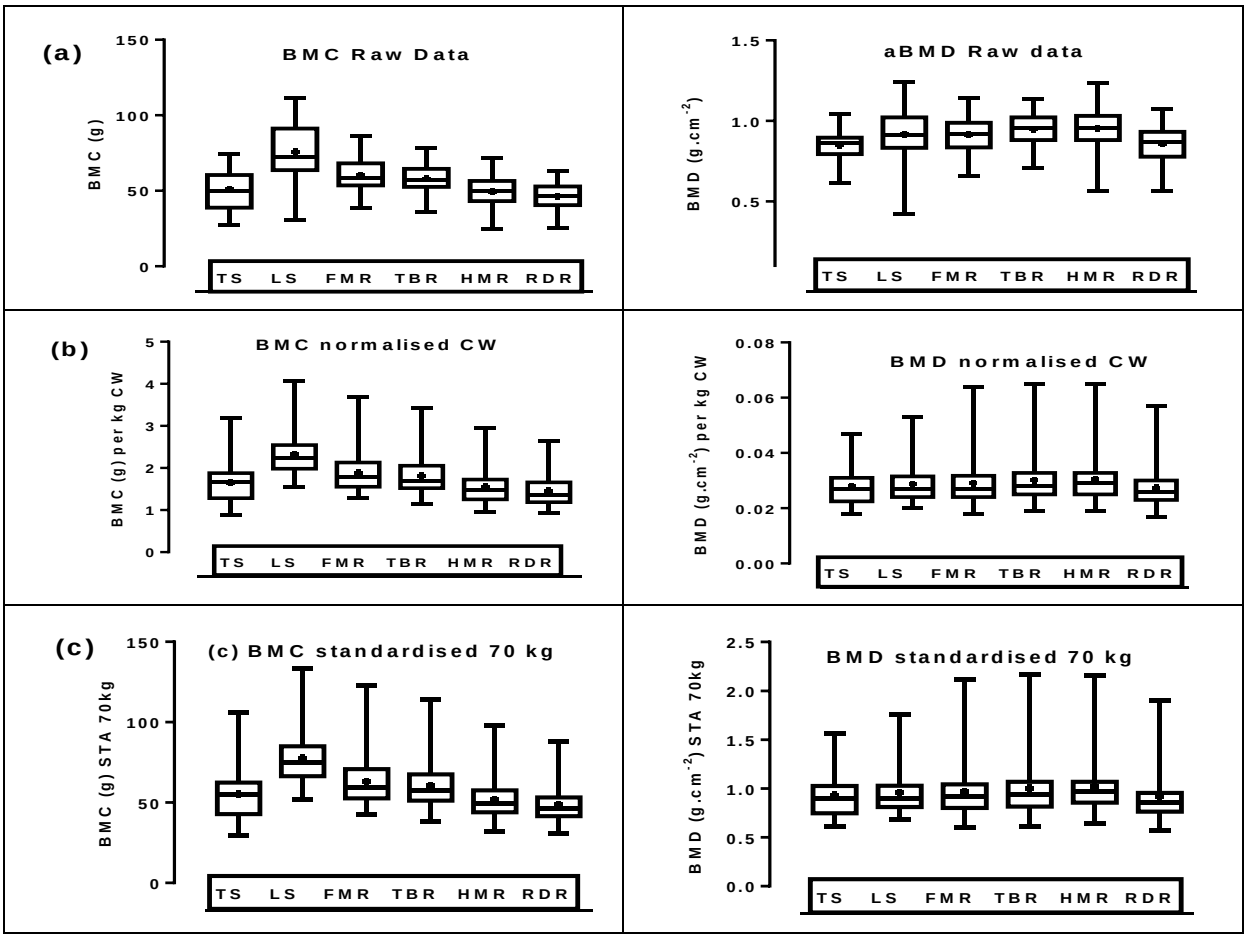

3.3.6: Correlation of bone quantity data between sites

Correlation analysis of whole bone sample density at each site showed strong associations (Table 3.1). Correlation coefficient 'r' for spinal and long bone sites varied from 0.7 to 0.8, between long bones was higher 0.8 to 0.9 and highest between bones of the same limb (0.89); the latter result presumably reflected similar loading within each respective limb.

Table 3.1: Simple correlation analysis (r) of BMD data across site for 6 vertebrae spinal and whole long bone samples in the ovine skeleton.

	FMR	TBR	HMR	RDR
Spine	0.71	0.72	0.81	0.82
FMR	-	0.89	0.82	0.79
TBR	-	-	0.84	0.84
HMR	-	-	-	0.89

3.3.7: Sub-regional bone density distribution

The relationship and inter-region analysis (ANOVA) of bone mineral content (BMC, g), area projection (EA, cm^2) and areal density (BMD, $g.cm^{-2}$) from rostral to caudal in spinal samples TS and LS are presented in Figures 3.10 and 3.11; and proximal to distal for hind-limb long bones FMR and TBR in Figures 3.12 and 3.13; and forelimb long bones HMR and RDR in Figures 3.14 and 3.15.

Figure 3.10: (a) BMC in g; (b) EA in cm^2 and (c) BMD in $g.cm^{-2}$ for R1 to R6 vertebrae in TS. [Median (bar), IQR (boxes), 10-90% (whiskers), mean (+) and outliers (·)]

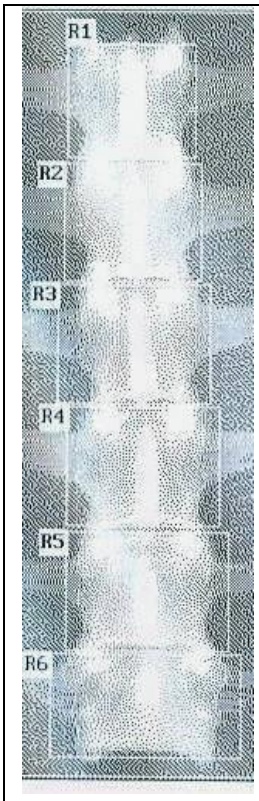

(a) BMC: TS R1 to R6; the box plot shows similar BMC for R1 to R3 then a gradual increase in BMC in R4 to R6. Statistical analysis (ANOVA) identified that *R5 was significantly higher BMC than R2 and R3 (P<0.05), and **R6 significantly higher BMC than R1 to 3 (P<0.01).

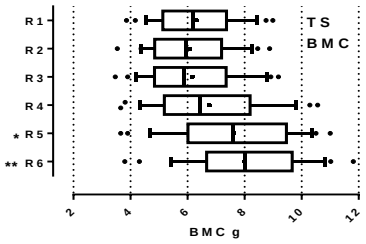

(b) EA: TS R1 to R6; greater projected area was detected in R4 to R6 compared to R1 to R3. ***R5 and R6 were significantly greater than R1 to R3 (P<0.001), R6 was significantly greater than R4 (P<0.05) and **R4 was significantly greater than R1 (P<0.01) and R2 (P<0.05).

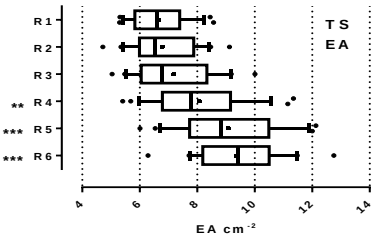

(c) a**BMD:** TS R1 to R6; relative increase in BMC R5 to R6 was less than EA and thus resultant BMD plot for TS shows an even density distribution over the entire segment from R2 to R6. Statistically; only BMD at *R1 was significantly different than R3, R4, R5 and R6 (P<0.05).

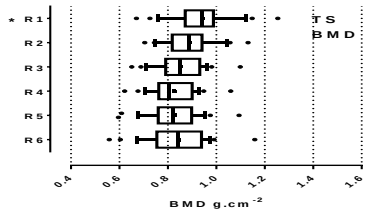

Figure 3.11: (a) BMC in g; (b) EA in cm^2 and (c) BMD in $g.cm^{-2}$ for R1 to R6 vertebrae in LS. [Median (bar), IQR (boxes), 95% (whiskers), mean (+) and outliers (·)]

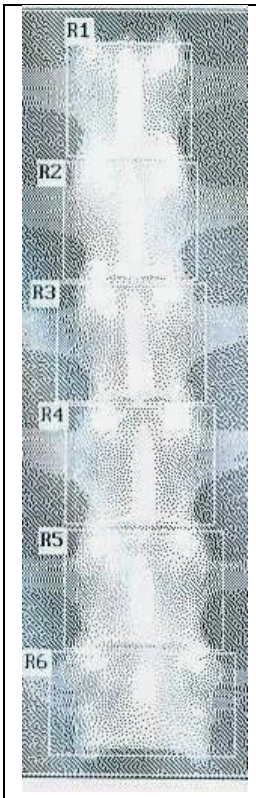

(a) BMC: LS R1 to R6; mean BMC was approximately 12±3g at each level and although the box plot shows a slight increase in median and mean BMC moving caudally from vertebrae R1 to R6, no statistical difference was detected in the amount of mineral at any level (P>0.05).

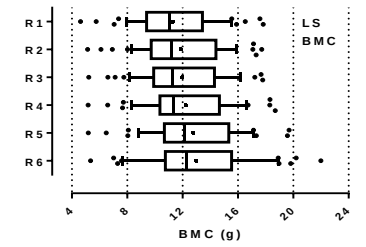

(b) EA: LS R1 to R6; EA increased significantly from R1 to R6. ***R6 was significantly greater than R1 to R4 (P<0.001); ***R5 was significantly greater than R4 (P<0.05) and R1 to R3 (P<0.001); **R4 was significantly greater than R1 to R2 (P<0.01); and, **R3 was significantly greater than R1 (P<0.01).

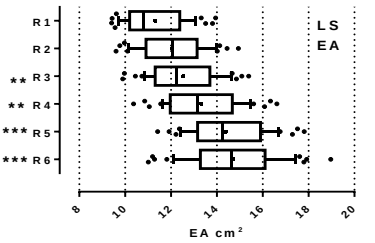

(c) BMD: LS R1 to R6; increasing EA with relatively constant mineral quantity at each level resulted in a slight fall in BMD at each vertebral level in the LS. Statistically, BMD at R5 and R6 were both significantly less than R2 (P<0.05) and R1 (P<0.01), respectively. No other differences were detected between any other levels.

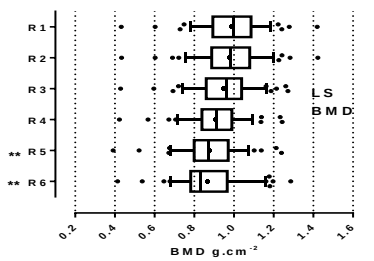

Figure 3.12: (a) BMC in g; (b) EA in cm^2 and (c) BMD in $g.cm^{-2}$ for R1 to R6 regions in FMR. [Median (bar), IQR (boxes), 95% (whiskers), mean (+) and outliers (˙)]

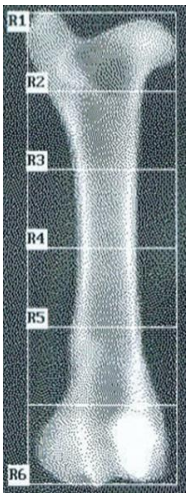

n=76 (M±SD)
Length 188±7mm
Width **(R1)** 65±3mm

(a) **BMC** in FMR: mineral content was similar in mid-shaft and metaphyses, higher proximally in head and neck but greatest in the distal condylar region. R1 had significantly greater BMC than R2 to R4 (*P*<0.001) and R5 (*P*<0.05); R5 was significantly greater than R4 (*P*<0.05); and, R6 was significantly greater than all regions R1-5 (*P*<0.001).

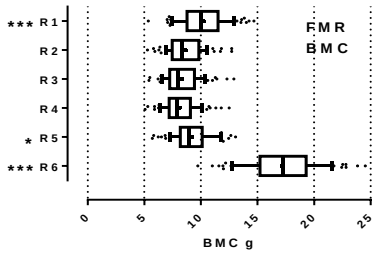

(c) **EA** in FMR. The graphical plot shows and picture shows EA greatest proximally and distally, tapering from the metaphyseal regions to the narrow mid-shaft. Statistically EA at R6 was significantly greater than all regions R1 to R5 (*P*<0.001); R1 was significantly greater than R2 to R5 (*P*<0.001); and R2 and R5 were both greater than R3 to R4 (*P*<0.001).

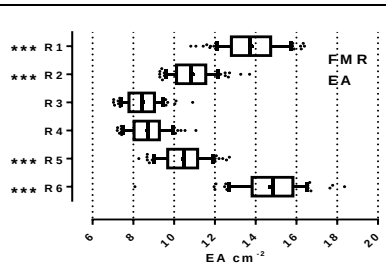

(c) **BMD** distribution in FMR. Lowest BMD occurred proximally and highest was in mid-shaft R3 to R4 and distal condylar region R6. Statistically R6 was significantly greater than R1 to R5 (*P*<0.001); mid-shaft regions R3 and R4 were greater than R1 to R2 and R5 (*P*<0.001); and R5 was greater than R1 to R2 (*P*<0.001).

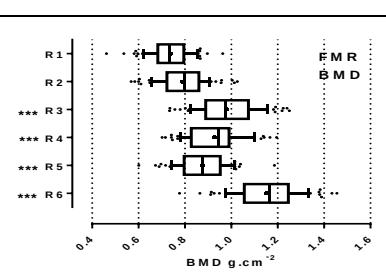

Figure 3.13: (a) BMC in g (b) EA (cm^2) and (c) BMD ($g.cm^{-2}$) for R1 to R6 regions in TBR. [Median (bar), IQR (boxes), 95% (whiskers), mean (+) and outliers (˙)]

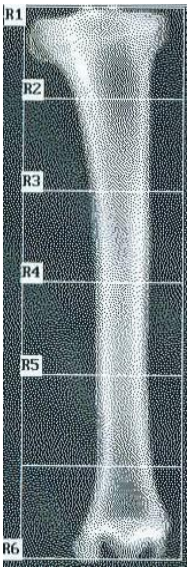

n=76 (M±SD)
Length 211±9mm
Width **(R1)** 55±4mm

(a) BMC in TBR; mineral content was greatest proximally in the tibial plateau region, was similar for all subsequent regions apart from the distal metaphysis. Statistically R1 had greater bone mineral content than all other regions R2 to R6 (*P*<0.001); and R5 also had less mineral content than R2 to R3 and R6 (*P*<0.001) and R4 (*P*<0.05).

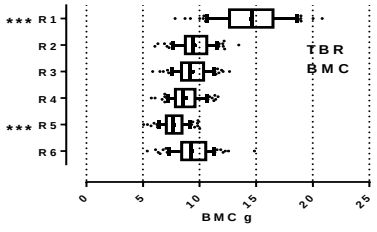

(b) EA in TBR was greatest in the load bearing proximal tibial plateau region, after which EA tapered into the narrow mid-shaft and then expanded distally at the malleolar region. Statistically R1 was greater than all other regions (*P*<0.001); R2 and R6 were greater in area than R3 to R5 (*P*<0.001); and lastly R3 was greater than R4 (*P*<0.05).

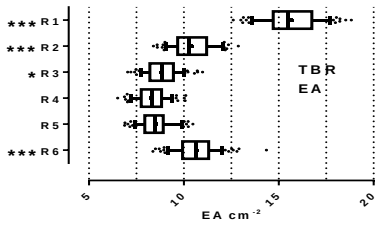

(c) BMD in TBR showed significantly higher BMD at mid-shaft regions than proximal and distal regions. Statistically R3 and R4 BMD was significantly greater than all other regions were (*P*<0.001); the only other difference detected was R6 was significantly greater than R1 (*P*<0.05).

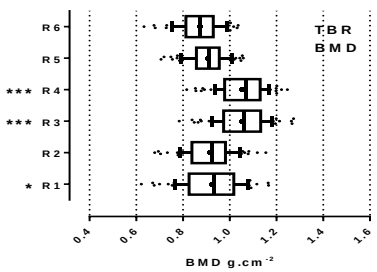

Figure 3.14: (a) BMC in g (b) EA in cm^2 and (c) BMD in $g.cm^{-2}$ for R1 to R6 regions in HMR. [Median (bar), IQR (boxes), 95% (whiskers), mean (+) and outliers (˙)]

n=76 (M±SD)
Length 156±6mm
Width **(R1)** 54±3mm

(a) BMC HMR: Analysis (ANOVA) of mineral content showed R2 and R6 to be significantly greater than R1 and R3 to R5 (P<0.001); R5 was greater than R1, R3 (P<0.001) and R4 (P<0.05); and R4 was greater than R3 (P<0.01).

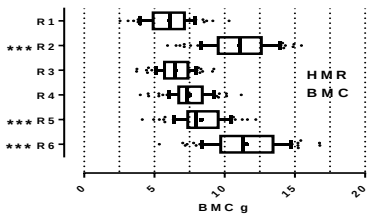

(b) EA HMR: R1, R3 and R5 were of similar area (P>0.05); R4 was significantly less (P<0.001) and R2 significantly greater than all other regions (P<0.001); and R6 was greater than R1, 3, 4 and 5 (P<0.001).

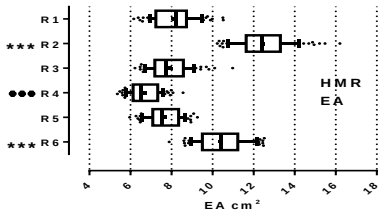

(c) BMD in HMR: When mineral content and area were combined analysis of regional BMD showed no differences between R4 and R6, and R4 to R6 to have significantly higher density than R1 to R3 (P<0.001). In the proximal humeral regions R2 was greater than R3 (P<0.05) and R1 (P<0.001); and R3 was greater than R1 (P<0.01).

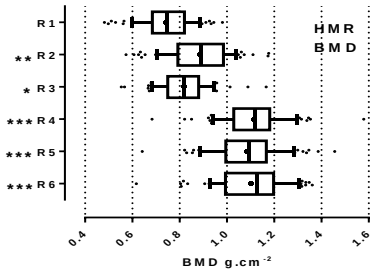

Figure 3.15: (a) BMC in g) (b) EA in cm^2 and (c) BMD in $g.cm^{-2}$ for R1 to R6 regions in RDR. [Median (bar), IQR (boxes), 95% (whiskers), mean (+) and outliers (˙)]

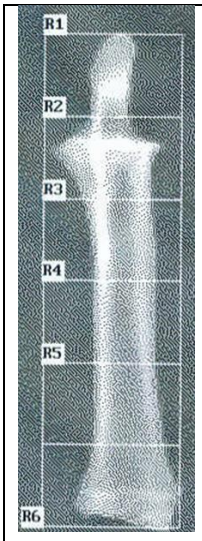

n=74 (M±SD)
Length 199±9mm
Width **(R1)** 40±3mm

(a) **BMC** in RDR: R1 (olecranon) had lower mineral content (P<0.001) and R2 greater mineral content than all other regions (P<0.001). R3 and R6 were greater than R4 to R5 (P<0.001); and R4 was greater than R5 (P<0.01).

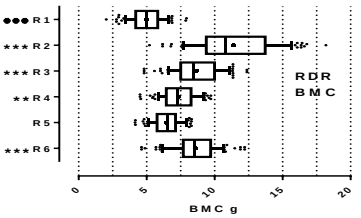

(b) **EA** in RDR: Projected area was less than and greater than all other regions for R1 and R6 respectively (P<0.001); additionally R2 was greater than R3 to R5 (P<0.001); and R3 (P<0.01) and R5 (P<0.001) were both greater than R4.

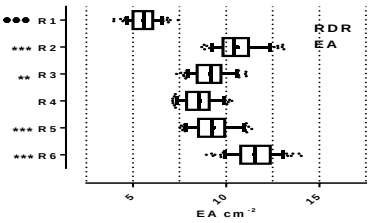

(c) **BMD** in RDR: R5 had lower density than all other regions (P<0.001) except R6; R2 was significantly higher in density than all other regions (P<0.001); R1 was similar in density to R3 and R4 (P>0.05); R3 was greater than R4 and regions R1, R3 and R4 were greater than R6 (P<0.001).

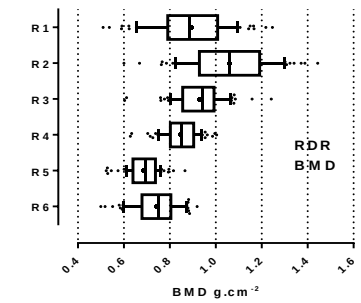

Bone mineral content, projected area, and bone density distribution in the long bones was highly related to morphology; the expected distribution of higher BMD in the mid-shaft regions R3 and R4 and lower BMD in proximal (R1 and R2) and distal (R5 and R6) sub-regions was only seen in the tibia. Distribution of BMD differed from the expected pattern with higher density assessed in distal condylar regions in FMR and HMR, and in RDR higher density proximally due to the presence of a reinforcing ulnar strut.

3.3.8: Region of interest

BMD in regions of high trabecular bone content were further examined in region of interest (ROI) scans within the proximal femur, humerus, tibia and distal radius. Figure 3.16 shows BMD data at the four regions of interest.

Figure 3.16: ROI (r1 to r3) BMD in (a) proximal femur (b) tibial plateau (c) proximal humerus and (d) distal radius. [Median (bar), IQR (boxes), 10-90% (whiskers), mean (+) and outliers (·)]

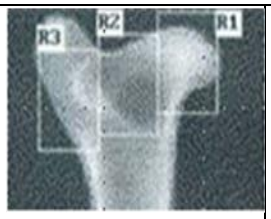	(a) BMD proximal femur: In the head (r1), was significantly greater than both other regions neck (r2) and inter-trochanteric region (r3) (*P*<0.001); the inter-trochanteric region r3 was also greater than r2 (*P*<0.001).	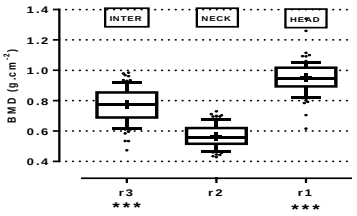
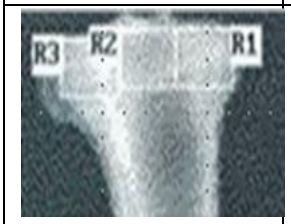	**(b)** BMD tibial plateau: Variation (medial to lateral) across the ovine tibial plateau; r1 and r2 were similar and r1 was significantly lower than r3 (*P*<0.01).	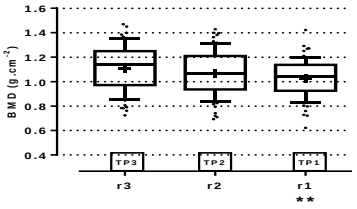
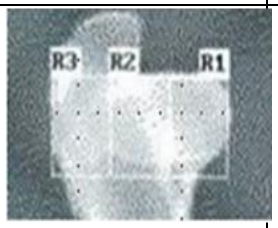	**(c)** BMD proximal humerus: r2 had significantly higher BMD than r1 and r3 (*P*<0.001) and the humeral head r1 was significantly greater than r3 (*P*<0.01).	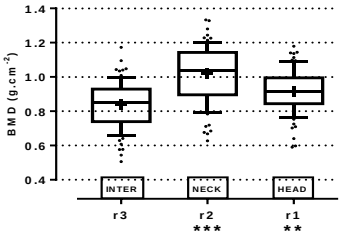
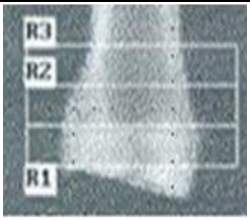	**(d)** BMD distal radius: In the distal epiphyseal region of the ovine radius r1 was significantly higher than r2 and r3 (*P*<0.001).	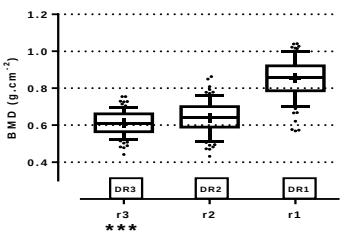

3.3.9: Summary of results

At levels of resolution used for human scanning, no inter-breed differences were detected in DXA derived bone quantity data for whole bone SRA and ROI in this sample of commercially reared Irish sheep. In analysis of seasonal effects (W/S vs. S/A) a difference was apparent within the r2 femoral neck region located in R1 the proximal femur (P<0.05). The relationship of bone quantity variables to animal mass (r^2) was better for BMD (~0.5) than either component of BMD, EA or BMC (~0.3 to 0.4). Correlation of BMD was good across all sites (r>0.7) and especially within the same limb (r >0.9), presumably reflecting similar loading conditions. BMD was evenly distributed from R2 to R6 in TS and in LS there was a gradual reduction in density from R1 to R6. In long bones, high density regions were present in all mid-shaft regions (R3 to R4) with additional high density regions in distal femoral and humeral condyles, and in the proximal radius due the presence of the ulnar reinforcing strut.

3.4: Discussion

The previous study (Chapter 2) highlighted technical and statistical inadequacies in previous validation studies of DXA measurement. This study provides data on effect of breed, seasonal variation, relationship of BMD with body mass, effects of normalisation and standardisation for body mass on bone quantity and profiles of bony quantity data across and within individual sub-regions at spinal and long bone sites. Additional background population data has thus been provided in a wider validation of the ovine large animal model. This study is to the author's knowledge the first to examine bone quantity variables in large *ex-vivo* bone samples from various skeletal sites, over range of body mass, breed and season typical of the normal Irish sheep population.

3.4.1: Sampling

Sampling was at the discretion of the meat rendering facility staff with occasional input from the author to ensure that the range of body mass of animals provided included some animals at the extremes of range of body mass. In earlier comparable studies sample sizes vary; body mass, breed and maturity are not usually stated or

poorly described, and seasonal effects are acknowledged but not accounted for; making the results of some interventional studies difficult to interpret (Newman *et al*., 1995; Turner *et al*., 1995a; Hornby *et al*., 1995). In this study the only information unavailable on the sample selected was the age profile of the sheep, however, according to meat rendering facility staff the animals sampled were all aged ewes 4 to 5 years or older and scan appearances all suggested that animals had reached skeletal maturity. However, determination of the exact age of the sheep scanned was beyond the scope of the study, in Ireland sheep are not tagged at birth and ewes coming to slaughter commercially are usually those that have been reared for commercial lambing (Personal communication, Veterinary Staff, Irish Country Meats, Navan, Ireland).

3.4.2: Inter-breed variation

Data grouped for breed were equally matched for body mass and showed no inter-breed effects in any BMD variables at any site; this is in contrast to the situation in human populations where racial differences are well known, such that in clinical usage for correct interpretation of BMD in Asian, Caucasian, African and Hispanic populations, different reference ranges are required (Cummings *et al*., 2002).

In comparison to previous studies in sheep, data for American ovine BMD (Turner *et al.,* 1995a) were higher; in the proximal femur 0.9 vs. approximately 0.8 $g.cm^{-2}$, distal femur 1.3 vs. approximately 1.2 $g.cm^{-2}$, proximal tibia 1.2 vs. approximately 1.0$g.cm^{-2}$ and proximal humerus 1.0 vs. approximately 0.7$g.cm^{-2}$, however this data could not be matched as body mass was not stated by the authors.

A more valid data comparison to French *in-vivo* DXA data matched to this study for; sample size, body mass, spinal level and partially matched for age, again showed slightly higher BMD of 0.915 vs. 0.842$g.cm^{2}$ and BMC of 36.6 vs. 39.6g (Pouilles *et al*., 2000). In conclusion, with effective matching for body mass and age, inter-breed differences in BMD in Irish sheep showed small insignificant differences, however, further studies would be required to examine variation of DXA derived data before homogeneity of ovine bone density could be confirmed for sheep worldwide.

3.4.3: Seasonal variation

Seasonal variation may theoretically manifest an effect on bone quantity through biological effects of sunlight hours on vitamin D concentration, on circadian rhythms and on cyclical changes in the levels of gonadal hormones during oestrus. In this study whole bone DXA data matched for body mass and grouped according to month and season of sacrifice only showed a statistically significant difference at one selected site, the r2 (neck) a sub-region within the most proximal part of the femur. Animal and human studies highlight seasonal variation as a possible disadvantage for the use of sheep as a large animal model. Human studies have generally shown lower BMD in the winter with fluctuating or no differences in PTH and Vitamin D levels (Overgaard *et al.,* 1988; Rosen *et al*., 1994). However, animal and human studies in extreme northern latitudes have also shown greater BMD changes associated with lower light levels in winter months in voles (Stevenson *et al.,* 2009), alpacas (Parker *et al*., 2002) and in humans (Gerdhem *et al.,* 2004).

In this study of Irish sheep living at typical European latitudes non-significant monthly and seasonal fluctuations in BMD were apparent and one might conclude that as the majority of sites evaluated showed no seasonal difference; that overall, the sheep skeleton is rather impervious to seasonal fluctuations. However, DXA does not delineate between trabecular and cortical bone and perhaps it is not sensitive enough to pick up seasonal changes in all but those sites with high trabecular bone content such as the femoral neck in our study. Arens *et al.* (2007) used pQCT to assess trabecular bone separately longitudinally, and reported higher BMD data during spring and summer months.

3.4.4: Body mass and bone density

In multiple linear regression models adjusted for age, oestrogen use and other lifestyle factors in women, total body mass and measures of body size seem to be the most consistent markers of bone mineral density at weight-bearing sites in the human skeleton, implying a mechanical effect of body mass on BMD (Edelstein & Barrett-Connor, 1993). In humans measures of body mass and body mass index have also been shown to account for between 9 to 20% of the variance in BMD for all sites (Felson *et al.,* 1993).

Genetic studies of BMD in Copworth sheep (Campbell *et al.,* 2000) documented that bone quantity was significantly correlated with muscle mass and body mass; and in the present study body mass accounted for between approximately 40 to 50% of the variance in BMD at four weight bearing long bone sites and at the lumbar spine. However, in the lower thoracic spine r^2 was much lower (30%) perhaps implying that this part of the spine in a sheep bears less load. Higher coefficients of determination could have resulted from quantification of factors such as age, diet and loading environment into a multiple regression analysis model, however, this was beyond the scope of the present study.

3.4.5: Effect of normalisation

When BMC (g) is divided by the projected area (cm^2) the computed data for bone quantity is essentially normalised by dividing by a measure of bone size at that particular site, the projected area, thus BMD is in itself is a form of "normalised" data. Further or alternative normalisation and standardisation procedures in this study by division of BMC and BMD by body mass, carcass mass a measure of lean body mass or standardising to a body mass of 70kg had no effect on inter-site differences in BMC and BMD. In human bone densitometry research, to account for differences in bone size and increase the predictive value of BMD in prediction of bone strength, various methods of normalisation have been employed. Various human studies have attempted to reduce the erroneous effects of bone size by normalizing area BMD measurement with an additional bone dimension from MRI scans and standard radiographs to generate estimated volumetric densities which aid prediction of bone strength in growing skeletons (Kröger *et al.,* 1995; Jiang *et al.,* 2000).

In another human study, Pors Nielsen *et al.* (1998) recommend either division of BMC or BMD data by body surface area or the square root of body surface area respectively, in order to normalise bone quantity in the lower and upper quartiles of body size. Whereas further measurements of the bones used in this study were possible it was beyond the scope of this current study, but the effect of normalisation procedures on BMD will be re-examined again in later chapters evaluating ovine bone quantity data in relation bone strength.

3.4.6: Correlation of bone quantity data between sites

The highest correlations of bone quantity between sites in the current study were detected between bones of the same limb, presumably a reflection of the same loading conditions. Correlation of bone quantity between and across sites *in-vivo* and *ex-vivo* has previously been reported (Turner *et al.*,1995a) and although correlation was higher overall in this *ex-vivo* study 'r' data were reasonably similar with higher association between vertebrae and lower correlation between vertebrae and long bone sites. Unfortunately, unlike Turner *et al.* (1995a) we did not perform an analysis of the sheep calcaneus which would be an easily scanned bone in live sheep which could provide a readily accessible site to follow bone density in further longitudinal studies.

3.4.7: Distribution of bone density

In a profile of bone density in skeletally mature Irish females (age range 25 to 30yr) Donne *et al.* (1996) reported mean (±SD) BMD to be 1.027±0.102 $g.cm^{-2}$ in the lumbar spine and 0.869±0.124 $g.cm^{-2}$ in the proximal femur. In this study standardised ovine BMD were 0.955±0.219 $g.cm^{-2}$ in the lumbar spine and 0.776 ± 0.196 $g.cm^{-2}$ in proximal femur. Thus ovine BMD data were reasonably similar to human data in the lumbar spine but were lower in the proximal femur again presumably reflecting different loading conditions at the femoral neck in bipeds and quadrupeds. Bone density distribution down the length of the lumbar spinal and long bone samples were in keeping with bone shape, size and function as they relate to the position in the sheep skeleton, with the longer tibia and radius showing more similar features than the femur and humerus.

In the spinal samples, vertebral aBMD was similar in the lower six thoracic vertebrae, however, down the length of the lumbar spine aBMD gradually diminished as the vertebrae got wider and a similar mineral content in each was distributed over a greater area; in the long bones mineral density was generally highest in the mid-shaft and lower in condylar regions but there were notable exceptions partly due to positioning of sub-regional scan boxes and partly due to shape of bony struts or processes.

3.4.8: Limitations of the study

In the interbreed analysis the sample size was possibly too small in some groups, power analysis in the previous study would indicate at least 20-30 animals in each breed would be necessary to show beyond doubt that breed differences do not exist. However, sample size did not restrict the seasonal analysis as there were adequate numbers in the winter/spring and summer/autumn groups. In the sub-regional analysis strict application of six equal length boxes did not necessarily capture anatomically regions in more atypical long bones, in retrospect it would possibly have been more beneficial perhaps to have five sub-regions, two each for proximal epiphysis and diaphysis regions, and one box to capture the mid-shaft region.

3.4.9: Conclusions

1. Despite the limitations alluded to above this is the first systematic evaluation of bone density in the ovine skeleton. Although incomplete in some aspects as it was not necessarily the primary focus of the overall work, this study provides a useful template of wider DXA validation procedures.

2. The study showed no substantive inter-breed variation in aBMD across the range of breeds seen in this sample of Irish sheep, however sample size for some breeds was small and it is still recommended that future researchers use the same breed of animal whenever possible in longitudinal studies.

3. A small seasonal effect was seen toward lower aBMD in Spring months when compared to late Summer Autumn. This was statistically significant at the proximal femoral site. In agreement with recommendations of previous research to maximise inter-group differences between bone wasting treatments and control animals in future longitudinal studies researchers should time sacrifice of animals for Spring months rather than late Summer months.

4. The BMD to body mass relationship charted for whole bone samples at six ovine skeletal sites; at a sub- regional level for individual vertebrae and six long bone sub-regions to provide a preliminary basic set of reference standards for ovine BMD across body mass for future comparative cross-sectional and longitudinal studies involving *ex-vivo* ovine bone.

CHAPTER 4

Short and long term effects of ovariectomy on ovine bone density

4.0: Summary / abstract

The ovariectomised sheep was initially thought a suitable large animal model for the study of human osteoporosis. However to date, *in* and *ex-vivo* studies of post-ovariectomy ovine bone density measured by DXA have only demonstrated small or inconsistent changes in BMD in timeframes suitable for research. This study aimed to systematically evaluate; at more than three skeletal sites, over a longer duration than previously studied and over DXA measurement ranges used in human osteoporosis; the effects of ovariectomy and an anti-resorptive drug in the ovine animal model. Seventy five healthy mature mixed breed ewes were randomised into two groups control (CON) and ovariectomy (OVX) for sacrifice at 12 (Y1) and 31 month (Y3); in the 31 month group, 4 OVX animals were withdrawn creating a fifth group which was treated with the long acting bisphosphonate, zoledronic acid (ZOL). *Ex-vivo* ovine bone density of lumbar spine, femur, tibia, humerus and radius were assessed using a Hologic QDR 4500 DXA scanner at whole bone (WB), sub-regional (R1-6) and within regions of interest (r1-3). Y1 and Y3, control and OVX data were analysed using 2 way ANOVA with *post-hoc* analysis using Tukey multiple comparison tests for effect of; time, treatment and interaction effects. Y3 data were further analysed across group (CON vs. OVX vs. ZOL) using Mann Whitney U tests with Bonferroni correction. Significant differences where detected were compared to scanner (95% LOA) measurement limits and for effect size (Cohen's d). No OVX effect on BMD was detected in WB at any site or any time point; however, moderate OVX effects were detected at Y3; of decreased BMD at the proximal humeral sites R1, r2 and r3; and an unusual finding of increased BMD at the tibial mid-shaft site R4. Although outside scanner measurement limits and of large effect size (d>0.9), proximal humeral changes were less than the -2.5 SD from the mean which define DXA diagnosis of osteoporosis in humans. In the ZOL analysis, the greatest BMD differences were detected between OVX and ZOL in WB, multiple regions within forelimb long bones and femoral mid-shaft, but not the spine. The results of the study suggest future research of bone quantity and quality relationships use the proximal humerus as this may be a more sensitive site to hormonal bone wasting effects of OVX. In respect to ZOL, again forelimb bones, humerus and radius, rather than the hind limb and spine are the optimal sites for further multi-disciplinary evaluation.

Key words: DXA, ovariectomy, sheep, zoledronic acid

4.1: Introduction

The ovariectomised (OVX) sheep model is purported to be a suitable large animal model of osteoporosis, due to cost, ease of handling in flock conditions, spontaneous ovulation, similar hormonal changes to humans during oestrus, and impaired remodelling post ovariectomy (Newman *et al*., 1995). In clinical assessment of human osteoporotic fracture risk, the need to treat is based on combination of individual clinical risk factors and DXA derived aBMD compared to population data at typical sites; usually proximal femora and lumbar spine (Kanis, 2002). Thus further criteria for clinical acceptability of sheep as a large animal model of osteoporosis should also include; easily quantifiable loss of bone mass post-ovariectomy (OVX) to differentiate between OVX and sham operated animals, no long term regain in bone mass post-ovariectomy and DXA quantifiable responses to a therapeutic agent known to ameliorate loss of bone mass or augment bone mass in human populations (Mosekilde, 1995).

DXA has been used to evaluate ovine bone density *in-vivo* post OVX at easily accessible skeletal sites such as the lumbar spine and calcaneus; unfortunately, longitudinal *in-vivo* studies of sheep bone at sites typical of human osteoporosis like the hip and spine are difficult due to imprecision (Turner, 1995a). Other confounding variables that have limited earlier studies include; small group sample sizes, difficulty with accurate repeat positioning of animals under anaesthesia, wide inter-animal variability in bone mass at baseline and changes in body mass over time (Hornby *et al*., 1995; Turner *et al*., 1995b; Turner *et al*., 1995c). Hornby *et al.* (1995) have also suggested that longitudinal sheep OVX studies take into account seasonal variations in BMD, recommending that OVX be performed in the summer months, and that BMD changes post-OVX may only be optimal in ewes aged seven years or older.

Results of previous studies charting *in-vivo* densitometric changes in ovine bone mass post-OVX have shown no major detectable changes or inconsistent results particularly in the lumbar spine (Turner *et al.,* 1995c; MacLeay *et al*., 2004 a, b). In the study by Turner *et al*. (1995c) small *in-vivo* vertebral changes detected by DXA at one vertebral level at six and twelve month were not detected at adjacent levels, over the lower three lumbar vertebrae when pooled together. Furthermore no significant differences in BMD were detected at long bone sites *ex-vivo* such as the proximal and distal femur, proximal tibia, and proximal humerus.

In later longitudinal *in-vivo* studies, as well as OVX, many researchers have incorporated bone wasting measures into their study design such as; steroid therapy, dietary induced acidaemia or calcium and vitamin D depletion diets. These additional measures have been necessary in order to produce DXA detectable BMD changes in the short term of similar magnitude to those seen in humans over several years characterising osteoporosis (MacLeay *et al*., 2003a,b; Lill *et al*., 2002a,b). Although these types of additional measures have induced significant decrements in bone quantity detectable by DXA, it is uncertain whether accompanying histomorphometric and mechanical changes would reflect those produced over the more insidious time course causing osteoporosis.

Bisphosphonates are pyrophosphate analogues, with the length and structure of the carbon side chains determining their potency. Oral bioavailability is low (<3%) being impaired by food, calcium, iron, coffee, tea and orange juice; but once absorbed they disappear rapidly from plasma, partly by binding to bone apatite and partly by renal excretion (Lin , 1996). In bone when liberated from apatite, they inhibit osteoclastic activity by; direct effects decreasing cellular metabolism and increasing apoptosis, and indirect effects by reducing recruitment. Newer more potent, amino-bisphosphonates such as zoledronic acid are now also known to inhibit the enzyme farnesyl pyrophosphate synthase (FPS). FPS is a key enzyme involved in biosynthesis of isoprenoids, compounds which regulate activity of guanosine triphosphate (GTP)-binding proteins, which are themselves key regulators of osteoclast activity (Graham & Russell, 2007). Bone absorption and renal excretion of bisphosphonates vary widely, however, bisphosphonates show no evidence of metabolism and thus renal excretion is the only route of elimination (Lin, 1996). In humans, bisphosphonates have been used as anti-bone resorptive medications for over 30 years; they are usually well tolerated albeit with mild gastrointestinal side effects. Serious side effects are rare but bone mineral defects and cardiac arrhythmias such as atrial fibrillation especially in patients with poor renal function have been reported with long-term use (Delmas, 2002).

In osteoporosis, anti-fracture efficacy is a major outcome measure and for the amino-bisphosphonates, namely; ibandronate and clodronate, there is strong evidence for reduction in vertebral and femoral neck fractures in human populations (McClung, 1996). Despite proven efficacy, compliance with oral bisphosphonates remains a

problem as they have to be taken for up to 3 years. However, long acting bisphosphonates like zoledronic acid can be given by infusions and promising initial short-term studies which showed decreased bone turnover and improved bone density after 12 month are now supported by evidence from a long-term, multicentre, randomized, double-blind, placebo-controlled study of women with post-menopausal osteoporosis showing single annual infusions of zoledronic acid (5 mg) for 3 years to be highly effective with a 35% risk reduction in fractures (Lyles *et al*., 2007). In large animal studies zolendronic acid has many advantages; it can be given by infusion avoiding poor bioavailability by the oral route, has a reasonable side effect profile, and re-distributes to bone its main site of action. Final criteria for acceptability of the ovine model would be to see OVX induced bone wasting effects reversed or prevented by such a therapeutic agent.

This study was part of the multidisciplinary 'Bone for Life' project, a series of collaborative studies in an ovariectomised sheep model of osteoporosis. A schematic overview of the project is shown in Figure 4.1. 'Bone for Life' project aims were to further elucidate bone quality and quantity relationships to bone strength through evaluation of bone quantity (DXA), histomorphometric analysis of ultra-structure (μCT) and remodelling (fluorescin dyes) and strength (various mechanical tests).

The specific aims of this DXA study were to systematically evaluate short- and long-term effects of ovariectomy on *ex-vivo* bone from spinal and long bone sites in the ovine skeleton at the three levels of analysis possible with DXA; whole bone (WB), equal length sub-regions (SRA) and within sub-regions of interest possessing high trabecular bone content (ROI). The final aim was to evaluate the effect of a long acting anti-osteoclastic bisphosphonate drug, zoledronic acid (ZOL).

Figure 4.1: Overview of the research components of the 'Bone for Life' Project

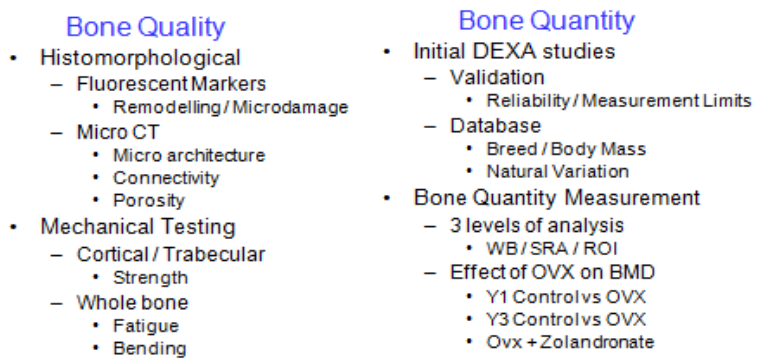

4.2: Methods

4.2.1 Animal selection and randomisation

Seventy five skeletally mature healthy Irish ewes aged between 5 and 8 years and of mixed breeds were selected for the study after purchase at local auction. Ewes were randomised to control group (CON) or to undergo ovariectomy (OVX); and then further sub-divided into four discrete groups with sacrifice at 12 (Y1) and 31 month (Y3).

4.2.2 Operative procedures, animal care and sacrifice

Ethical approval, animal husbandry, operative procedures, routine veterinary checks and fluorochrome dye injection procedures were all conducted and overseen by the staff of the University College Dublin, School of Veterinary Sciences (Lyons Estate, Newcastle Co. Kildare) under Department of Health license (No. B100/2443). A total of 38 animals underwent ovariectomy between the 17th and 21st of November 2003. All animals were housed and pastured in the same conditions over the time course of the study until sacrifice at a local meat rendering facility (Irish Country Meats, Navan, Co. Meath). Animal anaesthesia, ovariectomy, post-operative care procedures and subsequent fluorochrome dye injections, part of parallel studies on bone remodelling and microdamage are shown in Appendix 4. On the 22nd of November 2004, all the animals from the 12 month group were sacrificed and on 19th of June 2006, all 31 month animals were sacrificed.

4.2.3 Long acting anti-resorptive drug

In order to examine the effect of the anti-resorptive drug zoledronic acid a preliminary pharmokinetic study was conducted on five animals not part of the subsequent ovariectomy study. This preliminary study showed no adverse effects on serum calcium levels, cardiac, renal or liver function; all previously reported side effects of bisphosphonate treatment (Brennan, 2008). Subsequently four OVX sheep from the 31 month group were selected for injection of long acting bisphosphonate zoledronic acid (ZOL). Animals each received 5mg of zoledronic acid in 100mL of saline by infusion over 30 min via an indwelling jugular catheter. The infusion was repeated

weekly until all animals had received a total cumulative dose of 25mg of zoledronic acid.

4.2.4 Skeletal sites, sample preparation and data acquisition scan (WB)

Ex-vivo bones from five skeletal sites; the lower six lumbar vertebrae and right femur (FMR), tibia (TBR), humerus (HMR) and radius (RDR) were selected for DXA scanning. Following dissection of soft tissues, samples were positioned in a Perspex tank containing normal saline on the scanning platform of a Hologic QDR 4500 DXA scanner. A whole bone sample (WB) or data acquisition scan was performed, proximal to distal (T1) and distal to proximal (T2), generating estimated area projection (EA in cm^{-2}), bone mineral content (BMC in g) and bone mineral density (BMD in $g.cm^{-2}$) data.

4.2.5 Analysis of sub-regions (SRA) and regions of interest (ROI)

The Hologic human lumbar spine algorithm was used to analyse bone quantity in individual vertebrae or six equal length sub-regions (R1 to R6), and a further three smaller region of interest analyses (r1 to r3) within long bone regions of high trabecular bone content; R1 for FMR, TBR, HMR and R6 for RDR. All scan box sizes in SRA were relative to individual bone length and width and for ROI were relative to size of the scan box from which they were derived.

4.2.6 Data analysis

Data were grouped and tabulated on Excel spread sheet, underwent data cleaning and then were analysed Sigma Stat 3.5 statistical analysis software (Systat Software, Point Richmond, California). Data sets were analysed for normality using the D'Agostino and Pearson omnibus test; any non-normal data sets were re-analysed after logarithmic transformation. Non-repeated measures 2 way ANOVA was then used to test for effect of time, treatment (OVX) and treatment by time interaction; $P<0.05$ was considered significant. Where significant differences were detected *post-hoc* analysis was performed using Tukey multiple comparison tests. For Y3 ZOL data comparisons, where sample size in ZOL was very small, statistical comparison across groups was performed using the Mann Whitney U test with Bonferroni correction to account for the number of groups and $P<0.0166$ was therefore

considered significant. On completion of analysis for significant differences across groups the mean differences across groups were compared to the scanner measurement limits for each site and were also analysed for effect size using Cohen's 'd' statistic.

4.3: Results

4.3.1 Drop outs

A total of 10 animals died during the time course of the study; three OVX animals (4325, 4327 and 4330- see Chapter 4 Appendices) died following the initial surgical procedure. In 2004, a control animal (4336) died and OVX sheep (119) died of natural causes. In the 31 month group, one control animal (4351) died in February 2005 and an OVX animal (4338) died in May of 2006, again from natural causes. In December 2005 and January 2006, three animals (191, 4499 and 4477) became feverish and lethargic, unfortunately despite isolation and further veterinary care all three animals subsequently died. In view of this all remaining animals from the Y3 group underwent microbiological testing for common pathogens, and none were detected. Subsequent post-mortems revealed septicaemia in one animal and no obvious cause of death in the two others. In Y3, six animals were withdrawn (2 CON and 4 OVX) for a study into the effects of a long acting anti-resorptive bisphosphonate drug (ZOL). Two animals from the control group were used for a further pharmokinetic evaluation and four OVX animals received supra-physiological doses of zoledronic acid to study the effects of osteoclast inhibition in the ovariectomised animals. The total number of animals reaching sacrifice and whose results underwent statistical analysis therefore were 34 (18 CON and 16 OVX) at Y1 (12 month); and: 31 (16 CON and 11 OVX) plus 4 ZOL at Y3 (31 month).

4.3.2 Body mass

There were highly significant increases in body mass over time in both groups of equal magnitude ($P<0.001$), body mass changes in CON and OVX for both Y1 and Y3 are shown in Figure 4.3. No significant difference in body mass was apparent between groups at any time point, however, statistical analysis (ANOVA) revealed highly significant increase in body mass ($P<0.001$) between Y1 and Y3 at sacrifice,

and further *post-hoc* analysis (Tukey) revealed significant changes in both groups (+10kg) individually over time (CON; P=0.003, OVX; P=0.007).

Figure 4.3 Mean ± SEM body mass (kg) (a) across time and (b) comparison of body mass at sacrifice for CON and OVX, Y1 and Y3.

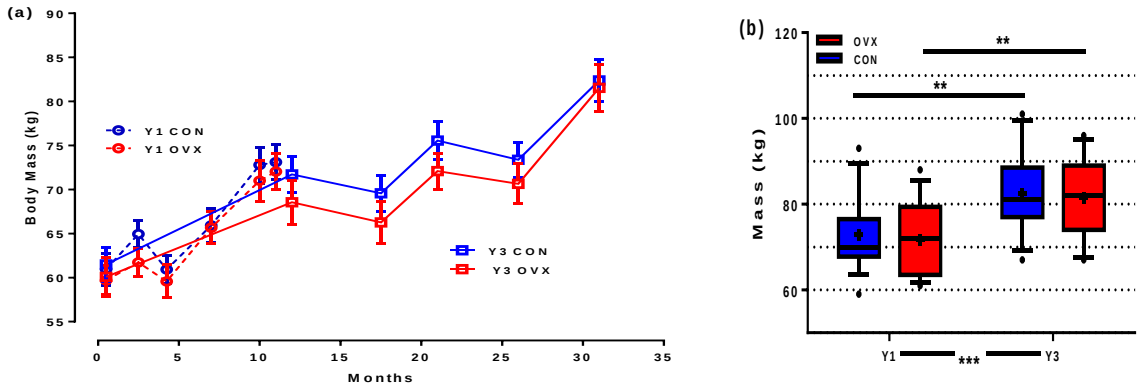

4.3.3 Whole bone sample data acquisition scan results

The results of whole bone (WB) analysis for estimated area (EA in cm^2), bone mineral content (BMC in g) and (BMD in $g.cm^{-2}$) are presented in Figure 4.4. At all sites no significant changes were detected in EA apart from HMR; however, there were changes in BMC and BMD. In whole bone BMC data, BMC was significantly greater in the Y3 animals at all sites except for FMR; *post-hoc* analysis identified this as primarily a group time effect at all sites except RDR where the difference was due to change in OVX. For whole bone sample BMD data a similar pattern to BMC emerged with significant group time effects at all sites except the femur and following *post-hoc* analysis of the group time effect, differences were attributed to OVX in LS and TBR and in both CON and OVX in RDR. Mean EA, BMC and BMD data normalised for body mass are presented in Figure 4.5.

Data normalisation had varying effects at different sites; in EA (cm^2), where there were no differences in the raw data across time, the effect of dividing by the greater Y3 body mass, as expected normalised EA ($cm^2.kg^{-1}$) was significantly lower at Y3 compared to Y1 at all sites. In the normalised BMC data there were no differences in LS, HMR and TBR; significantly smaller $BMC.kg^{-1}$ in FMR CON at Y3 and in RDR significantly greater $BMC.kg^{-1}$ in both CON and OVX at Y3. In the aBMD data normalisation for body mass nullified differences in raw BMD data seen across time in LS and RDR, but in FMR, HMR and TBR significant group time reductions became apparent at Y3.

Figure 4.4: Whole bone (a) BMC (b) EA and (c) aBMD in 6 vertebrae LS, and long bone sites FMR, TBR, HMR and RDR for CON and OVX at Y1 and Y3. [Mean (+), Median (bar), IQR (boxes), 10-90% (whiskers), outliers (·), and data tables in Appendix 4.2]

<table>
<tr>
<td> 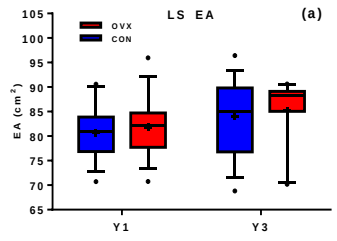
</td>
<td> 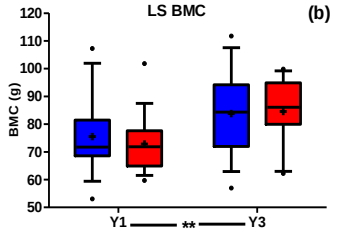
</td>
<td> 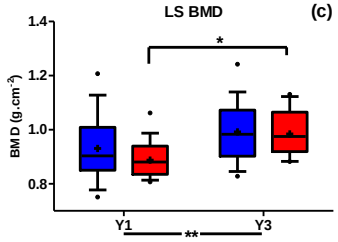
</td>
</tr>
<tr>
<td>All: group time ^{ns} OVX ^{ns} inter ^{ns}
Post hoc: CON time ^{ns} OVX time ^{ns}</td>
<td>All: group time ^{P<0.01} OVX ^{ns} inter ^{ns}
Post hoc: CON time ^{ns} OVX time ^{P=0.07}</td>
<td>All: group time ^{P<0.01} OVX ^{ns} inter ^{ns}
Post hoc: CON time ^{ns} OVX time ^{P=0.02}</td>
</tr>
<tr>
<td> 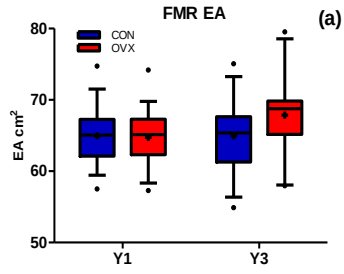
</td>
<td> 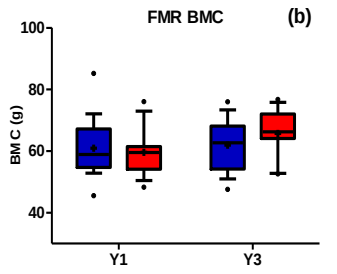
</td>
<td> 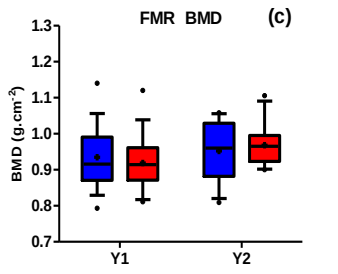
</td>
</tr>
<tr>
<td>All: group time ^{ns} OVX ^{ns} inter ^{ns}
Post Hoc: CON time ^{ns} OVX time ^{ns}</td>
<td>All: group time ^{ns} OVX ^{ns} inter ^{ns}
Post Hoc: CON time ^{ns} OVX time ^{ns}</td>
<td>All: group time ^{ns} OVX ^{ns} inter ^{ns}
Post Hoc: CON time ^{ns} OVX time ^{ns}</td>
</tr>
<tr>
<td> 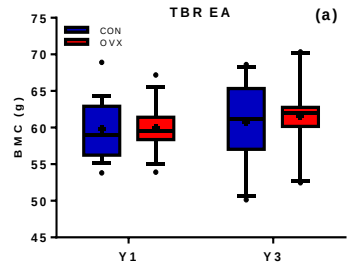
</td>
<td> 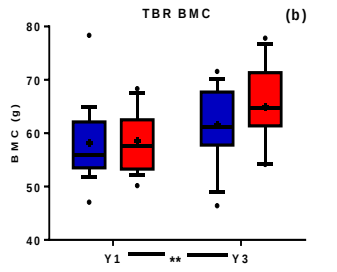
</td>
<td> 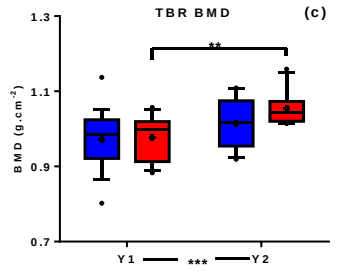
</td>
</tr>
<tr>
<td>All: group time ^{ns} OVX ^{ns} inter ^{ns}
Post Hoc: CON time ^{ns} OVX time ^{ns}</td>
<td>All: group time ^{P<0.01} OVX ^{ns} inter ^{ns}
Post Hoc: CON time ^{ns} OVX time ^{ns}</td>
<td>All: group time ^{P<0.01} OVX ^{ns} inter ^{ns}
Post Hoc: CON time ^{ns} OVX time ^{P<0.01}</td>
</tr>
<tr>
<td> 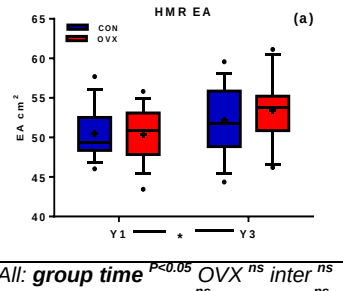
</td>
<td> 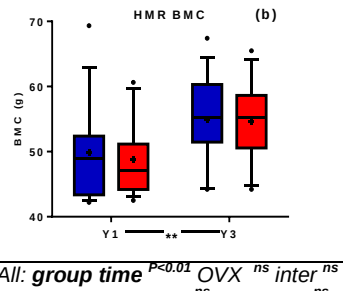
</td>
<td> 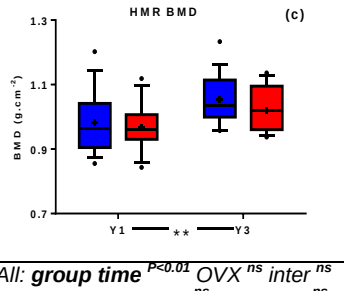
</td>
</tr>
<tr>
<td>All: group time ^{P<0.05} OVX ^{ns} inter ^{ns}
Post Hoc: CON time ^{ns} OVX time ^{ns}</td>
<td>All: group time ^{P<0.01} OVX ^{ns} inter ^{ns}
Post Hoc: CON time ^{ns} OVX time ^{ns}</td>
<td>All: group time ^{P<0.01} OVX ^{ns} inter ^{ns}
Post Hoc: CON time ^{ns} OVX time ^{ns}</td>
</tr>
<tr>
<td> 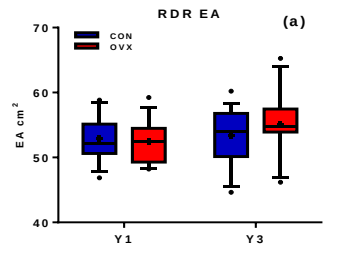
</td>
<td> 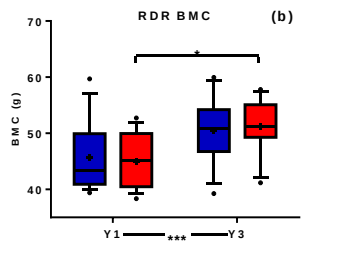
</td>
<td> 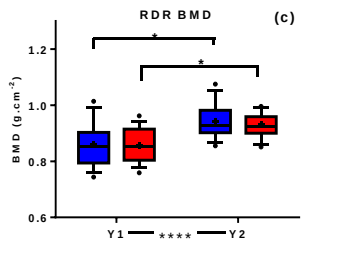
</td>
</tr>
<tr>
<td>All: group time ^{ns} OVX ^{ns} inter ^{ns}
Post Hoc: CON time ^{ns} OVX time ^{ns}</td>
<td>All: group time ^{P<0.01} OVX ^{ns} inter ^{ns}
Post Hoc: CON time ^{ns} OVX time ^{P<0.05}</td>
<td>All: group time ^{P<0.01} OVX ^{ns} inter ^{ns}
Post Hoc:CON time ^{P<0.05}OVX time ^{P<0.05}</td>
</tr>
</table>

Figure 4.5: whole bone (a) EA, (b) BMC and (c) BMD in LS FMR, TBR, HMR and RDR for CON and OVX at Y1 and Y3 normalised for body mass (data.kg^{-1}). [Mean (+), Median (bar), IQR (boxes), 10-90% (whiskers), and outliers (·), data tables in Appendix 4.2]

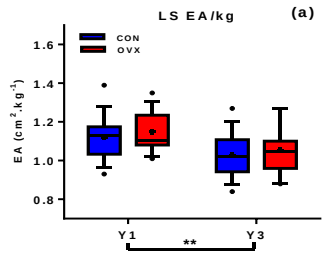	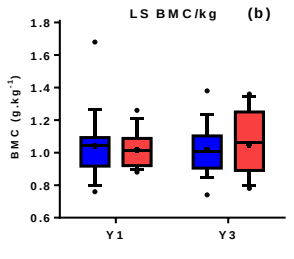	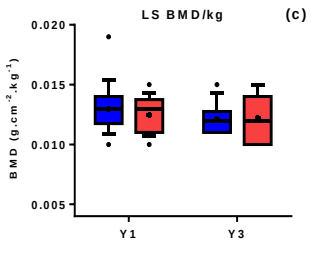
*All: **group time** $^{P<0.01}$ OVX ^{ns} inter ^{ns}* *Post hoc: CON time ^{ns} OVX time ^{ns}*	*All: group time ^{ns} OVX ^{ns} inter ^{ns}* *Post hoc: CON time ^{ns} OVX time ^{ns}*	*All: group time ^{ns} OVX ^{ns} inter ^{ns}* *Post hoc: CON time ^{ns} OVX time ^{ns}*
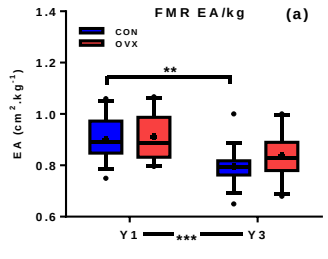	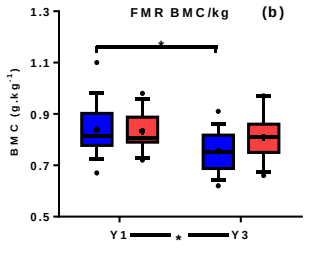	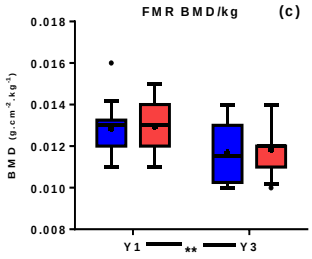
*All: **group time** $^{P<0.001}$ OVX ^{ns} inter ^{ns}* *Post Hoc: **CON time** $^{P<0.01}$ OVX time ^{ns}*	*All: **group time** $^{P<0.05}$ OVX ^{ns} inter ^{ns}* *Post Hoc: **CON time** $^{P<0.05}$ OVX time ^{ns}*	*All: **group time** $^{P<0.01}$ OVX ^{ns} inter ^{ns}* *Post Hoc: CON time ^{ns} OVX time ^{ns}*
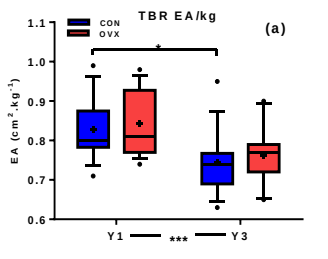	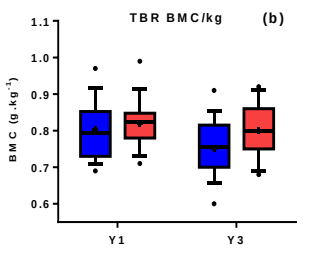	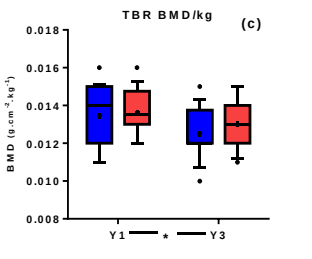
*All: **group time** $^{P<0.001}$ OVX ^{ns} inter ^{ns}* *Post Hoc: **CON time** $^{P<0.05}$ OVX time ^{ns}*	*All: group time ^{ns} OVX ^{ns} inter ^{ns}* *Post Hoc: CON time ^{ns} OVX time ^{ns}*	*All: **group time** $^{P<0.05}$ OVX ^{ns} inter ^{ns}* *Post Hoc: CON time ^{ns} OVX time ^{ns}*
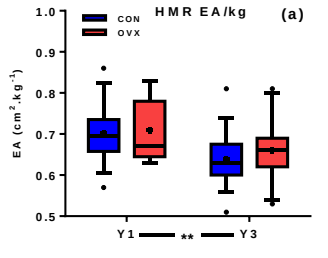	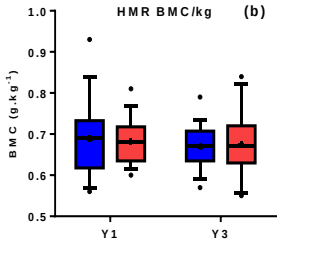	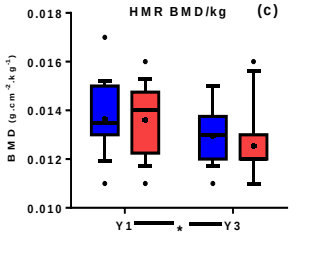
*All: **group time** $^{P<0.01}$ OVX ^{ns} inter ^{ns}* *Post Hoc: CON time ^{ns} OVX time ^{ns}*	*All: group time ^{ns} OVX ^{ns} inter ^{ns}* *Post Hoc: CON time ^{ns} OVX time ^{ns}*	*All: **group time** $^{P<0.05}$ OVX ^{ns} inter ^{ns}* *Post Hoc: CON time ^{ns} OVX time ^{ns}*
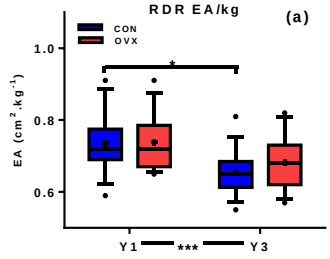	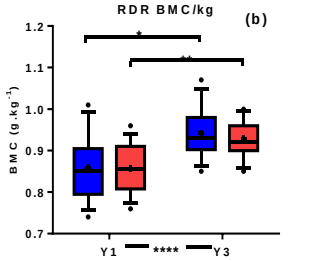	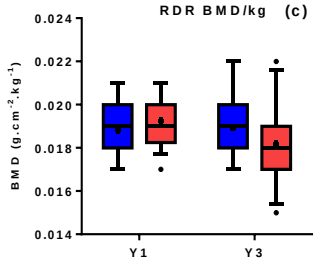
*All: **group time** $^{P<0.001}$ OVX ^{ns} inter ^{ns}* *Post Hoc: **CON time** $^{P<0.05}$ OVX time ^{ns}*	*All: **group time** $^{P<0.001}$ OVX ^{ns} inter ^{ns}* *Post Hoc: **CON time** $^{P<0.05}$ **OVX time** $^{P<0.01}$*	*All: group time ^{ns} OVX ^{ns} inter ^{ns}* *Post Hoc: CON time ^{ns} OVX time ^{ns}*

4.3.4 Sub-regional analysis results

BMD results for six sub-regions in spinal and long bone sample at Y1 and Y3 in CON and OVX animals are presented in Figures 4.6 to 4.10. For each site the sub-regions are represented from proximal to distal and to allow for ease of comparison across time. Y1 and Y3 results are represented on the same X-axis scale for each site. Results of statistical analysis (2-Way ANOVA with Tukey *post-hoc* analysis) for each sub-region are shown in the accompanying Table for each Figure, any non-parametric data underwent log^{10} transformation and were re-analysed. The primary aim of analysis was to identify sites in the axial and proximal sheep skeleton most affected by the OVX intervention.

Figure 4.6: Sub-regional BMD Lumbar Spine R1 to R6 at time points Y1 and Y3.
[Median (bar), IQR (boxes), 10-90% (whiskers), mean (+) and outliers (˙), data table in Appendix 4.2]

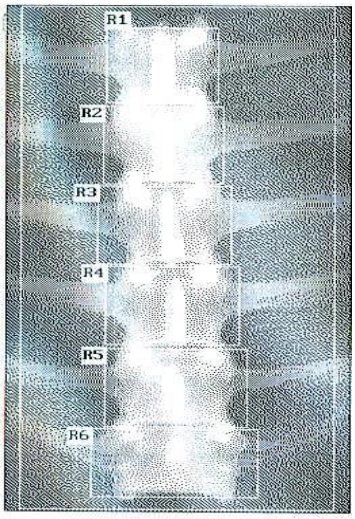

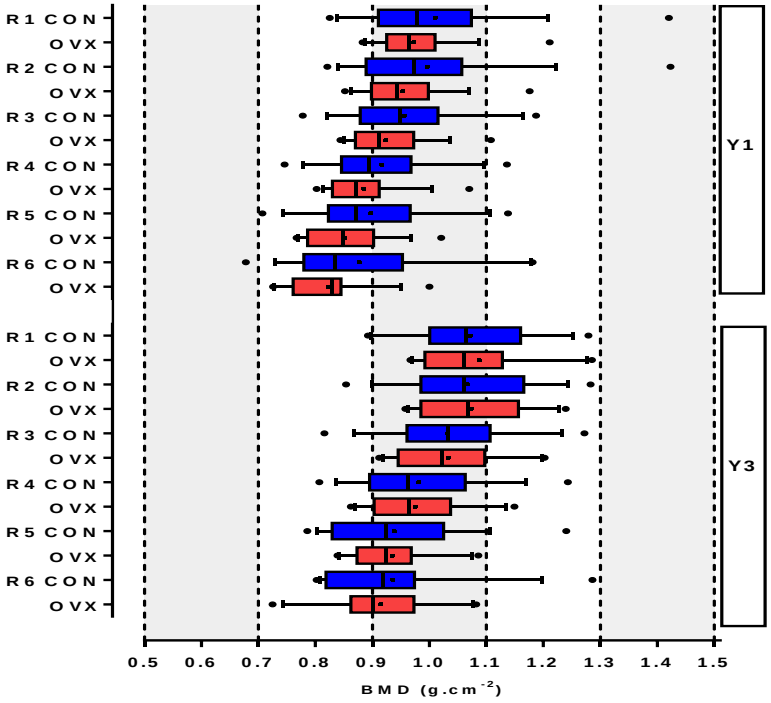

R	INT[n]	OVX	Time
1	ns	ns	<0.01 OVX
2	ns	ns	<0.01 OVX
3	ns	ns	<0.05 CHO
4	ns	ns	<0.05 OVX
5	ns	ns	<0.05 OVX
6	ns	ns	<0.05 OVX

Analysis of sub-regional BMD of the lumbar spine R1 to R6 revealed no significant difference between CON and OVX at any level and at any time point, Y1 or Y3. There were no interaction effects at any level; however, there was a significant overall group time effect (P<0.01) at all levels due to the significantly higher BMD in Y3 animals, *post-hoc* analysis showed that this was attributable to significantly higher BMD in OVX at all levels and in CON at R3.

Figure 4.7: Sub-regional BMD Femur R1 to R6 at time points Y1 and Y3.
[Median (bar), IQR (boxes), 10-90% (whiskers), mean (+) and outliers (·), data table in Appendix 4.2]

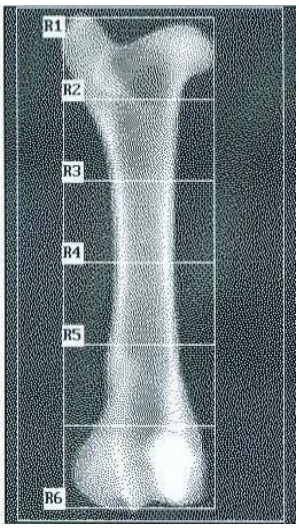

R	INT^{n}	OVX	Time
1	ns	ns	<0.01 ^{OVX}
2	ns	ns	<0.01 ^{OVX}
3	ns	ns	<0.05 $^{C+O}$
4	ns	ns	<0.05 ^{OVX}
5	ns	ns	<0.05 ^{OVX}
6	ns	ns	<0.05 ^{OVX}

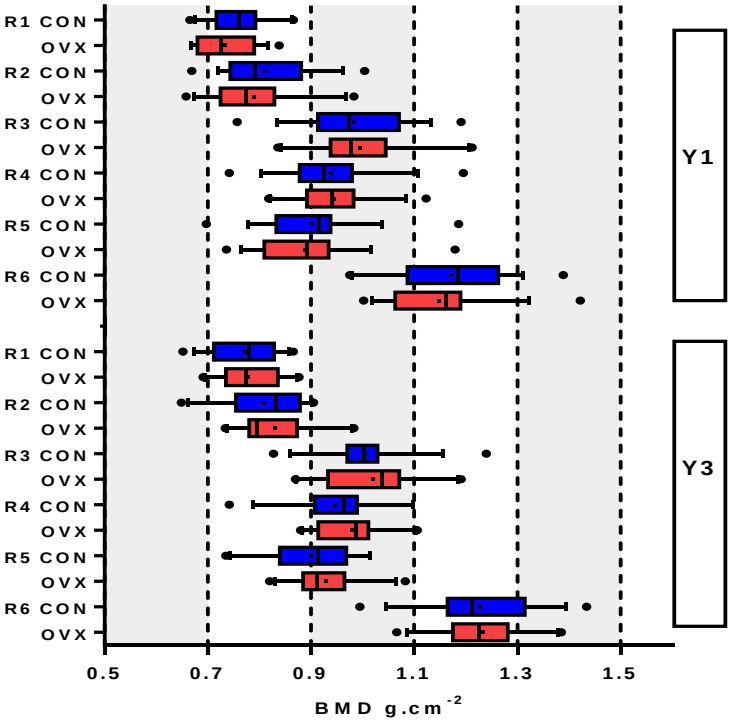

Figure 4.8: Sub-regional BMD Tibia R1 to R6 at time points Y1 and Y3.
[Median (bar), IQR (boxes), 10-90% (whiskers), mean (+) and outliers (·), data table in Appendix 4.2]

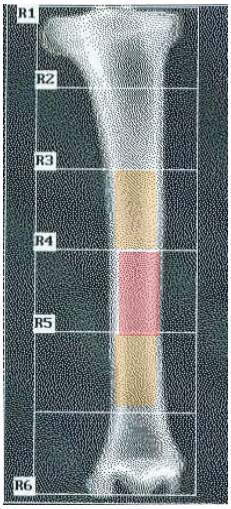

R	INT^{n}	OVX	Time
1	ns	ns	<0.05^{OVX}
2	ns	ns	ns
3	ns	0.06	<0.05^{OVX}
4	ns	0.04^{Y3}	<0.05^{OVX}
5	ns	0.08	<0.05^{C+O}
6	ns	ns	<0.01^{C+O}

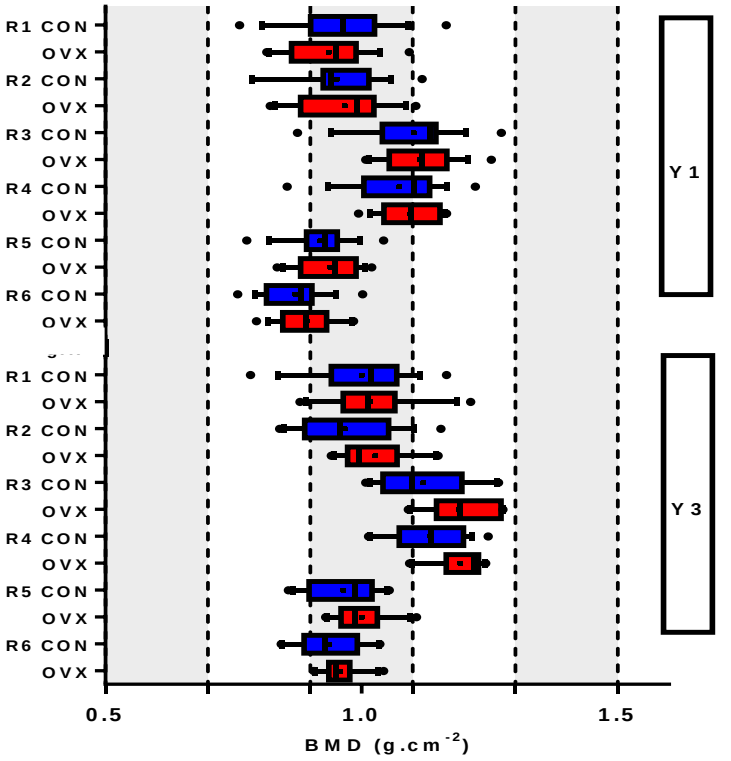

Figure 4.9: Sub-regional BMD Humerus R1 to R6 at time points Y1 and Y3.
[Median (bar), IQR (boxes), 10-90% (whiskers), mean (+) and outliers (·), data table in Appendix 4.2]

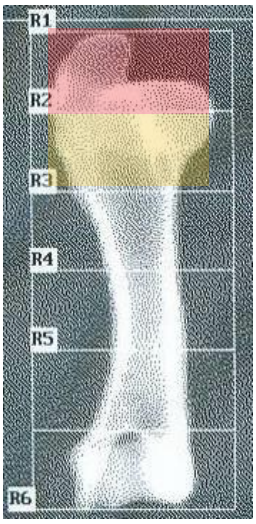

R	INT^{n}	OVX	Time
1	ns	0.03	<0.05
2	ns	0.06	ns
3	ns	ns	ns
4	ns	ns	<0.05 ^{CON}
5	ns	ns	<0.05 ^{CON}
6	ns	ns	<0.05 $^{C+O}$

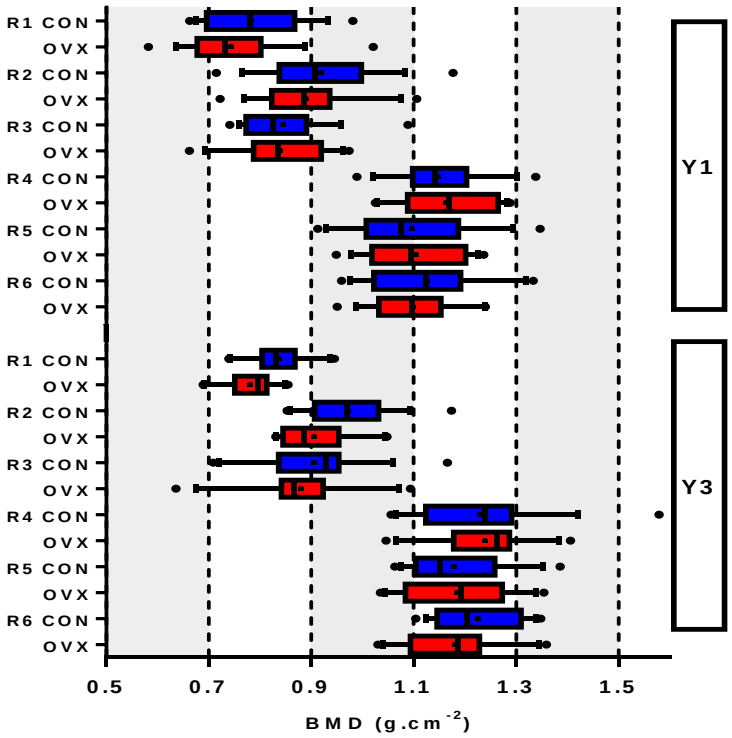

Figure 4.10: Sub-regional BMD Radius R1 to R6 at time points Y1 and Y3.
[Median (bar), IQR (boxes), 10-90% (whiskers), mean (+) and outliers (·), data table in Appendix 4.2]

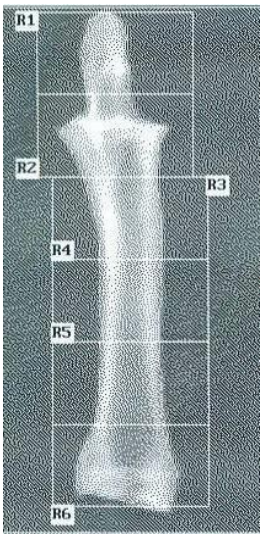

R	INT^{n}	OVX	Time
1	ns	ns	<0.05 ^{CON}
2	ns	ns	<0.01 $^{C+O}$
3	ns	ns	<0.01 $^{C+O}$
4	ns	ns	<0.05 $^{C+O}$
5	ns	ns	<0.05 ^{CON}
6	ns	ns	<0.01 ^{CON}

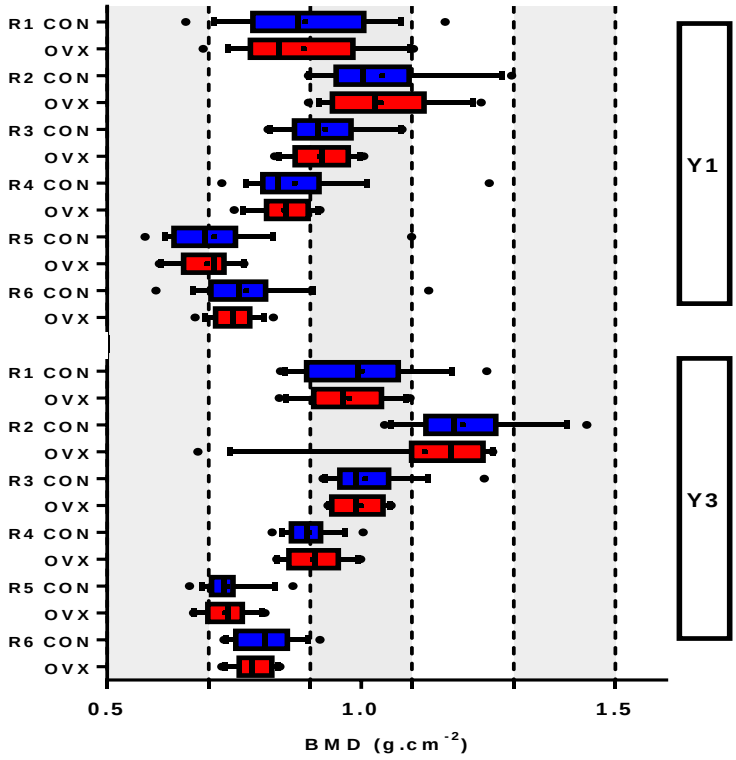

In FMR there were significant differences detected in BMD data across time at all levels R1 to R6. *Post-hoc* analysis (Tukey) revealed significantly higher BMD at all levels across time for OVX and at R3 for CON. However, no treatment effect (OVX) or interaction effect between time and treatment was detected globally or at any time point. In TBR again there was an overall global time effect with increased BMD detected at all levels apart from R2. A global OVX effect was apparent in R4 with *post-hoc* analysis identifying significantly increased BMD in the OVX treated group at Y3, and approaching significance at R3 and R5. In the humerus BMD was significantly greater at Y3 than Y1 in all regions except for R2 and R3. A global treatment effect (OVX) of reduced BMD was apparent R1 and approached significance at R2; however, post-hoc analysis (Tukey) did not detect any discrete treatment effect at each time point Y1 or Y3. In the radius BMD was greater at Y3 than Y1 at every level; however, no treatment effect (OVX) or interaction effect was apparent at any level. In summary, over R1 to R6 in the spinal and long bone samples assessed significantly lower BMD due to an OVX effect was only apparent in the proximal humerus and paradoxically higher BMD due to an OVX effect was seen in the mid-shaft of the tibia.

4.3.5 Region of interest (r1-3)

DXA sub-regional analysis within specific regions of high trabecular content r1-3 in the proximal femur, humerus, tibia and distal radius are presented in Figure 4.11.

Figure 4.11: Statistical analysis (2 way ANOVA and Tukey *post-hoc* analysis) of sub-regional BMD in r1-3, smaller sub-regions within FMR, HMR, TBR and RDR.

r	Int	OVX	Time	r	Int	OVX	Time	r	Int	OVX	Time	r	Int	OVX	Time
1	ns	ns	ns	1	ns	ns	$<0.05^{ovx}$	1	ns	ns	ns	1	ns	ns	$<0.05^{CON}$
2	ns	ns	ns	2	ns	ns	ns	2	ns	$<0.05^{Y3}$	ns	2	ns	ns	$<0.05^{CON}$
3	ns	ns	ns	3	ns	ns	$<0.05^{ovx}$	3	ns	$<0.05^{Y3}$	$<0.05^{C+O}$	3	ns	ns	$<0.05^{CON}$

Statistical significance in red and results of *post-hoc* analysis in superscript after each P value.

In HMR there was a significant treatment effect within r2 (neck) and r3 (inter-trochanteric region) at Y3. In all other regions of interest no OVX effect was detected, apart from significant time effects in TBR and RDR; and of note the proximal sheep

FMR, no treatment, interaction or time effect was detected in any region r1-3 (head, neck, trochanteric) at either time point Y1 or Y3.

4.3.6 Effect of zoledronic acid

Figure 4.12: (a) Mean (±SD) body mass (kg) in Y3 groups CON (n=16), OVX (n=11) and ZOL (n=4) across time (b) and comparison between T0 and sacrifice. [Median (bar), IQR (boxes), 10-90% (whiskers), mean (+) and outliers (◦), data tables in Appendix 4.2]

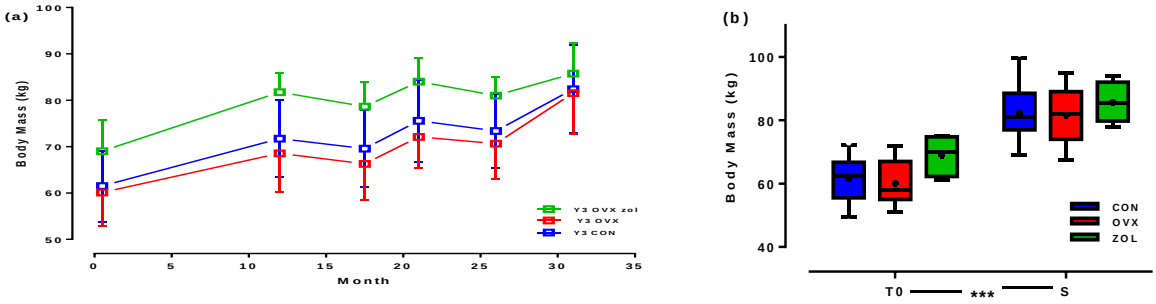

There was no significant inter-group difference in body mass at any individual time point (P<0.05) but a highly significant (P<0.001) increase in body mass occurred in all groups with a magnitude of 20kg for CON and OVX and 17 kg for ZOL across time from time points T0 to sacrifice (S). The effect of zoledronic acid on the lumbar spine is presented in Figure 4.13 and for the long bones in Figure 4.14.

Figure 4.13: Lumbar spine whole bone (WB) and sub-regional (R1 to R6) aBMD in CON, OVX and ZOL groups at Y3 sacrifice.
[Median (bar), IQR (boxes), 10-90% (whiskers), mean (+) and outliers (◦) data table in Appendix 4.2]

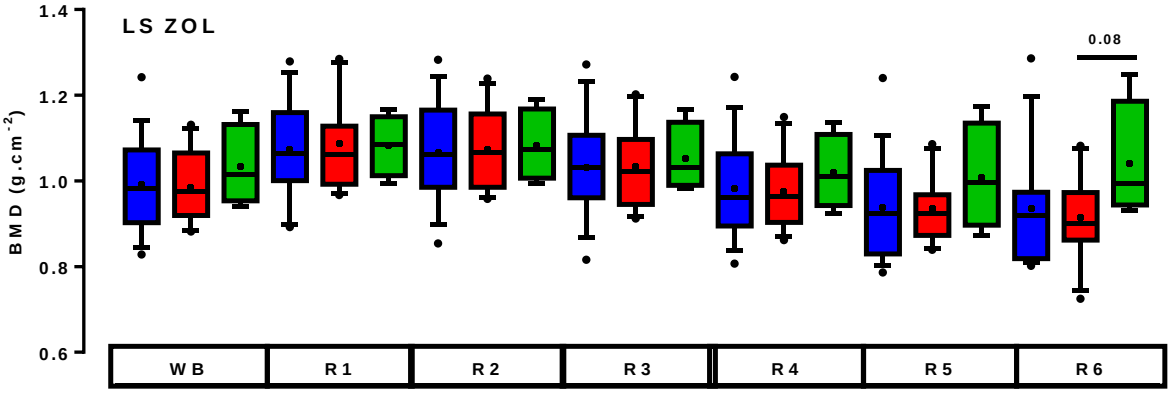

The graphical plot shows no significant difference between CON and OVX at any level of analysis; however, moving caudally in the lumbar spine from regions R4 to R6 a non-significant trend toward greater BMD (P=0.08) was apparent in the ovariectomised and zoledronic acid treated group (ZOL) when compared to OVX.

Figure 4.14: Whole bone sample (WB) and sub-regional (R1 to R6) aBMD for CON, OVX and ZOL in (a) FMR, (b) TBR, (c) HMR and (d) RDR at Y3 sacrifice.
[Median (bar), IQR (boxes), 10-90% (whiskers), mean (+) and outliers (˙) data tables in Appendix 4.2]

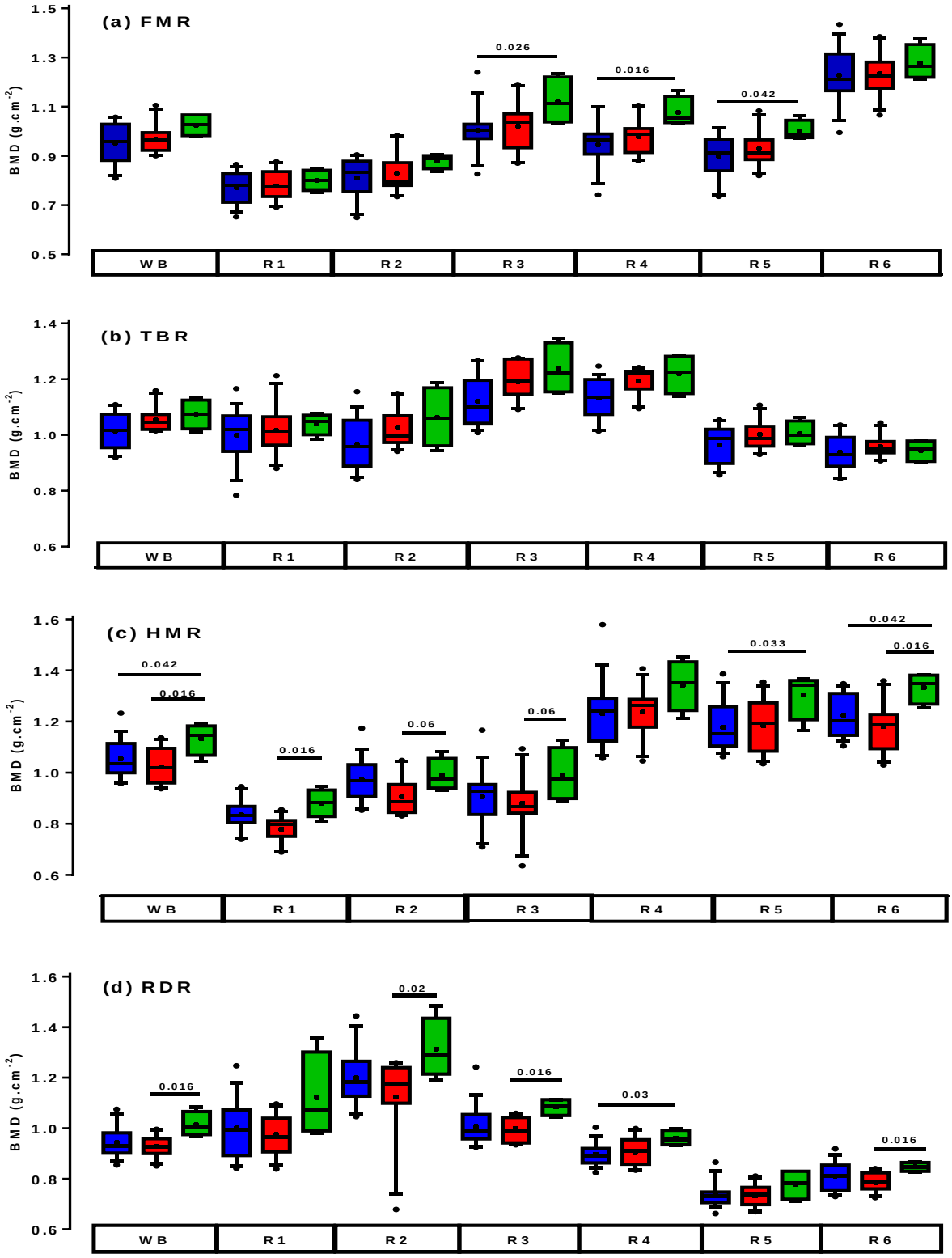

4.3.7 Summary of results

No post-ovariectomy changes in *ex-vivo* ovine BMD were detected at a whole bone level of analysis (WB) at either time point. In vertebral and long bone sub-regions no significant OVX effects were detected in the lumbar vertebra (LS) or femur (FMR), however, increased BMD was apparent in the mid-shaft region of the tibia (TBR) and decreased BMD in the proximal humerus (HMR). Analysis of small sub-regions rich in trabecular bone also showed DXA detectable reduction of BMD due to OVX in the proximal humerus. The addition of the therapeutic agent zoledronic acid to four OVX animals resulted in DXA detectable increases in BMD especially in the forelimb long bones humerus and radius, but significant change was also detected in the mid shaft of the femur and change approached significance in the lowest lumbar vertebrae.

4.4: Discussion

4.4.1 Study design

The DXA component of the greater 'Bone for Life' project was designed to enable a thorough examination of ovine BMD at a spinal and long bone sites post-ovariectomy albeit for a sample size of animals predetermined by the requirements of the greater study. The full measurement capability of the DXA device available for human scanning was employed and the study extended the usual 6 or 12 month timeframe of most previous studies to beyond 2 years.

Sheep have no natural menopause and even if ageing related unbalanced remodelling did occur in this species; it does not necessarily follow that BMD typically assessed at sites of bone fragility in human osteoporosis would be the same in an ovine large animal model. Therefore, due to inconsistency of BMD results reported in the literature for the usually selected sites, this study made no prior assumption about likely sites in the ovine skeleton which might be susceptible to bone mass change due to ovariectomy. In this study a systematic approach was taken whereby the *ex-vivo* ovine bone sites sampled were subjected to a thorough examination firstly; along their entire length in the whole bone scan; secondly for each individual vertebra in the lumbar spine and equal length sub-regions from proximal to distal epiphyseal regions in each long bone; and finally, areas of high trabecular content, the usual areas scanned in previous studies were examined.

The usual time frames employed by most previous DXA studies examining bone quantity change post-ovariectomy both *in* or *ex-vivo* have varied from 6 to 8 weeks to 3 to 6 month in the shorter studies to the upper limit of the longest previous study of 12 months. One study has assessed the long-term effect of OVX on bone quantity at up to 18 months but this study was limited to six sheep, only one site the distal radius was studied and BMD was assessed by pQCT so results are not directly comparable (Sigrist *et al*., 2007). This is the first study to examine bone quantity effects of ovariectomy at an initial time point of 12 month and then out to beyond 2 year at 31 month. This extended time course would be more reflective of the normal insidious time course of unbalanced bone remodelling following menopause or ovariectomy in human populations that gives rise to reduced bone quantity of osteoporosis.

4.4.2 Effect of OVX on Spinal BMD

Turner *et al.* (1995b) previously reported significant changes in spinal BMD ($P<0.08$) at 6 month post-OVX for the lowest three lumbar vertebrae L4 to L6 and L5 to L7. Although the significance level was not as stringent as the alpha level of this study, when BMD data for the lowest three vertebrae were combined and similarly analysed in this study a similar *P* value was obtained, with mean BMD for L4 to L6 in the OVX group lower than CON at the first time point, albeit in this case with the 12 month ($P=0.06$) approaching significance but not at the later time point of 30 month ($P=0.61$). At first glance the similarity of these results would possibly suggest that spinal BMD changes are transient, and that with increasing mass and age the OVX effect is minimised. In a further study of the effects of OVX and oestrogen replacement, Turner *et al.* (1995c) reported no change in L4 to L6 BMD at 6 and 12 month but reduced BMD; at L5 at 6 month and L4 at 12 month. This result is also similar to this study where no changes in BMD were apparent at any individual vertebral levels in any group; and, at any time point apart from those expected over time due to changes in body mass.

In relation to spinal BMD therefore, one could conclude that ovariectomy alone is insufficient to effect a significant long lasting DXA detectable change in bone mass. The reason for this probably lies in ovine vertebral structure; in contrast to human and primate vertebrae where most the mass resides in the trabecular network and cortical shell of the vertebral bodies, most ovine vertebral mass lies in the thick

posterior elements, which are cortical or plexiform type bone; which is not as susceptible to the bone wasting effects of low oestrogen levels post OVX (Deloffre *et al.,* 1995).

4.4.3 Effect of OVX on BMD at long bone sites

At a whole bone level DXA did not detect any whole bone BMD changes at 12 and 30 month post-OVX at any long bone site. The only region to show lower BMD in the OVX treatment group was the proximal humerus (R1) with; differences of 0.040 and 0.057 $g.cm^{-2}$ compared to control, which just reached and slightly exceeded DXA measurement limits (95% LOA: +0.050 to -0.043 $g.cm^{-2}$) at Y1 and Y3, respectively. These differences were further manifest within R1 areas of interest (r1 to r3), at the neck r2 and intertrochanteric r3 regions which also showed reduced bone density. Differences in neck and inter-trochanteric regions were inside measurement limits at Y1 (0.040 $g.cm^{-2}$) but well outside the measurement limits at Y3 (0.097 $g.cm^{-2}$). In analysis of significant differences at R1, r2 and r3, OVX effect size (Cohen's d) was moderate (~0.40) at Y1 and large at Y3 (~0.95-1.05). Thus further scrutiny of the results in the proximal humerus suggests it was a longer term effect of ovariectomy which produced a more significant result; that is differences in BMD between control and OVX well outside DXA scanner measurement limits and with a greater effect size.

The fact that significantly greater differences were seen in the proximal humerus rather than the proximal femur has not been previously described; but may not be surprising as the proximal humerus is bigger, contains more bone mass and more trabecular bone than the hind limb counterpart. Humeral head dimensions and morphology, that is a larger more spherical head and neck, are necessary to bear a more multidirectional ambient loading pattern than the head of the femur. The proximal part of the ovine femur is smaller, more peg like and has less mass than the humeral head; also the whole bone is orientated more horizontally from the acetabulum in contrast to the more vertical humeral alignment, see Figure 1.36.

Previous studies have reported differing results for *in-vivo* DXA BMD measures; Hornby *et al.* (1995) reported whole body *in-vivo* BMD loss at 15 week post-OVX and Turner *et al.* (1995b) reported no significant differences for *in-vivo* BMD

measurements at the calcaneus and distal radius at 6 month post-OVX. In a further study Turner *et al.* (1995c) reported no significant change in BMD of *ex-vivo* proximal and distal long bones at 12 month after ovariectomy. This is the first study to the author's knowledge to suggest that ovariectomy can produce a long-term effect in proximal humeral BMD.

The tibial mid-shaft changes of increased BMD at 31 month but not 12 month are difficult to explain. In Y3, the mean R4 mid shaft region BMD in the treatment group was 0.069 $g.cm^{-2}$ higher than the control, a statistically significant difference and nearly double the DXA scanner measurement limits described in Chapter 2 (95%LOA: ± 0.035 $g.cm^{-2}$); this along with a large effect size (0.86) suggest that there is a real OVX effect in cortical mid shaft BMD at Y3. The cortical steal phenomenon could explain increases in the mid-shaft but proximal and distal regions were unchanged and this phenomenon is usually associated with a treatment effect of anabolic agents rather than OVX alone (Mosekilde *et al*., 1995). Although not a true anabolic agent one might also have expected increased tibial BMD in the ZOL group, however, no such differences occurred.

This result was also not due to group variability in animal size as although Y3 animals continued to gain body mass throughout the time course of the study, there were no detectable differences between groups at sacrifice. A change in bone morphology either an increase or decrease in bone width would have affected the estimated area projection (EA, cm^2) and therefore reduced and increased the final BMD data in control and ovariectomised groups, respectively; again however, no significant differences were detected in overall bone dimensions at either time point so small changes in dimensions had no effect.

Seasonal variation in BMD is another possible explanation as previous studies have reported seasonal variation in BMD in both human and ovine studies (Rosen *et al*., 1994; Arens *et al.,* 2007; Turner, 2007). However, tibial BMD differences detected by repeated measures ANOVA were quantified on *post-hoc* analysis to be due to a difference between CON and OVX groups at Y3, that is the differences arose in animals which were all sacrificed at the same time point and thus seasonal variation could have had no bearing on this result.

Overall BMD results for the long bone sites in this study are similar to previous studies in that OVX does not produce large enough decrements in BMD at 12 month

to be considered similar to human osteoporosis (Turner *et al.,* 1985b; MacCleay *et al*., 2004a; Sigrist *et al*., 2007). However, at 31 month significant differences were detected, the magnitude of changes in the proximal humerus and mid-shaft of the tibia were associated with large effect sizes and were in excess of DXA measurement limits, albeit not of the order of - 2.5 standard deviations below the mean which define DXA aBMD criteria in human osteoporosis (Kanis, 2002).

In terms of an optimum site for study of the bone quantity to quality relationship the results suggest; that the proximal humerus, with the greatest bone quantity decrement due to OVX, rather than proximal femur or distal radius be the site to pursue in any future study. The findings in the tibia are unusual and unexpected and require further evaluation; they cannot be explained by breed, body mass, dimensional or seasonal changes and can only be attributed to either the small sample size in the OVX group at the second time point or some other biological process such as age related Haversian remodelling known to occur with ageing in sheep.

4.4.4 Effect of Zoledronic acid

In order to produce up to 30% reductions in bone mass typical of osteoporosis within 6 to12 months in an ovine model, most studies now employ OVX plus at least one or two other bone wasting strategies (Lill *et al*., 2002a, b; MacLeay *et al*., 2004a, b) or more recently two operative procedures OVX and pinealectomy (Egermann *et al*., 2011). Ovariectomy alone in the ovine model is not sufficient to produce BMD changes of the magnitude required for scientific study of bone quantity quality relationships typical of osteoporosis. Despite OVX producing DXA detectable changes at two sites the significant increases in bone quantity induced by the therapeutic agent used in this study were far more impressive, albeit with a very small sample size (n=4) in the treatment group (ZOL). Again the forelimb sites humerus and radius and not the hind limb, femur and tibia, or spinal site was where the greatest differences were demonstrated. In particular differences were predominantly detected in OVX vs. ZOL comparisons where non-significant decrease in BMD in the OVX group and BMD increases in the ZOL group magnified the differences. Despite non-parametric data analysis, large effect sizes and changes well in excess of measurement limits again suggest a real effect of ZOL.

The effect of Zoledronic acid infusion in post-menopausal women was examined in the HORIZON study (Black *et al*., 2007). At 36 month, a slightly longer end-point than this study, the % difference between placebo and zoledronic acid groups BMD were; 6.0, 6.7 and 5.1% for total hip, lumbar spine and femoral neck, respectively. At equivalent sites and regions in this study, using humeral rather than femoral data, differences between the OVX and the ZOL treated group at 31 month were; 13.1, 5.0 and 11.6% for R1 HMR, WB LS and neck r2 HMR, respectively. If one allows for an approximate 5% greater body mass in ZOL than OVX then the differences in humeral BMD due to supra-pharmacological dosing in the ovine model were similar to human data.

4.4.5 Limitations of the study

The sample size of the study was beyond the control of the author and was driven by economic constraints of funding the numerous components of the 'Bone for Life' project. Initial sample selection of 75 to 80 animals would have fulfilled sample size criteria recommended for a BMD study of 35 to 40 animals in each group, however further sub-division of the OVX and CON groups into Y1 and Y3 as the study was expanded to 31 month and the requirement for a pharmokinetic study and the long acting bisphosphonate ZOL treatment group further reduced the numbers in each of the sub-groups. Sample size was therefore well below that recommended by previous authors and in the validation study undertaken by this author in Study 1 (Turner *et al*., 1995c). Group size, especially at the second time point were uneven, 16 control vs. 11 ovariectomised and very small for the ZOL group (n=4). Although the study overall was underpowered the fact that an OVX effect was detected might indicate that the humeral site is more sensitive to hormonal effects and thus the best site to concentrate on in future *ex-vivo* OVX studies.

4.4.5a Animal selection and preparation

Hornby *et al*. (1995) when considering the large animal of osteoporosis suggested that only ewes aged over 7 year be used, that the weaning history be known and all animals be sacrificed at the same time point, preferably in the autumn to minimise the effect of seasonal changes. In this study a selection of mixed breed animals was

used and age although stated as mature and thought to be 5 to 7 year, was actually unknown. Weaning history of the animals was also unknown, the ovariectomy intervention was not matched by sham operations in the control group; and, Y1 and Y3 animals were sacrificed at a different time points. Initial study design was primarily set by others to meet criteria for study of bone quality and not DXA estimation of bone quantity by this author. Extra criteria for DXA evaluation of bone quantity would have included; a larger sample size of at least 18 to 20 animals in each group, confirmed age > 7 year, all of the same breed with weaning completed at least 12 months prior to the study, and an autumn sacrifice date would have also possibly further reduced natural variability in results.

One extra consideration in initial study design would have been the inclusion of an extra bone wasting intervention in addition to OVX. The work of MacCleay *et al*. (2004) on dietary metabolic acidosis was unknown at the time of the study design, however, previously inconsistent BMD results at both vertebral and long bone sites with OVX (Turner *et al*., 1995a, b and c; Deloffre *et al*., 1995; Hornby *et al*., 1995) and the two studies by Lill *et al*. (2002a and b) combining OVX and steroids were known at the time and recommendations especially in the latter two studies could have been used to improve the study design from a bone quantity point of view in the planning stages.

4.4.5b Scan settings

Box dimension settings for sub-regional analysis were standardised as far as possible at all sites. In the vertebral sample a standard antero-posterior scan image was used, thus the lamina and spines of the vertebrae were incorporated in the scan but lateral elements were excluded. Edge detection and lateral limits were set by the same operator for all scans, variation in scan box setting could be re-examined in a later study. In the long bone samples, it might have been better to tailor box dimensions to allow evaluation of the long bone from proximal epiphysis, metaphysis, diaphysis, to distal metaphysis and epiphysis, with five sub-regions boxes per long bone rather than six. Long bone scans could have also excluded some irregular features of the long bones such as the olecranon process of the radius. In the spine, a scan of the vertebral bodies with bone samples fixed to simulate a lateral scan may have negated the effect of the dense cortical posterior elements; again the subject for a possible re-analysis of data in a follow on study.

4.4.6 Conclusions

1. This study has confirmed that effect of ovariectomy and zoledronic acid on aBMD at 12 and 31 month at the ovine spinal site is not a useful model for the study of human vertebral osteoporosis.

2. Analysis of long term (31 month) differences in aBMD in the ovariectomy group in the proximal humerus were statistically significant, outside of scanner measurement limits and of a large enough effect size to warrant further investigation. The results suggest that the proximal humeral site may be more optimal model of human osteoporosis rather than the proximal femur and distal radius, the typical sites used in most previous research.

3. An unusual and unexpected finding of higher aBMD in the mid-shaft of the tibia in OVX compared to control at the second time point but was also significant, outside of scanner measurement limits and of large effect size. It cannot be explained on the grounds of differences in animal mass and bone dimensions, but possibly may be a seasonal effect or due to sampling error as sample sizes were unbalanced in the groups. Either way this finding warrants further investigation.

4. The effects of zoledronic acid were most evident in the forelimb long bones, humerus and radius, again stressing the importance of these two long bones rather than ovine hind limb site for future studies of bone quantity and quality relationships.

CHAPTER 5

Influence of DXA derived aBMD on strength and microdamage in ovine cortical bone

5.0 SUMMARY / ABSTRACT

The purpose of this study was firstly to evaluate the influence of DXA derived 'bone quantity' (aBMD) and structural geometric indices on cortical bone breaking strength; and secondly the influence of cyclic loading and regional stress on microdamage accumulation with and without aBMD stratification in a large animal model. Ovine whole radii across a range of low, medium and high bone density (Hologic QDR 4500, Waltham, USA) from control and ovariectomised sheep underwent mechanical loading on a material testing rig (Instron, 3600, Bucks., UK). Eight bones underwent three-point bending to failure to assess ultimate breaking load, breaking stress and structural analysis of geometric properties of cross-sections near point of fracture. A further ten bones underwent four-point cyclical loading (0.9kN) to $3x10^5$ and $1x10^6$ cycles in three dyes, to initiate and stain microdamage respectively. Analysis of three cross-sectional areas of regional stress (40, 60 and 80 MPa) was also made to evaluate influence of stress and cyclical loading on microdamage accumulation with and without aBMD stratification. In bending to failure, breaking force (F_{max}) was highly correlated with; whole bone aBMD (r=0.87), sub-regional aBMD (r=0.91); cross-sectional moment of area (r=0.83); and moderately correlated to section modulus (r=0.71) and cross-sectional centre of mass (r=0.58). Relationships of volumetric density (vBMD) to F_{max}; and, aBMD to breaking stress (σ_{max}) were moderate to poor (r<0.4). Individual bone microdamage data plots showed clear separation between bones with low, medium and high aBMD after cyclic loading. Correlation of aBMD to microdamage variables was good r > 0.75 and in pooled data there were highly significant differences in microdamage across aBMD at $1x10^6$ cycles (P<0.01). Analysis of microdamage across stress region at $1x10^6$ cycles, identified highly significant differences in microdamage across aBMD at 60MPa (P<0.01); but not at 80MPa (P=0.09) due to high data variance. In conclusion the strongest relationships to cortical bone bending strength in ovine radii were for DXA derived aBMD and cross-sectional moment of area (I). Results of four-point bending also suggested a relationship of low aBMD to higher crack numerical and surface density. Similar further studies would be required to confirm these findings with larger sample sizes and to examine ultimate strength, aBMD, and geometric structural relationships in ovine radii after prior cyclic loading to initiate microdamage.

Key words: bone density, bone geometry, microdamage, bending strength

5.1 INTRODUCTION

Bone is a natural composite material of mineral and organic content, micro- and macro-architecture scaled to achieve normal function with minimum mass for biological economy and safety limits (Currey, 2002). During normal everyday activity, cortical bone has to withstand compressive and tensile stresses and bending and torsional moments (Augat & Schorlemmer, 2006).

The mineral component, calcium hydroxyapatite, constitutes approximately 45% of bone and imparts stiffness; increasing bone mineral content increases stiffness further but with too much mineral bone becomes brittle (Zioupos & Currey, 1998). Small amounts of additional mineral laid down in areas of stress, in adaptation to loading changes, can increase strength by 60% and fatigue life one hundred fold (Turner, 2006). The organic component of bone, the collagen triple helix and its crosslinks, impart toughness the ability to absorb energy (Zioupos *et al*., 1999). The collagen component is especially important for long bone resistance to tensile bending stress; and decreases or increases above optimal in the amount of collagen or its cross-linking can reduce the capacity of bone to absorb energy (Currey, 2003b; Viguet-Carrin *et al.,* 2006).

Bone architecture has been described as a fabric woven at sub-microscopic, microscopic and macroscopic levels with optimal mass, size, and shape for strength (Yeni *et al.,* 1997). Cortical bone is comprised of osteons, lamellated tubular structures of alternately loosely and densely packed layers of mineralised collagen of different orientations surrounding a central Haversian canal. Long bone resistance to bending moments can be imparted, without any additional mass, by placement of the cortical shell away from the central axis thus increasing cross-sectional moment of area (Turner & Burr, 1993). Thus growth and remodelling of an initial genetically determined architectural template in response to ambient compressive and tensile stresses, modifies internal and external diameters of long bones creating elliptical or tubular cross-sections of varying thicknesses at different points (Martin & Atkinson 1977; Bouxsein *et al*., 1994).

However, bone is not a perfect structure and small cracks approximately 100 µm long are known to develop during normal loading (Taylor & Lee, 2003). If too many microcracks form, accumulated microdamage can result in failure but a limited amount of microcrack formation and propagation is beneficial, as it allows bone to

absorb and dissipate excess energy without fracture (Zioupos, 2001; Currey, 2002). Microcrack propagation is limited by osteonal structural properties of cement lines and alternating orientations of lamellae, and furthermore microcracks can be removed as bone remodelling units (BMUs) pass through bone in response to signals from the osteocyte cannalicular network. Following remodelling residual microdamage becomes confined to older more mineralised interstitial lamellae with newer undamaged osteons acting as bridges bearing loads that would otherwise cause microcrack extension (Nalla *et al.,* 2004). Mineral distribution therefore is not uniform through cortical bone, with newer less mineralised osteons alongside older more mineralised interstitial lamellae, remnants of partly remodelled osteons (Schaffler *et al*., 1995).

Degradation of material and structural properties occurs due to age related failure of modelling and remodelling in both genders; with ageing bone remodelling unit (BMU) repair of microdamage tends to remove more bone than it deposits, resulting in negative bone balance. In females post-menopause, with drug therapy, disuse and or disease, impaired remodelling accelerates resulting in greater cortical bone thinning, increased porosity, older more mineralised interstitial lamellae accumulating more microdamage, peripheral bone replacement by less mineralised bone, and overall loss of cortical bone stiffness and strength. Age related loss of cortical bone strength is partly offset by periosteal appositional modelling but this too may be affected by negative age related changes in osteoblast function (Seeman, 2003).

Bone densitometry or dual energy X-ray absorptiometry (DXA) is an effective non-invasive method for assessing bone quantity and fracture risk in humans (Delmas & Seeman, 2006). DXA estimates of bone quantity are based on the attenuation of photons at two energy levels passing through the bone sample. DXA derived bone mineral content (BMC; g) of the sample divided by the estimated area (EA; cm^2) of the projected image of the bone at the detector array thus gives an areal density measure of bone quantity (aBMD; $g.cm^{-2}$). DXA derived areal BMD is still a standard clinical measure of osteoporosis associated fracture risk and DXA derived aBMD expressed as T scores, and referenced to population databases have been incorporated into standard definitions of osteoporosis along with other clinical risk factors (Kanis, 2002; WHO, 2004).

Recently however DXA derived areal BMD has been criticised as many mistakenly assume it is a bone strength surrogate (Seeman, 2001; Seeman, 2002; Bolotin *et al*., 2004). Due to the popularity of DXA scanning many clinicians erroneously equate DXA derived aBMD with bone strength, unfortunately the reality is not so straight forward, and bone strength is ultimately a complex engineering problem (Beck, 2003). The major drawback of DXA, apart from misleading terminology, of areal density (aBMD) is that as a two-dimensional imaging technique, DXA conveys no information about other major determinants of bone strength; namely bone quality factors of material composition, structural design and microdamage (Delmas & Seeman, 2006).

In order to address DXA's geometric inadequacy new algorithms such as hip structural analysis (HSA) have been introduced in some newer generation DXA scanners (Beck, 2003). HSA incorporates geometric data from DXA scan images to generate cross-sectional moment of area data which in conjunction with aBMD purportedly improve prediction of fracture risk (Bouxsein & Seeman, 2009). However, the reliability of this data is highly dependent on positioning of the patient and is limited to prediction of bending strength in long bone sites such as the neck of femur (Beck, 2003). Other three dimensional imaging modalities such as quantitative computed tomography (QCT), high resolution peripheral quantitative computed tomography (pQCT) and MRI are now available for peripheral sites and are still under evaluation for imaging the lumbar spine and neck of femur (Bouxsein & Seeman, 2009). Despite recent criticism DXA remains the most utilised non-invasive investigation in clinical practice but in bone research invasive destructive investigations predominate. Questions with regard to DXA derived areal BMD data relationships to bone strength and bone quality factors such as microdamage and geometric structural variables still remain.

There are a variety of flexural test methods that can be performed on bone, and important questions arise in selection of appropriate tests for experimental work (Griffin *et al.*, 1999). In this study three-point bending tests were selected to ascertain ultimate breaking force as damage could be concentrated or narrowly focussed near the point of load application, thus allowing subsequent analysis of geometric structural properties in nearby cross-sections. In contrast to induce microdamage four -point bending was used to produce physiological axial bending stresses along the

'grain' that might be experienced by the bone in every day ambulation. Furthermore four-point bending produces tensile and compressive strains in gradient fashion, without transverse or shear strains in the cortical mid-shaft region and thus axial strains are consistent between loading points (Boyce *et al*. 1998; Griffin *et al.* 1999).

The general aim of this study was to examine the influence of DXA derived bone quantity in comparison to bone quality determinants of cortical bone strength. In the first part of the study, the influence of bone quantity and geometric indices on the capacity of pre-selected whole bones across a range of low medium and high aBMD values, to withstand fracture was examined in three point monotonic bending tests to failure. In the second part of the study, the aim was to examine the influence of aBMD, regional stress and cyclical loading on microdamage accumulation; physiological levels of loading generated by four point cyclic bending generated microdamage which was then analysed across cyclic loading and regional stress, with and without aBMD stratification.

5.2 METHODS

5.2.1 Study design

Dual energy X-ray absorptiometry assessment of bone quantity, whole bone data acquisition scan, and all subsequent sub-regional and region of interest analyses were conducted by the author. Assessment of cortical bone strength and microdamage accumulation in the mid-shaft of the ovine radius was conducted by Gerardo Presbitero (Presbitero, 2009).

5.2.2 Bone sample selection and DXA scanning

The ovine radius was selected for assessment of cortical bone strength, geometry and microdamage accumulation. The radius has been shown in a previous study to be suitable for mechanical testing under bending stresses, due to its high aspect ratio, minimal measurement error, and low measurement variability (Schriefer *et al.*, 2005). Four year 1 (Y1) radii from control (CON) and ovariectomised (OVX) groups exhibiting a range of low, medium and high aBMD according to whole bone and sub-regional aBMD determined by DXA scanning using a fan-beam X-ray bone densitometer (QDR 4500™ Elite, Hologic, Waltham, USA) were selected for monotonic and cyclic whole bone bending tests. DXA methods of sample positioning,

data acquisition scan and sub-regional analysis are given in Chapter 2. A sample whole bone (WB) and sub-regional analysis (R1-6) are presented in Figure 5.1.

Figure 5.1 DXA images of the ovine radius (a) whole bone data acquisition scan and (b) sub-regional analysis of R1 to 6. External loading points were placed in R3 and R5 regions and central loading point in R4 for three-point bending to failure tests; and in cyclic four-point bending at a constant load to initiate microdamage bones were also fixed in regions R3 and R5.	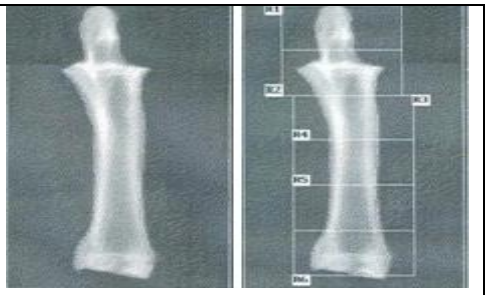

5.2.3 Monotonic three point loading to failure

Eight selected ovine radii underwent monotonic three-point bending on a material servo-hydraulic testing machine (Instron 8501, Buckinghamshire, UK) at a velocity of 1 mm.min^{-1} until fracture, to ascertain ultimate breaking strength (N). Loading was made over the radial mid-shaft, posterior surface upper most, with external loading points in the R3 and R5 regions and the central point of loading in the R4 region. Three-point bending was used to ensure stress concentration and fracture occurred near the central point (R4) of load application (Figures 5.1b and 5.4). Following fracture, cross-sections near point of failure were made and AutoCad software used to calculate cross-sectional moment of area (I) and distance from centroid to centre of mass (ω) in the cross-section. The section modulus (Z) was then calculated see equation 5.1.

Equation 5.1 $Z = I / \omega$	Where I is cross-sectional moment of area and ω is distance to the centre of mass from the centroid

5.2.4 Cyclic loading and analysis of microdamage

Ten ovine radii were placed under constant four-point bending loads of 0.9 kN at 3Hz to three hundred thousand and then to one million cycles using the same material testing machine (Instron 8501, Buckinghamshire, UK) in a bath of dyes to stain microcracks. Four-point bending external loading points were placed at the outer limits of regions R3 and R5 (Figure 5.2a). Prior to cyclic loading the organic content on the surface of the bones was removed and then proximal and distal ends wrapped to prevent the contamination of the dyes. Alizarin complexone, xylenol orange and

calcein dye were applied to stain microcracks; prior to cyclic loading *in vivo,* and during cyclic loading to $3x10^5$ and $1x10^6$ loading cycles, respectively (Figure 5.2).

Figure 5.2 (a) an alizarin stained bone sample within the experimental set up in preparation for cyclic loading with (b) xylenol orange for microdamage occurring during cyclic loading to $3x10^5$ cycles; and (c) to $1x10^6$ cycles using calcein blue.

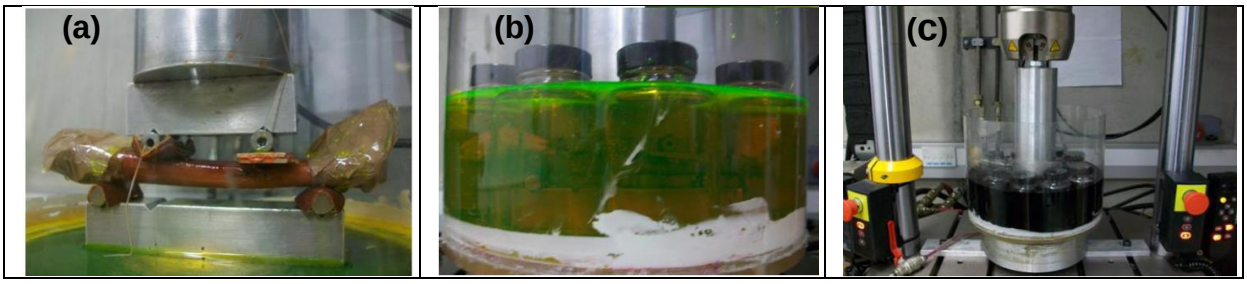

Following cyclic loading, three cross sections were cut at the middle of each bone and examined under epi-fluorescence microscopy for linear microdamage on compressive and tensile sides. Microdamage was recorded as: mean number of cracks occurring per section or crack numerical density (cracks occurring per mm^2), crack surface density (μm of crack length occurring per mm^2) and mean crack length. Analysis was then made of microdamage accumulation at different areas of stress within the cross-sections. AutoCAD 2010 software was used calculate the second moment of area (I); and results were substituted into the equation describing moment under bending stresses (Equation 5.2), to obtain selected stress values (σ) and distance from cross-sectional centre of mass (ω). A range of approximately ± 20% within each selected stress determined the area of subsequent observation for damage accumulation with variation in stress (Figure 5.3).

Equation 5.2: $\sigma = \frac{Mc}{I} = \frac{F\rho\omega}{I}$	Where; σ stress; *M* moment about the neutral axis; I second moment of area; *F* applied force; ω distance from cross-sectional centre of mass; and ρ distance between the loading points.

Figure 5.3: Schematic plot of three areas of regional stress (40, 60, 80 MPa) in a cross-section of the mid-shaft of ovine radius

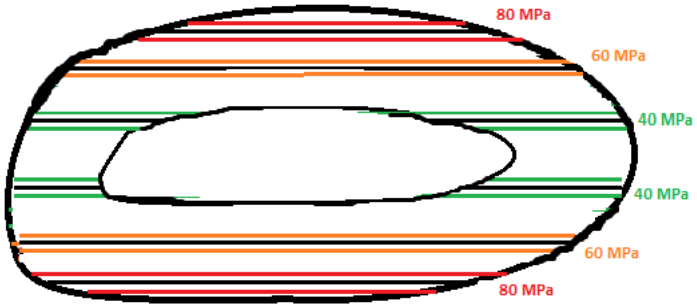

The regional stresses chosen to examine the relationship to microdamage accumulation were; 40, 60 and 80 MPa. In addition to microcrack distribution and variation within each stress region, analysis was made of microcrack propagation with and without variation in aBMD.

5.2.5 Data handling and statistical analysis

All data were recorded on Excel spread sheet and analysed for normality (D'Agostino) using Prism 6 (GraphPad Software, San Jose, USA). Year one radii analyses of aBMD, microdamage and bending strength for parametric data were performed using one way ANOVA with *post-hoc* analysis of significant differences using Student's T tests with Bonferroni correction; and for non-parametric data the Kruskal Wallis test with *post-hoc* analysis using Mann-Whitney U tests ALSO with Bonferroni correction.

5.3 RESULTS

5.3.1 DXA aBMD results for the radii

The aBMD of radii selected for monotonic loading (n=8) are presented in Table 5.1 and for cyclic loading tests (n=10) are presented in Table 5.2.

Table 5.1 Bone number, group, animal body mass, bone dimensions and whole bone and sub-regional aBMD (g.cm^{-2}) of radii selected for monotonic strength testing.

Bone Level /No.	Group	EBM kg	L mm	W mm	WB	R1	R2	R3	R4	R5	R6
H27	CON	93	213	38	1.014	1.165	1.249	1.079	0.986	0.796	0.880
H 2	CON	85	190	39	0.987	1.054	1.296	1.026	0.963	0.794	0.822
H18	OVX	85	201	38	0.925	0.953	1.174	0.983	0.884	0.718	0.782
M21	OVX	75	191	40	0.869	0.839	1.004	0.949	0.903	0.769	0.754
M26	OVX	64	188	40	0.827	0.917	1.031	0.830	0.794	0.644	0.755
M20	CON	68	204	42	0.822	0.817	0.992	0.946	0.837	0.632	0.702
L29	CON	66	202	39	0.773	0.717	0.897	0.817	0.803	0.660	0.711
L 4	OVX	62	196	39	0.759	0.689	0.926	0.871	0.750	0.607	0.673

Whole bone aBMD ranged from 0.759 to 1.014 g.cm^{-2} in bone samples selected for monotonic testing and aBMD was classified as high >0.900 g.cm^{-2}, mid-range ~ 0.900 to 0.800 g.cm^{-2} and low < 0.800 g.cm^{-2}. The range of whole bone aBMD for bones selected for cyclic loading was 0.744 to 0.985 g.cm^{-2}, and within the region R3

to 5, within the external loading points mean aBMD range, was from 0.716 to 0.916 g.cm^{-2}.

Table 5.2 Bone number, group, animal mass, dimensions and WB and sub-regional aBMD (g.cm^{-2}) of bones selected for cyclic loading for assessment of microdamage.

Bone No.	Group	EBM (kg)	L (mm)	W (mm)	aBMD WB	aBMD R3	aBMD R4	aBMD R5	R3 to 5 M±SD; g.cm^{-2}
H1	**CON**	**75**	**195**	**38**	**0.985**	**1.080**	**0.918**	**0.749**	**0.916 ± 0.166**
H25	**OVX**	**76**	**192**	**42**	**0.962**	**1.005**	**0.896**	**0.750**	**0.884 ± 0.128**
H8	**OVX**	**75**	**180**	**37**	**0.933**	**0.916**	**0.848**	**0.707**	**0.824 ± 0.107**
M3	**CON**	**64**	**196**	**41**	**0.919**	**0.990**	**0.838**	**0.630**	**0.819 ± 0.181**
M23	**OVX**	**65**	**205**	**38**	**0.828**	**0.931**	**0.855**	**0.727**	**0.838 ± 0.103**
M16	**CON**	**68**	**193**	**35**	**0.881**	**0.945**	**0.863**	**0.764**	**0.857 ± 0.091**
L19	**OVX**	**64**	**205**	**39**	**0.793**	**0.841**	**0.817**	**0.675**	**0.778 ± 0.090**
L10	**OVX**	**66**	**192**	**40**	**0.784**	**0.849**	**0.775**	**0.603**	**0.742 ± 0.126**
L17	**CON**	**68**	**189**	**40**	**0.777**	**0.820**	**0.832**	**0.681**	**0.778 ± 0.084**
L28	**CON**	**76**	**202**	**40**	**0.744**	**0.847**	**0.726**	**0.575**	**0.716 ± 0.136**

Statistical analysis of the aBMD of radii (17 CON / 16 OVX) from which bones were sampled for loading to failure (n=6) and fatigue loading (n=10) revealed no significant difference between CON and OVX groups for WB or any sub-region (P>0.05); and further analysis of the bones sampled for each test again revealed no significant difference between aBMD in the Y1 CON and OVX samples (P>0.05).

5.3.2 Monotonic 3 point bending tests to failure.

All eight bones fractured near the point of load application on the tensile side in the R4 sub-region in which the middle load point was applied (Figure 5.4a and b). Bone mineral density (g.cm^{-2}), bending strength (*Fmax*), distance from cross-sectional centre of mass (ω) and second moment of inertia (I) and applied stress to failure (σ_{max}) $_{of}$ each fractured bone are presented in Table 5.4.

Figure 5.4 (a) Bone sample undergoing 3 point bending and (b) a typical fracture.

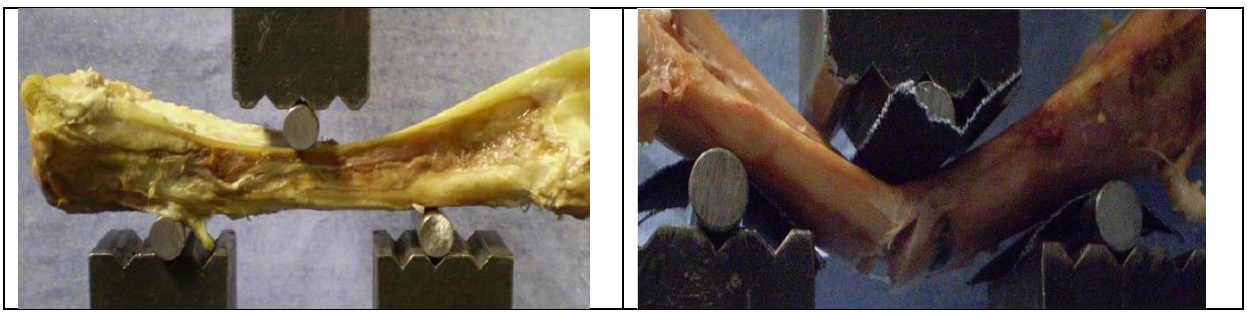

Table 5.3 Whole bone and R4 sub-region aBMD, geometric and mechanical properties of the bones fractured under three point bending.

Bone Level / no.	WB BMD ($g.cm^{-2}$)	R4 BMD ($g.cm^{-2}$)	ω (m)	I (m^4)	I / ω (m^3)	Fmax (N)	σ max (MPa)
H27	**1.014**	**0.986**	**7.76×10^{-3}**	**3.32×10^{-9}**	**4.55×10^{-7}**	**5232**	**205.07**
H2	**0.987**	**0.963**	**7.53×10^{-3}**	**3.59×10^{-9}**	**5.11×10^{-7}**	**5390**	**195.23**
H18	**0.925**	**0.884**	**6.94×10^{-3}**	**2.51×10^{-9}**	**3.77×10^{-7}**	**4479**	**157.74**
M21	**0.869**	**0.903**	**6.88×10^{-3}**	**2.45×10^{-9}**	**3.62×10^{-7}**	**4510**	**236.77**
M26	**0.827**	**0.794**	**6.80×10^{-3}**	**2.03×10^{-9}**	**3.81×10^{-7}**	**3030**	**164.64**
M20	**0.822**	**0.837**	**7.01×10^{-3}**	**2.15×10^{-9}**	**3.49×10^{-7}**	**4353**	**230.61**
L29	**0.773**	**0.803**	**7.01×10^{-3}**	**2.13×10^{-9}**	**3.54×10^{-7}**	**3050**	**153.08**
L4	**0.759**	**0.750**	**7.42×10^{-3}**	**2.52×10^{-9}**	**3.61×10^{-7}**	**3539**	**172.14**

Linear regression analysis of the relationships of whole bone and R4 sub-region bone density to breaking strength at the point of fracture are presented in Figure 5.5; and relationship of geometric parameters ω and I to breaking strength are presented in Figure 5.6.

Figure 5.5 Relationship of (a) whole bone sample and (b) sub-region R4 (region of fracture) areal bone mineral density ($g.cm^{-2}$) to maximum breaking force (F**max**).

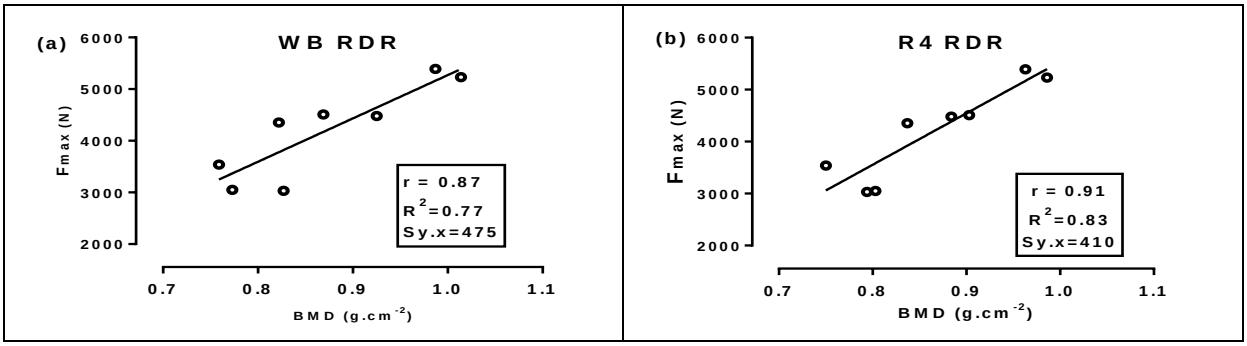

Figure 5.6 Relationships of (a) second moment of area (I) and (b) distance to the cross-sectional centre of mass (ω) to maximum breaking force (Fmax).

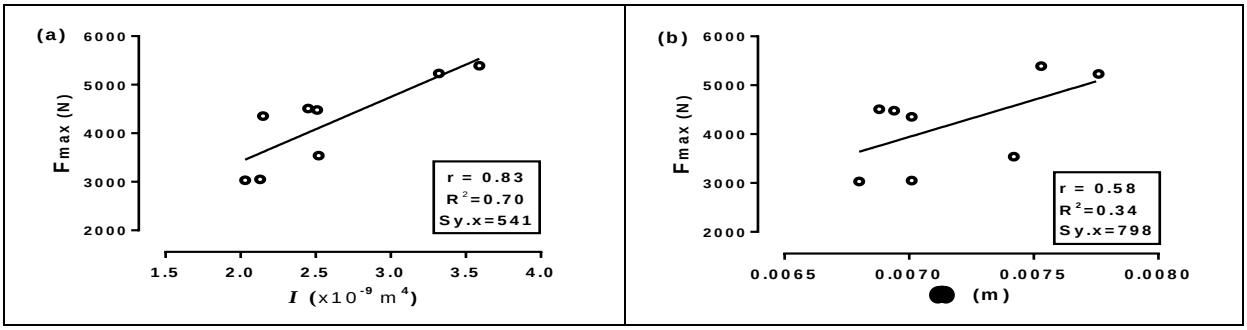

Analysis of scatter plots (Pearson product moment correlation coefficients) indicated mid-shaft cortical bone breaking strength (Fmax) in the ovine radius, albeit for a small number of bone samples tested, to be more strongly associated with DXA derived sub-regional aBMD (r=0.91) and whole bone aBMD (r=0.87) than to geometric

properties of cross-sectional moment of area (r=0.83), section modulus (r=0.71) and distance to cross-sectional centre of mass (r=0.58). Further analysis of whole bone and R4 sub-regional aBMD to σ_{max} at fracture showed r values < 0.4 indicating a poor association of aBMD to applied stress at the point of fracture.

The relationship of breaking force to various estimates of volumetric density ($g.cm^{-3}$) incorporating directly measured bone mineral content (BMC, g) divided by estimates of volume (cross-sectional area x section length) of the radial sections exposed to monotonic bending were less clear. The 'r' values of two estimated volumetric density measurements to breaking force were both less than 0.4 indicating a poor association of strength to estimated volumetric density. Therefore, in tests of monotonic bending to failure, DXA derived areal density measurement in units of $g.cm^{-2}$ over the whole bone and in particular the sub-region where fracture occurred were better associated with ultimate breaking strength of ovine radial mid shaft cortical bone than any other measured variable.

5.3.3 Four-point bending test results.

AutoCad software derived cross-section images of the ten bones selected for cyclic loading at 0.9 kN, to $3x10^5$ and $1x10^6$ cycles and subsequently undergoing analysis for microdamage are presented in Figure 5.7 and cross-sectional area and microdamage results in Table 5.4 are presented in order of magnitude of the bone sample aBMD.

Figure 5.7 Examples of the AutoCad software derived cross-sections for four of the ten bones sectioned following cyclic loading to 1 x 10^6 cycles at 0.9 kN.

The relationship of aBMD to microdamage accumulation variables is presented in Table 5.4; crack numerical density and surface density for individual bone samples and at high, medium and low aBMD levels are also presented graphically in Figures 5.8 and 5.9.

Table 5.4: aBMD (g.cm^{-2}), cross-sectional area (mm^2) and crack numerical and surface density *at T0,* 3x10^5 and 1x10^6 loading cycles in the entire cross-section.

Bone Level	aBMD (g.cm^{-2})	CSA (mm^2)	Numerical density (*n*.mm^{-2})			Surface density (μm.mm^{-2})			Mean crack length (μm)		
no.			*T0*	3x10^5	1x10^6	*T0*	3x10^5	1x10^6	*T0*	3x10^5	1x10^6
H 1	**0.916**	**508**	**0.02**	**0.05**	**0.21**	**2.2**	**8.3**	**28.0**	**102.5**	**168.0**	**134.0**
H25	**0.884**	**456**	**0.01**	**0.03**	**0.38**	**1.4**	**4.3**	**42.4**	**108.7**	**129.4**	**111.1**
H16	**0.857**	**352**	**0.01**	**0.04**	**0.24**	**0.7**	**4.2**	**22.7**	**87.1**	**106.3**	**95.1**
M23	**0.838**	**401**	**0.04**	**0.10**	**1.37**	**4.6**	**13.9**	**155.7**	**114.5**	**146.4**	**113.8**
M8	**0.824**	**431**	**0.02**	**0.04**	**2.81**	**1.5**	**4.0**	**258.2**	**70.2**	**115.3**	**91.9**
M3	**0.819**	**313**	**0.00**	**0.02**	**1.02**	**0.0**	**2.1**	**117.9**	**0.0**	**107.4**	**115.2**
L10	**0.778**	**367**	**0.03**	**0.32**	**5.59**	**2.7**	**30.2**	**519.1**	**89.4**	**93.2**	**92.8**
L17	**0.777**	**421**	**0.04**	**0.00**	**0.14**	**3.1**	**0.7**	**13.7**	**87.6**	**311.4**	**98.1**
L19	**0.742**	**366**	**0.08**	**0.08**	**4.32**	**6.4**	**9.9**	**403.3**	**83.5**	**129.0**	**93.4**
L28	**0.716**	**417**	**0.01**	**0.03**	**5.27**	**0.7**	**3.8**	**507.3**	**92.4**	**114.2**	**96.3**

Figure 5.8 Relationship of crack numerical density to (a) aBMD of individual bones; and (b) semi-log plot of mean (±SEM) microcrack numerical density grouped according to high, medium and low aBMD levels, *in vivo* and after cyclic loading.

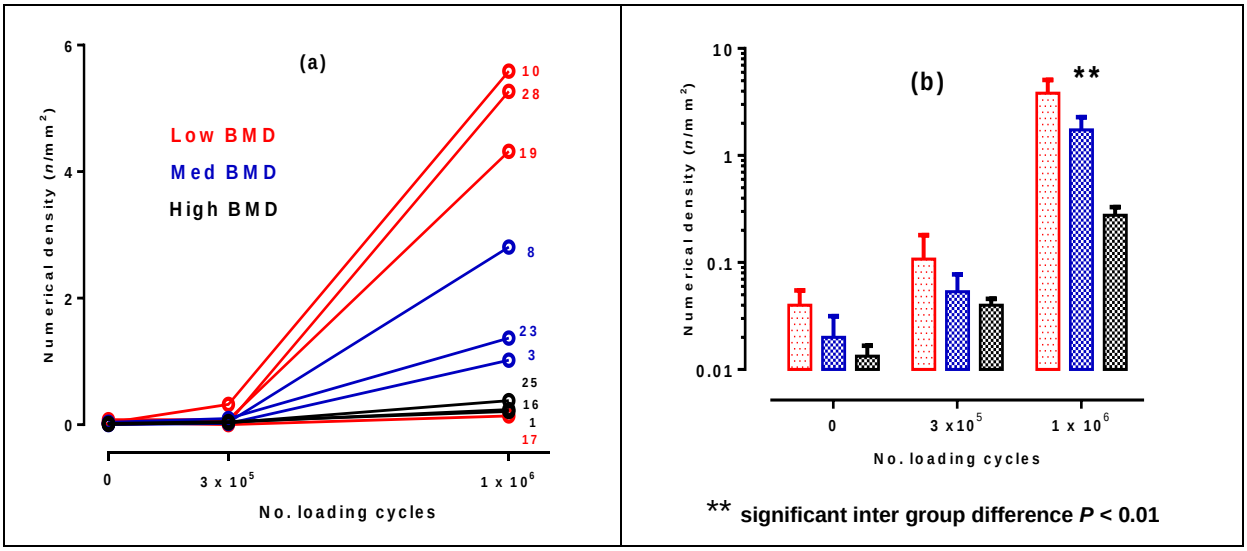

Figures 5.8a and 5.9a show microdamage accumulation for each individual bone with shading to indicate aBMD level, the individual plots clearly imply greater microdamage accumulation occurring in bone samples with lower aBMD, except for one outlier, *L17 where CSA and microdamage data resemble a high density bone. Initial statistical analysis within each level of loading at the three different aBMD levels for mean crack numerical and surface density (Figures 5.8b and 5.9b) revealed no significant difference between microdamage accumulation variables in bones of high, medium and low bone density.

Figure 5.9 Relationship of crack surface density to (a) aBMD of individual bones; and (b) semi-log plot of mean (±SEM) microcrack surface density grouped according to high, medium and low mean aBMD levels, *in vivo* and after cyclic loading.

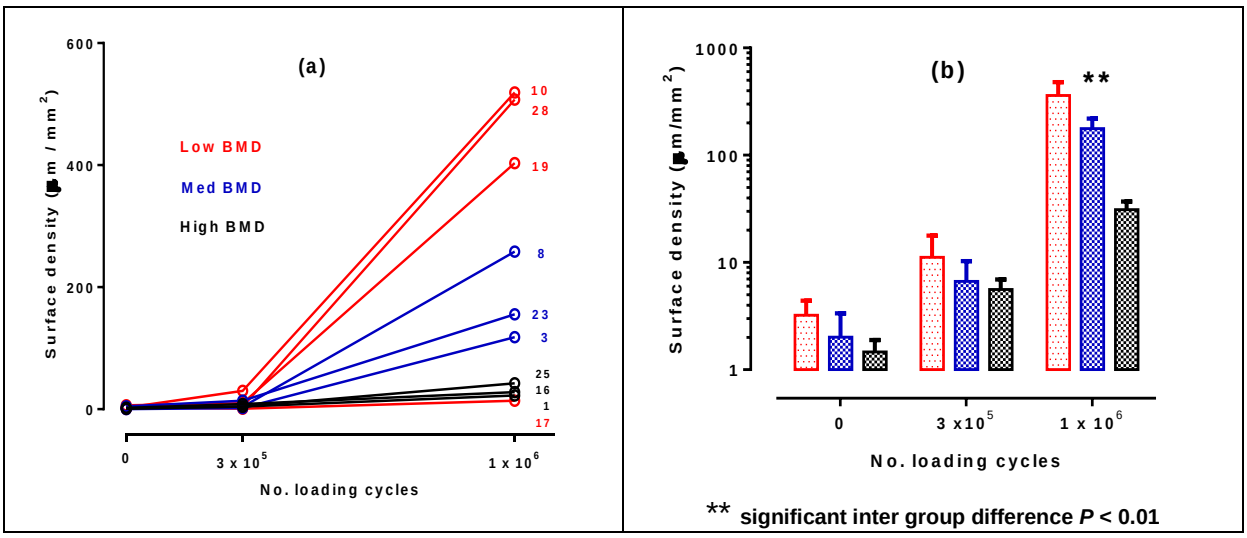

However, repeat analysis after removal of the outlier (L17) revealed a highly significant difference in both microdamage variables between aBMD groups at $1x10^6$ but not at 0 or $3x10^5$ cycles of loading (Kruskal Wallis $P = 0.0036$). Unfortunately the small sample size in each group precluded further statistical evaluation of the location of the differences between the aBMD groups at $1x10^6$ cycles. The level of association of aBMD to both microcrack numerical and surface density after $1x10^6$ cycles showed approximately similar r values of ~ 0.77 for both linear and non-linear curve fitting procedures but was best for a 3rd order polynomial (Figure 5.10).

Figure 5.10 Association of aBMD to microcrack (a) numerical density and (b) surface density after $1x10^6$ cycles of loading at 0.9kN.

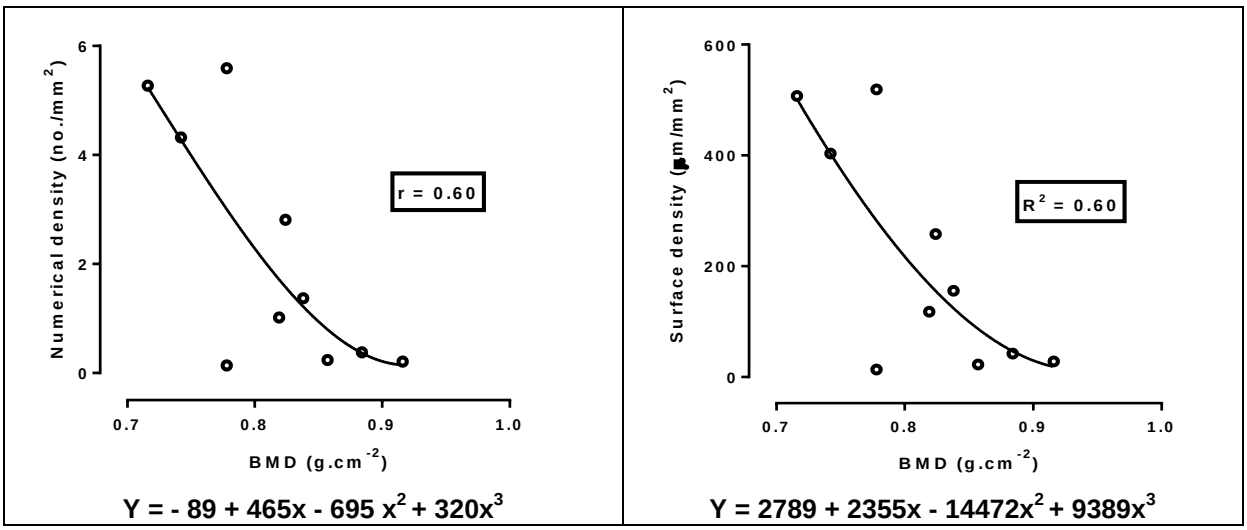

5.3.4 Conversion of load to stress

AutoCAD software derived cross-sectional area and Equation 5.1 were used to define discrete areas of stress; at 40, 60 and 80MPa (an example for Bone sample number 3 is presented in Figure 5.11). Cross-sectional area at each stress level for each individual bone is presented in Table 5.5 with microdamage variables at each stress region presented in Tables 5.6 and 5.7.

Figure 5.11: AutoCad derived cross-sectional areas for 40, 60 and 80 MPa (Bone 3).

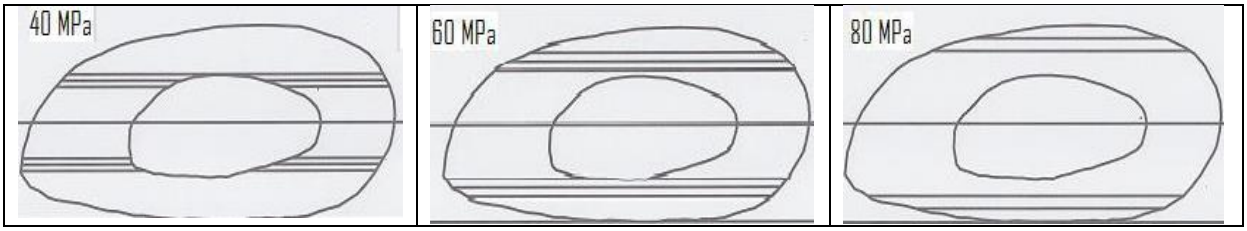

Table 5.5: Bone cross-sectional area (mm^2) for stress regions of 40, 60 and 80MPa

Bone	1	25	16	23	8	3	10	17	19	28
40MPa	135.7	93.3	42.5	60.9	73.6	49.7	36.1	57.3	44.9	93.1
60MPa	70.2	122.5	48.8	106.9	124.9	99.7	82.0	111.9	102.2	121.3
80Mpa	-	39.0	87.3	80.1	57.5	3.8	100.6	100.5	98.3	1.9

Table 5.6: Microcrack numerical density ($n.mm^{-2}$) of bone samples ranked according to aBMD ($g.cm^{-2}$) at three cross-sectional areas of stress; 40, 60 and 80MPa.

Bone	aBMD	*In vivo*			$3x10^5$ cycles			$1x10^6$ cycles		
Level/No.	$g.cm^{-2}$	40 MPa	60 MPa	80 MPa	40 MPa	60 MPa	80 MPa	40 MPa	60 MPa	80 MPa
H1	0.916	0.00	0.14	-	0.01	0.20	-	0.27	0.41	-
H25	0.884	0.01	0.01	0.08	0.02	0.02	0.20	0.15	0.64	1.15
H16	0.857	0.00	0.02	0.00	0.00	0.12	0.07	0.00	0.74	0.42
M23	0.838	0.07	0.00	0.02	0.00	0.09	0.15	0.30	2.68	2.83
M8	0.824	0.00	0.07	0.00	0.00	0.06	0.09	3.91	3.28	1.34
M3	0.819	0.00	0.00	0.00	0.00	0.04	0.00	0.18	1.49	9.37
L10	0.778	0.00	0.01	0.03	0.14	0.45	0.14	3.49	8.11	3.00
*L17	0.778	0.00	0.00	0.12	0.00	0.00	0.01	0.00	0.03	0.18
L19	0.742	0.00	0.01	0.26	0.00	0.10	0.09	3.72	4.23	3.25
L28	0.716	0.01	0.00	1.08	0.05	0.06	2.17	5.20	5.16	32.50

Table 5.7: Microcrack surface density ($\mu m.mm^2$) of bone samples ranked according to aBMD ($g.cm^{-2}$) at three cross-sectional areas of stress; 40, 60 and 80MPa.

Bone	aBMD	*T0*			$3x10^5$ cycles			$1X10^6$ cycles		
Level/No.	$g.cm^{-2}$	40 MPa	60 MPa	80 MPa	40 MPa	60 MPa	80 MPa	40 MPa	60 MPa	80 MPa
H1	**0.916**	**0.0**	**14.4**	**-**	**0.8**	**31.8**	**-**	**28.7**	**67.5**	**-**
H25	**0.884**	**1.3**	**0.7**	**8.7**	**2.0**	**2.2**	**26.3**	**21.1**	**69.5**	**110.0**
H16	**0.857**	**0.0**	**1.9**	**0.0**	**0.0**	**15.1**	**8.2**	**0.00**	**75.8**	**40.1**
M23	**0.838**	**7.5**	**0.0**	**2.7**	**0.0**	**14.6**	**19.9**	**36.7**	**287.5**	**321.2**
M8	**0.824**	**0.0**	**5.1**	**0.0**	**0.0**	**6.9**	**10.6**	**362.4**	**301.7**	**109.1**
M3	**0.819**	**0.0**	**0.0**	**0.0**	**0.0**	**3.7**	**0.00**	**27.1**	**174.3**	**807.3**
L10	**0.778**	**0.0**	**1.0**	**2.8**	**13.8**	**40.3**	**16.5**	**322.9**	**731.4**	**283.7**
L17	**0.778**	**0.0**	**0.0**	**10.2**	**0.0**	**0.00**	**3.1**	**0.00**	**2.4**	**22.7**
L19	**0.742**	**0.0**	**0.9**	**21.6**	**0.0**	**10.4**	**15.4**	**348.9**	**404.3**	**315.0**
L28	**0.716**	**1.0**	**0.0**	**101.9**	**6.4**	**6.6**	**247.9**	**508.0**	**529.5**	**3144.1**

5.3.5 Cyclic loading, regional stress and microdamage.

Initial statistical analysis (D'Agostino) of microdamage results for normality showed the majority of data sets were non-normal. Therefore the non-parametric Kruskal Wallis test was used to assess differences in microdamage data across stress region (40, 60 and 80 MPa) within each level of cyclic loading and across cyclic loading (0, $3x10^5$ and $1x10^6$ cycles) within each stress region. Further *post-hoc* analyses of detected statistical differences were performed using the Mann-Whitney test with Bonferroni correction to account for the number of groups and $P<0.05$ was considered significant. Results of statistical analysis of the microdamage variables numerical density and surface density across cyclic loading and across stress level without stratification for aBMD level are presented in Figures 5.12 and Figure 5.13.

Analysis of crack numerical density results across stress regions (40, 60 and 80MPa) revealed no inter group differences *in vivo* and at $1x10^6$ cycles ($P>0.05$). However, significant inter-group differences across stress regions were noted at $3x10^5$ cycles due to significant differences between 40MPa vs. 60 and 80MPa ($P<0.05$) but not 60 vs. 80MPa. The graphical plot of data at $1x10^6$ cycles of loading (Figure 5.12a) at first glance would seem to suggest differences across stress region; however, error bars indicated a considerable degree of variance within each group and consequently statistical analysis revealed no significant difference across stress level at this cyclic loading.

Figure 5.12: Microdamage results analysis with no aBMD stratification: mean (±SEM) numerical density (a) across stress region within 0, $3x10^5$ and $1x10^6$ cycles of loading; and (b) across loading cycles within regional stresses 40, 60 and 80MPa.

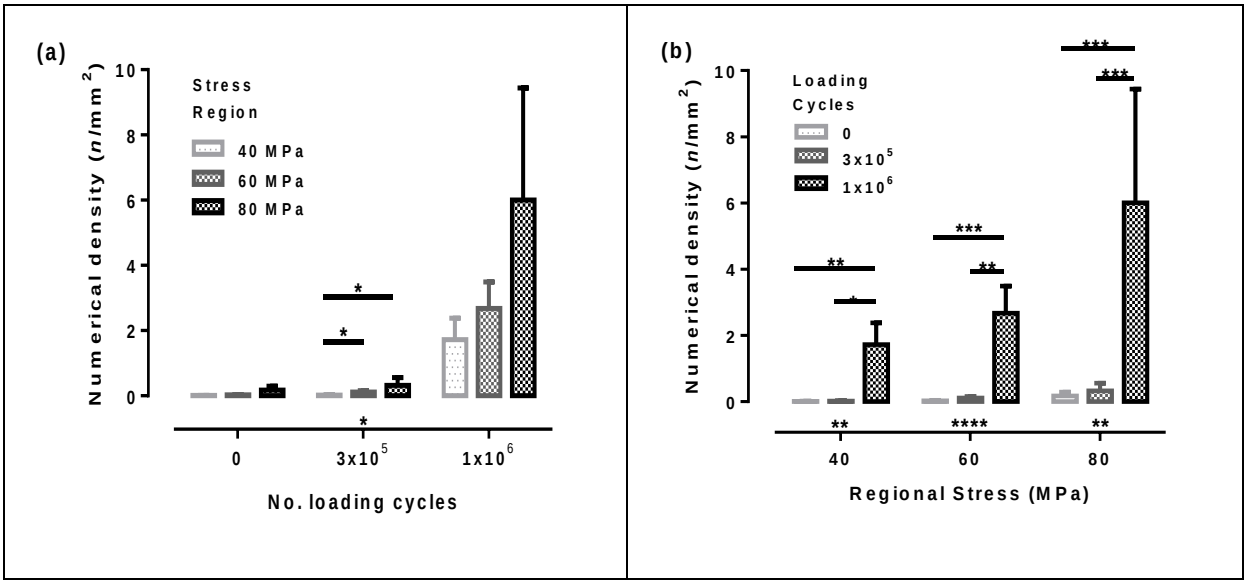

In contrast, analysis of crack numerical density data across cyclic loading level (Figure 5.12b) revealed significant differences at every level of regional stress; and further *post-hoc* analysis identified these differences at all levels of regional stress to be between 0 and $3x10^5$ cycles with $1x10^6$ cycles (P<0.01), with no significant effect detected between 0 and $3x10^5$ cycles of loading for any regional stress (P>0.05).

Analysis of crack surface density results revealed significant differences across stress region at every level of cyclic loading (P<0.01) and across cyclic loading at every level of stress (Figure 5.13). Again, similar to the numerical density data, *post-hoc* analysis across level of cyclic loading at each regional stress detected significant differences between $1x10^6$ cycles and both 0 and $3x10^5$ cycles; but not between 0 and $3x10^5$ cycles of loading.

Figure 5.13: Microdamage results analysis with no aBMD stratification: mean (±SEM) surface density (a) across stress region within 0, $3x10^5$ and $1x10^6$ cycles of loading; and (b) across loading cycles within regional stresses 40, 60 and 80MPa.

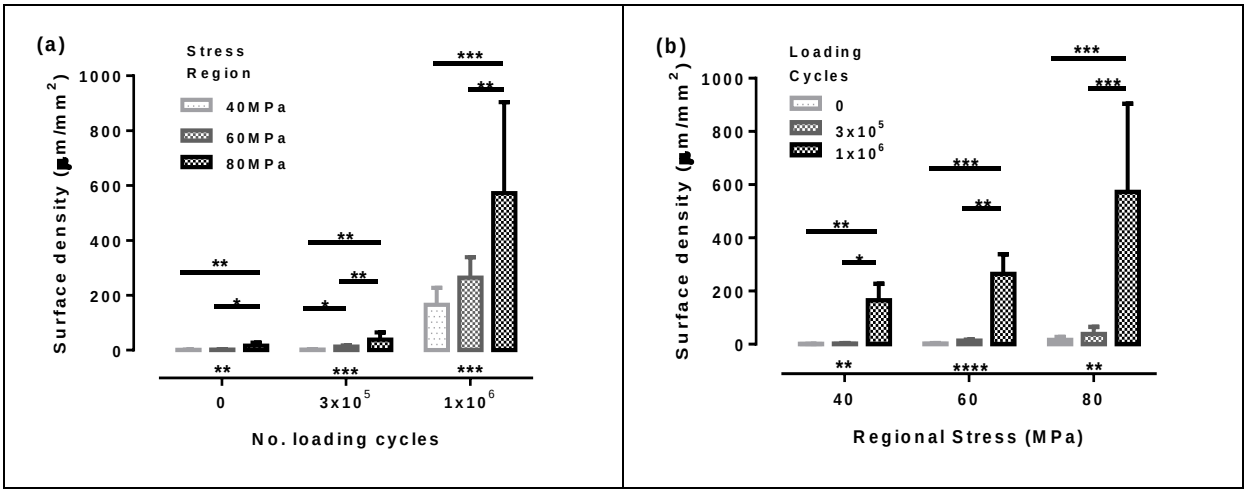

Statistical analysis of results without aBMD stratification suggests that the number of loading cycles is a more important determinant of crack numerical density than regional stress; whereas analysis of surface density results revealed significant increases in microdamage with any increase in regional stress or increase in cyclic loading over $3x10^5$ loading cycles at 0.9kN in four point bending. In the next analysis microdamage data were stratified as high, medium and low BMD to examine the influence of DXA derived bone quantity measurement (aBMD) with microdamage accumulation during cyclic loading.

5.3.6 Cyclic loading, regional stress and microdamage with aBMD stratification

The influence of aBMD on microdamage variables in the three stress regions in individual bones ranked according to aBMD are presented in Table 5.6 and Table 5.7; and non-parametric statistical analysis (Kruskal Wallis) of microdamage data occurring across stress regions at 40, 60 and 80MPa with aBMD stratified at high, medium and low levels are presented in the graphical plots Figures 5.14 and 5.15.

There were no significant differences between crack numerical density at 0 and 3 $x10^5$ cycles of loading at any level of aBMD at any regional stress ($P>0.05$). At $1x10^6$ cycles at 40MPa no significant difference was detected across aBMD level even when outlier (L17) was removed ($P=0.09$); at 60MPa with removal of the outlier (L17) there was a highly significant difference detected ($P<0.01$); and at 80MPa while the graphical plot is suggestive of an aBMD effect; large data variance and small sample size resulted in no significance even with removal of the outlier ($P=0.09$).

Figure 5.14: Mean (±SEM) crack numerical density ($n.mm^{-2}$) in high, medium and low aBMD bones at 40, 60 and 80 MPa.

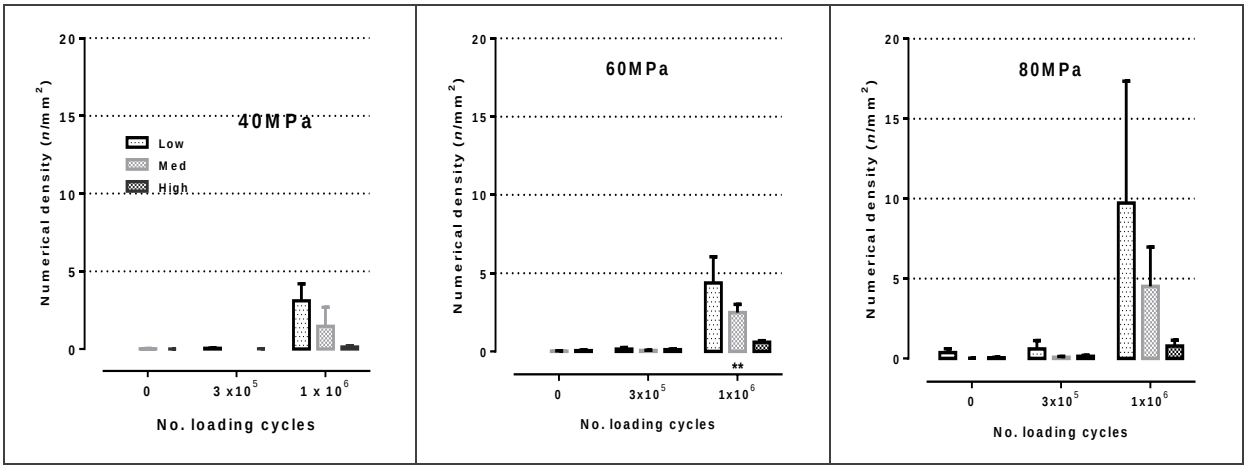

Figure 5.15: Mean (±SEM) crack surface density ($\mu m.mm^{-2}$) in high, medium and low density bone at 40, 60 and 80 MPa.

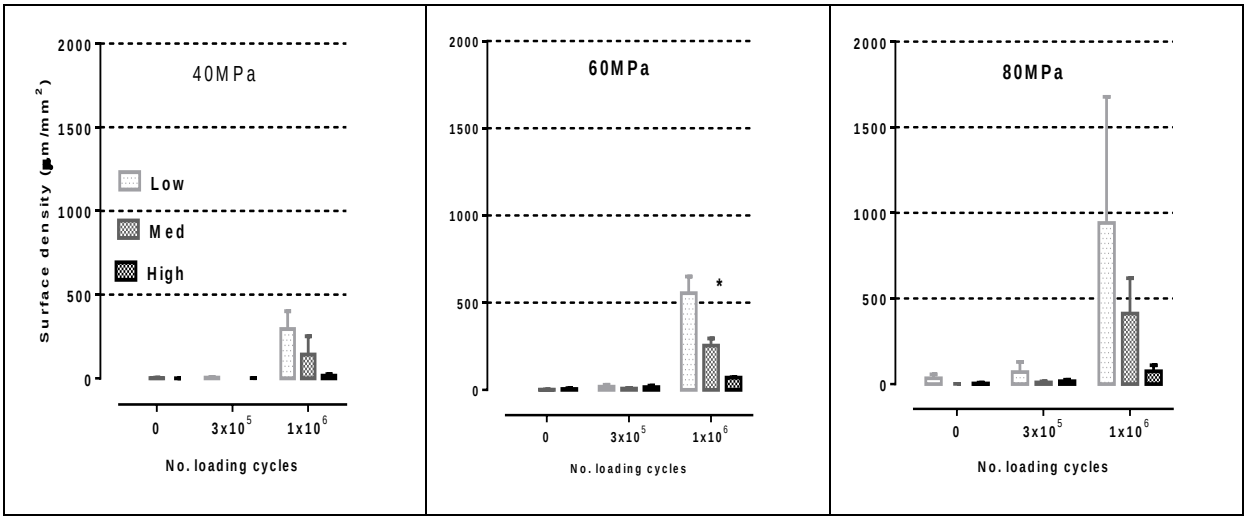

In analysis of microcrack surface density at 40, 60 and 80MPa no significant differences were apparent between aBMD levels *in vivo* (0 cycles) and at 3 x 10^5 cycles loading at any regional stress. A similar pattern also emerged with respect to data analysis at 1x10^6 cycles in that with removal of the outlier there was no significant inter-group difference at 40MPa, a significant difference at 60MPa (P<0.05) and at 80MPa again although the graphical plot suggests an aBMD effect this was not significant due to variance in data and small sample size.

Note at 80MPa numbers in the high density group in both analyses were reduced to two as AutoCad software derived data could not define a stress region within the cross-section of bone number 1.

5.4 DISCUSSION

5.4.1 Bone quantity in ovine radii selected for mechanical testing

DXA derived areal aBMD at five sites in the ovine skeleton including the ovine radii are presented and discussed in detail in Chapter 4. In the sub sample of Y1 ovine radii selected for monotonic tests to failure and four point bending, no differences were detected in areal BMD for CON vs. OVX at a whole bone level or in any of the sub-regions subjected to loading; namely, R4 for three-point bending and R3-5 for four-point bending. Thus the sample selection procedures, of bones across a wide range of density from both groups, did not result in a subsequent confounding effect due to OVX treatment on aBMD for testing to failure or for cyclic loading.

In analysis of the two components of aBMD for the bones undergoing 3 point bending to failure; much greater variability was apparent in bone mineral content (BMC; g) than areal projection (EA; cm^2) a marker of bone size or in this case the bone width. This has implications for interpretation of aBMD and geometric strength relationships in the next section, as there was greater variability in BMC than EA this might suggest that aBMD values in this part of the study were more related to differences in mineral content, rather than bone width. BMC variability results either from differences in material density, more mineral along the path length of the beam or differences in cross-sectional thickness of bone with same material density creating longer or shorter path length for attenuation of the beam.

5.4.2 Cortical bone density, geometry and breaking strength in ovine radii

In three point bending to failure of the radius, breaking force (Fmax) was highly correlated with; whole bone aBMD (r=0.87), sub-regional aBMD (r=0.91) at the site of fracture; cross-sectional moment of area (r=0.83) at site of fracture; and moderately correlated to section modulus (r=0.71) and cross-sectional centre of mass from the centroid (r=0.58). However, the relationships of estimated volumetric density (vBMD) to breaking force (F_{max}); and, of aBMD to breaking stress (σ_{max}) at the fracture site were poor ($r<0.4$). These findings, albeit for a small number of bones sampled, agree with numerous previous studies where the best predictors of fracture load in various human long bones were bone quantity; followed by geometric properties dependent

on cortical area and width (Alho *et al*., 1988; Beck *et al*., 1990; Augat *et al*., 1996; Courtney *et al*., 1997).

Coefficients of determination (r^2) data for DXA derived aBMD and cross-sectional moment of area, in this study could account for approximately 80 and 75% of whole bone strength, respectively. Again, very similar to data commonly quoted in the literature for cortical bone (Augat & Schorlemmer, 2006); and more moderate association of strength to section modulus and distance to the cross-sectional centre of mass was possibly due to elliptical rather than perfectly tubular cross-sections, and biological variability in cross-sectional thickness in different parts of the bone (Figure 5.11).

However, the relationships of aBMD to bending stress (σ_{max}) at fracture, and any estimated vBMD to any strength variable at the site of failure, only showed poor to moderate association. Strømsøe *et al*. (1995) reported similar findings in cortical bone of human femora; where DXA and QCT derived aBMD data were better associated with three point bending strength than QCT derived vBMD. Muehleman *et al.* (2000) assessing human metatarsals reported similar correlations between directly measured QCT derived vBMD and DXA derived aBMD; however, correlations of r~0.4 were much lower than those recorded for aBMD in this study illustrating variance in results between studies due to the cantilever loading method used in mechanical testing. Courtney *et al.* (1997) used a four point bending tests on metatarsals, and association between failure load and aBMD were much higher (r~0.8) and more in keeping with this study.

The strong relationship of aBMD to strength for the radii was not unexpected. DXA data essentially integrates a bone quantity factor (BMC) with a bone dimensional factor area projection (EA). Therefore, it is not surprising that together they show better association with bone strength; especially at cortical long bone sites, such as the mid shaft of the radius, with relatively thick cortices with uniformly distributed material through the cross-section (Beck *et al*., 1990). In addition it could be argued that BMC, if material density is constant between specimens and there is not much variability in bone size, would also be representative of geometry as greater attenuation and higher BMC values would be produced by a greater distance travelled across a section. In analysis of the two components of BMD in this study greater variability was seen in BMC, the mineral quantity component where

coefficient of variation (CV%) was 16%, than the dimensional width component EA; where CV% was approximately 5%. Interestingly CV% for I data was 18%, and therefore similar to BMC, this might suggest that the variation in BMD across the samples was due to differences in the inner cortical diameter or cortical cross-sectional thickness rather than an increase in tissue mineral density.

Tommasini *et al*. (2005) has reported that more slender long bones offer lower mechanical resistance, and suggested that slender bones may be at increased risk for fatigue fractures. However, variability in slenderness of selected mid-shaft ovine radii did not cause a problem for this study, and a size correction was not needed, as the range of width was very uniform in the central mid-shaft (38 to 42 mm).

Beck (2007) has shown how simple geometric properties like Z and I can be extracted from DXA scan data in an attempt to increase the predictive value of DXA in estimating fracture risk. In this study Z was determined from direct measurement of cross-sections using AutoCad software again not unexpectedly for a beam in bending to failure there was a strong relationship between section modulus (Z) to F_{max} (r=0.71); in newer generation DXA scanners, including the latest Hologic scanner it is possible to incorporate such geometrical data in addition to aBMD in hip structural analysis (HSA) scanner algorithms; it remains to be seen however whether aBMD and structural indices together will improve fracture risk prediction.

5.4.3 Cortical bone density and microdamage accumulation in the ovine radii

Fazzalari *et al*. (1998) stated that it would be useful if the burden of microdamage in bone could be assessed by non-invasive radiological measures. The results of this study, although of a small sample size, provide a preliminary insight as few studies have directly related non-invasive bone quantity radiological techniques to microdamage, an important bone quality factor in bone fragility and human osteoporosis.

Initial graphical plots of data for microcrack numerical density (Figure 5.8) and surface density (Figure 5.9) for individual samples showed a clear separation between low, medium and high density bone samples occurring with increased cyclic loading. Correlation of aBMD to microdamage variables was good r > 0.75, and R square data suggest that aBMD could account for approximately 60% of the

differences in microdamage occurring at the higher level of cyclic loading. When data were pooled and an outlier removed from analysis, highly significant differences in microdamage were apparent across aBMD level at $1x10^6$ loading cycles ($P<0.01$). In further analysis of microdamage across three stress regions at $1x10^6$ cycles, again, highly significant differences in microdamage variables were identified across aBMD level at 60MPa ($P<0.01$); and at 80MPa, although data analysis was highly suggestive of a difference across aBMD; differences did not attain significance ($P=0.09$) due to high data variance.

Stepan *et al*. (2007) investigated accumulation of microdamage in bone in post-menopausal women who had undergone long-term treatment with alendronate; and after adjustment for potential confounding variables, reported; lower femoral neck aBMD, increased age and alendronate treatment to be associated with microdamage accumulation; and that femoral neck aBMD was an independent predictor of microdamage. Fazzalari *et al.* (1998) studied bone quantity, compressive strength, stiffness, and micro-damage in the proximal femur of patients with osteoarthrosis; and reported bone mineral density and crack density to be major determinants of trabecular bone strength; and, bone mineral density and anisotropy major determinants of bone stiffness. However, compressive strength test results showed no relationship to aBMD and, therefore, the authors did not recommend aBMD for monitoring mechanical changes due to microdamage accumulation.

This might be true for the femoral neck in humans which is largely made up of trabecular bone and a small cortical shell, but, may not be true for bone with a high cortical bone component such as the ovine radii, where bending test results were highly related to aBMD. Therefore, in order to investigate the aBMD microdamage strength relationship further, mechanical testing to failure data for ovine radii which have undergone prior cyclical loading would be required, in a similar manner to the Fazzalari *et al.* (1998) study where trabecular bone samples which had undergone cyclical loading and were then compressed to failure.

5.4.4 Study limitations

The results of this study were almost certainly limited by the sample size, in the first part of the study when looking at levels of association between variables it is usually

recommended that at least a third of samples are at the extremes of range of values seen in the normal population. In this study that would have necessitated the availability of at least 4 to 6 low, medium and high density specimens. The availability of bone samples over a such a range of densities was partly limited by the sample size of the parent 'Bone for life' study and the requirement to split samples into two groups, one for whole bone tests to failure and the other to assess microdamage with cyclical loading.

The effect of low sample size has follow on effects on subsequent correlation analyses, and these results should therefore be interpreted with caution. Regression analyses, with small sample sizes tend to produce higher levels of association. In this study r and r^2 values were therefore presented with accompanying standard error of the estimate (Sy.x) values to quantify the predictive capacity of computed relationships. Calculated Sy.x data from regression analysis to F_{max} in this study were approximately 400 to 450 N for any of the associated variables measured, this represents approximately 20% of the total measurement range (3000 to 5000 N), and as such implies a significant degree of biological variation was present.

The lack of correlation of vBMD to F_{max} and σ_{max} was most likely due to the fact the volumetric density was not a directly measured variable; the calculated vBMD values were based on CSA measured by AutoCad software and section lengths. This calculation method assumed that the CSA measurement was constant along the section length, and the section lengths themselves were arbitrarily determined. Thus vBMD data were probably inaccurate which partly explains the poor levels of association to mechanical properties. It should be noted however that the literature reports even directly measured rather than estimated vBMD values used in this study, have also been found be a poor predictor of fracture load (Fmax). Beck, 2007 reported pQCT and DXA derived aBMD to be better predictors of whole bone failure in cortical bone than pQCT derived vBMD. The lack of strong associations of measured variables to σ_{max} data may also be due to the fact that CSA was not measured at the actual site of fracture.

In the second part of the study analysis of the results of microdamage accumulation with stratification for aBMD showed a statistically significant finding of greater microdamage with decreasing aBMD. These results should also be interpreted with

caution as sample size in the groups was very small, and there was a great degree of variability detected in data especially at $1x10^6$ cycles of loading. Furthermore, data analysis could only be performed using non-parametric rank order type statistical tests which are less robust, therefore, overall although significant differences were found they were small and warrant further investigation.

5.4.5 Conclusions and suggestions for future research

Despite the limitations mentioned above the following conclusions can be drawn from the results of the study:

1. The small differences in bone quantity detected between CON and OVX, bones selected for mechanical testing of bone strength and microdamage analysis did not attain statistical significance and nor were there any inter-group differences due to OVX on F_{max}, σ_{max} or any geometric structural bone quality property (I, ω or Z) related to bone strength. Ovariectomy alone does not induce any changes in bone quantity or quality at the radial site in an ovine animal model.

2. In three-point bending to failure the strongest associations of cortical bone breaking strength (F_{max}) were to DXA derived aBMD, and the structural variables cross-sectional moment of area (I) and section modulus (Z). Levels of association of aBMD and geometric variables to material strength (σ_{max}) were at best moderate, and vBMD relationships to any mechanical strength variable were poor. A further study using pQCT would allow more accurate direct measurement of cross-sectional areas and section volumetric BMD at the site of failure and would possibly improve the relationships of σ_{max} and vBMD to the other measured variables.

3. Similar levels of association of aBMD and I to F_{max}, as well as similar levels of variability in I and BMC, the bone quantity component of aBMD possibly suggest that the DXA aBMD measurement in this study was more reflective of differences in cross-sectional thickness rather than changes in tissue mineral material density. A further study might be possible involving HSA analysis on a third generation DXA device to ascertain DXA derived structural variables I and Z from the original radial scans, this data could then possibly be compared to the directly measured data to

further investigate the utility of DXA in prediction of geometric structural indices and their relation to mechanical properties.

4. The results of microdamage analysis following cyclic loading suggest lower areal BMD is related to higher levels of microdamage, in terms of crack numerical and surface density. However, further studies would be required to confirm these findings with much larger sample sizes. Additionally, to examine aBMD, microdamage and strength relationships, further studies are required of mechanical testing to failure in the ovine radii which have undergone prior exposure to cyclic loading to initiate microdamage.

CHAPTER 6

Influence of aBMD and microarchitecture on strength in ovine trabecular bone

6.0: Summary / Abstract

This study examined the influence and inter-relationships of bone quantity and quality factors on trabecular bone strength in an ovine animal model of osteoporosis. Trabecular cores (50mm long x 7mm diameter) were removed from the femoral necks of *ex vivo* ovine bones at two time points (12 month; Y1) and (31 month; Y3) post ovariectomy (OVX) and in control animals (CON). A further sub-group of 4 animals in Y3 OVX were treated with a long acting bisphosphonate drug zoledronic acid (ZOL). All whole bone samples underwent prior DXA scanning (Hologic QDR4500, USA); mid-sections of core samples (20mm x 7mm) subsequently underwent micro computed tomography (µCT40 Scanco, Switzerland) followed by compressive mechanical testing (Instron, UK). DXA derived bone quantity (aBMD), µCT volumetric density (vBMD) and trabecular microarchitectural variables (BV/TV; Tb.N; Tb.Th; Tb.Sp; and DA); and, mechanical test data; ultimate compressive stress (UCS), compressive modulus (*E*) and energy to failure (EN) data were compared for effect of time (Y1/Y2) and treatment (CON / OVX / ZOL). Results of mechanical tests revealed significant inter-group differences in UCS and *E* between CON and OVX at Y1 and all mechanical test variables at Y3; and in EN a significant increase in ZOL vs. OVX at Y3. No significant differences were detected in aBMD or vBMD between groups at any time point. In microarchitecture; Tb.Th. showed significant reduction in OVX vs. CON with large effect size at Y3; there were non-significant osteopaenic changes in most other variables at both time points; and in Y3 ZOL vs. OVX difference in Tb.Th approached significance. Relationships of bone quantity and quality to mechanical properties were best in Y1 CON for aBMD vs. UCS (r^2~0.5); BV/TV vs. UCS & *E* (r^2~0.7 to 0.8) and Tb.Sp vs. UCS & *E* (r^2~0.5 to 0.6); at Y3 and in OVX at both time points relationships were weaker for all variables. In conclusion inter-group differences in trabecular mechanical strength were most likely due to changes in microarchitecture, in particular decrements in trabecular thickness and increase in trabecular spacing. Relationships of bone quantity and quality variables were strongest at the first time point in the control group and were best for DXA derived areal density; BV/TV a marker of apparent density; and, trabecular spacing.

Key words: trabecular bone, bone quantity, microarchitecture, mechanical properties

6.1: Introduction

Bone's ability to resist fracture depends on the amount of bone mass, the spatial distribution of bone mass and intrinsic properties of bone material (Bouxsein, 2007). At the macroscopic structural level, bone is made up of two distinct types; cortical or compact bone, the predominant form in long bone diaphyses, and cancellous or trabecular bone predominantly found within vertebrae and at the expanded ends of long bones such as the proximal femur (Figure 6.1).

Figure 6.1: (a) Section through the proximal femoral trabecular bone and (b) Culman's crane and trabecular patterns described by von Meyer 1867 and later used by Wolff 1892 (adapted from Jacobs 2000).

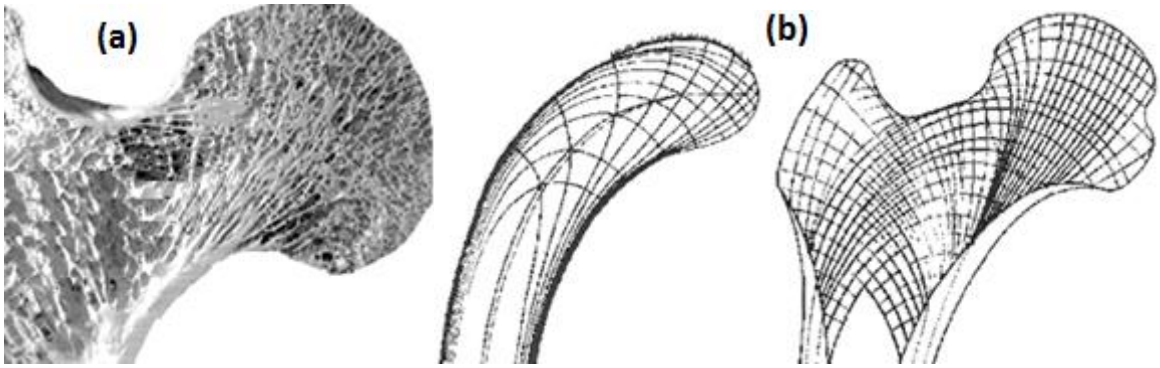

Cancellous bone is made up of a complex network of interconnecting struts and plates or trabeculae, arranged in varying forms, with thicker trabeculae orientated along lines of ambient stress (Gibson & Ashby, 1997; Jacobs, 2000). Trabeculae bear multidirectional loads, within the proximal and distal long bones, and effectively re-distribute these forces to the cortex of the mid-shafts (Turner, 2006). In vertebrae, axial compressive forces predominate and lighter porous trabeculae in the form of interconnected plates, absorb energy by deformation. However, trabeculae stiffness is reduced and vertebrae cannot withstand the peak loads seen in long bones (Turner, 2002). Trabecular volumetric density and vertebral height are similar across gender, and strength differences due to gender or ethnicity are usually dimensional; that is stronger vertebrae are wider, have greater cross-sectional area and greater trabecular thickness (Homminga *et al*., 2002; Duan *et al.,* 2006).

Degradation of structural and material properties in trabeculae occurs when ageing related failure of remodelling results in more bone being removed than deposited and an overall negative bone balance (Bouxsein & Seeman, 2009). In spinal trabecular bone, a porous material, strength declines by a factor of 4 to 5 from 20 to 80 years,

however, apparent density only halves this can be explained by the power relationship between apparent density and strength in trabecular bone (Carter & Hayes, 1977). In their original paper Carter and Hayes (1977) considered trabecular bone as open-celled rigid plastic foam or aerated porous concrete. In these types of porous materials, apparent density is a key factor determining mechanical properties and the relationship of elastic modulus and strength to apparent density can generally be described using the power relationship formulae shown in Equation 6.1.

Equation 6.1: $\gamma = A\rho^B$	Where; γ = strength or modulus, ρ is apparent density A and B = experimentally derived constants

Equation 6.1 can be rewritten in logarithmic form Equation 6.2.

Equation 6.2: log γ = log A + B log ρ	The constant 'B' is given by the slope of the linear regression line and 'log A' is the intercept.

The relationship between strength or modulus and apparent density is therefore linear on logarithmic plots. In addition to using the above equations to derive power relationships for apparent density and strength in bovine and human trabecular bone Carter and Hayes (1977) also recognised that this was not the only factor determining trabecular bone strength. They also recommended that any evaluation of bone tissue behaviour, should also include; analysis of ultra-structure, mineralization, trabecular orientation (anisotropy), both with and without the presence of marrow and over a range of densities to more accurately describe mechanical properties of bone.

Therefore, power relationships can partly explain why small changes in trabecular bone mass due to age related impairment of remodelling, coupled with further detrimental effects of; menopause, ovariectomy, drugs, disease or disuse, can have marked effects on structural competence. The typical features of osteoporotic age related bone loss in trabecular bone are; thinning (Parfitt *et al*., 1983), decreased connectivity (Martin & Ishida, 1989), and increased anisotropy (Mosekilde *et al.*, 2000). Ultimately, reduction in bone mass and quality falls to the point where the bone fails spontaneously or when some unusual loading outside of normal direction or magnitudes, say during a fall for example, may cause failure (Frost, 1997).

The Consensus Development Conference in Osteoporosis in Copenhagen in 1990 defined osteoporosis as ''a disease characterised by low bone mass and microarchitectural deterioration of bone tissue, leading to enhanced bone fragility and a consequent increase in fracture risk.'' Diagnosis of osteoporosis is usually based

on assessment of well-defined risk factors in a patient's history and dual-energy X-ray absorptiometry (DXA) measurement of areal bone mineral density (aBMD) at the neck of the femur and the lumbar spine (Kanis, 2002). However, it is increasingly recognised that DXA derived aBMD is a poor predictor of fracture risk as it lacks both sensitivity and specificity (Johnell *et al.,* 2005). The majority of people with osteoporosis by DXA criteria do not develop fractures (Schuit *et al.*, 2004), more than 50% of those who develop a fragility fracture do not have osteoporosis (Wainwright *et al*., 2004); and, BMD change only accounts for approximately 30% of the reduction seen in fracture risk with drug therapy (Delmas & Seeman, 2004).

The relationships of mass and strength have been studied in small and large animal studies. Ammann (2009) reported vertebral BMD in rats to predict 60% of the variance in maximal load; and, improved predictions of fracture load to 71.5 and 95% could be made with the addition of modulus (elastic tissue properties) and hardness (plastic tissue properties), respectively. Mittra *et al.* (2005) studied µCT variables in low, medium, and high strength trabecular bone samples from sheep; and reported structural model index (SMI) and density indices of bone volume fraction (BV/TV), with r^2 values of 0.85 and 0.81 respectively, as the best predictors of ultimate strength. Mittra *et al.* (2005) also reported bone loss affected trabecular connectivity and number, and increased strength was better associated with increase in trabeculae thickness rather than connectivity.

At the beginning of the previous decade the prevailing view was that human trabecular bone mechanical properties mainly depended on bone mass and the influence of bone quality factors remained uncertain (Keaveny *et al.*, 2001). However, recent research indicates aBMD, while still important clinically, is insufficient to accurately predict fracture risk or drug treatment effects; and further understanding of bone quality data from animal studies suggest that a combination of bone quantity and quality data may improve prediction of fracture risk and monitoring of patients receiving osteoporosis treatment in the future (Felsenberg & Boonen, 2005).

The 'Bone for Life' project consisted of a number of studies on bone quality in an ovariectomised ovine animal model. In one such study, Brennan (2008), investigated the 'microarchitectural bone quality' determinants of trabecular bone strength, and dovetailing with this work in the aim of the present study was to add a 'whole bone quantity determination' to the overall evaluation of trabecular bone strength in the

ovariectomised animal model. The specific aim of this part of the work was therefore to examine the influence of DXA derived 'whole bone quantity' (aBMD) on mechanical and microstructural properties of trabecular bone sampled from the ovine femoral neck. In particular the study aimed to show whether DXA aBMD, a whole bone measure incorporating both cortical and trabecular bone, could predict changes in strength in isolated trabecular cores from an ovariectomised animal model at two time points.

6.2: METHODS

6.2.1 Study design

Dual energy X-ray absorptiometry assessment of bone quantity, whole bone data acquisition scan, and all subsequent sub-regional and region of interest analyses were conducted by the author. Assessment of strength and micro-architectural variables of trabecular core samples taken from proximal ovine femora were conducted by Orlaith Brennan (Brennan, 2008).

6.2.2 Bone sample selection and DXA scanning

The proximal right femur was selected for micro-architectural studies and assessment of trabecular bone strength. Femora from all five groups Y1 CON and OVX, and Y3 CON, OVX and ZOL were scanned using a Hologic QDR4500 fan beam bone densitometer. Bone sample alignment protocols, DXA acquisition scan and sub-regional analysis algorithms for the femoral scans are documented in Chapter 2. In addition to WB and R1-6 scans, in the proximal femoral neck region smaller region of interest scans were also performed to chart BMD in head (r1); neck (r2) and intertrochanteric (r3) areas; namely, the region where trabecular core samples for assessment were collected from. Sample DXA scan images for WB, R1-6; and r1-3 are presented in Figure 6.2.

Figure 6.2: (a) Whole bone acquisition scan image (WB); (b) sub-regional analysis (SRA R1-6); and (c) region of interest analysis (ROI) r1 head; r2 neck and r3 intertrochanteric region for the right ovine femur covering the area of core trabecular samples.

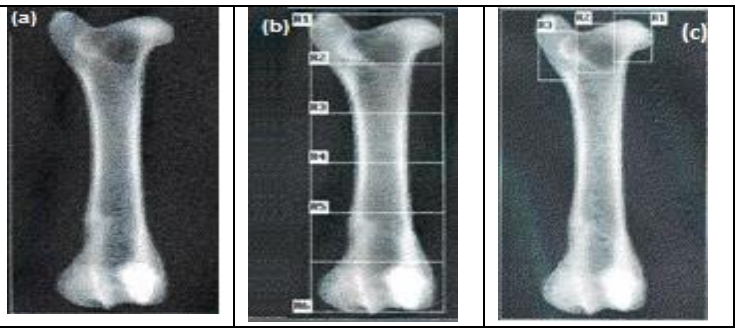

6.2.3 Femoral trabecular bone core sampling

Cylindrical cores of trabecular bone were obtained from the proximal femur using a diamond tipped coring tool (Cajero, Kent, UK); samples (7 mm diameter and 50 mm long) were removed in the coronal plane from the fovea to the greater trochanter (Figure 6.3). Test samples were then assessed at 15 mm from the point of entry, maintaining a length to diameter ratio of 2:1 as recommended for trabecular bone compression tests (Keaveny *et al.,* 1993). The 20 mm long samples were extracted from the cores using a diamond saw (Accutom-50, Struers, Denmark) for micro computed tomography (µCT) analysis and strength testing.

Figure 6.3: (a) alignment of femoral core sampling; and (b) schematic 7 x 50mm core sample, with 20 mm sample removed for mechanical testing at 15 mm distance.

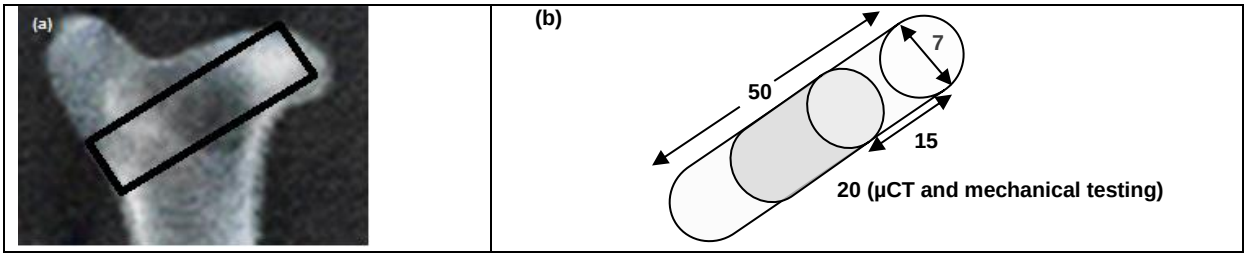

6.2.4 Micro computed tomography

Proximal femur trabecular architecture was analysed by micro computed tomography (µCT40, Scanco, Wangen-Brüttisellen, Switzerland). The 20 mm long cylinders were wrapped in saline soaked gauze to ensure hydration and scanned at a resolution of 8µm, at 70kVp and 114µA; 3-D images were obtained from 10mm mid-sections of the 20mm core cylinder scanned at a threshold value of 210, with sigma and support values of 0.8 and 1, respectively. The threshold value was selected to discriminate between bone, air and marrow. Trabecular bone volume fraction (BV/TV), trabecular number (Tb.N; $n.mm^{-1}$); trabecular thickness (Tb.Th; mm); trabecular separation (Tb.Sp; mm), and bone mineral volumetric density (BMC; $mg.mm^{-3}$) were recorded for analysis.

6.2.5 Trabecular core uniaxial compression tests

Uniaxial compression tests were carried out on the core samples in a material testing machine (Instron, Buckinghamshire, UK). The cylindrical cores were first press fitted into brass end-caps, attached to steel plates and following five pre-conditioning loads

of 20N were compressed to failure at a rate of 1mm.min^{-1}. Load displacement curves were plotted, and ultimate compressive strength, energy to failure and compressive modulus from the elastic region of the curves were interpolated. Non-attached peripheral trabeculae and the architectural variables, bone volume fraction and trabecular separation are known to influence mechanical properties and were factored into subsequent compressive modulus (*E*; MPa) calculations (Un *et al.,* 2006; Brennan, 2008). Ultimate compressive strength (*UCS*; MPa) was calculated by taking the maximum stress on the sample and dividing by the cross-sectional area of the cylinder. The energy absorption to failure (*Energy*; kJ.m^{-3}) of the specimen at the point of maximum stress was determined from the area underneath the stress-strain curve; by integration of the equation for the line between zero and the point of maximum stress (Figure 6.6).

Un et al. (2006) states that peripheral unattached trabeculae, do not contribute to the overall strength of the sample; and, that trabecular architecture parameters of BV/TV and Tb.Sp also influence modulus values. Thus corrections were made to mechanical test data of trabecular cylinders in compression using microCT data and Equation 6.1 a correction factor α.

Equation 6.1	*Where:* E_{True} = corrected modulus; $E_{Measured}$ = measured modulus when diameter is 7mm; and a and b are constants
$$\alpha = \frac{E_{True}}{E_{Measured}} = \frac{a \times Tb.Sp + b}{D}$$	

As Tb.Sp is inversely correlated with BV/TV, the correction factor can be expressed as a function of bone volume fraction, using Equation 6.2:

Equation 6.2	*Where:* c and d represent the slope and intercept, respectively, for Tb.Sp vs. BV/TV regression
$Tb.Sp = c \times BV/TV + d$	

Ultimate compressive strength (UCS), maximum load divided by the cross sectional area of the cylinder; with a correction factor α can also be expressed as shown in Equation 6.3.

Equation 6.3	*Where:* β = t / d; d = original diameter (7mm) and t is thickness of bone affected by side artefact. A new diameter D-t was used to determine the cross sectional area.
$$\alpha = \left(\frac{1}{1-2\beta}\right)^2$$	

The energy absorption at failure ($kJ.m^{-3}$) or energy absorbed by the cylinder at maximum stress was also calculated, by determination of the area underneath the stress-strain curve, by integration of the equation of the line between zero and maximum stress on the stress strain plots.

6.2.6 Data handling and statistical analysis

Microarchitectural and mechanical raw data corrected for the effects of unconnected trabeculae (Brennan, 2008) were re-analysed by the author. All data were recorded on Excel spread sheet and analysed for normality (D'Agostino) using Prism 6 (GraphPad Software, San Jose, USA). Femoral BMD, bone microarchitecture and strength in CON and OVX groups at Y1 and Y3 were compared using two way ANOVA using Sigma Stat 3.5 (Systat Software, CA, USA) with *post-hoc* analysis (Tukey multiple comparison tests) used to isolate differences. A further analysis was performed on Y3 femoral trabecular core data for differences between CON, OVX and ZOL; and, as there were only 4 animals in the ZOL group, non-parametric analysis (Kruskal Wallis) with *post-hoc* (Mann Whitney) with Bonferroni correction was employed. Further linear regression analysis was used to determine association between BMD and microarchitectural determinants of trabecular bone strength.

6.3: Results

DXA bone mineral density, µCT derived mineral content and micro-architectural data, and mechanical test results are presented in Table 6.1. Analysis of bone quantity and quality data and across time and group are presented in Figures 6.1 to 6.3.

Table 6.1: Mean (±SD) trabecular bone quantity, quality and strength of ovine femora from CON, OVX and zolendronic acid treated animals at 12 (Y1) and 31 month (Y3).

	Bone Quantity					**Bone Quality**				**Bone Strength**		
	DXA R1 $g.cm^{-2}$	**DXA r1** $g.cm^{-2}$	**DXA r2** $g.cm^{-2}$	**DXA r3** $g.cm^{-2}$	**µCT** $mg.mm^{-3}$	**BV/TV** ratio	**Tb. N** $n.mm^{-1}$	**Tb.Th** mm	**Tb.Sp** mm	***UCS*** MPa	***E*** MPa	***Energy*** $kJ.m^{-3}$
Y1 CON n=12	0.76 (0.07)	0.96 (0.06)	0.60 (0.06)	0.80 (0.10)	0.90 (0.24)	0.30 (0.08)	1.61 (0.32)	0.21 (0.04)	0.64 (0.12)	14.04 (4.45)	510 (176)	691 (74)
Y1 OVX n=13	0.74 (0.06)	0.98 (0.08)	0.58 (0.06)	0.77 (0.07)	0.89 (0.36)	0.26 (0.07)	1.62 (0.38)	0.19 (0.03)	0.69 (0.09)	11.26 (2.24)	378 (78)	621 (202)
Y3 CON n=16	0.77 (0.06)	0.99 (0.08)	0.58 (0.06)	0.81 (0.10)	0.91 (0.27)	0.24 (0.05)	1.52 (0.31)	0.17 (0.02)	0.71 (0.12)	11.75 (3.40)	604 (145)	547 (561)
Y3 OVX n=11	0.77 (0.06)	0.99 (0.08)	0.58 (0.06)	0.81 (0.10)	0.91 (20.3)	0.22 (0.05)	1.36 (0.28)	0.15 (0.01)	0.72 (0.13)	8.80 (3.48)	432 (159)	103 (79)
Y3 ZOL n=4	0.80 (0.04)	1.04 (0.05)	0.61 (0.03)	0.84 (0.04)	0.93 (0.05)	0.26 (0.04)	1.56 (0.27)	0.17 (0.00)	0.64 (0.11)	12.32 (2.40)	525 (185)	387 (224)

6.3.1 Femoral bone density data analysis

DXA derived femoral areal BMD (g.cm^{-2}) and micro CT derived volumetric density at two time points; 12 month (Y1) CON and OVX and 31 month (Y3) CON, OVX and Zolendronic acid treated group are presented in Figure 6.1. In the DXA results the r2 area of interest within proximal sub region R1 represented the areal BMD closest to the portion of bone sampled from the trabecular core for micro CT and strength testing.

No significant differences in DXA derived areal BMD were detected across group or time and there was no interaction effect between group or time for any region analysed R1 or r1-3 (two way ANOVA; *P*>0.05); further analysis of Y3 data revealed no significant differences in median data for CON, OVX and ZOL in any region (Kruskal Wallis; *P*>0.05).

Figure 6.4: (a) DXA bone mineral density (g.cm^{-2}) of whole bone (WB), proximal femoral sub-region (R1) and head, neck and intertrochanteric regions r1-3; and (b) µCT volumetric density (µg.mm^{-3}) of the trabecular core sample mid-sections.

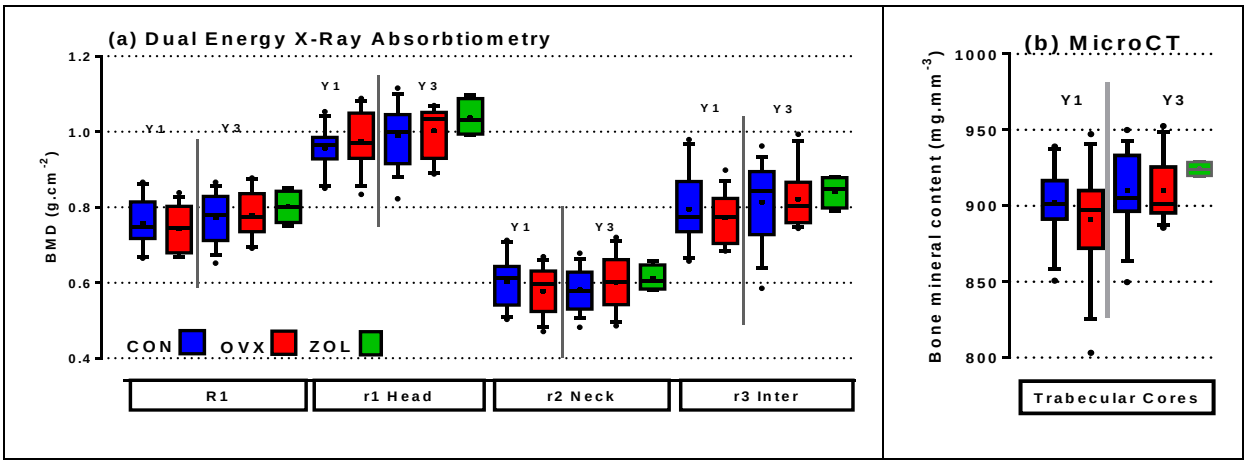

[Mean (+), median (bar), IQR (box), 10-90% (whiskers), outliers (·), data table in Appendix 6]

Analysis of µCT derived volumetric density (mg.mm^{-3}) of the trabecular core sample mid-sections also revealed no significant difference between Y1 and Y3, CON and OVX groups (2 way ANOVA; *P*>0.05) and in further analysis of Y3 groups there was no differences detected in median data for CON, OVX and ZOL (Kruskal Wallis; *P*>0.05).

6.3.2 Femoral trabecular microarchitecture data analysis

Femoral trabecular µCT data from proximal femur trabecular core samples are presented graphically with statistical analysis included in Figure 6.4. Analysis of BV/TV ratio revealed a significant difference between the CON groups at the two

levels of time Y1 and Y3 (2 way ANOVA; *P*<0.05), but there was no difference between OVX groups across time and no interaction effect detected between time and group. Analysis within Y3 groups revealed no significant differences in median data for CON, OVX and ZOL treated groups (Kruskal Wallis; *P*>0.05).

Figure 6.5: µCT micro-architectural data (a) bone volume fraction (b) trabecular number (n.mm^{-1}) (c) trabecular thickness (mm) and (d) trabecular spacing (mm).

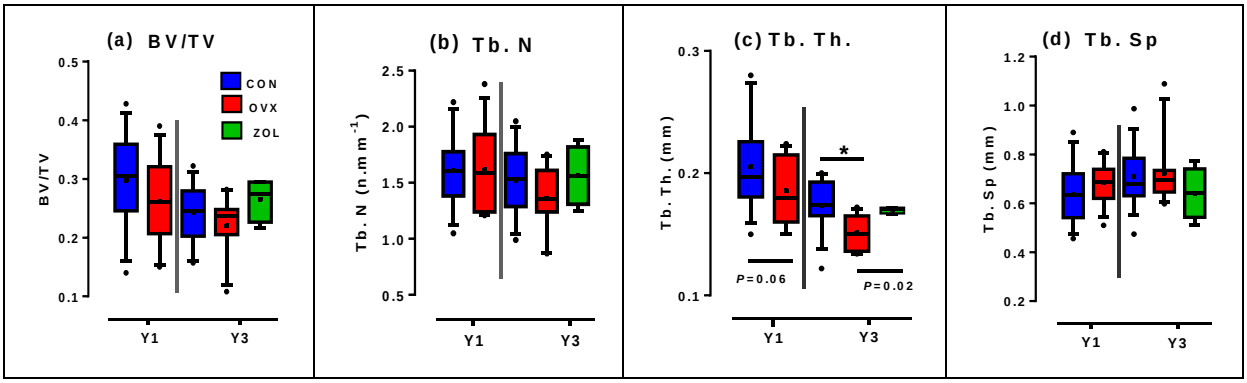

[Mean(+), median(bar), IQR(box), 10-90%(whiskers), outliers(·), * denotes *P*<0.05, data in Appendix 6]

In analysis of trabecular number (Tb.N) no significant difference was detected at any level of time (Y1 vs. Y3) or group (CON vs. OVX), there was no interaction effect between time and group (2 way ANOVA; *P*>0.05); and further analysis of Y3 groups revealed no significant difference between CON, OVX and ZOL treated groups (Kruskal Wallis; *P*>0.05).

Analysis of trabecular thickness (Tb.Th) data revealed significant inter-group differences, with a highly significant reduction detected within groups CON and OVX across time (*P*<0.01), analysis of between group differences (CON vs. OVX) approached significance at Y1 (*P*=0.056) and were significantly different at Y3 (*P*=0.028). However, no interaction effect was detected between group and time; further comparison of Y3 groups median data again showed a significant difference between CON and OVX (Mann Whitney; *P*<0.05) but differences between either CON or OVX with ZOL, after Bonferroni correction, did not reach significance. Analysis of trabecular spacing (Tb.Sp) revealed no significant difference at any level of time (Y1 vs. Y3) or group (CON vs. OVX) and no interaction effect between time and group (2 way ANOVA; *P*>0.05); within Y3 there were no significant differences between CON, OVX and ZOL (Kruskal Wallis; *P*>0.05).

6.3.3 Femoral trabecular strength data analysis

A typical stress strain curve for a trabecular core under compression is presented in Figure 6.6. Statistical analysis of; ultimate compression strength (UCS; MPa), compressive modulus (*E;* MPa) from the elastic region of the stress strain curves, and energy to failure (EN; kJ) derived from the area under the stress strain curves for Y1 and Y3 CON

Figure 6.6: Trabecular core compression stress strain curve

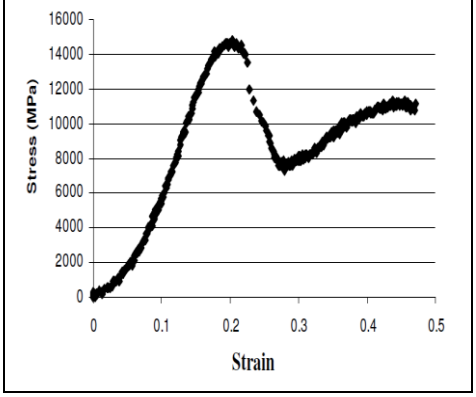

and OVX groups; and Y3 CON, OVX and ZOL groups are presented in Figure 6.7. Analysis (2 way ANOVA) of ultimate compressive strength (Figure 6.7a) revealed a significant overall time effect (Y1 vs. Y3; $P<0.05$) and a highly significant effect of group (CON vs. OVX; $P<0.01$) but no interaction effect. *Post-hoc* multiple comparison tests (Tukey) revealed no significant difference in strength within group across year (both $P=0.09$) but did detect significant strength reductions due to treatment CON vs. OVX within year at Y1 ($P=0.05$) and Y3 ($P<0.05$).

Figure 6.7: Trabecular core compression test to failure (a) ultimate strength (MPa) (b) modulus (MPa) and (c) energy to failure (kJ).

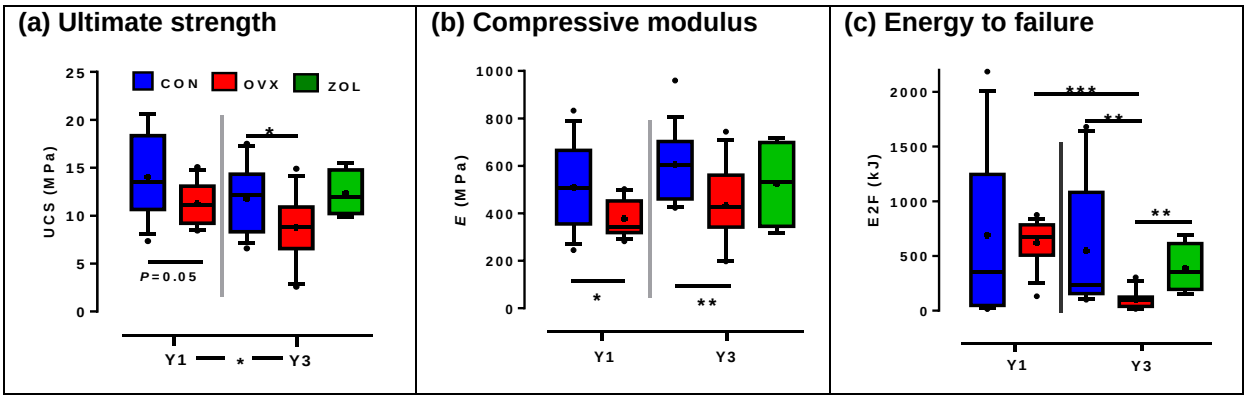

[Mean (+), median (bar), IQR (box), 10-90% (whiskers), outliers (˙) and * denotes $P<0.05$; ** $P<0.01$; *** $P<0.001$, for data tables see Appendix 6]

Analysis of compressive modulus (*E*) (Figure 6.7b) revealed no significant time effect Y1 vs. Y3 (2 way ANOVA; $P<0.05$) but there were significant differences between groups (CON vs. OVX) at each time point; with $P=0.025$ at Y1 and $P=0.004$ at Y3. Further analysis of median data of Y3 groups again showed significant strength reduction comparing OVX and CON (Mann Whitney; $P<0.05$), however, *post- hoc*

analysis with Bonferroni correction revealed no significant differences between both CON and OVX with ZOL (Mann Whitney; $P>0.05$).

Energy to failure (kJ) data (Figure 6.7c) were difficult to interpret due to wide dispersion of data in Y1 and Y3 CON; the raw data set failed normality testing and prior to analysis (2 way ANOVA) data therefore underwent Log 10 transformation. Further confounding data interpretation; a highly significant interaction effect was detected between time and group ($P<0.001$); as well as a highly significant reduction in energy to failure in OVX compared to CON at Y3 ($P<0.001$) but not at Y1, and highly significant reduction in energy to failure data for Y3 compared to Y1 in OVX. Analysis of median data within Y3 for the effects of Zolendronic acid again showed similar reduction in energy to failure for OVX vs. CON ($P<0.001$) but also a significantly higher energy to failure in ZOL compared to OVX, but not ZOL vs. CON.
Initial scrutiny of results suggested that reductions in ultimate compressive strength and compressive modulus of ovine femoral neck trabecular core samples in the OVX group were the result of a reduction in trabecular thickness, that is a reduction in bone quality rather than bone quantity as there were no significant inter-group differences detected in DXA areal BMD ($g.cm^{-2}$) or µCT volumetric BMD ($mg.mm^{-3}$) variables. In an attempt to quantify the strength, if any, of relationships between variables, regression analysis of bone quantity (BMD) and quality (micro-architecture) to bone strength was performed. Additionally as no statistically significant effect of OVX was apparent, the relationships of stratified BMD data, to bone strength variables was conducted, similar to the cortical bone analysis presented earlier in Chapter 5.

6.3.4 Relationships of bone quantity and quality to strength

Linear regression analysis; Pearson correlation coefficient (r) and coefficient of determination (r^2) and standard error of the estimate (Sy.x); of bone quantity, DXA whole bone (WB) and sub-regional (SR1, sr2) area BMD and µCT volumetric BMD and bone quality factors; bone volume fraction (BV:TV), trabecular number (Tb. *n*), thickness (Tb. Th.) and spacing (Tb. Sp.) in relation to ultimate compressive strength and compressive modulus (*E*) are presented in Table 6.2. Linear regression analysis for energy to failure data are not presented as data variability was too large to make meaningful interpretation.

Table 6.2: Global linear regression of bone quantity and quality factors to mechanical properties of all femoral neck trabecular core samples (n=56).

		Ultimate strength			Modulus		
	Variable	**r**	**R^2**	**Sy.x** (MPa)	**r**	**R^2**	**Sy.x** (MPa)
Bone quantity	**WB aBMD**	0.20	0.04	3.65	0.13	0.02	165.5
	R1 aBMD	**0.28**	0.08	3.59	0.17	0.03	161.1
	r2 aBMD	**0.28**	0.08	3.58	0.15	0.02	164.9
	Tb vBMD	0.02	<0.01	3.73	<0.01	<0.01	166.9
Bone quality	**BV:TV**	**0.69**	**0.47**	2.72	**0.46**	0.21	148.1
	Tb. *n.*	**0.58**	**0.33**	3.05	**0.37**	0.13	155.3
	Tb. Th.	0.30	0.09	3.56	0.04	<0.01	166.8
	Tb. Sp.	**0.59**	**0.36**	3.02	**0.45**	0.20	149.3

Figure 6.8: Global relationships of bone quantity and quality to ultimate compressive strength in: (a) r2 aBMD (b) BV fraction and (c) trabecular spacing.

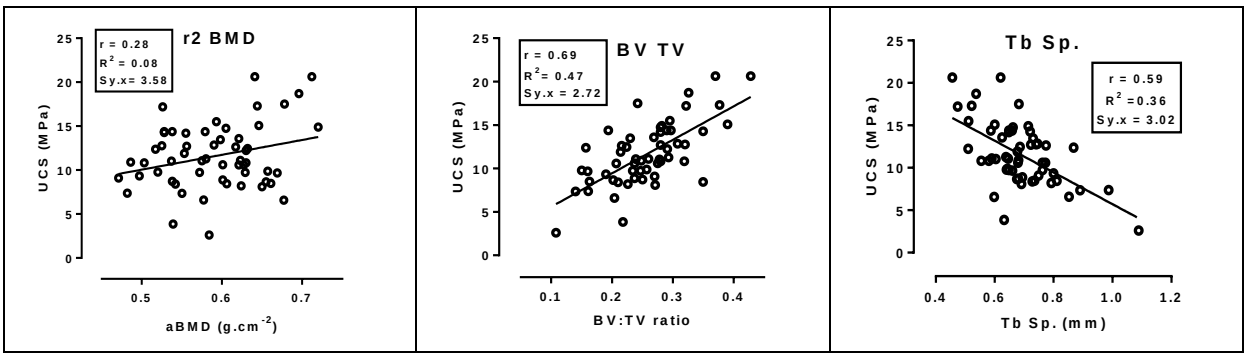

Results of linear regression for the trabecular samples in compression showed absent or poor association for all bone quantity factors to the three bone strength variables measured. The highest r values (~0.3) were seen for the relationship R1 and r2 to ultimate strength, association with compressive modulus was weaker (r<0.2) and there was no association with energy to failure. µCT derived volumetric BMD (mg.mm^{-3}) showed no association to any strength variable. The association of architectural variables to mechanical properties, although much better than for bone quantity, was at best moderate.

Bone volume fraction BV/TV a marker of apparent density had the highest level of association; r~0.7 for strength and r~0.5 for modulus and energy to failure. Trabecular number and spacing recorded r data of ~0.6 for strength and 0.3 to 0.4 for modulus and energy to failure. Trabecular thickness was of a similar level of association to mechanical properties as the bone quantity variables. Linear regression analysis of bone quantity and quality to ultimate strength for Y1 and Y3, CON and OVX groups are presented in Tables 6.3 and 6.4 and sample scatter plots are depicted in Figure 6.9 and 6.10. The Y3 ZOL group is not presented as sample size was too small (n=4) to make any meaningful assumptions.

Table 6.3: Y1 CON (n=12) and OVX (n=13) linear regression of bone quantity and quality factors to mechanical properties of all femoral neck trabecular core samples.

	Y1	CON			OVX		
	Variable	**r**	**R^2**	**Sy.x** (MPa)	**r**	**R^2**	**Sy.x** (MPa)
Bone quantity	**WB aBMD**	0.44	0.19	4.18	0.37	0.13	2.18
	R1 aBMD	**0.75**	**0.55**	3.11	0.50	0.25	2.03
	r2 aBMD	**0.70**	**0.49**	3.34	0.34	0.12	2.20
	Tb vBMD	0.39	0.02	4.61	0.10	0.01	2.33
Bone quality	**BV:TV**	**0.86**	**0.74**	2.37	0.47	0.22	2.07
	Tb. *n.*	0.42	0.18	4.23	0.45	0.20	2.09
	Tb. Th.	0.03	<0.01	4.66	**0.62**	0.39	1.83
	Tb. Sp.	**0.68**	0.46	3.42	0.35	0.13	2.19

Figure 6.9: Relationships of bone quantity and quality to ultimate compressive strength in Y1 CON: (a) r2 aBMD (b) BV fraction and (c) trabecular spacing.

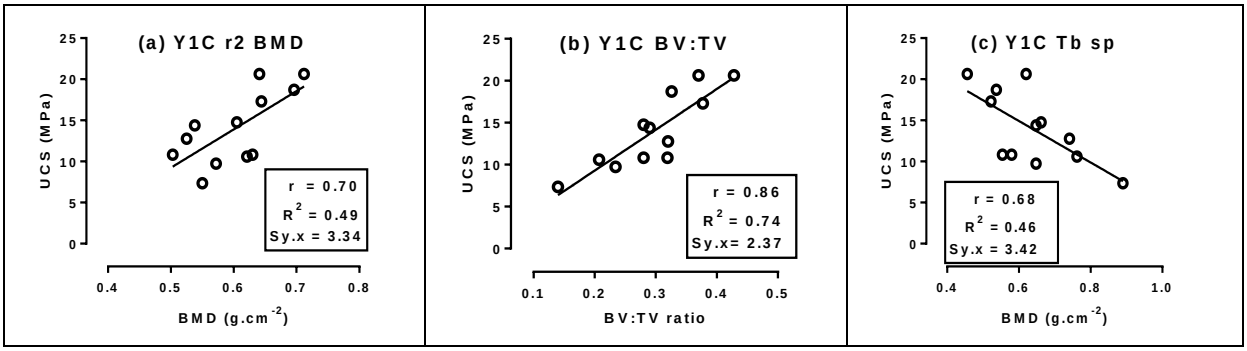

In Y1 association with ultimate compressive strength was strongest in the control group for bone volume fraction (r~0.9), good for R1 BMD, r2 BMD and trabecular spacing (r~0.7) and moderate to poor for all other variables. In the OVX group there was moderate association for trabecular thickness (r~0.6), but poor association for all other bone quantity and quality parameters.

Table 6.4: Y3 CON (n=16) and OVX (n=11) linear regression of bone quantity and quality factors to ultimate compressive strength of all trabecular core samples.

	Y3	CON			OVX		
	Variable	**r**	**R^2**	**Sy.x** (MPa)	**r**	**R^2**	**Sy.x** (MPa)
Bone quantity	**WB aBMD**	0.10	0.01	3.50	0.38	0.15	3.40
	R1 aBMD	0.10	0.01	3.50	0.19	0.03	3.61
	r2 aBMD	0.05	<0.01	3.51	0.31	0.09	3.50
	Tb vBMD	0.01	<0.01	3.52	0.25	0.07	3.55
Bone quality	**BV:TV**	0.47	0.22	3.11	**0.79**	**0.63**	2.25
	Tb. *n.*	**0.69**	0.47	2.56	**0.79**	**0.63**	2.25
	Tb. Th.	0.05	<0.01	3.51	0.16	0.03	3.62
	Tb. Sp.	**0.66**	0.43	2.65	0.41	0.17	3.35

Figure 6.10: Relationships of bone quantity and quality to ultimate compressive strength in Y3 OVX: (a) r2 aBMD (b) BV fraction and (c) trabecular spacing.

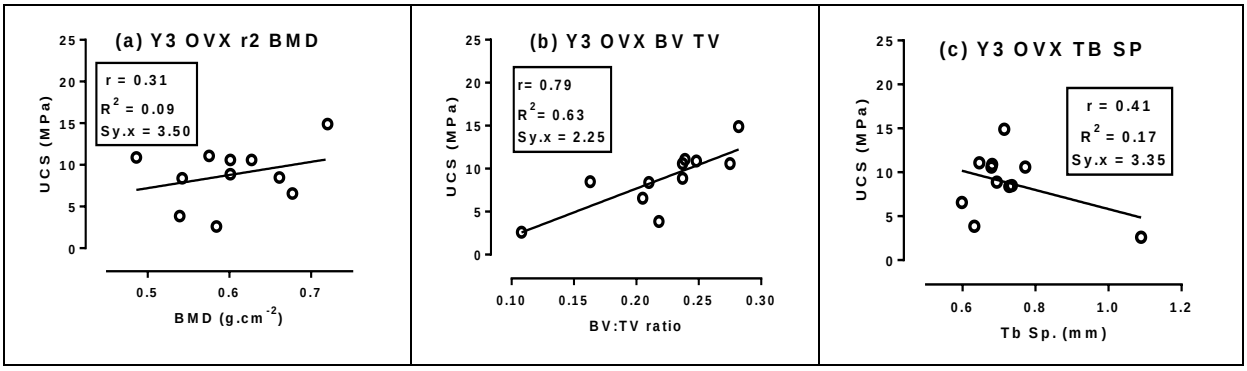

In Y3 the strongest associations with ultimate compressive strength were for bone quality factors, in OVX; bone volume fraction and trabecular number (r~0.8); in CON; association was also moderate for trabecular number, spacing and bone volume fraction (r~0.5 to 0.6). However, bone quantity variables only recorded moderate to poor association with strength in OVX (r ~ 0.2 to 0.4) and were poor in CON (r < 0.2). Greater correlation with strength in both Y1 and Y3 groups should be interpreted with caution, higher r values were largely due to smaller sample sizes in individual groups especially in Y3 OVX.

Standard errors of the estimate (Sy.x), for the different variables assessed, were similar (2 to 4 MPa) when data were analysed globally or for individual groups, and therefore change in r values were thus largely attributable to change in sample size. Computed Sy.x data also indicated a considerable degree of biological variation in strength across bone quantity and quality variables when it is considered that they account for at best ~15% and at worst ~30% of the total data range of ultimate compressive strength measured during mechanical testing of the trabecular cores.

6.4.5 Trabecular strength and microarchitecture data with BMD stratification

In this section the relationship of high, medium and low areal BMD to ultimate compressive strength, modulus and µCT data are presented stratified for high, medium and low BMD derived from DXA data at the r2 site in Figure 6.2. In analysis of low, medium and high BMD trabecular cores to ultimate compressive strength there were non-significant trends of increased strength across density in CON and OVX; and, when grouped according to year; at Y1, the high density group was significantly stronger than medium and low density cores. There were no differences in modulus data across density in CON or OVX and at Y3 or Y1. In µCT data

stratified for BMD there were non-significant trends across density of increased bone volume fraction in CON, increased trabecular number across density in all groups, increased trabecular thickness in CON and decreased in OVX, and significantly reduced trabecular spacing in the high density group when compared to low and medium density bone in Y1 ($P<0.05$).

Figure 6.11: Mechanical and microarchitectural properties of trabecular cores; for all, CON/OVX and Y1/Y3 data stratified by DXA derived r2 sub-region area BMD.

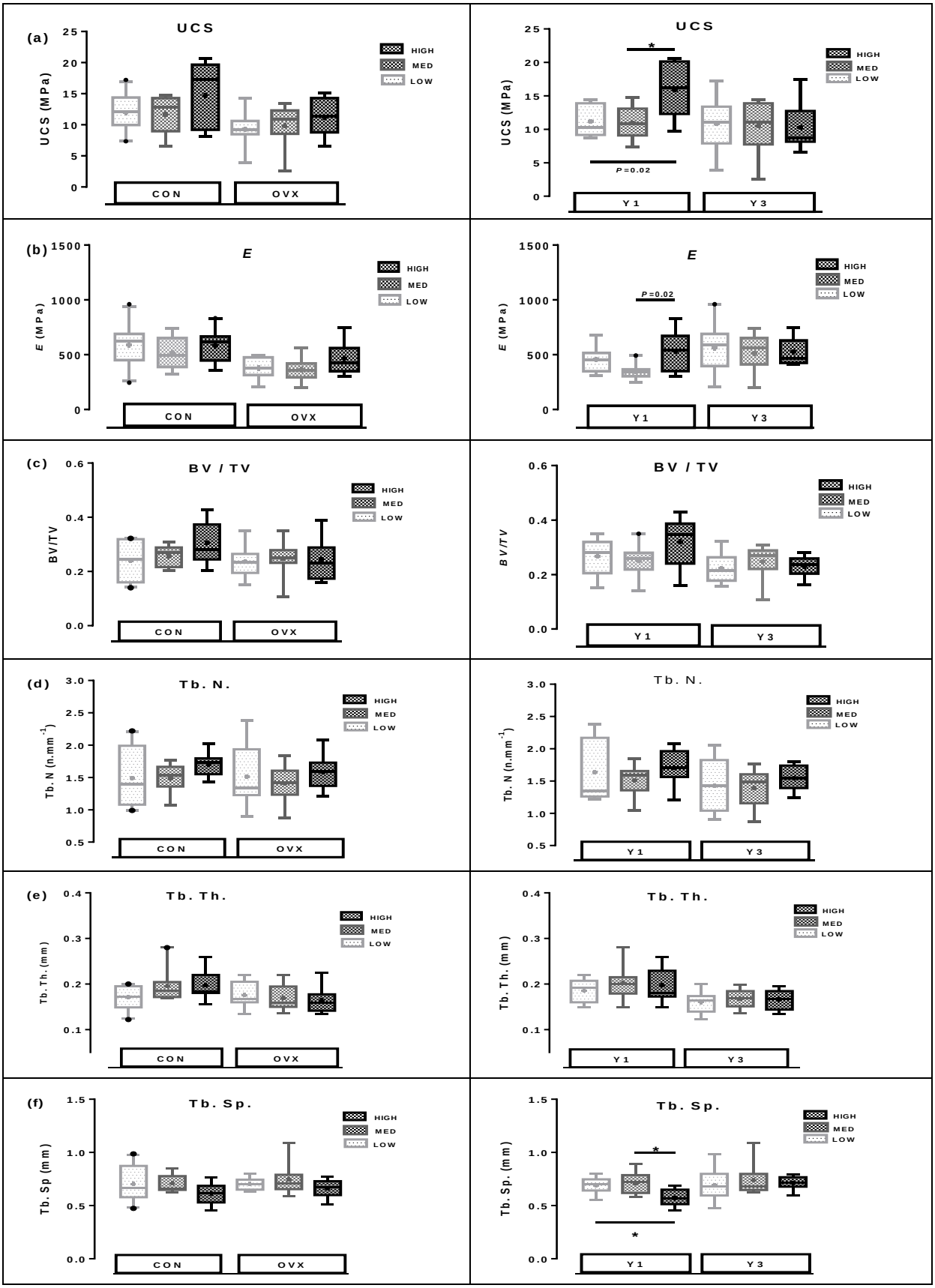

[Mean (+), median (bar), IQR (box), 10-90% (whiskers), outliers (·) and * denotes $P<0.05$, for data tables see Appendix 6]

6.3.6 Summary of results

Results are summarised below as mean inter-group differences (%), in Table 6.5 for mechanical properties, and in Tables 6.6 and 6.7 for bone quantity and micro-architectural data. Where significant differences in raw data comparisons were detected the mean inter-group % differences have been highlighted. A summary of linear regression analyses of bone quantity and quality to bone strength is presented in Table 6.8 for Y1 and Table 6.9 for Y3 groups.

Table 6.5: Trabecular mechanical properties: Mean inter-group differences (%).

	Y1	Y3		
Variable	**OVX - CON**	**OVX-CON**	**ZOL-OVX**	**ZOL-CON**
Compressive strength (UCS)	↓20%	↓25%	↑ 40%	↑ 5%
Compressive modulus (*E*)	↓26%	↓29%	↑ 22%	↓ 13%
Energy to failure (EN)	↓10%	↓81%	↑278%	↓ 29%

Table 6.6: Trabecular bone quantity: Mean inter-group differences (%)

	Y1	Y3		
Variable	**OVX-CON**	**OVX-CON**	**ZOL-OVX**	**ZOL-CON**
DXA R1 BMD	↓ 2%	↑ 1%	↑3%	↑4%
DXA r2 BMD	↓ 4%	↑ 3%	↑2%	↑5%
Micro CT vBMD	↓ 1%	↔ 0%	↑2%	↑2%

Table 6.7: Trabecular bone microarchitecture: Mean inter-group differences (%)

	Y1	Y3		
Variable	**OVX-CON**	**OVX-CON**	**ZOL-OVX**	**ZOL-CON**
Bone volume fraction **(BV / TV)**	↓12%	↓ 10%	↑21%	↑10%
Trabecular number **(Tb. N.)**	↓ 1%	↓ 11%	↑15%	↑3%
Trabecular thickness **(Tb. Th.)**	↓10%	↓ 15%	↑12%	↓3%
Trabecular spacing **(Tb. Sp.)**	↑ 8%	↑ 2%	↓11%	↓9%
Degree of anistropy **(DA)**	↑ 8%	↑ 8%	↓ 4%	-

Table 6.8: Relationships (r^2 values) for trabecular bone quantity and micro-architecture variables to strength and stiffness in **CON** and OVX groups at Y1.

	R1 aBMD	r2 aBMD	vBMD	BV / TV	Tb. N.	Tb. Th.	Tb. Sp.
UCS	**0.56** 0.25	**0.49** 0.12	**0.02** 0.00	**0.74** 0.22	**0.18** 0.20	**0.00** 0.39	**0.46** 0.13
E	**0.15** 0.03	**0.12** 0.06	**0.00** 0.12	**0.83** 0.14	**0.55** 0.03	**0.00** 0.10	**0.57** 0.03

Table 6.9: Relationships (r^2 values) for trabecular bone quantity and micro-architecture variables to mechanical properties in **CON** and OVX groups at Y3.

	R1 aBMD	r2 aBMD	vBMD	BV / TV	Tb. N.	Tb. Th.	Tb. Sp.
UCS	**0.01** 0.03	**0.00** 0.09	**0.00** 0.06	**0.21** 0.63	**0.46** 0.62	**0.00** 0.02	**0.43** 0.41
E	**0.02** 0.13	**0.08** 0.50	**0.09** 0.35	**0.29** 0.39	**0.31** 0.12	**0.00** 0.09	**0.49** 0.10

6.4: DISCUSSION

6.4.1: Trabecular bone strength and stiffness in the proximal ovine femur

Ultimate compressive strength and modulus were significantly reduced in OVX when compared to CON at both time points Y1 and Y3. However, energy to failure (kJ) data were widely dispersed, non-normal and exhibited a significant interaction effect. The significant inter-group difference in energy to failure apparent in OVX when compared to CON at Y3; and in OVX over time should be interpreted with caution. Y3 data analysis also detected significantly higher energy to failure data in ZOL compared to OVX but not in comparison to CON.

In this study there were 20 and 26% differences in UCS and *E* of femoral neck trabecular bone samples across treatment group at Y1 and 25 and 29% differences between CON and OVX groups in Y3. Lill *et al*. (2002) reported reductions in compressive failure load of up to 40% in ovine lumbar vertebrae but not in femoral head trabecular biopsies, in ovariectomised and steroid treated animals when compared to control. However, significant reduction in stiffness were reported at both sites; 25% in the vertebrae and 35% in femoral head biopsies. In a study on the effects of ovariectomy and 12 month steroid therapy, Schorlemmer *et al*. (2005) reported a 55% reduction in cancellous bone compressive stiffness in ovine cancellous bone samples from the proximal tibia. The reductions, or more correctly differences, in trabecular bone strength and stiffness in these studies occurring over shorter or equivalent timeframes, were 10 to 20% greater than those observed in the current study.

The Y3 zoledronic acid group results are difficult to interpret due to the small sample size (n=4) and wide data dispersion in CON for the energy to failure data. Differences in strength and stiffness expressed relative to OVX (40 and 22%, respectively) although impressive were not statistically significant, and the highly significant rise in energy to failure in ZOL in comparison to the OVX is also difficult to interpret due to significant interaction effect and small sample size. However, given these caveats the findings possibly suggest that zolendronic acid reversed the strength decrements due to ovariectomy and this observation clearly warrants further study with a larger sample size.

Given the significant ovariectomy induced differences in strength, stiffness and energy to failure recorded for trabecular bones tested in compression the question therefore arises whether these differences were due to decrements in bone quantity or in degradation of microarchitectural bone quality.

6.4.2: Proximal femoral bone quantity

DXA derived areal BMD at five sites in the ovine skeleton are presented and discussed in detail in Chapter 4. In the proximal ovine femora, the regions of trabecular core sampling, analysis of BMD; in proximal sub-region R1 and r1-3; head, neck and intertrochanteric sub-regions, revealed no significant differences in aBMD across time (Y1 vs. Y3), across group (CON vs. OVX) and no ZOL effect in Y3. Furthermore, analysis of µCT derived volumetric BMD ($mg.mm^{-3}$) of sampled trabecular cores also revealed no significant differences in bone quantity across any group at any time point, and no ZOL effect.

A possible confounding variable in the bone quantity analysis was that Y1 and Y3 animals underwent sacrifice in different seasons, Y1 animals were sacrificed in early November 2004 and the Y3 group in late June 2006. Seasonal effects of sunlight on vitamin D production and subsequent changes in aBMD cannot be discounted as statistically significant seasonal fluctuations in aBMD were reported for the proximal femoral site in Chapter 2; and, in Chapter 4 an unexpected finding of a significant increase in aBMD in the cortical mid-shaft of the tibia in Y3 OVX compared to CON indicated possible bone mass accrual in the long bone mid-shafts.

Hornby *et al.* (1995) reported short-term decreases in total body BMD following ovariectomy in an *in vivo* study investigating ovariectomy in sheep, however, they also noted several confounding factors. These included seasonal BMD variation, reversible reduction in bone quantity as a result of lactation, and BMD changes associated with age of sheep at ovariectomy. Age at sacrifice and weaning history of sheep in the current study were not known and seasonal effects on BMD that may have occurred due to timing of sacrifice, were previously noted in a sample of Irish sheep at the proximal femoral site and were reported Chapter 2. Turner *et al.* (1995b) reported significant short-term changes in BMD post-ovariectomy *in vivo*; however, in the same study BMD changes in *ex vivo* bone samples, including the proximal femur were not detected. In a recent ovine bone study, Wu *et al.* (2011) reported a 25 to

30% decrement in DXA derived BMD in L3 to L6 vertebrae at 12 months post-ovariectomy and following a low calcium diet.

The non-significant trends documented in Table 6.6 of reduced BMD in OVX when compared to control at Y1 with a return of BMD to similar levels at Y3 is in agreement with a recent study by Sigrist *et al.* (2007). In this study, Sigrist *et al.* (2007) reported short-term decreases in oestrogen concentration, reduced cancellous BMD at the distal radius, and osteopaenic type trabecular microarchitecture in iliac crest biopsies at 6 and 9 month post-ovariectomy. However, oestrogen and microarchitecture variables subsequently returned to normal by 12 to 15 months and the non-significant decreases from baseline in BMD began to increase back to baseline. Consequently, the authors criticised the use of the ovariectomised ovine model as a suitable model for the study of osteoporosis.

6.4.3: Trabecular microarchitecture in the ovine femora

No significant differences were apparent in trabecular number and spacing across time or due to ovariectomy, and although a significant reduction in bone volume fraction was apparent across time in the control groups this was not apparent in the OVX groups. The main finding in femoral bone quality analyses were highly significant inter-group differences in trabecular thickness across time in both CON and OVX, and at Y3 a significant treatment effect of OVX. The magnitude of inter-group differences across time and at Y3 between groups had large effect sizes (Cohen's d = 1.0 to 1.2) indicating that a meaningful changes had occurred. Analysis of Y3 microarchitecture revealed a ZOL effect of increased trabecular thickness approaching but not quite reaching significance when comparing OVX and ZOL.

The mean inter-group differences in microarchitectural data summarised in Table 6.8 are in agreement with the expected trends previously reported by Lill *et al*. (2002a) and Schorlemmer *et al.* (2003). However, recorded mean inter-group differences in bone quality variables of between 8 and 15% were lower in magnitude than those reported in studies employing additional bone weakening measures. Lill *et al.* (2002a) reported the following changes in sheep iliac crest biopsy microarchitecture data; BV/TV, Tb.N. and Tb.Th. decreased by 42, 17 and 30%, respectively; and Tb.Sp. increased by 34%; following a 7 month osteoporosis induction regimen consisting of ovariectomy, low calcium diet and steroid therapy. The inter-group

differences in microarchitectural bone quality indices reported by Lill *et al.* (2002a) were all significant and associated with a 10 to 12% decrement in vertebral BMD and were two to four times greater than changes recorded in the current study.

In analysis of differences between ZOL and OVX groups; decrements in OVX were possibly too small or increase in ZOL was not large enough, or most likely sample size was too small, to attain statistical significance. Consequently, inter-group differences were only suggestive of a protective effect on microarchitecture for bone volume fraction (+21%); and trabecular thickness differences (+12%) did not quite reach significance, after statistical correction for the number of groups. Previously, protective effects of bisphosphonates have been reported in the literature. Meunier and Boivin (1997) investigating non-human primates demonstrated similar results to the current study with matrix mineralisation data in OVX animals treated with alendronate closer to the control group than OVX group. Komatsubara *et al.* (2003), in a study on vertebral trabecular microarchitecture, strength and microdamage highlight the necessity of adequate sample size (n=10 per group), they reported significant effects of long term bisphosphonate administration on vertebral trabecular microarchitectural variables; bone volume fraction, trabecular thickness and trabecular spacing in control vs. incadronate treated dogs over 3 years.

6.4.4: Trabecular bone quantity and quality vs. compressive strength

Overall the relationships between microarchitectural variables and mechanical properties were better than for bone quantity. Correlation was best ($r \sim 0.8$) for bone volume fraction in Y1, most consistent across time for trabecular spacing ($r \sim 0.4$ to 0.6), and least well correlated to trabecular number and thickness. DXA derived areal BMD was better correlated to strength than µCT derived volumetric BMD; however, correlation to compressive strength and modulus was poor for any bone quantity variable ($r<0.3$). In Y1, quantity and quality variables association with strength were best for bone volume fraction ($r \sim 0.9$), good for areal BMD and trabecular spacing ($r \sim 0.7$) in CON, but moderate to poor for all other variables. In Y3, association with ultimate compressive strength and modulus were best for BV/TV and Tb. N. ($r \sim 0.8$) in OVX, but only moderate for BV/TV, Tb. N. and Tb.Sp. ($r \sim 0.5$ to 0.6) in CON; and all bone quantity variables at Y3 recorded only moderate to poor correlation with mechanical properties in either group.

Relationship of variables stratified according to BMD with strength measures revealed non-significant trends of increased strength across density in both CON and OVX. When grouped according to time the Y1 high density cores were significantly stronger than medium and low density cores. However, no significant differences in modulus were detected across density in any group. Relationships of microarchitectural data stratified for BMD, as expected, identified non-significantly higher bone volume fraction, trabecular number, trabecular thickness across density; significantly reduced trabecular thickness across density in OVX; and, reduced spacing in the high density group in Y1 (P<0.05).

Review of Tables 6.8 and 6.9 indicated that bone volume fraction (BV/TV), an index of apparent density, had the strongest association with compressive strength and modulus. Regression analysis of logarithmic plots of bone quantity/density markers, areal (aBMD), volumetric (vBMD) and apparent density (BV/TV) vs. strength and modulus also revealed BV/TV to be the best associated variable. Carter and Hayes (1977) reported that vertebral strength was proportional to the square of the density and modulus was proportional to the cube of density. In the current study, analysis of volumetric density data ($mg.mm^{-3}$) revealed that strength was proportional to vBMD to the power of ~1.6 and modulus to the power of ~3.3, approximately similar figures.

The relationship of DXA derived aBMD to strength and modulus was difficult to interpret, in Y1 both R1 and r2 areal BMD were only reasonably associated with ultimate compressive strength but not with modulus, in Y3 animals there was essentially no association detected between any bone quantity variable and mechanical indices. One possible explanation for the lack of association lies in the fact that the density data were a measure of both trabecular and cortical bone, and a better test for DXA derived BMD to strength therefore would have been a whole bone test of the neck of femur. Cheng *et al.* (1997) performed testing on human femoral necks *in vitro* on a specially designed jig created to impart a bending load at the femoral neck. The authors reported much higher levels of association for DXA derived aBMD (r^2 ~0.6 to 0.9); and interestingly human BMD at Ward's triangle reported by Cheng *et al.* (1997) were very similar to the range of ovine r2 aBMD in the current study (0.57 to. 0.63 $g.cm^{-2}$). Therefore, in a more realistic investigation of DXA derived aBMD and whole bone breaking strength, the relationships were much stronger than that observed for compressive testing of isolated trabecular cores.

6.4.5 Limitations of the study

There were a number of confounding factors in this study which may have reduced the strength of relationships between DXA derived aBMD measurements and mechanical properties. Firstly the DXA measurement was conducted at a whole bone level and thus aBMD represented X-ray attenuation through three layers of bone tissue; cortical shell - inner trabeculae - cortical shell; and no direct DXA measurement was made on the cores of trabecular bone isolated from the cortical shell. The positioning, dimensions and orientation of the DXA r2 region of interest analysed in the whole bone sample (Figure 6.2) may not have exactly corresponded to the site of trabecular core sampling used in each case.

Furthermore, if one examines variation of proximal femoral DXA r1-3 aBMD data; mean (±SD) aBMD for the head (r1), neck (r2) and trochanteric region (r3) were 0.98±0.07; 0.59±0.06; and 0.80±0.09 $g.cm^{-2}$ respectively, thus small deviations in the site of r2 scan box, toward r3 the trochanteric region laterally or the r1 head region medially could have increased the aBMD value by 10-20%. Repeat positioning over a site of interest is critical in human DXA scanning and similarly in this research setting it is entirely possible, that small discrepancies in scan box positioning and orientation in relation to the trabecular sampling site could have introduced significant error in aBMD representation of the trabecular core sampled, with a subsequent knock on effect of poor relationships to mechanical testing data in correlation analyses.

Similarly errors could have also could also have been introduced on the mechanical testing side of the examined relationships. Ensuring consistency in quality of the trabecular cores, could have been affected by the site selection, sampling technique, fitting of end caps, pre-loading protocols, and marrow effects during the mechanical tests. The number and quality of connected trabecular would have been affected by the ratio of the core diameter to the actual femoral neck diameter in each case. The trabecular core sample dimensions and orientation were dictated by the site selected, the femoral neck. The core dimensions met a previously recommended ratio of length to diameter but with smaller samples a greater degree of disconnection is introduced on the edges of the specimen in relation to the absolute size of the specimen.

The orientation of the core sampling also may not have represented the predominant alignment of the major trabecular, in a previous study in humans, all femoral bone core samples were aligned to the central medullary cavity of the shaft, and were thus

in the orientation of the major load bearing trabeculae (Fazzalari et al., 1998). Adjustment of mechanical test data was made to account for unconnected trabecular by co-workers using previously described formulae (Un *et al.*, 2006), but it would be necessary to compare unadjusted raw data to aBMD in order to fully determine edge effects on strength in this particular model.

The fitting of non-perforated end caps could have caused further degradation of mechanical properties prior to the loading to failure procedure as could a one size fits all pre-loading protocol. The presence of marrow in trabecular cores is known to effect mechanical test data, the use of perforated end caps or cleaning of marrow using water jets ameliorates possible confounding hydraulic effects of marrow during compressive mechanical tests (Ding *et al*., 1996). Interpolation of ultimate compressive strength, compressive modulus and energy to failure from stress strain curves is also subject to interpolation error especially in compressive tests where the sample material compresses down on itself making it sometimes difficult to interpret a firm end point to the elastic limit on the stress strain curves.

A validation study, similar to that carried out in Chapter 2 for DXA methods examining the confounding variables, disconnections of trabeculae and size of the sample in relation to femoral neck dimensions would have been useful in assessing and reducing natural biological variability during mechanical testing prior to compressive testing of bone samples from the intervention study. Additionally, although only known after the femoral study, the larger proximal humeral head may have provided a much more suitable site for sampling of larger trabecular samples along the alignment of the major load bearing trabeculae. An additional benefit of this site was that data analysis in Chapter 4 revealed it to be the only ovine skeletal site to show significant intergroup differences in bone quantity due to OVX; and, therefore it may have provided a better substrate for examination of trabecular bone quantity and quality relationships to compressive strength and stiffness post ovariectomy.

6.4.6 Conclusions

1. Ovariectomy caused significant inter-group differences in compressive strength and stiffness at 12 and 31 months, comparable in magnitude but over much longer time frames than recently reported in the literature. Results also suggest a possible protective effect on trabecular bone strength and stiffness of a long acting

bisphosphonate drug in ovariectomised animals, however further studies, with a larger sample size (minimum 8 to 12 animals in the treatment group) should be undertaken before this finding can be confirmed in this animal model.

2. Ovariectomy did not cause any short or long-term decrements in bone quantity at the ovine proximal femoral site similar to those defining human osteoporosis. The suggested reasons for this are either; lack of an osteopaenic effect of OVX at this site or confounding factors not accounted for in the initial study design of; age, weaning history, and seasonal effects on sheep bone metabolism; and especially in Y3 small sample sizes. The magnitude of OVX induced differences in areal BMD would not appear large enough to account for differences in mechanical properties.

3. Non-significant inter-group differences in microarchitecture variables were highly suggestive of an ovariectomy effect although of lower magnitude than those recently reported in the literature which suggest osteoporosis induction procedures resulting in a 10% reduction in bone mass are required to produce statistically significant change in all microarchitecture variables. However, the differences in trabecular thickness were significant, of large effect size, and changes in trabecular thickness were the most likely explanation for differences in mechanical strength and stiffness.

4. Linear regression relationships of bone quantity to compressive strength and modulus of trabecular cores isolated from the cortical shell were weak for both aBMD and vBMD. However, examination of vBMD power relationships to compressive strength and stiffness were similar to that reported in the literature. Despite a better ‘fit’ of vBMD power relationships to strength indices bone quality relationships were still much stronger; and, in overall conclusion, the results of this study would support the view that microarchitectural bone quality factors; in particular BV/TV, trabecular thickness and spacing; should be incorporated with bone quantity data to further improve predictions of fracture risk in bone with a high trabecular bone content.

CHAPTER 7

General discussion

7.0 GENERAL DISCUSSION

7.1 Study design

At the inception of the 'Bone for Life Project' the focus of bone research was moving from small animal models, such as rat and mice models, to larger animal models such as dogs, sheep and non-human primates. The advantage of scaling-up to animals of comparative dimensions to humans was to allow for investigation at a more realistic scale of factors affecting bone fragility, especially microarchitectural and material bone quality factors, efficacy of new drug treatments and orthopaedic implants (Mosekilde, 1995). The ovine animal model emerged as a possible suitable large animal model in the early 90's due to its purported advantages of cost, ease of handling, similarity of hormonal changes during oestrus and bone remodelling rates to humans (Hornby *et al*., 1995; Newman *et al.,* 1995). Early studies on the effects of ovariectomy in sheep had shown short-term changes in biochemical markers of bone remodelling and decreased oestrogen levels but substantive changes in bone density were not evident (Turner *et al.,* 1995b; Turner *et al.,* 1995c). However, the balance of available evidence, and, therefore, the prevailing view at the time, was that bone samples from an ovariectomised ovine model would possibly provide a useful substrate for further investigation of bone quantity, quality and bone strength.

The 'Bone for Life' project commenced with selection of 75 animals at a local auction. The sample size was initially thought, following power analysis calculations, to be sufficient for the general requirements of a series of studies evaluating the realtionships of bone quality to bone strength, using fluorochrome dyes as a marker of bone turnover, various microstructural analyses of bone quality using μCT and microscopy techniques, and assessment of strength indices by mechanical testing.

The scope of the 'Bone for Life' project was subsequently expanded to include DXA, a routine clinical investigation of bone quantity used in the evaluation of fracture risk in human osteoporosis, as well as animal research. Grier and Turner (1996) had estimated, assuming DXA aBMD precision (CV%) of the order of 2 to 3%, that any experimental study would require a minimum of 75 animals to detect a 1% change at a significance level of P <0.05. The greater 'Bone for Life project with an initial sample size of 75, was subsequently extended from 12 to 31 month and with two discrete groups (Con and OVX) in each year, consequently, the total number of animals was reduced to approximately 16-18 animals per group. Therefore, from the

outset, in order to detect a significance outcome based on the actual sample sizes (17-18) per group, any inter-group differences in aBMD would have to be greater than 5 to 10%. A further adaptation of the study design was made, necessitating the withdrawal of further number of animals from Y3 OVX group, to examine the effects of the long acting amino bisphosphonate drug zolendronic acid. This lead to a further reduction and slight imbalance in sample size between control and treatment groups in Y3. The control group (n=17) exceeded the OVX group (n=11) by nearly a third, and in the zoledronic acid group (n=4) the number of animals was so small that subsequent data analysis was severely restricted.

In studies employing a repeated measures design with serial *in vivo* measurements of the same animals over time, the initial sample size selected and group assignation would probably have been acceptable, however, such a design was impractical from both experimental and economic reasons. Considering the study design employed, evaluating inter-group differences in *ex-vivo* bone samples at two time points, sample sizes possibly fell below the optimum for statistical analysis of bone quantity data previously suggested for DXA. Inter-group comparisons of DXA derived aBMD for an effect of ovariectomy, strength, microdamage and microarchitecture were possibly just acceptable in Y1, but were possibly underpowered and slightly unbalanced in Y3 data. Furthermore, based on sample size (n=4) criteria alone, any conclusions drawn from comparisons of zoledronic acid group DXA data to control and OVX groups in Y3 should be interpreted with great caution.

Sheep ages in this study were purportedly between 5 to 8 years when purchased at auction (Brennan, 2008); unfortunately in Ireland, sheep, unlike cattle, are not tagged at birth and the exact age of sheep in this study was therefore unknown. In young sheep, bone is of a plexiform type, and older sheep are known to undergo Haversian remodelling in later life from 7 to 9 years (Newman *et al.*, 1995). Haversian remodelling changes have been reported in both the ovine radius and femur, the sites used for comparative analyses of aBMD and mechanical properties in Chapters 5 and 6. In terms of ovariectomy as a bone wasting intervention some authors have also suggested that only sheep over 7 years of age are susceptible to ovariectomy, and younger sheep whose skeletons are still growing should not be used (Hornby *et al.*, 1995). Sample size and further confounding factors; mixed breed selection, unknown weaning history, different time points of sacrifice in Y1 (November ‘04) and

Y3 (June 06) were beyond the author's control and posed a significant challenge to data analysis and interpretation in later parts of the study.

In order to minimise the impact of these confounding factors two preliminary studies were undertaken prior to the assessment of bone quantity changes with ovariectomy described in Chapter 4; and bone quantity relationships to strength and quality indices in Chapters 5 and 6. The first study was a thorough validation of DXA scanning methodology for use in assessment of *ex vivo* ovine bone samples (Chapter 2); and a second study evaluated normal levels of biological or natural variation present in ovine aBMD in a sample of the normal Irish sheep population of different breeds, across body mass (as a marker of size and age) and for the effect of seasonal timing of sacrifice (Chapter 3).

7.2 Validation of DXA methodology for *ex-vivo* large animal bones

In any study employing a new measurement technique experimentally researchers should firstly ensure that the measurement is reliable and accurate, and that there is no drift in measurement reliability over time. On this basis, using previous DXA methodology for *ex vivo* bones reported in the literature (Kaymakci & Wark, 1994; Turner *et al*., 1995a; Pouilles *et al*., 2000) and a recommended statistical approach to the determination of reliability (Atkinson & Nevill, 1998); DXA scanning methods and sub-regional analysis of *ex vivo* bone samples was further adapted, improved and validated.

Kaymakci and Wark (1994) defined optimum depth of fluid immersion for scanning; Turner *et al*. (1995a) compared *in vivo* to *ex vivo* DXA results on different scanners; and Pouilles *et al.* (2000) defined DXA precision. However, on review of these studies, all had identified areas of weakness which needed to be addressed to further validate DXA methods in the ovine animal model. In particular, each study was limited by sampling restriction in terms of age of animals, breed selection, skeletal site selection and especially sample size. Therefore, despite widespread use of DXA in this large animal model, validity had not been fully determined over a range of animal sizes, breed and body mass existing in the normal sheep population. In addition these studies examined North American and Australian breeds; and no

study had examined the Irish sheep population; the population from which animals were to be selected for the ‘Bone for Life’ project.

The validation studies undertaken documented the repeatability and reliability of the DXA measurement methods used; but also defined systematic bias and scedasticity of data, which were then used to determine the correct expression of measurement limits of the technique. This last point is important, as well-defined measurement limits were necessary for evaluation of data in later parts of the overall work. These measurement limits were used to confirm the real significance of inter-group differences in the longitudinal studies in Chapters 4, 5 and 6. The magnitude of any detected inter-group differences in these later studies due to OVX or some other intervention would have to be both statistically significant and greater than DXA scanner measurement limits, in order for subsequent inference of any meaningful difference.

The DXA methods employed had similar reliability and accuracy to that reported previously for both human scanning and scanning of small animal models (Gluer *et al*., 1995; Libouban *et al*., 2002). The present study, to the author’s knowledge, is the first to suggest based on scedasticity results, that correct expression of measurement limits for fan beam DXA scanning in this animal model should be expressed as limits of agreement (95% LOA); and, not the often quoted statistic; coefficient of variation (CV%), seen in most, if not all, previously reported ovine DXA studies in the literature. The statistic CV% is normally used to define linearity or long-term drift in aBMD of whole block phantoms measured during DXA start-up calibration procedures and is a more appropriate statistic defining measurement variation in heteroscedastic data sets. Furthermore, the computed measurement limits (95%LOA) defined for each skeletal site should be useful to future researchers in any DXA study of ovine bone examining aBMD changes in longitudinal studies utilising bone wasting measures. These measurement limits, as well as statistical analysis, define minimum changes needed to indicate a true change outside of that occurring due to measurement variation.

7.3 Natural variation in areal BMD at five sites in the ovine skeleton

In Study 1, DXA was shown be a reliable device to measure aBMD across a variety of sites in the ovine skeleton. Study 2 further validated the animal model by addressing the next research question; what is the level of natural or biological variation in aBMD present in a sample of the Irish sheep population? Although a widely used model for over 10 years, natural variation in sheep aBMD has not been defined to the same extent as that for human populations. The purpose of this study was not to create a database of DXA values similar to those used in clinical assessments of fracture risk in humans; but it was necessary to examine biological variation in bone density at some level prior to later longitudinal studies. This study, examined aBMD at ovine spinal and long bone sites with variation in mass, breed and across month of sacrifice.

The study showed ovine aBMD across five skeletal sites standardised for body mass to be very similar to human female populations (Donne *et al.*, 1996; Donne & O'Brien, 2007); however, unlike humans where aBMD can vary significantly with ethnicity (Cummings & Melton, 2002), no significant differences were detected in ovine BMD across breed. In terms of variation of aBMD and body mass the results suggested approximately 50% of the variation in ovine aBMD could be accounted for by change in animal mass. However, further normalisation of data for mass had little or no effect. This is not surprising as DXA aBMD data essentially captures or incorporate a measure of mass (BMC) and size (EA) already; therefore, providing that the selection of groups in the later interventional studies were matched for mass and size, there would seem to be no logical reason to employ any further normalisation procedures to correct for body mass.

The study made one further important finding with respect to a possible flaw in the initial study design which could have had a potential knock-on effect on subsequent data interpretation in Chapter 6. That is, non-significant trends were detected towards higher aBMD in late summer and autumn than winter / spring at most sites. In the r2 neck region of the proximal femur, the region of interest and site of trabecular core sampling in Chapter 6, the seasonal effect on aBMD detected was statistically significant. Seasonal variation has been reported in the literature in both human and various animal species including sheep living in northern latitudes (Arens *et al*., 2007; Gerdhem *et al.,* 2004; Turner, 2007). However, but perhaps fortunately for the

subsequent data analyses in Chapter 6, the magnitude of the difference at the r2 site had only a poor effect size (Cohen's d = 0.4). The different time points of sacrifice of Y1 and Y3 animals and a potential seasonal effect on aBMD, although statistically significant, were unlikely to be large enough to affect subsequent analyses of trabecular aBMD to strength. Overall, biological or natural variation across Irish breeds, in animals of body mass ranging from 35 to 105 kg revealed a range of aBMD from 0.6 to 1.2 $g.cm^{-2}$, and although a small seasonal effect was detected, this was too small to cause a major confounding effect in later studies.

7.4 Short- and long-term effect of ovariectomy on ovine BMD

There is no doubt given the current state of knowledge that the ovine animal model has been a useful large animal model for bone research. However, to produce the magnitude of reductions, in bone quantity and quality over short time frames, required for research that typify osteopaenia, seen in humans over a life time, most large animal studies now employ extra bone wasting measures in addition to ovariectomy (Lill *et al*., 2002a, b; MacCleay *et al*., 2004a, b; Turner, 2007). The aBMD differences in the ovine skeleton in the present study (Chapter 4), also suggest ovariectomy alone is insufficient to produce significant changes in aBMD over short time frames necessary for research, as there was no significant ovariectomy effect in bone quantity at any site at the 12 month time point. However, at the second 31 month time point, there were two significant OVX effects, one that might have been expected, of lower aBMD than control in the proximal humerus; and, one unexpected finding of higher aBMD than control in the mid shaft of the tibia. The effects were statistically and clinically significant as computed effect sizes were large, and differences exceeded the scanner measurement limits previously described for these sites in Chapter 2.

The aBMD differences detected at 31 month raise two important issues for research in the ovine large animal model. Firstly, most previous ovine bone research assumes that the proximal femur, distal radius and lumbar spine, the common sites of menopause or ovariectomy induced osteopaenia and bone fragility in humans, will be the same sites affected when the quadrupedal sheep skeleton is exposed to a similar intervention. At all these homologous anatomical sites no differences were detected between OVX and control at either time point. Secondly, given that ageing and

menopause related changes characterising osteopaenia and osteoporosis take many years to develop in humans, why should they develop in ovariectomy treated ewes in 12 months? By extending the study to 31 month and demonstrating significant bone quantity differences between OVX and control in the proximal humerus, the current study has demonstrated the utility of the ovine model at one site, and given the restricted sample sizes there possibly could have been more with changes at other sites. Furthermore, slower changes over a similar time course to the human condition may produce a more accurate simulation of human osteopaenia in the ovine model than those studies employing combinations of ovariectomy, steroid therapy, acidaemic and low calcium and vitamin D diets, which degrade bone at pathophysiological rates not generally observed in nature.

The unusual and unexpected finding of increased aBMD in the mid-shaft of the tibia, at the second but not the first time point is an unusual finding, and had a large effect size (Cohen's d=0.8) and was greater than scanner measurement limits. The possible explanations for this finding have been discussed in Chapter 4; but to summarise, it is unlikely that this finding was due the confounding effects of breed, animal mass, and whole bone dimensions as these were all evenly matched across all groups. In terms of the two components of BMD there was a greater difference in BMC values in the tibial cortex than EA values which were similar; this would suggest an increase in cortical thickness due to a reduction of the inner cortical radius.

A follow-on study by Keeley *et al.* (2008) examining the pull out forces of interosseus screws reported significantly increased cortical thickness and holding strength of tibial screws at the mid-shaft of the ovine tibia in OVX compared to control animals. The results of both the current study and Keeley *et al.* (2008), possibly indicate some form of cortical steal phenomenon due to OVX, this is a new finding that has not been previously reported in the literature and requires further evaluation.

7.5 Influence of aBMD on ovine cortical bone strength and microdamage

In the first part of this study, bone samples from control and OVX animals sacrificed at the 12 month time point underwent three-point bending to failure to compare aBMD and structural indices at the point of fracture to long bone bending strength. The results of the first part of the study clearly showed DXA derived aBMD, and the

structural variables CSMI and section modulus to be the best predictors of breaking strength (Fmax) in three-point bending to failure of the ovine radius.

In hip structural analysis (HSA) algorithms of newer generation DXA scanners it has been possible to incorporate aBMD, with estimates of CSMI, section modulus and buckling ratio derived from pixel analysis of DXA data (Beck, 2003). It was initially thought that combining aBMD and HSA data might improve prediction of fracture risk in humans (Beck, 2003); however, only minor improvements in fracture risk prediction over and above aBMD measurement alone have been disappointing (Bonnick, 2007). Similar to this study, where any estimate of volumetric density was reported to be a poor predictor of breaking strength and stiffness; research using multi slice CT scanning to generate cross-sectional measures and density to estimate volumetric bone density and relationship to fracture risk have also been disappointing, and come with the disadvantage of high radiation exposure (Beck, 2003). However, the combination of bone density and geometric properties in finite element analysis in order to enhance the predictability of osteoporotic fractures seems to be more promising (Lang *et al*., 1997b; Keyak & Falkinstein, 2003).

As microdamage in cortical bone accumulates with increasing age, there is a concomitant progressive increase in microcrack density (Schaffler *et al.,* 1995). Although microcrack formation is thought to be an effective way of energy dissipation, microcracks also impose adverse effects on the mechanical competence of bone. Stiffness and strength have been shown to decrease as the amount of microdamage in bone increases (Zioupos, 2001). It remains unclear, however, to what extent microdamage accumulation contributes to an increase in fracture risk (Augat & Schorlemmer, 2006). In the second part of this study, radial long bones, over a range of low, medium and high densities, were exposed to cyclical four-point bending at normal physiological loads to examine for possible relationships of aBMD to microdamage accumulation.

The results of this part of the study showed a clear separation between levels of microdamage and aBMD in all, bar one, of the bones analysed individually, and with removal of an obvious outlier, statistical analysis of microdamage data stratified for low, medium or high density also suggested the potential of DXA to possibly discriminate between bones with different levels of microdamage. However, although results were limited by small sample size, the results still warrant further

investigation. In particular, a further study of fracture load on bones following prior exposure to similar levels of cyclical loading would be very useful to determine whether aBMD and associated levels of microdamage could be used to predict fracture load in bending to failure.

Radiographic approaches for the assessment of micro-structural properties are constrained by the limited resolution of non-invasive imaging systems. Therefore, although DXA may be related to microdamage, DXA is likely to be far too insensitive to measure microdamage in a meaningful way that will ultimately effect predictions of bone strength. The development of future imaging techniques will have to concentrate on functional biological imaging of bone at high enough spatial resolution to estimate microstructural properties (Augat & Schorlemmer, 2006). Nicolella *et al.* (2011) have used a novel non-destructive imaging technique, nuclear magnetic resonance (NMR), to investigate microdamage accumulation in human cortical bone under four-point bending. The technique was assessed alongside standard histological methods in the evaluation of bone porosity and microdamage in unloaded and fatigued cortical bone after cyclic loading to various levels of modulus degradation and microdamage. However, the authors were able to relate a damage parameter to a crack density parameter through their effects on the modulus reduction.

7.6 Influence of aBMD and microarchitecture on ovine trabecular bone strength

The primary aim of the ‘Bone for life’ project studies was the further evaluation of bone quality determinants of bone strength in animal model of osteoporosis, and the project was extended to include determination of bone quantity by DXA. The ovine femoral neck was the initial site chosen for evaluation of the mechanical competence in compression of trabecular cores taken from control and ovariectomised sheep at 12 and 31 month time points post-ovariectomy. Analysis of DXA and µCT results indicated inter-group differences in µCT derived microarchitectural variables, especially trabecular thickness at Y3, to be the most likely explanation for the significant 20 to 30% degradation in mechanical properties, Fmax, *E* and energy to failure, detected in OVX compared to control core samples at both time points. The large effect sizes (Cohen’s d= 0.9 to 1.0) of inter-group differences seen in mechanical properties suggest that these were real changes, and differences in DXA

derived bone quantity data could not predict these differences, whereas µCT derived microarchitectural data could.

The lack of DXA sensitivity in this study was possibly due to confounding effects detailed earlier, and limitations detailed in previous chapters may have had a role. Inaccurate placement of DXA regions of interest over the exact site of trabecular core sample, and the effect of the cortical shell component of aBMD masking change in the trabecular component due to OVX, are two possible reasons for lack of DXA association with mechanical properties. Further examination of the data by re-analysis of trabecular cores with similar dimensions and orientations of ROIs to the angle of trabecular core, and comparison of DXA data to whole bone mechanical testing at the femoral neck would likely answer these questions.

However, it is probable, unlike predictive capacity in the long bone bending, that the resolution capacity of DXA is too limited to detect change in trabecular bone. A similar study from the 'Bone for Life' group (Kennedy *et al.,* 2008) of bone turnover, bone quantity and mechanical properties on whole ovine L3 vertebral bodies from Y1 documented similar results to the current study; namely, difference due to OVX in trabecular bone turnover and microarchitecture (bone quality factors) better explained trabecular bone compressive mechanical behaviour than differences in DXA derived aBMD. The results of the current study and Kennedy *et al*. (2008) would therefore seem to be agreement with previous studies, which suggest that DXA has insufficient resolution to detect early changes in trabecular bone structure in OVX sheep (Turner *et al*., 1995b; Chavassieux *et al*., 2001).

7.7: Overall conclusions

1. The overall study design enabled detection of significant ovariectomy effects on ovine bone turnover and bone quality variables at a number of skeletal sites at both the 12 month (short-term post-OVX) and 31 month (long-term post-OVX) time points. However, by DXA bone quantity measurement criteria, the overall study sample size was perhaps too small to allow for the detection of significant bone quantity changes with only one bone wasting intervention. Statistical analysis of zoledronic acid effects was restricted by sample size.

2. Study 1; clearly demonstrated the validity and defined measurement limits of fan beam DXA protocols utilised to examine aBMD in this animal model, and,

furthermore, the model developed would appear be a useful template for other researchers aiming to perform DXA scanning of *ex–vivo* bone samples in humans or large animal species.

3. Study 2; examined bone quantity in the ovine large animal model by systematic examination of variability in DXA derived aBMD data in the Irish sheep population across breed, mass, season of sacrifice and skeletal site. Data indicated no breed effect, but similar variation in aBMD with body mass and seasonal variation similar to that reported in humans. The addition of age, as a legal requirement in Irish sheep husbandry, would further improve the overall validity of the model.

4. Study 3; demonstrated no short-term ovariectomy effect on DXA derived bone quantity at 12 month and but a significant longer-term effect of reduced aBMD in the proximal humerus at 31 month, at both time points the results may have been limited by sample size and the timing of sacrifice. An unexpected finding of increased aBMD in the mid-shaft of the tibia at Y3 in the ovariectomised group warrants further evaluation in future studies with larger sample size, if confirmed; a paradoxical cortical steal effect of ovariectomy may limit future use of this skeletal site in this animal model.

5. Study 4; this investigation clearly showed the utility of DXA derived bone quantity and geometric structural indices in the prediction of fracture load at cortical bone sites. The study suggests a possible relationship of lower cortical bone aBMD to greater microdamage accumulation that warrants further investigation with larger sample sizes and correlation to mechanical tests to failure of varying density whole bones which have undergone prior cyclic loading.

6. Study 5; in contrast to Study 4 and with the caveat of certain limitations that require further re-evaluation, demonstrated that whole bone DXA measurement is not sensitive enough to detect changes due to time and ovariectomy that predict the compressive strength of isolated trabecular bone.

REFERENCES

Aerssens J, Boonen S, Lowet G & Dequeker J (1998). Interspecies differences in bone composition, density, and quality: Potential implications for *in-vivo* bone research. *Endocrinology* **139**, 663–670.

Alho A, Husby T & Høiseth A (1988). Bone mineral content and mechanical strength: An *ex vivo* study on human femora at autopsy. *Clin Orthop Relat Res* **27**, 292-297.

Altman D & Bland J (1983). Measurement in medicine: The analysis of method comparison studies. *Statistician* **32**, 307-317.

Ammann P (2009). Bone strength and ultrastructure. *Osteoporos Int* **20**, 1081-1083.

Arens D, Sigrist I, Alini M, Schawalder P, Schneider E & Egermann M (2007). Seasonal changes in bone metabolism in sheep. *Vet J* **174**, 585-591.

Arnett T & Boyd T (2006): www.ucl.ac.uk/anatomy/boneresearch/histology.html. Last accessed December 2005.

Aszodi A, Bateman JF, Gustafsson E, Boot-Handford R & Fassler R (2000). Mammalian skeletogenesis and extracellular matrix: what can we learn from knockout mice? *Cell Structure & Function* **25**, 73–84

Atkinson G & Nevill A (1998). Statistical methods for assessing measurement error (reliability) in variables relevant to sports medicine. *Sports Med* **26**, 217-328.

Augat P, Reeb H & Claes L. (1996): Prediction of fracture load at different skeletal sites by geometrical properties of the cortical shell. *J Bone Miner Res* **11**, 1356–63.

Augat P, Schorlemmer S, Gohl C, Iwabu S, Ignatius A & Claes L. (2003) Glucocorticoid-treated sheep as a model for osteopaenic trabecular bone in biomaterials research. *J Biomed Mater Res* **66A**, 457-462.

Augat P & Schorlemmer S (2006). The role of cortical bone and its microstructure in bone strength. *Age Ageing* **35**, S2: ii27–ii31.

Baron R (2003): General Principles of Bone Biology. In: Primer on the Metabolic Bone Diseases and Disorders of Mineral Metabolism. Favus M (Ed.) 5th Edition. American Society for Bone and Mineral Research, Washington DC. pp. 1–8.

Beck T, Ruff C, Warden K, Scott W & Rao G (1990). Predicting femoral neck strength from bone mineral data a structural approach. *Invest Radiol* **25**, 6-18.

Beck T (2003). Measuring the structural strength of bones with dual-energy X-ray absorptiometry: principles, technical limitations, and future possibilities. *Osteoporos Int* **14**, S81-S88.

Beck T (2007). Extending DXA beyond bone mineral density: understanding hip structural analysis. *Curr Osteoporos Rep* **5**, 49-55.

Bevill G, Eswaran SK, Gupta A, Papadopoulos P & Keaveny T (2006). Influence of bone volume fraction and architecture on computed large-deformation failure mechanisms in human trabecular bone. *Bone* **39,** 1218–1225

Black D, Delmas P, Eastell R, Reid I & Boonen S (2007). Once-yearly zoledronic acid for treatment of postmenopausal osteoporosis. *N Eng J Med* **356**, 1809-1822.

Blake G & Fogelman I (1997). Technical principles of dual energy x-ray Absorptiometry. *Semin Nucl Med* **27**, 210-28.

Bland J & Altman D (1986). Statistical methods for assessing agreement between two methods of clinical measurement. *Lancet* **8**, 307-310.

Bland J & Altman D (1996). Statistics notes: Measurement error and correlation coefficients. *BMJ* **313**, 41-42.

Bolotin H (2004). The significant effects of bone structure on inherent patient-specific DXA *in vivo* bone mineral density measurement inaccuracies. *Med Phys* **31**, 774-788.

Bolotin H (2007). DXA *in-vivo* BMD methodology: An erroneous and misleading research and clinical gauge of bone mineral status, bone fragility, and bone remodelling. *Bone* **41**, 138-154.

Bone Academy: Amgen Clinical Resources (2006). The critical role of RANK/RANK Ligand / OPG in bine remodelling. Last accessed on line at www.amgen.com May 2006.

Bonjour JP, Amman P & Rizzoli R (1999). Importance of preclinical studies in the development of drugs for treatment of osteoporosis: A review related to the 1998 WHO guidelines. *Osteoporos Int* **9**, 379-393.

Boskey A, Wright T & Blank R (1999). Perspective: Collagen and bone strength. *J Bone Miner Res* **14**, 330-335.

Boskey A (2003): Bone mineral crystal size. *Osteoporos Int* **14**, 16–21.

Bouxsein M, Myburgh K, van der Meulen M, Lindenberger E & Marcus R (1994). Age-related differences in cross-sectional geometry of the forearm bones in healthy women. *Calcif Tissue Int* **54**, 113-118.

Bouxsein M (2007). Biomechanics of age-related fractures. In: Marcus R, Feldman D, Nelson D, Rosen C, editors. Osteoporosis. 3rd edn San Diego, CA: Elsevier Academic Press. pp. 601–616.

Bouxsein M & Seeman E (2009). Quantifying the material and structural determinants of bone strength. *Best Pract Res Cl Rh* **23**, 741–753.

Boyce T, Fyhrie D, Glotkowski M, Radin E & Schaffler M. Damage type and strain mode associations in human compact bone bending fatigue. *J Orthopaed Res* **16**, 322-329

Boyle W, Simonet W & Lacey D (2003). Osteoclast differentiation and activation. *Nature* **423**, 337–342.

Burr D, Martin B, Schaffler M & Radin E (1990). Bone remodeling in response to *in vivo* fatigue microdamage. *J Biomech* **18**, 189–200.

Brennan O (2008). PhD Thesis, University of Dublin. Bone quality and its relationship with bone fragility and osteoporosis. Cpt 2, pp. 39-47.

Campbell A, Bain W, McRae A, Broad T, Johnstone P, Dodds K, Veenvliet B, Greer G, Glass B, Beattie A, Jopson N & McEwan J (2003). Bone density in sheep: genetic variation and quantitative trait loci localisation. *Bone* **33**, 540-548.

Carter D & Hayes W (1976): Bone compressive strength: The influence of density and strain rate. *Science* **194**, 1174-75

Carter D & Hayes W (1977). The compressive behaviour of bone as a two-phase porous structure. *J Bone Joint Surg Am* **59**, 954-962.

Carter D, Bouxsein M & Marcus R. (1992): New approaches for interpreting projected bone density data. *J Bone Min Res* **7**, 137-145

Chavassieux P, Garnero P, Duboeuf F, Vergnaud P, Brunner-Ferber F, Delmas P & Meunier P (2001). Effects of a new selective estrogen receptor modulator (MDL 103,323) on cancellous and cortical bone in ovariectomized ewes: a biochemical, histomorphometric, and densitometric study. *J Bone Miner Res* **16**, 89–96.

Cheng X, Lowet G, Boonen S, Nicholson P, Brys P, Nijs J & Dequeker J (1997). Assessment of the strength of proximal femur *in vitro*: relationship to femoral bone mineral density and femoral geometry. *Bone* **20**, 213-218.

Christoffersen J, Landis WJ (1991) A contribution with review to the description of mineralization of bone and other calcified tissues in vivo. *Anat Rec* **230**, 435–450.

Consensus Development Conference on Osteoporosis. Copenhagen, Denmark (1991). *Am J Med* **91**, S1–S68.

Courtney A, Davis B, Manning T & Kambic H (1997). Effects of age density and geometry on the bending strength of human metatarsals. *Foot Ankle Int.* **18**, 216–221.

Crabtree N, Kroger H, Martin A, Pols H, Lorenc R, Nijs J, Stepan J, Falch J, Miazgowski T, Grazio S, Raptou P, Adams J, Collings A, Khaw K, Rushton N, Lunt M, Dixon A & Reeve J (2002). Improving risk assessment: hip geometry, bone mineral distribution and bone strength in hip fracture cases and controls: the EPOS study. *Osteoporos Int* **13**, 48–54.

Cummings S, Cosman F & Jamal S (2002). Osteoporosis; an evidence-based guide to prevention and management. *American College of Physicians, Women's Health Series*.

Cummings S & Melton L (2002). Epidemiology and outcomes of osteoporotic fractures. *Lancet* **359**, 1761–1767.

Currey J (1984). Mechanical properties and histology of bone. *Amer Zool* **24**, 5-12.

Currey J (2002). Bones: structure and mechanics. Princeton University Press, Princeton, NJ.

Currey J (2003a). The many adaptations of bone. *J Biomech* **36**, 1487-1495.

Currey J (2003b). Role of collagen and other organics in the mechanical properties of bone. *Osteoporos Int* **14**, S29-S36.

Dahlberg G (1940). Statistical methods for medical and biological students. London: Allen Unwin, Diem K & Lentner C (Eds) 1974 pp. 122-132.

Delany A, Amling M, Priemel M, Howe C, Baron R & Canalis E (2000). Osteopenia and decreased bone formation in osteonectin-deficient mice. *J Clin Invest* **105**, 915-923.

Delmas P (2002): Treatment of post-menopausal osteoporosis. *Lancet* **359**, 2018–2026.

Delmas P & Seeman E (2004). Changes in bone mineral density explain little of the reduction in vertebral or non-vertebral fracture risk with anti-resorptive therapy. *Bone* **34**, 599–604.

Delmas P & Seeman E (2006). Bone quality - the material and structural basis of bone strength and fragility. *N Engl J Med* **354**, 2250-6.

Deloffre P, Hans D, Rumelhart C, Mitton D, Tsouderos Y & Meunier P (1995). Comparison between bone density and bone strength in glucocorticoid-treated aged ewes. *Bone* **17**, 409S-414S.

Donne B, Kelly M, Kelly A, Barniville G & O'Brien M (1996) Bone density profiles and osteoporosis incidence in Irish females. *Ir Med J* **89**, 92-94.

Donne B & O'Brien M (2007). A longitudinal investigation into the effects of menstrual cycle restoration in females with anorexia nervosa: possible analogies with the female athletic triad. Proceedings of the 12th Annual Congress of the European College of Sports Sciences 11th - 14th July 2007 Jyvaskala, Finland, 524-525.

Ding M, Dalstra M, Danielsen C, Kabel J, Hvid I & Linde F (1997). Age variations in the properties of human tibial trabecular bone. *J Bone Joint Surg* **79**, 995-1002.

Dong X & Guo X. (2004). The dependence of transversely isotropic elasticity of human femoral cortical bone on porosity. *J Biomech* **37**, 1281–1287.

Duan Y, Duboeuf F, Munoz F, Delmas P & Seeman E (2006). The fracture risk index and bone mineral density as predictors of vertebral structural failure. *Osteoporos Int* **17**, 54–60.

Ducy P, Desbois C, Boyce B, Pinero G, Story B, Dunstan C, Smith E, Bonadio J, Goldstein S, Gundberg C, Bradley A & Karsenty G (1996). Increased bone formation in osteocalcin-deficient mice. *Nature* **382**, 448–452.

Edelstein S & Barrett-Connor E (1993). Relation between body size and bone mineral density in elderly men and women. *Am J Epidemiol.* **138**, 160-169.

Egermann M, Gerhardt C, Barth A, Maestroni G, Schneider E & Alini M. (2011). Pinealectomy affects bone mineral density and structure - an experimental study in sheep. Bio Med Central Musculoskeletal Disorders. 12:271. Accessed on line at http://www.biomedcentral.com/1471-2474/12/271

Einhorn T (1996). The bone organ system; form and function. In: Osteoporosis, Marcus R, Feldman D & Kelsey J (Eds), San Diego, CA, USA, Academic Press, 3-22.

Fazzalari N, Forwood M, Smith K, Manthey B & Herreen P. (1998): Assessment of cancellous bone quality in severe osteoarthrosis: Bone mineral density, mechanics, and microdamage. *Bone* **22**, 381–388.

Felson D, Zhang Y, Hannan M & Anderson J (1993). Effects of weight and body mass index on bone mineral density in men and women: The Framingham study. *J Bone Miner Res* **8**, 567-573

Felsenberg D & Boonen S (2005). The bone quality framework: determinants of bone strength and their interrelationships, and implications for osteoporosis management. *Clin Ther* **27**, 1-11.

Frost H (1960). Presence of microscopic cracks in vivo in bone. *Henry Ford Hospital Med Bull* **8**, 25–35.

Frost H (1994). Wolff's Law and bone's structural adaptations to mechanical usage: an overview for clinicians. *Angle Orthod* **64**, 175-188.

Frost H (1997). Defining osteopaenias and osteoporoses: Another view with insights from a new paradigm. *Bone* **20**, 385-391.

Gallagher C & Sai A (2010). Molecular biology of bone remodeling: Implications for new therapeutic targets for osteoporosis. *Maturitas* **65**, 301–307.

Genant H, Faulkner K & Gluer C (1991). Measurement of bone mineral density: current status. *Am J Med* **91**, Suppl, 49S-53S.

Genant H & Compston J (2004). Epidemiology and diagnosis of post-menopausal osteoporosis. In: Atlas of post-menopausal osteoporosis, Rizzoli R (Ed.) Science Press Ltd, 26.

Gerdhem P, Mallmin H, Akesson K & Obrant K (2004). Seasonal variation in bone density in postmenopausal women. *J Clin Densitom* **7**, 93-100.

Gibson L (1985). The mechanical behaviour of cancellous bone. *J Biomech* **18**, 317-328.

Gibson L & Ashby M (1997). Cellular solids: Structure and properties. 2nd Edition Cambridge University Press, 429-450.

Gore C. (2005). Physiological tests for elite athletes. Australian Sports Commission. Human Kinetics, Champaign Il, USA. pp. 83-85.

Goto R & Mascie-Taylor N (2007). Precision of measurement as a component of human variation. *J Phys Anthropol* **26**, 253–256.

Gluer C, Blake G, Lu Y, Blunt B, Jergas M & Genant H (1995). Accurate assessment of precision errors: How to measure the reproducibility of bone densitometry techniques. *Osteoporos Int* **5**, 262-270.

Graham R & Russell G. (2007). Bisphosphonates: Mode of action and pharmacology. *J Pediatr* **119**, S150.

Grier S & Turner A (1996). The use of dual-energy X-ray absorptiometry in animals. *Invest Radiol* **31**, 50-62.

Griffin L, Gibeling J, Martin R, Gibson V & Stover S (1999). The effects of testing methods on the flexural fatigue life of human cortical bone. *J Biomech* **32,** 105-109.

Harris E & Smith R (2009). Accounting for measurement error: A critical but overlooked process. *Arch Oral Biol* **54s**, 107-117.

Havill L, Mahaney M, Czerwinski S, Carey K, Rice K & Rogers J (2003): Bone mineral density reference standards in adult baboons (Papio hamadryas) by sex and age. *Bone* **33**, 877-888.

Hofbauer L & Schoppet, M (2004) Clinical implications of the osteoprotegerin/RANK Ligand/RANK system for bone and vascular diseases. *JAMA* **292**, 490-495.

Homminga J, McCreadie B, Ciarelli T, Weinans H, Goldstein S & Huiskes R (2002): Cancellous bone mechanical properties from normals and patients with hip fractures differ on the structure level, not on the bone hard tissue level. *Bone* **30**, 759-764.

Hornby S, Ford S, Mase C & Evans G (1995). Skeletal changes in the ovariectomised ewe and responses to treatment with 17β oestradiol. *Bone* **17**, 389S-394S.

Heinonen A (2001). Physical activity and bone health, Khan K, McKay H, Kannus P, Bailey D, Wark J & Bennell K (Eds), Human Kinetics, 23-32.

Jacobs C (2000). The mechanobiology of cancellous bone structural adaptation. J *Rehabil Res Dev* **37**, 209-216.

Jerome C, Lees C & Weaver D (1995). Development of osteopenia in ovariectomized Cynomolgus monkeys. *Bone* **17**, 403S~.08S

Jiang C, Giger M, Kwak S, Chinander M, Martell J & Favus M (2000). Normalised BMD as a predictor of bone strength. *Acad Radiol* **7**, 33-39.

Johnell O, Kanis J, Oden A, Johansson H, De Laet C, Delmas P, Eisman J, Fujiwara S, Kroger H, Mellstrom D, Meunier P, Melton L, O'Neill T, Pols H, Reeve J, Silman A & Tenenhouse A (2005). Predictive value of BMD for hip and other fractures. *J Bone Miner Res* **20**, 1185–1194.

Kanis J (1994). Osteoporosis. Blackwell Science, 4-36.

Kanis J (2002). Diagnosis of osteoporosis and assessment of fracture risk. *Lancet* **359**, 1929-1936

Kanis J, Delmas P, Burckhardt P, Cooper C & Torgerson D (1997). Guidelines for diagnosis and management of osteoporosis. *Osteoporos Int* **7**, 390-406.

Kaymakci B & Wark J (1994). Precise accurate measurements of excised sheep bone using X-ray densitometry. *Bone and Mineral* **25**, 231-246.

Keaveny T & Hayes W (1993). A 20-year perspective on the mechanical properties of trabecular bone. *J Biomech Eng* **15**, 534–542.

Keaveny T, Morgan E, Niebur G & Yeh O (2001). Biomechanics of trabecular bone. *Ann Rev Biomed Eng* **3**, 307–333.

Keeley B, Heidari B, Mahony N, Rackard S, O'Brien F, Lee T, Brennan O, Kennedy O & FitzPatrick D (2008). Biomechanical comparison of the pull-out properties of external skeletal fixation pins in the tibiae of intact and ovariectomised ewes. *Vet Comp Orthop Traumatol* **21**, 418-26.

Kennedy O, Brennan O, Mahony N, Rackard S, O'Brien F, Taylor D & Lee C (2008). Effects of high bone turnover on the biomechanical properties of the L3 vertebra in an ovine model of early stage osteoporosis. *Spine* **33**, 2518-2523.

Keyak J & Falkinstein Y (2003). Comparison of in situ and in vitro CT scan-based finite element model predictions of proximal femoral fracture load. *Med Eng Phys* **25**, 781-787.

Khan K, McKay H, Kannus P, Bailey D, Wark J & Bennell K (2001). Physical activity and bone health. Human Kinetics.

Klein-Nulend J, Bacabac R & Mullender M (2005). Mechano-biology of bone tissue. *Pathol Biol* **53**, 576-580.

Komatsubara S, Mori S, Mashiba T, Ito M, Li J, Kaji Y, Akiyama T, Miyamoto K, Cao Y, Kawanishi J & Norimatsu H (2003). Long-term treatment of incadronate disodium accumulates microdamage but improves the trabecular bone microarchitecture in dog vertebra. *J Bone Miner Res* **18**, 512-520.

Kröger H, Vainio P, Nieminen J & Kotaniemi A (1995). Comparison of different models for interpreting bone mineral density measurements using DXA and MRI technology. *Bone* **17**, 157-159.

Lacey D, Timms E, Tan H, Kelley M, Dunstan C, Burgess T, Elliott R, Colombero A, Elliott G, Scully S, Hsu H, Sullivan J, Hawkins N, Davy E, Capparelli C, Eli A, Qian Y, Kaufman S, Sarosi I, Shalhoub V, Senaldi G, Guo J, Delaney J & Boyle W (1998). Osteoprotegerin ligand is a cytokine that regulates osteoclast differentiation and activation. *Cell* **93**, 165-176.

Lang T, Keyak J, Heitz M, Augat P, Lu Y, Mathur A, & Genant H (1997a). Volumetric quantitative computed tomography of the proximal femur: precision and relation to bone strength. *Bone* **21**, 101-108.

Lang T, Guglielmi G, Van Kuijk C, De Serio A, Cammisa M & Genant H (1997b). Measurement of bone mineral density at the spine and proximal femur by volumetric quantitative computed tomography and dual-energy x-ray absorptiometry in elderly women with and without vertebral fractures. *Bone* **30**, 247–250.

Lee C & Taylor D (1999). Bone remodelling should we cry Wolff? *Ir J Med Sci* **168**, 102-105

Lee T &Taylor D (2003). Quantification of ovine bone adaptation to altered load, morphometry, density, and surface strain. *Eur J Morphol* **41**, 117-125.

Libouban H, Simon Y, Silve C, Legrand E, Basle, MF, Audran M & Chappard D. (2002). Comparison of pencil, fan, and cone beam dual energy X-ray absorptiometers for evaluation of bone mineral content in excised rat bone. *J Clin Densitom* **5**, 355-361.

Lill C, Gerlach U, Eckhardt C, Goldhahn J & Schneider E. (2002a). Bone changes due to glucocorticoid application in an ovariectomized animal model for fracture treatment in osteoporosis *Osteoporos Int* **13**, 407-414.

Lill C, Fluegel A, Schneider E (2002b). Effect of ovariectomy, malnutrition and glucocorticoid application on bone properties in sheep: A pilot study. *Osteoporos Int* **13**, 480-486.

Lin J (1996). Bisphosphonates: A review of their pharmacokinetic properties. *Bone* **18**, 75-85.

Lochmuller E, Groll O, Kuhn V & Eckstein F (2002). Mechanical strength of the proximal femur as predicted from geometric and densitometric bone properties at the lower limb versus the distal radius. *Bone* **30**, 207–216.

Lyles K, Colon-Emeric C, Magaziner J, Adachi J , Pieper C, Mautalen C, Hyldstrup L, Recknor C, Nordsletten L, Moore K, Lavecchia C, Zhang J, Mesenbrink P, Hodgson P, Abrams K, Orloff J, Horowitz Z, Eriksen E & Boonen S (2007). Zoledronic acid and clinical fractures and mortality after hip fracture. *N Eng J Med* **357**, 1799-1809.

Marshall D, Johnell O & Wedel H (1996). Meta-analysis of how well measures of bone mineral density predict occurrence of osteoporotic fracture. *BMJ* **312**, 1254-1259.

Martin R & Atkinson P (1977). Age and sex-related changes in the structure and strength of the human femoral shaft. *J Biomech* **10**, 223-231.

Martin R. & Burr. D (1989). The structure and function and adaptation of compact bone. New York. Raven Press.

Martin R (1991). Determinants of the mechanical properties of bones. *J Biomech* **24**, 79-88.

Martin R & Ishida J (1989). The relative effects of collagen fiber orientation, porosity, density, and mineralization on bone strength. *J Biomech* **22**, 419–426.

MacLeay J, Olson J & Turner S (2004a). Effect of dietary-induced metabolic acidosis and ovariectomy on bone mineral density and markers of bone turnover. *J Bone Miner Metab* **22**, 561–568.

MacLeay J, Olson J, Enns R, Les C, Toth C, Wheeler D & Turner A (2004b). Dietary-induced metabolic acidosis decreases bone mineral density in mature ovariectomized ewes. *Calcif Tissue Int* **75**, 431–437.

McClung M (1996). Current bone mineral density data on bisphosphonates in postmenopausal osteoporosis. *Bone* **19**, 195S-198S.

Meunier P & Boivin G (1997). Bone mineral density reflects bone mass but also the degree of mineralization of bone: therapeutic implications. *Bone* **21**, 373-377.

Miller S, Bowman B & Jee W (1995). Available animal models of osteopaenia-small and large. *Bone* **17**, 117S-123S

Mittra E, Rubin C & Qin Y (2005). Interrelationship of trabecular mechanical and microstructural properties in sheep trabecular bone. *J Biomech* **38**, 1229–1237.

Morgan E, Bayraktar H, Yeh O & Keaveny T (2003). Contribution of inter-site variations in architecture to trabecular bone apparent yield strain. *J Biomech* **37**, 1413–1420.

Mosekilde L, (1993). Normal age-related changes in bone mass, structure and strength consequences of the remodelling process. *Dan Med Bull* **1**, 65-84.

Mosekilde L (1995). Assessing bone quality - animal models in preclinical osteoporosis. *Bone* **17**, 343S-352S.

Mosekilde L, Ebbesen E, Tornvig L & Thomsen J (2000). Trabecular bone structure and strength -remodelling and repair. *J Musculoskel Neuron Interact* **1**, 25-30.

Muehleman C, Lidtke R, Berzins A, Becker J, Shott S & Sumner D (2000). Contributions of bone density and geometry to the strength of the human second metatarsal. *Bone* **27**, 709–714.

Murshed M, Harmey D, Millán J, Mckee M & Karsenty G (2005). Unique co-expression in osteoblasts of broadly expressed genes accounts for the spatial restriction of extra-cellular matrix mineralization to bone. *Gene Dev* **19**, 1093-1104.

Nalla R, Kruzic J, Kinney J & Ritchie R (2004). Effect of aging on the toughness of cortical bone: Evaluation by R-curves. *Bone* **35**, 1240.

Newman E, Turner A & Wark J (1995). The potential of sheep for the study of osteopaenia: current status and comparison with other animal models. *Bone* **16**, 277S-284S

Nicolella D, Ni Q & Chan K (2011). Non-destructive characterization of micro-damage in cortical bone using low field pulsed NMR. *J Mech Behav Biomed Mater* **4**, 383-391.

Overgaard K, Nilas L, Sidenius Johansen J & Christiansen C (1988). Lack of seasonal variation in bone mass and biochemical estimates of bone turnover. *Bone* **9**, 285-288.

Parfitt A, Mathews CH & Villanueva (1983). Relationships between surface, volume, and thickness of iliac trabecular bone in aging and in osteoporosis. Implications for the microanatomic and cellular mechanisms of bone loss. *J Clin Invest* **72**, 1396-1409.

Parker J, Timm K, Smith B, Van Saun R, Winters K, Sukon P & Snow C (2002). Seasonal interaction of serum vitamin D concentration and bone density in alpacas. *Amer J Vet* **63**, 948-953.

Pouilles J, Collard P, Tremollieres F, Frayssinet P, Railhac J, Cahuzac J, Autefage A & Ribot C (2000). Accuracy and precision of *in-vivo* mineral measurements in sheep using dual-energy X-ray absorptiometry. *Calc Tissue Int* **66**, 70-73.

Pors Nielsen S, Kolthoff N, Barenholdt O, Kristensen B, Abrahamsen B, Hermann A & Brot C (1998). Diagnosis of osteoporosis by planar densitometry can body size be disregarded. *Brit J Radiol* **71**, 934-943.

Presbitero G (2009). Microcrack distributions in bone: Effects of stress and bone mineral density. PhD thesis, Trinity College Dublin

Puustjärvi K, Nieminen J, & Räsänen T (1999). Do more highly organized collagen fibrils increase bone mechanical strength in loss of mineral density after one-year running training? *J Bone Miner Res* **14**, 321–329.

Reginster J & Burlet N (2006). Osteoporosis a still increasing prevalence. *Bone* **38**, S4-S9.

Rho J & Kuhn-Spearing L (1998). Mechanical properties and the hierarchical structure of bone. *Med Eng Phys* **20**, 92-102.

Rice J, Cowin S & Bowman J (1988): On the dependence of the elasticity and strength of cancellous bone on apparent density. *J Biomech* **21**, 155–168.

Ritchlin C (2004). Mechanisms of erosion in rheumatoid arthritis. *J Rheumatol* **31**, 1229-1237.

Rizzoli R, Slosman D & Bonjour J (1995). The role of dual energy X-ray absorptiometry of lumbar spine and proximal femur in the diagnosis and follow-up of osteoporosis. *Am J Med* **98**, 33S–36S.

Rizzoli R (2004). Atlas of postmenopausal osteoporosis. Science Press Ltd.

Robling A, Hinant F, Burr D & Turner C (2002). Improved bone structure and strength after long-term mechanical loading is greatest if loading is separated into short bouts. *J Bone Miner Res* **17**, 1545-1554.

Rosen C, Morrison A, Zhou H, Storm D, Hunter S, Musgrave K, Chen T, Wei W & Holick M (1994). Elderly women in northern New England exhibit seasonal changes in bone mineral density and calciotropic hormones. *Bone Miner* **25**, 83–92.

Rubin C & Lanyon L (1982). Limb mechanics as a function of speed and gait: a study of functional strains in the radius and tibia of horse and dog. *J Exp Biol* **101**, 187-211.

Rubin C, Turner AS, Mueller R, Mittra E, McLeod K, Lin W & Qin Y (2002). Quantity and quality of trabecular bone in the femur are enhanced by a strongly anabolic, non-invasive mechanical intervention. *J Bone Miner Res* **17**, 349–357.

Rubin C (2005). Emerging concepts in osteoporosis and bone strength. *Curr Med Res Opin* **21**, 1049–1056.

Sato M (1995). Comparative X ray densitometry of bones from ovariectomised rats. *Bone* **17**, 157S-162S.

Schaffler M, Choi K & Milgrom C (1995). Aging and matrix microdamage accumulation in human compact bone. *Bone* **17**, 521–525.

Schorlemmer S, Gohl C, Iwabu S, Ignatius A, Claes L & Augat P (2003). Glucocorticoid treatment of ovariectomized sheep affects mineral density, structure, and mechanical properties of cancellous bone. *J Bone Miner Res* **18**, 2010-2015.

Schorlemmer S, Ignatius A, Claes L & Augat P (2005). Inhibition of cortical and cancellous bone formation in glucocorticoid-treated OVX sheep. *Bone* **37**, 491-496

Schriefer J, Robling A, Warden S, Fourniera A, Masone J & Turner C (2005). A comparison of mechanical properties derived from multiple skeletal sites in mice. *J Biomech* **38**, 467-475.

Schuit S, van der Klift M, Weel A, de Laet C, Burger H, Seeman E, Hofman A, Uitterlinden A, van Leeuwen J & Pols H (2004). Fracture incidence and association with bone mineral density in elderly men and women: the Rotterdam study. *Bone* **34**, 195–202.

Seeman E (2001). Sexual dimorphism in skeletal size, density and strength. *J Clin Endocrinol Metab* **86**, 4576-4584.

Seeman E (2002): Pathogenesis of bone fragility in women and men. *Lancet* **359**, 1841-1850.

Seeman E (2003). Bone quality. *Osteoporos Int* **14**, S3–S7.

Seeman E (2008). Bone quality: the material and structural basis of bone strength. *J Bone Miner Metab*. **26**, 1-8.

Sievänen H, Kannus P, Neiminen V, Heinonen A, Oja P & Vuori I (1996). Estimation Of Various Mechanical Characteristics Of Human Bones Using Dual Energy X Ray Absorptiometry: Methodology And Precision. *Bone* **18**, 17S-27S.

Sigrist I, Gerhardt C, Alini M, Schneider E & Egermann M (2007). The long-term effects of ovariectomy on bone metabolism in sheep. *J Bone Miner Metab* **25**, 28-35.

Soames R, Pegington J, Boyde A & Jones S (1995). Skeletal connective tissues. In: Gray's Anatomy 38th edition Williams P (Ed), Churchill Livingstone, NY, USA, 6, 443-482.

Sommerfeldt D & Rubin C (2001). Biology of the bone and how it orchestrates the form and function of the skeleton. *Eur Spine J* **10**, S86–S95.

Simonet W, Lacey D, Dunstan C, Kelley M, Chang M, Lüthy R, Nguyen H, Wooden S, Bennett L, Boone T, Shimamoto G, DeRose M, Elliott R, Colombero A, Tan H, Trail G, Sullivan J, Davy E, Bucay N, Renshaw-Gegg L, Hughes T, Hill D, Pattison W, Campbell P, Sander S, Van G, Tarpley J, Derby P, Lee R & Boyle W (1997). Osteoprotegerin: a novel secreted protein involved in the regulation of bone density. *Cell* **89**, 309–319.

Stepan J, David B, Burr D, Pavo I, Sipos A, Michalska D, Li J, Fahrleitner-Pammer A, Petto H, Westmore M, Michalsky D, Sato M & Dobnig H (2007). Low bone mineral density is associated with bone microdamage accumulation in postmenopausal women with osteoporosis. *Bone* **41**, 378–385.

Stevenson K, van Tets I & Chon D (2009). Making no bones about it: bone mineral density changes seasonally in a non-hibernating Alaskan rodent. *J Mammal* **90**, 25-31.

Strømsøe K., HØiseth A, Alho A & Kok W (1995). Bending strength of the femur in relation to non-invasive strength assessment. *J Biomech* **28**, 857-861.

Taylor D & Lee C (2003). Microdamage and mechanical behaviour: predicting failure and remodelling in compact bone. *J Anat* **203**, 203–211.

Thompson D, Simmons H, Pirie C & Ke H (1995). FDA Guidelines and animal models for osteoporosis. *Bone* **17**, 125S-133S.

Tommasini S, Nasser P, Schaffler M & Jepsen K (2005). Relationship between bone morphology and bone quality in male tibias. *J Bone Miner Res* **20**, 1372-1380.

Turner C & Burr D (1993). Basic biomechanical properties of bone: a tutorial. *Bone* **14**, 595-608.

Turner A, Mallinckrodt C, Alvis M & Bryant H (1995a). Dual energy X-ray absorptiometry in sheep: experiences with *in-vivo* and *ex-vivo* studies. *Bone* **17**, 381S-387S.

Turner A, Alvis M, Myers W, Stevens M & Lundy M (1995b). Changes in bone mineral density and bone specific alkaline phosphatise in ovariectomised ewes. *Bone* **17**, 395S-402S.

Turner A, Mallinckrodt C, Alvis M & Bryant H (1995c). Dose-response effects of oestradiol implants on bone mineral density in ovariectomised ewes. *Bone* **17**, Suppl 421-427.

Turner A (2002). The sheep as a model for osteoporosis in humans. *Vet J* **163**, 232-239

Turner A (2007). Seasonal changes in bone metabolism in sheep: Further characterization of an animal model for human osteoporosis. *Vet J* **174**, 460-461.

Turner C (2002). Biomechanics of bone: determinants of skeletal fragility and bone quality. *Osteoporos Int* **13**, 97-104.

Turner C (2006). Bone strength: Current concepts. *Ann N.Y. Acad Sci* **1068**, 429-446.

Un K, Bevill G & Keaveny T (2006). The effects of side-artefacts on the elastic modulus of trabecular bone. *J Biomech* **39**, 1955-1963.

Van der Linden J, Homminga J, Verhaar J & Weinans H (2001). Mechanical consequences of bone loss in cancellous bone. *J Bone Min Res* **16**, 457–465.

Viguet-Carrin S, Garnero P & Delmas P (2006). The role of collagen in bone strength. *Osteoporos Int* **17**, 319–336.

Wang X, Bank R, TeKoppele J & Agrawal C (2001). The role of collagen in determining bone mechanical properties. *J Orthop Res* **19**, 1021–1026.

Wang X, Shen X,. Li X & Mauli Agrawal C (2002). Age-related changes in the collagen network and toughness of bone. *Bone* **31**, 1–7.

Wachter N, Krischak G & Mentzel M (2002). Correlation of bone mineral density with strength and microstructural parameters of cortical bone *in vitro*. *Bone* **31**, 90-95.

Wainwright S, Marshall L, Ensrud K, Cauley J, Black J ; Hillier T, Hochberg M, Vogt T & Orwoll E (2005). Hip fracture in women without osteoporosis. *J Clin Endocrinol Metab* **90**, 2787–2793.

Warden S, Hurst J, Sanders M, Turner C, Burr D & Jiliang L (2005). Bone adaptation to a mechanical loading program significantly increases skeletal fatigue resistance. *J Bone Miner Res* **20**, 809-816.

WHO Study Group (1994). WHO Technical Report Series S43, WHO Geneva, Switzerland, 1-129.

WHO Study Group (2004). On the assessment of osteoporosis at primary health care level summary meeting report. Brussels, Belgium, 5-7 May 2004.

Wolff J (1892). "The Law of Bone Remodeling". Berlin Heidelberg New York: Springer, 1986 (translation of the German 1892 edition)

Wu Z, Liu D, Wan S, Cui G, Zhang Y & Lei W (2011). Sustained-release rhBMP-2 increased bone mass and bone strength in an ovine model of postmenopausal osteoporosis. *J Orthop Sci* **16**, 99–104.

Yagami K, Suh J, Enomoto-Iwamoto M, Koyama E, Abrams W, Shapiro I, Pacifici M & Iwamoto M (1999). Matrix GLA protein is a developmental regulator of chondrocyte mineralization and, when constitutively expressed, blocks endochondral and intramembranous ossification in the limb. *J Cell Biol* **147**, 1999 1097-1108.

Yamaguchi A, Komori T & Suda T (2000) Regulation of osteoblast differentiation mediated by bone morphogenetic proteins, Hedgehogs, and Cbfa1. *Endocr Rev* **21**, 393–411

Yeni Y, Brown CU, Wang Z & Norman T (1997). The influence of bone morphology on fracture toughness of the human femur and tibia. *Bone* **21**, 453–459.

Zioupos P & Currey J (1998). Changes in the stiffness, strength, and toughness of human cortical bone with age. *Bone* **22**, 57-66.

Zioupos P, Currey J & Hamer A (1999). The role of collagen in declining mechanical properties of aging human cortical bone. *J Biomed Mater Res* **45**, 108-116.

Zioupos P (2001). Accumulation of in-vivo fatigue microdamage and its relation to biomechanical properties in ageing human cortical bone. *J Microsc* **201**, 270-278

Zioupos P, Cook R & Hutchinson R (2008). Some basic relationships between density values in cancellous and cortical bone. *J Biomech* **41**, 1961-1968.

APPENDIX 1

Common Terms Used in Bone Density Assessment (Cummings *et al.,* 2002)

Bone mass
A nonspecific term that refers to the amount of bone tissue. This may refer to the total amount of protein and mineral, or to the amount of mineral in the whole skeleton or in a particular segment of bone.

Bone mineral content
The amount of mineral measured in a defined section of bone. *Total body bone mineral content* refers to the mineral content of the whole skeleton.

Bone density or bone mineral density
The average concentration of mineral in a two- or three-dimensional image or average concentration in a defined section of bone. This term is also used to refer to the results of all types of bone densitometry.

Areal bone density
The bone mineral content divided by the area of the image of a bone projected in two dimensions. This is the type of "bone density" that is produced by dual and single energy x-ray absorptiometry.

Volumetric bone density
The bone mineral content of a section of bone divided by the volume of that section. This type of bone density is produced by quantitative computed tomographic (QCT) scans.

Trabecular bone density
The mineral density of a section of bone that contains only or largely trabecular bone.

Microfracture or microdamage
Cracks in bone that remain localized to a very small place in a bone. These are not detected by standard radiographs but by special microscopic techniques in bone samples.

T score
The difference between the value for an individual and the mean value of a group of young (usually 20–30 year old) adults of the same gender. Both the mean value and the size of a standard deviation of the measurement vary between techniques and between sites of measurement.

Z score
The difference between the mean value of the individual and a group of people of the same gender and same age.

Osteoporosis
Defined by a Working Group of the World Health Organization as a T score of at least –2.5 (also called *densitometric osteoporosis* to distinguish this from a diagnosis of osteoporosis made on the basis of the presence of a vertebral fracture on x-ray).

Osteopenia
A term coined by the World Health Organization to refer to T scores between –1.0 and –2.5.

Bone ultrasound attenuation
A slope of the line connecting the amount of attenuation of sound energy across a spectrum of sound frequencies.

Speed of sound
The fastest rate of transmission of a specific frequency of sound through a defined section of bone.

Coefficient of variation
A measurement of reproducibility defined as the standard deviation of repeated measurements divided by the mean value for the measurement in the group tested, expressed as a percent.

APPENDIX 2

Figure 2.4 Repeatability (ICC) & Reliability (%TEM) data for FMR (Figure 2.4)

FMR	n=77	Min	25%	Med	75%	Max	M	SD	SEM	ICC	%TEM
WB	WB S1	0.479	0.834	0.918	0.991	1.140	0.909	0.113	0.013		
	WB S2	0.401	0.838	0.912	0.983	1.140	0.908	0.118	0.013	0.99	0.91
SRA	R1 S1	0.358	0.676	0.733	0.790	0.956	0.730	0.099	0.011		
	R1 S2	0.245	0.682	0.736	0.795	0.969	0.731	0.106	0.012	0.99	1.85
	R2 S1	0.412	0.714	0.801	0.861	1.022	0.784	0.111	0.013		
	R2 S2	0.347	0.715	0.798	0.859	1.030	0.781	0.114	0.013	0.99	1.27
	R3 S1	0.529	0.888	0.974	1.068	1.251	0.974	0.132	0.015		
	R3 S2	0.451	0.882	0.968	1.069	1.249	0.972	0.136	0.016	0.99	1.11
	R4 S1	0.489	0.822	0.943	0.986	1.193	0.921	0.122	0.014		
	R4 S2	0.420	0.825	0.945	0.988	1.197	0.921	0.125	0.014	0.99	1.09
	R5 S1	0.446	0.797	0.873	0.955	1.179	0.870	0.114	0.013		
	R5 S2	0.367	0.793	0.872	0.951	1.193	0.870	0.120	0.014	0.99	1.26
	R6 S1	0.627	1.046	1.164	1.254	1.463	1.144	0.152	0.017		
	R6 S2	0.562	1.059	1.158	1.237	1.446	1.147	0.154	0.018	0.99	1.54
ROI	r1 S1	0.550	0.877	0.939	1.019	1.339	0.945	0.119	0.014		
	r2 S2	0.429	0.881	0.950	1.015	1.340	0.940	0.125	0.014	0.99	1.69
	r2 S1	0.304	0.514	0.565	0.617	0.731	0.563	0.082	0.009		
	r2 S2	0.218	0.513	0.561	0.614	0.728	0.559	0.087	0.010	0.99	1.69
	r3 S1	0.371	0.685	0.779	0.861	0.997	0.771	0.123	0.014		
	r3 S2	0.247	0.679	0.771	0.852	0.972	0.763	0.128	0.015	0.99	1.81

APPENDIX 3

Figure 3.4 data table inter-breed variation in aBMD (g.cm^{-2}) in TS and LS sites

TS	n	25%	Med	75%	10%	90%	M	SD	SEM
All breeds	26	0.794	0.863	0.896	0.710	0.953	0.847	0.093	0.018
Suffolk	13	0.791	0.886	0.919	0.683	0.962	0.853	0.094	0.026
Suffolk (x)	4	0.805	0.889	0.923	0.778	0.933	0.872	0.066	0.033
Texel (x)	5	0.808	0.825	0.862	0.798	0.867	0.833	0.028	0.013
Others	4	0.678	0.796	0.998	0.660	1.044	0.824	0.168	0.084
LS	**n**	**25%**	**Med**	**75%**	**10%**	**90%**	**M**	**SD**	**SEM**
All breeds	48	0.840	0.914	1.026	0.734	1.098	0.927	0.143	0.021
Suffolk (x)	22	0.827	0.903	0.971	0.737	1.069	0.907	0.125	0.027
Cheviot	5	0.926	1.029	1.099	0.882	1.119	1.016	0.093	0.042
Kerry	5	0.801	0.899	0.955	0.751	0.959	0.882	0.085	0.038
Texel (x)	5	0.774	0.969	1.045	0.735	1.073	0.921	0.142	0.064
Others	11	0.837	1.007	1.096	0.597	1.212	0.952	0.204	0.062

Figure 3.5 (a) and (b) data tables for interbreed variation in aBMD (g.cm^{-2}) in FMR WB and sub-region R1

(a) FMR WB	n	25%	Med	75%	10%	90%	M	SD	SEM
All breeds	75	0.836	0.917	0.989	0.790	1.051	0.915	0.103	0.012
Suffolk	15	0.835	0.940	0.988	0.764	1.094	0.913	0.111	0.029
Suffolk (x)	24	0.838	0.925	0.973	0.801	1.025	0.913	0.085	0.017
Texel	6	0.823	0.872	0.996	0.800	1.040	0.899	0.095	0.039
Texel (x)	5	0.806	0.925	1.011	0.771	1.014	0.912	0.106	0.047
Cheviot	6	0.892	0.963	1.079	0.827	1.140	0.977	0.113	0.046
Kerry	5	0.874	0.914	0.996	0.873	1.048	0.931	0.072	0.032
Others	14	0.772	0.924	1.007	0.682	1.065	0.897	0.137	0.037
(a) FMR R1	**n**	**25%**	**Med**	**75%**	**10%**	**90%**	**M**	**SD**	**SEM**
All breeds	76	0.683	0.736	0.796	0.622	0.854	0.737	0.090	0.010
Suffolk	15	0.660	0.704	0.794	0.573	0.857	0.715	0.092	0.024
Suffolk (x)	25	0.680	0.759	0.780	0.620	0.834	0.735	0.073	0.015
Texel	6	0.668	0.712	0.785	0.663	0.796	0.722	0.057	0.023
Texel (x)	5	0.662	0.702	0.842	0.624	0.857	0.742	0.097	0.043
Cheviot	5	0.717	0.721	0.818	0.716	0.853	0.758	0.060	0.027
Kerry	6	0.700	0.777	0.866	0.684	0.866	0.779	0.077	0.031
Other	14	0.630	0.749	0.856	0.525	0.930	0.740	0.136	0.036

APPENDIX 3

Figure 3.6 data table for pooled spinal and femoral aBMD across time of sacrifice

Spine	n	25%	Med	75%	10%	90%	M	SD	SEM
Feb	8	0.755	0.877	0.932	0.660	1.044	0.856	0.120	0.042
Mar	7	0.781	0.798	0.860	0.778	0.933	0.823	0.056	0.021
Apr	6	0.722	0.873	0.912	0.684	0.961	0.837	0.106	0.043
Jun	11	0.784	0.885	0.969	0.639	1.019	0.864	0.121	0.036
Sep	6	0.747	0.825	0.951	0.712	1.213	0.866	0.179	0.073
Nov	20	0.848	0.903	1.013	0.754	1.116	0.917	0.141	0.032
W/S	21	0.780	0.857	0.894	0.694	0.958	0.840	0.095	0.021
S/A	37	0.815	0.882	0.972	0.725	1.092	0.893	0.140	0.023
FMR	**n**	**25%**	**Med**	**75%**	**10%**	**90%**	**M**	**SD**	**SEM**
Feb	8	0.785	0.890	0.966	0.704	1.078	0.885	0.121	0.043
Mar	8	0.796	0.834	0.951	0.786	1.081	0.871	0.105	0.037
Apr	7	0.905	0.944	0.995	0.827	1.004	0.935	0.060	0.023
Jun	11	0.840	0.913	1.008	0.726	1.112	0.921	0.126	0.038
Sep	6	0.782	0.836	0.911	0.728	1.038	0.851	0.103	0.042
Nov	20	0.866	0.916	0.994	0.797	1.044	0.925	0.103	0.023
W/S	23	0.827	0.905	0.973	0.777	1.048	0.895	0.100	0.021
S/A	37	0.838	0.913	0.992	0.757	1.054	0.912	0.111	0.018

Figure 3.7 data table for femoral sub-region R1 / r2 aBMD across time of sacrifice

FMR R1	n	25%	Med	75%	10%	90%	M	SD	SEM
Feb	8	0.639	0.688	0.764	0.588	0.852	0.704	0.083	0.029
Mar	8	0.635	0.661	0.753	0.597	0.830	0.684	0.080	0.028
Apr	7	0.700	0.735	0.798	0.581	0.800	0.729	0.075	0.028
Jun	11	0.693	0.743	0.826	0.548	0.890	0.737	0.109	0.033
Sep	6	0.628	0.684	0.784	0.617	0.963	0.717	0.127	0.052
Nov	20	0.716	0.761	0.815	0.666	0.863	0.750	0.092	0.020
W/S	23	0.638	0.689	0.773	0.592	0.818	0.705	0.078	0.016
S/A	37	0.698	0.734	0.810	0.612	0.864	0.741	0.101	0.017
FMR r2	**n**	**25%**	**Med**	**75%**	**10%**	**90%**	**M**	**SD**	**SEM**
Feb	8	0.465	0.533	0.578	0.443	0.603	0.524	0.059	0.021
Mar	8	0.476	0.505	0.566	0.460	0.682	0.527	0.073	0.026
Apr	7	0.533	0.569	0.611	0.428	0.624	0.557	0.066	0.025
Jun	11	0.509	0.547	0.618	0.437	0.724	0.570	0.093	0.028
Sept	6	0.471	0.539	0.622	0.457	0.704	0.552	0.094	0.038
Nov	20	0.541	0.593	0.643	0.504	0.696	0.589	0.085	0.019
W/S	23	0.469	0.533	0.584	0.450	0.619	0.535	0.065	0.014
S/A	37	0.521	0.581	0.636	0.455	0.701	0.577	0.087	0.014

APPENDIX 3

Figure 3.9 data tables for ovine BMC (g) / aBMD (g.cm^{-2}) data normalisation effects (a) raw data (b) normalised to carcass weight (c) standardised to mass of 70 kg.

(a) BMC	n	min	25%	Med	75%	max	M	SD	SEM
TS	26	27.17	38.77	50.04	60.47	74.51	51.26	13.66	2.68
LS	49	30.83	63.76	72.43	91.26	111.80	75.85	18.67	2.67
FMR	76	38.89	53.65	58.49	68.22	86.40	60.26	10.59	1.22
TBR	76	35.96	52.54	57.42	64.58	78.35	58.07	9.06	1.04
HMR	76	24.82	43.24	49.60	56.59	71.64	49.55	9.42	1.08
RDR	75	25.01	40.56	46.36	52.89	63.19	46.33	8.70	1.01
aBMD	**n**	**min**	**25%**	**Med**	**75%**	**max**	**M**	**SD**	**SEM**
TS	26	0.617	0.794	0.863	0.896	1.044	0.847	0.093	0.018
LS	49	0.420	0.833	0.912	1.023	1.242	0.917	0.159	0.023
FMR	76	0.660	0.836	0.916	0.989	1.140	0.915	0.102	0.012
TBR	76	0.706	0.881	0.953	1.022	1.137	0.947	0.091	0.010
HMR	76	0.563	0.882	0.958	1.031	1.233	0.954	0.120	0.014
RDR	75	0.563	0.778	0.871	0.932	1.075	0.858	0.103	0.012

(b) BMC	n	min	25%	Med	75%	max	M	SD	SEM
TS	26	0.890	1.283	1.660	1.878	3.190	1.654	0.504	0.099
LS	49	1.540	1.985	2.250	2.545	4.080	2.327	0.550	0.079
FMR	76	1.290	1.555	1.780	2.130	3.690	1.886	0.477	0.055
TBR	76	1.140	1.520	1.690	2.055	3.420	1.819	0.432	0.050
HMR	76	0.960	1.255	1.485	1.728	2.950	1.559	0.370	0.042
RDR	75	0.920	1.190	1.370	1.660	2.640	1.456	0.346	0.040
aBMD	**n**	**min**	**25%**	**Med**	**75%**	**max**	**M**	**SD**	**SEM**
TS	26	0.018	0.023	0.027	0.031	0.047	0.028	0.008	0.002
LS	49	0.020	0.024	0.027	0.032	0.053	0.029	0.007	0.001
FMR	76	0.018	0.024	0.027	0.032	0.064	0.029	0.008	0.001
TBR	76	0.019	0.025	0.028	0.033	0.065	0.030	0.008	0.001
HMR	76	0.019	0.025	0.029	0.033	0.065	0.031	0.008	0.001
RDR	75	0.017	0.023	0.026	0.030	0.057	0.027	0.008	0.001

(c) BMC	n	min	25%	Med	75%	max	M	SD	SEM
TS	26	29.78	42.77	55.37	62.45	106.20	55.15	16.77	3.29
LS	49	51.77	66.40	75.16	85.00	133.30	77.48	16.32	2.33
FMR	76	42.89	52.60	59.55	70.75	123.00	62.90	15.44	1.77
BMC	76	38.09	51.19	57.28	67.51	114.00	60.64	13.94	1.60
BMC	76	32.09	43.92	49.52	57.54	98.18	51.96	11.86	1.36
RDR	75	30.66	41.55	46.48	53.16	88.10	48.54	11.09	1.28
aBMD	**n**	**min**	**25%**	**Med**	**75%**	**max**	**M**	**SD**	**SEM**
TS	26	0.872	0.942	0.989	0.761	1.122	0.942	0.130	0.025
LS	49	0.818	0.889	0.941	0.749	1.043	0.889	0.103	0.020
FMR	76	0.791	0.852	0.932	0.709	0.964	0.851	0.099	0.019
TBR	76	0.763	0.807	0.900	0.708	0.929	0.827	0.096	0.019
HMR	76	0.760	0.821	0.898	0.677	0.952	0.829	0.109	0.021
RDR	75	0.755	0.844	0.939	0.673	0.973	0.845	0.127	0.025

APPENDIX 3

*Figure 3.10 data tables (a) BMC (g); (b) EA (cm^2) and (c) aBMD ($g.cm^{-2}$) for sub-regions R1 to R6 in **TS**.*

BMC	n	25%	Med	75%	10%	905	M	SD	SEM
R1	26	5.14	6.20	7.37	4.55	8.42	6.30	1.40	0.28
R2	26	4.85	5.96	7.20	4.38	8.26	6.07	1.42	0.28
R3	26	4.84	5.88	7.35	4.21	8.79	6.17	1.62	0.32
R4	26	5.19	6.45	8.20	4.34	9.80	6.77	1.92	0.38
R5	26	6.01	7.60	9.47	4.69	10.37	7.63	2.05	0.40
R6	26	6.67	8.02	9.67	5.41	10.82	8.00	2.06	0.40
EA	**N**	**25%**	**Med**	**75%**	**10%**	**90%**	**M**	**SD**	**SEM**
R1	26	5.83	6.60	7.39	5.40	8.23	6.66	0.96	0.19
R2	26	5.99	6.53	7.88	5.41	8.41	6.79	1.13	0.22
R3	26	6.05	6.79	8.34	5.52	9.16	7.18	1.35	0.26
R4	26	6.79	7.78	9.16	5.99	10.57	8.07	1.64	0.32
R5	26	7.73	8.83	10.49	6.70	11.89	9.09	1.72	0.34
R6	26	8.19	9.43	10.51	7.75	11.46	9.36	1.48	0.29
aBMD	**n**	**25%**	**Med**	**75%**	**10%**	**90%**	**M**	**SD**	**SEM**
R1	26	0.872	0.942	0.989	0.761	1.122	0.942	0.130	0.025
R2	26	0.818	0.889	0.941	0.749	1.043	0.889	0.103	0.020
R3	26	0.791	0.852	0.932	0.709	0.964	0.851	0.099	0.019
R4	26	0.763	0.807	0.900	0.708	0.929	0.827	0.096	0.019
R5	26	0.760	0.821	0.898	0.677	0.952	0.829	0.109	0.021
R6	26	0.755	0.844	0.939	0.673	0.973	0.845	0.127	0.025

*Figure 3.11 data tables (a) BMC (g); (b) EA (cm^2) and (c) aBMD ($g.cm^{-2}$) for sub-regions R1 to R6 in **LS**.*

BMC	N	25%	Med	75%	10%	90%	Mean	SD	SEM
R1	49	9.40	11.03	13.44	7.92	15.55	11.30	2.95	0.42
R2	49	9.74	11.23	14.41	8.31	15.89	11.87	3.02	0.43
R3	49	9.92	11.24	14.30	8.16	16.17	11.96	2.97	0.42
R4	49	10.36	11.36	14.66	8.31	16.60	12.23	3.10	0.44
R5	49	10.68	12.14	15.35	8.83	17.11	12.77	3.25	0.46
R6	49	10.76	12.30	15.54	7.64	18.91	12.97	3.68	0.53
EA	**N**	**25%**	**Med**	**75%**	**10%**	**90%**	**Mean**	**SD**	**SEM**
R1	49	10.20	10.81	12.38	9.73	13.07	11.30	1.31	0.19
R2	49	10.91	12.05	13.14	10.17	13.97	12.05	1.36	0.19
R3	49	11.31	12.23	13.70	10.85	14.65	12.53	1.44	0.21
R4	49	11.97	13.16	14.68	11.62	15.49	13.33	1.57	0.22
R5	49	13.16	14.23	15.91	12.41	16.67	14.38	1.59	0.23
R6	49	13.29	14.65	16.10	12.12	17.41	14.72	1.88	0.27
aBMD	**n**	**25%**	**Med**	**75%**	**10%**	**90%**	**M**	**SD**	**SEM**
R1	49	0.894	0.999	1.086	0.780	1.185	0.988	0.173	0.025
R2	49	0.888	0.982	1.080	0.758	1.199	0.977	0.178	0.025
R3	49	0.860	0.963	1.039	0.742	1.162	0.946	0.163	0.023
R4	49	0.839	0.913	0.990	0.718	1.091	0.908	0.154	0.022
R5	49	0.799	0.873	0.972	0.680	1.073	0.879	0.159	0.023
R6	49	0.782	0.832	0.966	0.681	1.161	0.869	0.168	0.024

APPENDIX 3

*Figure 3.12 data tables (a) BMC (g); (b) EA (cm^2) and (c) aBMD ($g.cm^{-2}$) for sub-regions R1 to R6 in **FMR.***

BMC	n	25%	Med	75%	105	905	M	SD	SEM
R1	76	8.77	10.03	11.51	7.41	12.91	10.22	1.98	0.23
R2	76	7.46	8.34	9.82	6.91	10.57	8.60	1.57	0.18
R3	76	7.23	7.96	9.42	6.59	10.35	8.31	1.51	0.17
R4	76	7.19	7.85	9.07	6.42	10.05	8.10	1.45	0.17
R5	76	8.18	8.93	10.11	7.29	11.75	9.19	1.63	0.19
R6	76	15.22	17.21	19.29	12.76	21.61	17.18	3.15	0.36
EA	**n**	**25%**	**Med**	**75%**	**10%**	**90%**	**M**	**SD**	**SEM**
R1	76	12.82	13.73	14.74	12.10	15.73	13.78	1.32	0.15
R2	76	10.12	10.81	11.55	9.59	12.14	10.88	0.99	0.11
R3	76	7.79	8.44	9.04	7.39	9.44	8.45	0.79	0.09
R4	76	8.03	8.74	9.28	7.51	9.93	8.71	0.86	0.10
R5	76	9.69	10.48	11.15	9.03	11.92	10.44	1.01	0.12
R6	76	13.83	14.84	15.83	12.69	16.52	14.73	1.57	0.18
aBMD	**n**	**25%**	**Med**	**75%**	**10%**	**90%**	**M**	**SD**	**SEM**
R1	76	0.683	0.736	0.796	0.622	0.854	0.737	0.090	0.010
R2	76	0.723	0.801	0.860	0.657	0.907	0.788	0.103	0.012
R3	76	0.890	0.973	1.074	0.824	1.156	0.980	0.123	0.014
R4	76	0.827	0.947	0.990	0.780	1.098	0.927	0.112	0.013
R5	76	0.797	0.876	0.953	0.744	1.012	0.876	0.105	0.012
R6	76	1.056	1.165	1.246	0.976	1.333	1.153	0.140	0.016

*Figure 3.13 data tables (a) BMC (g); (b) EA (cm^2) and (c) aBMD ($g.cm^{-2}$) for sub-regions R1 to R6 in **TBR.***

BMC	n	25%	Med	75%	10%	90%	M	SD	SEM
R1	76	12.64	14.65	16.48	10.67	18.58	14.58	2.78	0.32
R2	76	8.75	9.41	10.63	7.67	11.53	9.52	1.49	0.17
R3	76	8.40	9.19	10.35	7.58	11.28	9.34	1.40	0.16
R4	76	7.87	8.57	9.59	7.19	10.68	8.76	1.33	0.15
R5	76	7.07	7.65	8.45	6.44	9.16	7.73	1.08	0.12
R6	76	8.41	9.23	10.55	7.27	11.30	9.33	1.64	0.19
EA	**n**	**25%**	**Med**	**75%**	**10%**	**90%**	**M**	**SD**	**SEM**
R1	76	14.71	15.51	16.75	13.61	17.70	15.66	1.45	0.17
R2	76	9.67	10.25	11.21	9.04	12.05	10.39	1.04	0.12
R3	76	8.21	8.87	9.45	7.76	9.99	8.84	0.88	0.10
R4	76	7.76	8.34	8.83	7.19	9.37	8.29	0.81	0.09
R5	76	7.94	8.47	8.92	7.42	9.92	8.53	0.84	0.10
R6	76	9.93	10.65	11.31	9.18	12.02	10.66	1.13	0.13
aBMD	**n**	**25%**	**Med**	**75%**	**10%**	**90%**	**M**	**SD**	**SEM**
R1	76	0.826	0.934	1.018	0.765	1.080	0.926	0.120	0.014
R2	76	0.839	0.926	0.982	0.786	1.044	0.915	0.100	0.011
R3	76	0.974	1.060	1.133	0.925	1.180	1.054	0.104	0.012
R4	76	0.978	1.069	1.130	0.935	1.168	1.055	0.097	0.011
R5	76	0.858	0.913	0.956	0.792	1.009	0.905	0.080	0.009
R6	76	0.813	0.875	0.930	0.754	0.991	0.872	0.086	0.010

APPENDIX 3

*Figure 3.14 data tables (a) BMC (g); (b) EA (cm^2) and (c) aBMD ($g.cm^{-2}$) for sub-regions R1 to R6 in **HMR.***

BMC	n	25%	Med	75%	10%	90%	M	SD	SEM
R1	76	4.91	6.13	7.14	4.01	7.91	6.08	1.52	0.17
R2	76	9.55	11.12	12.61	8.31	13.97	11.07	2.12	0.24
R3	76	5.72	6.47	7.39	5.09	7.98	6.50	1.13	0.13
R4	76	6.73	7.32	8.42	6.01	9.23	7.51	1.37	0.16
R5	76	7.38	7.99	9.54	6.42	10.46	8.34	1.61	0.18
R6	76	9.73	11.31	13.44	8.41	14.74	11.55	2.42	0.28
EA	**n**	**25%**	**Med**	**75%**	**10%**	**90%**	**M**	**SD**	**SEM**
R1	76	7.24	8.20	8.73	6.94	9.47	8.12	0.99	0.11
R2	76	11.64	12.39	13.31	10.77	14.20	12.46	1.31	0.15
R3	76	7.19	7.75	8.58	6.72	9.11	7.94	0.96	0.11
R4	76	6.13	6.54	7.33	5.78	7.60	6.70	0.72	0.08
R5	76	7.09	7.56	8.35	6.57	8.66	7.67	0.77	0.09
R6	76	9.51	10.43	11.23	8.93	12.17	10.40	1.13	0.13
aBMD	**n**	**25%**	**Med**	**75%**	**10%**	**90%**	**M**	**SD**	**SEM**
R1	76	0.685	0.746	0.820	0.600	0.885	0.744	0.115	0.013
R2	76	0.793	0.892	0.985	0.706	1.038	0.887	0.133	0.015
R3	76	0.750	0.819	0.881	0.685	0.945	0.819	0.107	0.012
R4	76	1.029	1.120	1.181	0.941	1.296	1.116	0.137	0.016
R5	76	0.995	1.094	1.167	0.888	1.284	1.083	0.144	0.016
R6	76	0.994	1.128	1.198	0.927	1.303	1.102	0.145	0.017

*Figure 3.15 data tables (a) BMC (g); (b) EA (cm^2) and (c) aBMD ($g.cm^{-2}$) for sub-regions R1 to R6 in **RDR.***

BMC	n	25%	Med	75%	10%	90%	M	SD	SEM
R1	96	4.20	4.97	5.82	3.41	6.60	4.98	1.18	0.12
R2	96	9.38	10.77	13.72	7.73	15.68	11.36	2.89	0.30
R3	96	7.50	8.41	10.00	6.60	11.08	8.66	1.70	0.17
R4	96	6.44	7.28	8.27	5.90	9.15	7.37	1.21	0.12
R5	96	5.77	6.51	7.13	5.14	7.92	6.45	1.00	0.10
R6	96	7.70	8.55	9.71	6.20	10.69	8.61	1.62	0.17
EA	**n**	**25%**	**Med**	**75%**	**10%**	**90%**	**M**	**SD**	**SEM**
R1	74	5.00	5.60	6.06	4.70	6.57	5.57	0.72	0.08
R2	74	9.83	10.44	11.20	9.27	12.34	10.61	1.12	0.13
R3	74	8.45	9.20	9.72	7.94	10.56	9.16	0.91	0.11
R4	74	7.88	8.54	9.09	7.36	9.86	8.58	0.84	0.10
R5	74	8.52	9.25	9.92	7.86	10.95	9.32	1.00	0.12
R6	74	10.78	11.53	12.37	9.95	13.05	11.54	1.16	0.13
aBMD	**n**	**25%**	**Med**	**75%**	**10%**	**90%**	**M**	**SD**	**SEM**
R1	74	0.791	0.886	1.009	0.657	1.097	0.894	0.163	0.019
R2	74	0.929	1.062	1.191	0.826	1.299	1.062	0.178	0.021
R3	74	0.856	0.944	0.993	0.802	1.065	0.929	0.109	0.013
R4	74	0.803	0.850	0.904	0.752	0.937	0.847	0.076	0.009
R5	74	0.640	0.693	0.737	0.611	0.760	0.685	0.067	0.008
R6	74	0.679	0.752	0.805	0.599	0.872	0.740	0.092	0.011

APPENDIX 3

Figure 3.16 data tables for ROI (r1 to r3) aBMD in (a) proximal femur (b) tibial plateau (c) proximal humerus and (d) distal radius

FMR	n	25%	Med	75%	10%	90%	M	SD	SEM
r1	77	0.894	0.944	1.018	0.821	1.055	0.949	0.109	0.012
r2	77	0.517	0.561	0.620	0.463	0.679	0.565	0.077	0.009
r3	77	0.689	0.773	0.855	0.620	0.922	0.773	0.113	0.013
TBR	**n**	**25%**	**Med**	**75%**	**10%**	**90%**	**M**	**SD**	**SEM**
r1	76	0.925	1.043	1.138	0.833	1.195	1.028	0.150	0.017
r2	76	0.936	1.068	1.209	0.835	1.315	1.071	0.176	0.020
r3	76	0.972	1.137	1.250	0.851	1.354	1.111	0.188	0.022
HMR	**n**	**25%**	**Med**	**75%**	**10%**	**90%**	**M**	**SD**	**SEM**
r1	76	0.844	0.915	0.995	0.764	1.089	0.913	0.124	0.014
r2	76	0.896	1.041	1.143	0.795	1.203	1.019	0.162	0.019
r3	76	0.740	0.853	0.929	0.659	0.999	0.836	0.136	0.016
RDR	**n**	**25%**	**Med**	**75%**	**10%**	**90%**	**M**	**SD**	**SEM**
r1	76	0.786	0.858	0.922	0.698	0.998	0.853	0.112	0.013
r2	76	0.590	0.643	0.700	0.511	0.762	0.641	0.090	0.010
r3	76	0.565	0.608	0.661	0.522	0.695	0.610	0.068	0.008

APPENDIX 4.1

Anaesthetic and Surgical Procedures for Ovariectomy (OVX)

Anaesthetic Procedures
Animals for surgery were grouped in an indoor pen the neck was clipped in the region of external jugular vein and intravenous Sodium Thiopentone was administered as induction agent. Animals were placed in dorsal recumbency on the operating table, hind limbs were tethered to maintain position and were intubated with size 7 or 8 rubber cuffed endotracheal tubes. Anaesthesia was maintained with 3-4% Halothane (Merial Animal Health, Harlow, UK)

Pre-operative procedures
Lower ventral abdomen from mammary gland to umbilicus was close clipped, shaved with disposable razor and skin preparation solution, chlorhexidine and alcohol, applied. Table tilted to displace abdominal contents caudally for ease of identification of uterus and ovaries. The operative field was covered with surgical drapes, fenestrated over site of incision, secured with towel clips

Operative protocol
A 10 cm ventral midline incision was made from just cranial to the umbilicus. Sub cutaneous fat/facia teased apart by blunt dissection, the milk veins were carefully avoided, and branches were ligated. The linea alba was incised using scalpel and scissors, uterus identified and exteriorised to allow identification of the ovaries. Ovarian vessels were ligated with 3 metric polydioxannone (PDS, Ethicon, Johnson and Johnson, Brussels, Belgium) and ovaries were resected and pedicles checked for haemorrhage, when no haemorrhage was evident pedicles were returned to the abdomen. The linea alba closed by continuous suture (5 metric polydioxannone, PDS, Ethicon), subcutaneous tissues were opposed (3 metric polydioxannone, PDS, Ethicon) and skin closed by continuous sutures (3 metric polypropylene, Proline, Ethicon).

Anti sepsis and Analgesia
Intra-peritoneal Benzyl Penicillin (10 $mg.kg^{-1}$, Crystapen, Schering Plough Animal Health, Ireland) was administered prophylactically before closure to protect against peritonitis. The surgical wound was sprayed with aluminium powder based wound spray (Alluspray, Vetoquinol Ireland Ltd, Dublin) and long acting amoxicillin was given IM (15 mg/kg, Betamox LA, Norbrook Laboratories Ltd, Ireland). Oxytetracycline (50 mg/kg, Terramycin LA, Norbrook Labarotories Ltd, Ireland) was given intravenously just prior to anaesthetic recovery. An analgesic medication, Flunixin meglumine (2.2 $mg.kg^{-1}$, Flunixin Inj., Norbrook Laboratories Ltd, Dublin) was administered intramuscularly (see Table below).

Fluorochrome *in vivo* injection regimen BFL project.

Fluorochrome Agent	Solution Concentrations	Intravenous Dosage
Oxytetracycline (Pfizer Animal Health, Dublin)	200 $g.L^{-1}$	50 $mg.kg^{-1}$ *
Alizarin complexone (Lennox Laboratory Supplies, Dublin)	30 $g.L^{-1}$	25 $mg.kg^{-1}$ *
Calcein (Sigma Aldrich, Dublin)	5 $g.L^{-1}$	10 $mg.kg^{-1}$ * #
Xylenol orange (Sigma Aldrich, Dublin)	90 $g.L^{-1}$	90 $mg.kg^{-1}$ * #
Calcein blue (Sigma Aldrich, Dublin)	30 $g.L^{-1}$	30 $mg.kg^{-1}$ * #

***** From Lanyon *et al.* (1982); # from Rahn (1977).

Post-operative care
Sheep were observed for return of swallowing reflex, and then extubated, further observation was conducted in the indoor holding pen until full recovery and normal ambulation. 24 hours post op a second analgesic injection was given (flunixin meglumine). 48 hours post op all surgical wounds were inspected for swelling, infection or breakdown. At 10 days post op wounds were again inspected and skin sutures removed.

APPENDIX 4.2

Figure 4.3 (a) data table mean (±SD) body mass (kg) across time

Time (week)	**0**	**10**	**17**	**28**	**40**	**44**
Y1 CON	61(8)	65 (7)	61 (7)	66 (8)	73 (9)	73 (9)
Y1 OVX	60 (7)	62 (7)	60 (8)	66 (8)	71 (9)	72 (8)
Time (week)	**0**	**48**	**70**	**84**	**104**	**130**
Y3 CON	62 (8)	72 (8)	70 (8)	76 (9)	73 (8)	82 (9)
Y3 OVX	60 (7)	69 (8)	66 (8)	72 (7)	71 (8)	82 (9)
Y3 ZOL	69 (7)	82 (4)	79 (5)	84 (5)	81 (4)	86 (7)

Figure 4.3 (b) data table comparison of body mass at sacrifice for CON and OVX, at Y1 and Y3.

	n	**25%**	**Med**	**75%**	**10%**	**90%**	**M**	**SD**	**SEM**
Y1 CON	18	68	70	77	64	89	73	9	2
Y1 OVX	16	64	72	79	62	86	72	9	2
Y3 CON	16	77	81	89	69	100	82	9	2
Y3 OVX	11	74	82	89	68	95	82	9	3

*Figure 4.4: Data table for whole bone sample (a) EA, (b) BMC and (c) aBMD in CON and OVX at Y1 and Y3 for **LS***

BMC	**n**	**25%**	**Med**	**75%**	**10%**	**90%**	**M**	**SD**	**SEM**
Y1 CON	18	68.60	71.74	81.46	59.41	101.90	75.52	14.04	3.31
Y1 OVX	16	64.93	71.83	77.65	61.52	87.51	72.83	10.08	2.52
Y3 CON	16	71.97	84.30	94.16	62.93	107.50	83.81	14.83	3.71
Y3 OVX	11	79.96	86.06	94.87	62.97	99.20	84.54	11.94	3.60
EA	**n**	**25%**	**Med**	**75%**	**10%**	**90%**	**M**	**SD**	**SEM**
Y1 CON	17	77.38	81.03	84.05	72.62	90.21	81.17	5.47	1.33
Y1 OVX	15	77.56	81.96	85.02	73.10	92.62	81.69	6.28	1.62
Y3 CON	16	76.79	84.96	89.81	71.65	93.37	84.06	7.94	1.98
Y3 OVX	11	85.04	88.27	89.13	70.53	90.52	85.17	7.18	2.17
aBMD	**n**	**25%**	**Med**	**75%**	**10%**	**90%**	**M**	**SD**	**SEM**
Y1 CON	18	0.850	0.903	1.009	0.777	1.128	0.931	0.120	0.028
Y1 OVX	16	0.835	0.881	0.940	0.813	0.987	0.888	0.067	0.017
Y3 CON	16	0.902	0.983	1.072	0.846	1.140	0.992	0.109	0.027
Y3 OVX	11	0.919	0.975	1.065	0.883	1.122	0.985	0.082	0.025

APPENDIX 4.2

Figure 4.4: Data table for whole bone sample (a) EA, (b) BMC and (c) aBMD in CON and OVX at Y1 and Y3 ***FMR***

BMC	n	25%	Med	75%	10%	90%	M	SD	SEM
Y1 CON	18	54.71	58.90	67.16	52.82	72.06	60.93	8.90	2.10
Y1 OVX	16	54.15	59.55	61.47	50.47	72.94	59.59	7.32	1.83
Y3 CON	16	54.20	62.72	68.12	50.98	73.39	61.95	8.15	2.04
Y3 OVX	11	64.09	66.27	72.01	52.79	75.83	65.71	7.35	2.22
EA	**n**	**25%**	**Med**	**75%**	**10%**	**90%**	**M**	**SD**	**SEM**
Y1 CON	18	62.12	65.08	67.26	59.45	71.51	64.97	4.17	0.98
Y1 OVX	16	61.28	65.37	67.64	56.37	73.26	64.97	5.53	1.38
Y3 CON	16	62.31	65.13	67.30	58.34	69.79	64.74	4.17	1.04
Y3 OVX	11	65.15	68.76	69.85	58.07	78.55	67.85	6.22	1.87
aBMD	**n**	**25%**	**Med**	**75%**	**10%**	**90%**	**M**	**SD**	**SEM**
Y1 CON	18	0.871	0.916	0.991	0.829	1.056	0.935	0.085	0.020
Y1 OVX	16	0.882	0.960	1.029	0.820	1.056	0.952	0.079	0.020
Y3 CON	16	0.871	0.914	0.961	0.817	1.039	0.919	0.076	0.019
Y3 OVX	11	0.923	0.965	0.995	0.902	1.091	0.968	0.059	0.018

Figure 4.4: data table for whole bone sample (a) EA, (b) BMC and (c) aBMD in CON and OVX at Y1 and Y3 ***TBR***

(a) EA	n	25%	Med	75%	10%	90%	M	SD	SEM
Y1 CON	34	57.68	59.38	61.99	55.36	64.29	59.82	3.53	0.61
Y1 OVX	27	57.09	61.52	64.00	52.14	68.83	61.12	5.41	1.04
Y3 CON	16	58.36	59.50	61.43	54.96	65.49	59.89	3.40	0.85
Y3 OVX	11	60.16	61.96	62.75	52.64	70.22	61.58	5.48	1.65
(b) BMC	**n**	**25%**	**Med**	**75%**	**10%**	**90%**	**M**	**SD**	**SEM**
Y1 CON	34	53.49	56.99	62.27	52.36	66.80	58.39	6.27	1.08
Y1 OVX	27	57.81	63.19	68.52	53.34	71.80	63.00	7.08	1.36
Y3 CON	16	53.30	57.69	62.51	52.13	67.60	58.62	5.70	1.43
Y3 OVX	11	61.37	64.79	71.35	54.26	76.80	64.99	7.19	2.17
(c) aBMD	**n**	**25%**	**Med**	**75%**	**10%**	**90%**	**M**	**SD**	**SEM**
Y1 CON	34	0.921	0.992	1.021	0.888	1.047	0.975	0.067	0.012
Y1 OVX	27	0.984	1.025	1.073	0.941	1.110	1.030	0.061	0.012
Y3 CON	16	0.913	0.999	1.020	0.890	1.053	0.978	0.058	0.014
Y3 OVX	11	1.020	1.045	1.073	1.014	1.150	1.055	0.046	0.014

APPENDIX 4.2

Figure 4.4: Data table for whole bone sample (a) EA, (b) BMC and (c) aBMD in CON and OVX at Y1 and Y3 ***HMR***

(a) EA	n	25%	Med	75%	10%	90%	M	SD	SEM
Y1 CON	18	48.37	49.38	52.53	46.85	56.12	50.55	3.26	0.77
Y1 OVX	16	48.84	51.82	55.87	45.45	58.10	52.10	4.43	1.11
Y3 CON	16	47.84	50.86	53.09	45.41	54.92	50.39	3.32	0.83
Y3 OVX	11	50.86	53.76	55.21	46.60	60.44	53.43	4.13	1.25
(b) BMC	**n**	**25%**	**Med**	**75%**	**10%**	**90%**	**M**	**SD**	**SEM**
Y1 CON	18	43.36	48.93	52.38	42.49	62.85	49.91	7.78	1.83
Y1 OVX	16	51.47	55.31	60.32	44.29	64.48	54.97	6.67	1.67
Y3 CON	16	44.20	47.09	51.15	43.17	59.74	48.78	5.77	1.44
Y3 OVX	11	50.56	55.21	58.63	44.75	64.12	54.58	5.83	1.76
(c) aBMD	**n**	**25%**	**Med**	**75%**	**10%**	**90%**	**M**	**SD**	**SEM**
Y1 CON	18	0.905	0.964	1.042	0.875	1.145	0.983	0.096	0.023
Y1 OVX	16	0.999	1.034	1.114	0.958	1.162	1.054	0.076	0.019
Y3 CON	16	0.930	0.961	1.007	0.858	1.096	0.967	0.074	0.019
Y3 OVX	11	0.960	1.019	1.095	0.941	1.128	1.021	0.065	0.020

Figure 4.4: data table for whole bone sample (a) EA, (b) BMC and (c) aBMD in CON and OVX at Y1 and Y3 ***RDR***

(a) EA	n	25%	Med	75%	10%	90%	M	SD	SEM
Y1 CON	17	50.62	52.21	55.14	47.84	58.53	52.93	3.37	0.82
Y1 OVX	16	50.15	53.99	56.78	45.49	58.29	53.36	4.30	1.08
Y3 CON	16	49.29	52.51	54.50	48.24	57.71	52.44	3.33	0.83
Y3 OVX	11	53.92	54.78	57.46	46.86	63.97	55.13	4.86	1.47
(b) BMC	**n**	**25%**	**Med**	**75%**	**10%**	**90%**	**M**	**SD**	**SEM**
Y1 CON	33	40.57	43.40	49.52	39.91	53.60	45.27	5.59	0.97
Y1 OVX	27	47.21	51.26	54.30	41.75	58.08	50.74	5.38	1.03
Y3 CON	16	40.46	45.22	49.94	39.34	51.88	44.93	4.85	1.21
Y3 OVX	11	49.27	51.26	55.07	42.09	57.38	51.23	4.70	1.42
(c) aBMD	**n**	**25%**	**Med**	**75%**	**10%**	**90%**	**M**	**SD**	**SEM**
Y1 CON	17	0.794	0.853	0.903	0.758	0.992	0.859	0.080	0.019
Y1 OVX	16	0.902	0.930	0.982	0.868	1.054	0.943	0.061	0.015
Y3 CON	16	0.804	0.853	0.915	0.777	0.942	0.856	0.059	0.015
Y3 OVX	11	0.900	0.925	0.959	0.859	0.993	0.930	0.043	0.013

APPENDIX 4.2

*Figure 4.5: data table for whole bone (a) EA, (b) BMC and (c) BMD in **LS** for CON and OVX at Y1 and Y3 normalised for body mass (data.kg^{-1}).*

(a) EA/kg	n	25%	Med	75%	10%	90%	M	SD	SEM
Y1 CON	18	1.03	1.13	1.18	0.97	1.28	1.12	0.11	0.03
Y1 OVX	16	0.94	1.02	1.11	0.88	1.20	1.03	0.11	0.03
Y3 CON	16	1.08	1.11	1.24	1.02	1.31	1.15	0.10	0.03
Y3 0VX	11	0.96	1.05	1.10	0.88	1.27	1.05	0.13	0.04
(b) BMC/kg	**n**	**25%**	**Med**	**75%**	**10%**	**90%**	**M**	**SD**	**SEM**
Y1 CON	18	0.92	1.05	1.09	0.80	1.27	1.04	0.20	0.05
Y1 OVX	16	0.91	1.01	1.10	0.85	1.23	1.02	0.15	0.04
Y3 CON	16	0.92	1.02	1.09	0.89	1.21	1.02	0.12	0.03
Y3 0VX	11	0.89	1.06	1.25	0.80	1.34	1.05	0.19	0.06
(c) aBMD/kg	**n**	**25%**	**Med**	**75%**	**10%**	**90%**	**M**	**SD**	**SEM**
Y1 CON	18	0.012	0.013	0.014	0.011	0.015	0.013	0.002	0.000
Y1 OVX	16	0.011	0.012	0.013	0.011	0.014	0.012	0.001	0.000
Y3 CON	16	0.011	0.013	0.014	0.011	0.014	0.013	0.001	0.000
Y3 0VX	11	0.010	0.012	0.014	0.010	0.015	0.012	0.002	0.001

*Figure 4.5: data table for whole bone (a) EA, (b) BMC and (c) BMD in **FMR** for CON and OVX at Y1 and Y3 normalised for body mass (data.kg^{-1}).*

(a) EA/kg	n	25%	Med	75%	10%	90%	M	SD	SEM
Y1 CON	34	0.84	0.89	0.98	0.80	1.06	0.91	0.09	0.02
Y1 OVX	27	0.77	0.80	0.84	0.70	0.98	0.81	0.08	0.02
Y3 CON	16	0.83	0.89	0.99	0.80	1.06	0.91	0.09	0.02
Y3 0VX	11	0.78	0.83	0.89	0.69	1.00	0.84	0.10	0.03
(b) BMC/kg	**n**	**25%**	**Med**	**75%**	**10%**	**90%**	**M**	**SD**	**SEM**
Y1 CON	18	0.78	0.82	0.90	0.72	0.98	0.84	0.10	0.02
Y1 OVX	16	0.69	0.75	0.82	0.64	0.86	0.75	0.08	0.02
Y3 CON	16	0.79	0.81	0.89	0.73	0.96	0.83	0.08	0.02
Y3 0VX	11	0.75	0.81	0.86	0.67	0.97	0.81	0.09	0.03
(c) aBMD/kg	**n**	**25%**	**Med**	**75%**	**10%**	**90%**	**M**	**SD**	**SEM**
Y1 CON	18	0.012	0.013	0.013	0.011	0.014	0.013	0.001	0.000
Y1 OVX	16	0.010	0.012	0.013	0.010	0.014	0.012	0.001	0.000
Y3 CON	16	0.012	0.013	0.014	0.011	0.015	0.013	0.001	0.000
Y3 0VX	11	0.011	0.012	0.012	0.010	0.014	0.012	0.001	0.000

*Figure 4.5: data table for whole bone (a) EA, (b) BMC and (c) BMD in **TBR** for CON and OVX at Y1 and Y3 normalised for body mass (data.kg^{-1}).*

(a) EA/kg	n	25%	Med	75%	10%	90%	M	SD	SEM
Y1 CON	18	0.78	0.80	0.88	0.74	0.96	0.83	0.08	0.02
Y1 OVX	16	0.69	0.74	0.77	0.64	0.87	0.74	0.08	0.02
Y3 CON	16	0.77	0.81	0.93	0.75	0.97	0.84	0.08	0.02
Y3 0VX	11	0.72	0.77	0.79	0.65	0.89	0.76	0.08	0.02
(b) BMC/kg	**n**	**25%**	**Med**	**75%**	**10%**	**90%**	**M**	**SD**	**SEM**
Y1 CON	18	0.73	0.80	0.85	0.71	0.92	0.80	0.08	0.02

APPENDIX 4.2

Y1 OVX	16	0.70	0.76	0.82	0.66	0.85	0.75	0.08	0.02
Y3 CON	16	0.78	0.83	0.85	0.73	0.91	0.82	0.06	0.02
Y3 0VX	11	0.75	0.80	0.86	0.69	0.91	0.80	0.07	0.02
(c) aBMD/kg	**n**	**25%**	**Med**	**75%**	**10%**	**90%**	**M**	**SD**	**SEM**
Y1 CON	18	0.012	0.014	0.015	0.011	0.015	0.013	0.002	0.000
Y1 OVX	16	0.012	0.012	0.014	0.011	0.014	0.013	0.001	0.000
Y3 CON	16	0.013	0.014	0.015	0.012	0.015	0.014	0.001	0.000
Y3 0VX	11	0.012	0.013	0.014	0.011	0.015	0.013	0.001	0.000

*Figure 4.5: data table for whole bone (a) EA, (b) BMC and (c) BMD in **HMR** for CON and OVX at Y1 and Y3 normalised for body mass (data.kg^{-1}).*

(a) EA/kg	**n**	**25%**	**Med**	**75%**	**10%**	**90%**	**M**	**SD**	**SEM**
Y1 CON	18	0.66	0.70	0.74	0.61	0.82	0.70	0.07	0.02
Y1 OVX	16	0.60	0.63	0.68	0.56	0.74	0.64	0.07	0.02
Y3 CON	16	0.65	0.67	0.78	0.63	0.83	0.71	0.07	0.02
Y3 0VX	11	0.62	0.66	0.69	0.54	0.80	0.66	0.08	0.02
(b) BMC/kg	**n**	**25%**	**Med**	**75%**	**10%**	**90%**	**M**	**SD**	**SEM**
Y1 CON	18	0.62	0.69	0.73	0.57	0.84	0.69	0.09	0.02
Y1 OVX	16	0.64	0.67	0.71	0.59	0.73	0.67	0.05	0.01
Y3 CON	16	0.64	0.68	0.72	0.61	0.77	0.68	0.06	0.01
Y3 0VX	11	0.63	0.67	0.72	0.56	0.82	0.67	0.08	0.02
(c) aBMD/kg	**n**	**25%**	**Med**	**75%**	**10%**	**90%**	**M**	**SD**	**SEM**
Y1 CON	18	0.013	0.014	0.015	0.012	0.015	0.014	0.001	0.000
Y1 OVX	16	0.012	0.013	0.014	0.012	0.015	0.013	0.001	0.000
Y3 CON	16	0.012	0.014	0.015	0.012	0.015	0.014	0.001	0.000
Y3 0VX	11	0.012	0.012	0.013	0.011	0.016	0.013	0.001	0.000

*Figure 4.5: data table for whole bone (a) EA, (b) BMC and (c) BMD in **RDR** for CON and OVX at Y1 and Y3 normalised for body mass (data.kg^{-1}).*

(a) EA/kg	**n**	**25%**	**Med**	**75%**	**10%**	**90%**	**M**	**SD**	**SEM**
Y1 CON	17	0.69	0.72	0.78	0.62	0.89	0.74	0.08	0.02
Y1 OVX	16	0.61	0.65	0.69	0.57	0.75	0.65	0.06	0.02
Y3 CON	16	0.67	0.72	0.79	0.66	0.88	0.74	0.08	0.02
Y3 0VX	11	0.62	0.68	0.73	0.58	0.81	0.68	0.07	0.02
(b) BMC/kg	**n**	**25%**	**Med**	**75%**	**10%**	**90%**	**M**	**SD**	**SEM**
Y1 CON	17	0.80	0.85	0.91	0.76	0.99	0.86	0.08	0.02
Y1 OVX	16	0.90	0.93	0.98	0.86	1.05	0.94	0.06	0.02
Y3 CON	16	0.81	0.86	0.91	0.77	0.94	0.86	0.06	0.01
Y3 0VX	11	0.90	0.92	0.96	0.86	1.00	0.93	0.04	0.01
(c) aBMD/kg	**n**	**25%**	**Med**	**75%**	**10%**	**90%**	**M**	**SD**	**SEM**
Y1 CON	17	0.018	0.019	0.020	0.017	0.021	0.019	0.001	0.000
Y1 OVX	16	0.018	0.019	0.020	0.017	0.022	0.019	0.002	0.000
Y3 CON	16	0.018	0.019	0.020	0.018	0.021	0.019	0.001	0.000
Y3 0VX	11	0.017	0.018	0.019	0.015	0.022	0.018	0.002	0.001

APPENDIX 4.2

*Figure 4.6 aBMD (g.cm^{-2}) data table for **HMR** sub-regions R1 to R6 CON and OVX at Y1 and Y3.*

Y1	n	25%	Med	75%	10%	90%	M	SD	SEM
R1 CON	18	0.911	0.979	1.074	0.839	1.209	1.010	0.141	0.033
OVX	16	0.925	0.964	1.010	0.887	1.087	0.973	0.079	0.020
R2 CON	18	0.889	0.974	1.057	0.840	1.221	0.997	0.144	0.034
OVX	16	0.899	0.943	0.998	0.863	1.070	0.953	0.078	0.019
R3 CON	18	0.879	0.948	1.015	0.820	1.165	0.955	0.107	0.025
OVX	16	0.870	0.913	0.972	0.850	1.036	0.923	0.069	0.017
R4 CON	18	0.846	0.895	0.968	0.778	1.096	0.916	0.104	0.024
OVX	16	0.830	0.872	0.912	0.813	1.005	0.885	0.069	0.017
R5 CON	18	0.823	0.871	0.966	0.743	1.106	0.897	0.118	0.028
OVX	16	0.786	0.849	0.902	0.769	0.968	0.852	0.072	0.018
R6 CON	18	0.780	0.835	0.953	0.729	1.178	0.877	0.147	0.035
OVX	16	0.761	0.829	0.845	0.727	0.951	0.823	0.075	0.019
Y3	**n**	**25%**	**Med**	**75%**	**10%**	**90%**	**M**	**SD**	**SEM**
R1 CON	16	1.001	1.065	1.160	0.898	1.252	1.072	0.110	0.028
OVX	11	0.992	1.061	1.128	0.970	1.276	1.087	0.104	0.031
R2 CON	16	0.985	1.061	1.166	0.900	1.243	1.067	0.115	0.029
OVX	11	0.985	1.067	1.156	0.962	1.227	1.073	0.093	0.028
R3 CON	16	0.961	1.032	1.107	0.867	1.232	1.032	0.114	0.029
OVX	11	0.945	1.022	1.097	0.918	1.197	1.033	0.094	0.028
R4 CON	16	0.895	0.962	1.063	0.837	1.170	0.981	0.114	0.028
OVX	11	0.903	0.964	1.037	0.870	1.134	0.975	0.087	0.026
R5 CON	16	0.829	0.924	1.025	0.803	1.107	0.939	0.122	0.030
OVX	11	0.873	0.924	0.968	0.842	1.076	0.935	0.076	0.023
R6 CON	16	0.819	0.919	0.974	0.809	1.199	0.935	0.134	0.033
OVX	11	0.862	0.901	0.973	0.743	1.077	0.914	0.102	0.031

APPENDIX 4.2

*Figure 4.7 aBMD (g.cm^{-2}) data table for **FMR** sub-regions R1 to R6 CON and OVX at Y1 and Y3.*

Y1	n	25%	Med	75%	10%	90%	M	SD	SEM
R1 CON	18	0.717	0.761	0.792	0.675	0.864	0.760	0.061	0.014
OVX	16	0.680	0.725	0.790	0.668	0.818	0.734	0.056	0.014
R2 CON	18	0.744	0.792	0.881	0.720	0.961	0.811	0.090	0.021
OVX	16	0.725	0.775	0.829	0.674	0.968	0.789	0.090	0.022
R3 CON	18	0.913	0.974	1.071	0.834	1.133	0.983	0.108	0.025
OVX	16	0.938	0.977	1.045	0.842	1.206	0.995	0.107	0.027
R4 CON	18	0.878	0.925	0.980	0.804	1.108	0.938	0.108	0.026
OVX	16	0.892	0.942	0.982	0.821	1.085	0.945	0.083	0.021
R5 CON	18	0.833	0.915	0.938	0.777	1.037	0.901	0.107	0.025
OVX	16	0.809	0.892	0.934	0.764	1.017	0.888	0.101	0.025
R6 CON	18	1.087	1.185	1.263	0.980	1.311	1.171	0.113	0.027
OVX	16	1.063	1.162	1.190	1.017	1.323	1.148	0.106	0.026
Y3	**n**	**25%**	**Med**	**75%**	**10%**	**90%**	**M**	**SD**	**SEM**
R1 CON	16	0.712	0.781	0.829	0.674	0.857	0.772	0.064	0.016
OVX	11	0.735	0.775	0.836	0.695	0.873	0.778	0.061	0.018
R2 CON	16	0.755	0.833	0.879	0.662	0.902	0.809	0.082	0.021
OVX	11	0.780	0.795	0.873	0.737	0.980	0.830	0.083	0.025
R3 CON	16	0.970	1.004	1.029	0.860	1.155	1.005	0.096	0.024
OVX	11	0.933	1.038	1.071	0.871	1.184	1.020	0.102	0.031
R4 CON	16	0.907	0.964	0.990	0.788	1.098	0.946	0.095	0.024
OVX	11	0.914	0.987	1.011	0.883	1.103	0.979	0.074	0.022
R5 CON	16	0.840	0.914	0.968	0.743	1.015	0.900	0.087	0.022
OVX	11	0.885	0.911	0.965	0.830	1.066	0.928	0.070	0.021
R6 CON	16	1.165	1.213	1.315	1.045	1.395	1.227	0.113	0.028
OVX	11	1.175	1.226	1.281	1.086	1.378	1.234	0.089	0.027

APPENDIX 4.2

*Figure 4.8 aBMD (g.cm^{-2}) data table for **TBR** sub-regions R1 to R6 CON and OVX at Y1 and Y3.*

Y1	n	25%	Med	75%	10%	90%	M	SD	SEM
R1 CON	18	0.901	0.964	1.026	0.806	1.091	0.963	0.098	0.023
OVX	16	0.863	0.951	0.989	0.819	1.036	0.936	0.079	0.020
R2 CON	18	0.925	0.941	1.014	0.786	1.057	0.952	0.084	0.020
OVX	16	0.881	0.991	1.024	0.832	1.086	0.968	0.089	0.022
R3 CON	18	1.041	1.133	1.145	0.941	1.203	1.102	0.095	0.023
OVX	16	1.054	1.118	1.166	1.015	1.207	1.113	0.069	0.017
R4 CON	18	1.004	1.102	1.133	0.933	1.166	1.073	0.092	0.022
OVX	16	1.044	1.096	1.153	1.016	1.163	1.095	0.056	0.014
R5 CON	18	0.893	0.929	0.953	0.819	0.996	0.919	0.063	0.015
OVX	16	0.881	0.949	0.990	0.848	1.007	0.938	0.058	0.015
R6 CON	18	0.814	0.882	0.903	0.791	0.950	0.871	0.061	0.014
OVX	16	0.846	0.891	0.932	0.818	0.981	0.893	0.054	0.013
Y3	**n**	**25%**	**Med**	**75%**	**10%**	**90%**	**M**	**SD**	**SEM**
R1 CON	16	0.941	1.019	1.069	0.836	1.114	1.000	0.096	0.024
OVX	11	0.964	1.013	1.065	0.891	1.185	1.017	0.086	0.026
R2 CON	16	0.889	0.959	1.053	0.849	1.102	0.968	0.095	0.024
OVX	11	0.973	0.995	1.069	0.946	1.146	1.027	0.069	0.021
R3 CON	16	1.042	1.100	1.196	1.016	1.265	1.120	0.086	0.022
OVX	11	1.146	1.193	1.272	1.093	1.275	1.189	0.067	0.020
R4 CON	16	1.073	1.135	1.199	1.016	1.216	1.134	0.070	0.018
OVX	11	1.165	1.219	1.228	1.099	1.241	1.192	0.049	0.015
R5 CON	16	0.898	0.988	1.021	0.867	1.050	0.964	0.065	0.016
OVX	11	0.960	0.988	1.031	0.933	1.095	1.000	0.052	0.016
R6 CON	16	0.888	0.929	0.991	0.845	1.033	0.937	0.063	0.016
OVX	11	0.936	0.950	0.977	0.908	1.032	0.958	0.038	0.011

APPENDIX 4.2

*Figure 4.9: aBMD (g.cm^{-2}) data table for **HMR** sub-regions R1 to R6 CON and OVX at Y1 and Y3.*

Y1	n	25%	Med	75%	10%	90%	M	SD	SEM
R1 CON	18	0.696	0.781	0.868	0.676	0.932	0.783	0.096	0.023
OVX	16	0.678	0.732	0.802	0.636	0.887	0.743	0.101	0.025
R2 CON	18	0.838	0.907	0.998	0.765	1.083	0.919	0.114	0.027
OVX	16	0.823	0.886	0.936	0.769	1.075	0.890	0.096	0.024
R3 CON	18	0.773	0.826	0.891	0.759	0.959	0.845	0.087	0.020
OVX	16	0.787	0.836	0.920	0.694	0.961	0.838	0.088	0.022
R4 CON	18	1.098	1.141	1.203	1.020	1.301	1.148	0.089	0.021
OVX	16	1.088	1.170	1.265	1.029	1.282	1.163	0.091	0.023
R5 CON	18	1.008	1.076	1.188	0.928	1.293	1.097	0.126	0.030
OVX	16	1.019	1.095	1.201	0.977	1.224	1.104	0.090	0.022
R6 CON	18	1.022	1.124	1.192	0.975	1.319	1.127	0.113	0.027
OVX	16	1.032	1.098	1.153	0.987	1.239	1.099	0.081	0.020
Y3	**n**	**25%**	**Med**	**75%**	**10%**	**90%**	**M**	**SD**	**SEM**
R1 CON	16	0.804	0.832	0.868	0.743	0.937	0.837	0.057	0.014
OVX	11	0.751	0.797	0.813	0.691	0.848	0.780	0.051	0.015
R2 CON	16	0.907	0.969	1.031	0.859	1.092	0.973	0.083	0.021
OVX	11	0.845	0.886	0.954	0.832	1.043	0.906	0.074	0.022
R3 CON	16	0.837	0.928	0.954	0.721	1.059	0.906	0.109	0.027
OVX	11	0.842	0.866	0.923	0.676	1.070	0.879	0.110	0.033
R4 CON	16	1.124	1.240	1.291	1.065	1.421	1.230	0.132	0.033
OVX	11	1.178	1.262	1.287	1.065	1.384	1.238	0.093	0.028
R5 CON	16	1.104	1.151	1.258	1.075	1.352	1.178	0.098	0.024
OVX	11	1.084	1.193	1.273	1.044	1.338	1.185	0.096	0.029
R6 CON	16	1.146	1.205	1.310	1.124	1.338	1.226	0.081	0.020
OVX	11	1.094	1.187	1.228	1.041	1.345	1.181	0.093	0.028

APPENDIX 4.2

*Figure 4.10 aBMD (g.cm^{-2}) data table for **RDR** sub-regions R1 to R6 CON and OVX at Y1 and Y3.*

Y1	n	25%	Med	75%	10%	90%	M	SD	SEM
R1 CON	18	0.787	0.876	1.005	0.711	1.079	0.890	0.138	0.033
OVX	16	0.782	0.839	0.984	0.739	1.095	0.887	0.128	0.032
R2 CON	18	0.951	1.003	1.094	0.897	1.276	1.041	0.126	0.030
OVX	16	0.944	1.028	1.124	0.917	1.221	1.039	0.105	0.026
R3 CON	18	0.869	0.915	0.980	0.820	1.079	0.929	0.078	0.018
OVX	16	0.870	0.922	0.975	0.838	0.998	0.919	0.056	0.014
R4 CON	18	0.807	0.837	0.917	0.773	1.013	0.870	0.115	0.027
OVX	16	0.814	0.852	0.896	0.768	0.915	0.848	0.051	0.013
R5 CON	18	0.632	0.692	0.753	0.614	0.826	0.711	0.115	0.027
OVX	16	0.651	0.710	0.730	0.606	0.768	0.697	0.052	0.013
R6 CON	18	0.704	0.760	0.812	0.670	0.905	0.774	0.115	0.027
OVX	16	0.714	0.747	0.781	0.693	0.809	0.748	0.041	0.010
Y3	**n**	**25%**	**Med**	**75%**	**10%**	**90%**	**M**	**SD**	**SEM**
R1 CON	16	0.893	0.994	1.073	0.851	1.179	1.001	0.118	0.029
OVX	11	0.907	0.964	1.040	0.852	1.089	0.976	0.076	0.023
R2 CON	16	1.127	1.183	1.265	1.059	1.405	1.200	0.114	0.029
OVX	11	1.099	1.177	1.240	0.742	1.258	1.125	0.167	0.050
R3 CON	16	0.958	0.990	1.054	0.929	1.132	1.008	0.079	0.020
OVX	11	0.942	0.990	1.043	0.936	1.057	1.000	0.046	0.014
R4 CON	16	0.863	0.893	0.920	0.845	0.969	0.898	0.045	0.011
OVX	11	0.858	0.910	0.955	0.834	0.995	0.904	0.058	0.018
R5 CON	16	0.706	0.730	0.748	0.686	0.831	0.737	0.048	0.012
OVX	11	0.698	0.738	0.766	0.671	0.804	0.733	0.044	0.013
R6 CON	16	0.753	0.812	0.855	0.734	0.896	0.812	0.058	0.015
OVX	11	0.760	0.785	0.824	0.731	0.837	0.785	0.036	0.011

APPENDIX 4.2

Figure 4.12 data tables for (a) Mean (±SD) body mass (kg) in Y3 groups CON (n=16), OVX (n=11) and ZOL (n=4) across time and (b) comparison of body mass (kg) between T0 and sacrifice.

(a) Time (week)	0	48	70	84	104	130
Y3 CON	62 ± 8	72 ± 8	70 ± 8	76 ± 9	73 ± 8	82 ± 9
Y3 OVX	60 ± 7	69 ± 8	66 ± 8	72 ± 7	71 ± 8	82 ± 9
Y3 ZOL	69 ± 7	82 ± 4	79 ± 5	84 ± 5	81 ± 4	86 ± 7

(b) Y3	n	25%	Med	75%	10%	90%	M	SD	SEM
T0 CON	16	55.5	62.5	66.8	49.4	72.3	61.5	7.7	1.9
T0 OVX	11	55.0	58.0	67.0	51.2	71.8	60.1	7.2	2.2
T0 ZOL	4	62.3	70.0	74.8	61.0	75.0	69.0	6.7	3.3
S CON	16	77.0	81.0	88.5	69.1	99.6	82.4	9.4	2.4
S OVX	11	74.0	82.0	89.0	67.6	95.0	81.6	8.8	2.7
S ZOL	4	79.8	85.5	92.0	78.0	94.0	85.8	6.6	3.3

*Figure 4.13 data table for whole bone (WB) and sub-regional (R1- R6) aBMD ($g.cm^{-2}$) in Y3 CON, OVX and ZOL (shaded) for **LS**.*

Y3	n	25%	Med	75%	10%	90%	M	SD	SEM
WB CON	16	0.902	0.983	1.072	0.846	1.140	0.992	0.109	0.027
OVX	11	0.919	0.975	1.065	0.883	1.122	0.985	0.082	0.025
ZOL	4	0.953	1.016	1.132	0.940	1.163	1.034	0.095	0.048
R1 CON	16	1.001	1.065	1.160	0.898	1.252	1.072	0.110	0.028
OVX	11	0.992	1.061	1.128	0.970	1.276	1.087	0.104	0.031
ZOL	4	1.012	1.084	1.150	0.994	1.166	1.082	0.072	0.036
R2 CON	16	0.985	1.061	1.166	0.900	1.243	1.067	0.115	0.029
OVX	11	0.985	1.067	1.156	0.962	1.227	1.073	0.093	0.028
ZOL	4	1.007	1.073	1.168	0.994	1.190	1.082	0.084	0.042
R3 CON	16	0.961	1.032	1.107	0.867	1.232	1.032	0.114	0.029
OVX	11	0.945	1.022	1.097	0.918	1.197	1.033	0.094	0.028
ZOL	4	0.990	1.032	1.137	0.981	1.166	1.053	0.080	0.040
R4 CON	16	0.895	0.962	1.063	0.837	1.170	0.981	0.114	0.028
OVX	11	0.903	0.964	1.037	0.870	1.134	0.975	0.087	0.026
ZOL	4	0.943	1.010	1.109	0.925	1.137	1.020	0.088	0.044
R5 CON	16	0.829	0.924	1.025	0.803	1.107	0.939	0.122	0.030
OVX	11	0.873	0.924	0.968	0.842	1.076	0.935	0.076	0.023
ZOL	4	0.897	0.996	1.135	0.872	1.173	1.009	0.126	0.063
R6 CON	16	0.819	0.919	0.974	0.809	1.199	0.935	0.134	0.033
OVX	11	0.862	0.901	0.973	0.743	1.077	0.914	0.102	0.031
ZOL	4	0.944	0.993	1.186	0.931	1.247	1.041	0.141	0.070

APPENDIX 4.2

*Figure 4.14 (a) data table for whole bone sample (WB) and sub-regional (R1 to R6) aBMD ($g.cm^{-2}$) for CON, OVX and ZOL (shaded) in **FMR** at Y3 sacrifice.*

(a) Y3 FMR	n	25%	Med	75%	10%	90%	M	SD	SEM
WB CON	16	0.882	0.960	1.029	0.820	1.056	0.952	0.079	0.020
OVX	11	0.923	0.965	0.995	0.902	1.091	0.968	0.059	0.018
ZOL	4	0.983	1.028	1.067	0.980	1.067	1.026	0.047	0.024
R1 CON	16	0.712	0.781	0.829	0.674	0.857	0.772	0.064	0.016
OVX	11	0.735	0.775	0.836	0.695	0.873	0.778	0.061	0.018
ZOL	4	0.760	0.802	0.842	0.750	0.851	0.801	0.043	0.021
R2 CON	16	0.755	0.833	0.879	0.662	0.902	0.809	0.082	0.021
OVX	11	0.780	0.795	0.873	0.737	0.980	0.830	0.083	0.025
ZOL	4	0.848	0.888	0.902	0.837	0.904	0.879	0.030	0.015
R3 CON	16	0.970	1.004	1.029	0.860	1.155	1.005	0.096	0.024
OVX	11	0.933	1.038	1.071	0.871	1.184	1.020	0.102	0.031
ZOL	4	1.038	1.114	1.221	1.035	1.235	1.124	0.098	0.049
R4 CON	16	0.907	0.964	0.990	0.788	1.098	0.946	0.095	0.024
OVX	11	0.914	0.987	1.011	0.883	1.103	0.979	0.074	0.022
ZOL	4	1.035	1.054	1.142	1.033	1.167	1.077	0.062	0.031
R5 CON	16	0.840	0.914	0.968	0.743	1.015	0.900	0.087	0.022
OVX	11	0.885	0.911	0.965	0.830	1.066	0.928	0.070	0.021
ZOL	4	0.974	0.985	1.045	0.971	1.064	1.001	0.042	0.021
R6 CON	16	1.165	1.213	1.315	1.045	1.395	1.227	0.113	0.028
OVX	11	1.175	1.226	1.281	1.086	1.378	1.234	0.089	0.027
ZOL	4	1.220	1.264	1.353	1.210	1.377	1.279	0.071	0.036

APPENDIX 4.2

*Figure 4.14 (b) data table for whole bone sample (WB) and sub-regional (R1 to R6) aBMD (g.cm^{-2}) for CON, OVX and ZOL (shaded) in **TBR** at Y3 sacrifice.*

(b) TBR Y3	n	25%	Med	75%	10%	90%	M	SD	SEM
WB CON	16	0.955	1.017	1.075	0.924	1.108	1.013	0.065	0.016
OVX	11	1.020	1.045	1.073	1.014	1.150	1.055	0.046	0.014
ZOL	4	1.022	1.074	1.125	1.010	1.136	1.073	0.053	0.027
R1 CON	16	0.941	1.019	1.069	0.836	1.114	1.000	0.096	0.024
OVX	11	0.964	1.013	1.065	0.891	1.185	1.017	0.086	0.026
ZOL	4	1.001	1.050	1.071	0.985	1.077	1.040	0.039	0.020
R2 CON	16	0.889	0.959	1.053	0.849	1.102	0.968	0.095	0.024
OVX	11	0.973	0.995	1.069	0.946	1.146	1.027	0.069	0.021
ZOL	4	0.961	1.061	1.170	0.945	1.189	1.064	0.108	0.054
R3 CON	16	1.042	1.100	1.196	1.016	1.265	1.120	0.086	0.022
OVX	11	1.146	1.193	1.272	1.093	1.275	1.189	0.067	0.020
ZOL	4	1.155	1.222	1.330	1.151	1.348	1.236	0.094	0.047
R4 CON	16	1.073	1.135	1.199	1.016	1.216	1.134	0.070	0.018
OVX	11	1.165	1.219	1.228	1.099	1.241	1.192	0.049	0.015
ZOL	4	1.148	1.226	1.282	1.138	1.285	1.219	0.072	0.036
R5 CON	16	0.898	0.988	1.021	0.867	1.050	0.964	0.065	0.016
OVX	11	0.960	0.988	1.031	0.933	1.095	1.000	0.052	0.016
ZOL	4	0.969	0.999	1.050	0.961	1.064	1.006	0.043	0.022
R6 CON	16	0.888	0.929	0.991	0.845	1.033	0.937	0.063	0.016
OVX	11	0.936	0.950	0.977	0.908	1.032	0.958	0.038	0.011
ZOL	4	0.906	0.949	0.978	0.899	0.980	0.944	0.039	0.019

APPENDIX 4.2

*Figure 4.14 (c) data table for whole bone sample (WB) and sub-regional (R1 to R6) aBMD (g.cm^{-2}) for CON, OVX and ZOL (shaded) in **HMR** at Y3 sacrifice.*

(c) HMR Y3	n	25%	Med	75%	10%	90%	M	SD	SEM
WB CON	16	0.999	1.034	1.114	0.958	1.162	1.054	0.076	0.019
OVX	11	0.960	1.019	1.095	0.941	1.128	1.021	0.065	0.020
ZOL	4	1.068	1.147	1.183	1.045	1.192	1.133	0.063	0.031
R1 CON	16	0.804	0.832	0.868	0.743	0.937	0.837	0.057	0.014
OVX	11	0.751	0.797	0.813	0.691	0.848	0.780	0.051	0.015
ZOL	4	0.829	0.884	0.933	0.811	0.948	0.882	0.056	0.028
R2 CON	16	0.907	0.969	1.031	0.859	1.092	0.973	0.083	0.021
OVX	11	0.845	0.886	0.954	0.832	1.043	0.906	0.074	0.022
ZOL	4	0.940	0.974	1.056	0.930	1.082	0.990	0.065	0.032
R3 CON	16	0.837	0.928	0.954	0.721	1.059	0.906	0.109	0.027
OVX	11	0.842	0.866	0.923	0.676	1.070	0.879	0.110	0.033
ZOL	4	0.899	0.976	1.098	0.885	1.127	0.991	0.104	0.052
R4 CON	16	1.124	1.240	1.291	1.065	1.421	1.230	0.132	0.033
OVX	11	1.178	1.262	1.287	1.065	1.384	1.238	0.093	0.028
ZOL	4	1.243	1.353	1.433	1.212	1.454	1.343	0.100	0.050
R5 CON	16	1.104	1.151	1.258	1.075	1.352	1.178	0.098	0.024
OVX	11	1.084	1.193	1.273	1.044	1.338	1.185	0.096	0.029
ZOL	4	1.207	1.343	1.361	1.163	1.366	1.304	0.094	0.047
R6 CON	16	1.146	1.205	1.310	1.124	1.338	1.226	0.081	0.020
OVX	11	1.094	1.187	1.228	1.041	1.345	1.181	0.093	0.028
ZOL	4	1.268	1.348	1.381	1.252	1.382	1.332	0.062	0.031

APPENDIX 4.2

*Figure 4.14 (d) data table for whole bone sample (WB) and sub-regional (R1 to R6) aBMD (g.cm^{-2}) for CON, OVX and ZOL (shaded) in **RDR** at Y3 sacrifice.*

(d) RDR Y3	n	25%	Med	75%	10%	90%	M	SD	SEM
WB CON	16	0.902	0.930	0.982	0.868	1.054	0.943	0.061	0.015
OVX	11	0.900	0.925	0.959	0.859	0.993	0.930	0.043	0.013
ZOL	4	0.976	1.002	1.066	0.970	1.084	1.015	0.049	0.025
R1 CON	16	0.893	0.994	1.073	0.851	1.179	1.001	0.118	0.029
OVX	11	0.907	0.964	1.040	0.852	1.089	0.976	0.076	0.023
ZOL	4	0.990	1.073	1.301	0.982	1.358	1.121	0.170	0.085
R2 CON	16	1.127	1.183	1.265	1.059	1.405	1.200	0.114	0.029
OVX	11	1.099	1.177	1.240	0.742	1.258	1.125	0.167	0.050
ZOL	4	1.214	1.288	1.435	1.190	1.484	1.312	0.123	0.062
R3 CON	16	0.958	0.990	1.054	0.929	1.132	1.008	0.079	0.020
OVX	11	0.942	0.990	1.043	0.936	1.057	1.000	0.046	0.014
ZOL	4	1.051	1.088	1.113	1.046	1.114	1.084	0.033	0.017
R4 CON	16	0.863	0.893	0.920	0.845	0.969	0.898	0.045	0.011
OVX	11	0.858	0.910	0.955	0.834	0.995	0.904	0.058	0.018
ZOL	4	0.935	0.957	0.992	0.933	0.998	0.961	0.030	0.015
R5 CON	16	0.706	0.730	0.748	0.686	0.831	0.737	0.048	0.012
OVX	11	0.698	0.738	0.766	0.671	0.804	0.733	0.044	0.013
ZOL	4	0.719	0.783	0.830	0.713	0.830	0.777	0.061	0.031
R6 CON	16	0.753	0.812	0.855	0.734	0.896	0.812	0.058	0.015
OVX	11	0.760	0.785	0.824	0.731	0.837	0.785	0.036	0.011
ZOL	4	0.830	0.849	0.864	0.828	0.865	0.848	0.019	0.009

APPENDIX 6

Figure 6.4 data tables for (a) DXA derived aBMD ($g.cm^{-2}$) of whole bone (WB), proximal femoral sub-region (R1) and head, neck and intertrochanteric regions r1-3; and (b) µCT volumetric density ($\mu g.mm^{-3}$) of the trabecular core sample mid-sections.

(a) DXA aBMD		**n**	**25%**	**Med**	**75%**	**10%**	**90%**	**M**	**SD**	**SEM**
R1	Y1 CON	12	0.717	0.747	0.814	0.668	0.862	0.757	0.065	0.019
	OVX	13	0.679	0.744	0.802	0.668	0.826	0.742	0.059	0.016
	Y3 CON	16	0.712	0.781	0.829	0.674	0.857	0.772	0.064	0.016
	OVX	11	0.735	0.775	0.836	0.695	0.873	0.778	0.061	0.018
	ZOL	4	0.760	0.802	0.842	0.750	0.851	0.801	0.043	0.021
r1	Y1 CON	12	0.928	0.964	0.985	0.856	1.042	0.956	0.056	0.016
	OVX	13	0.929	0.970	1.049	0.856	1.082	0.975	0.074	0.021
	Y3 CON	16	0.915	1.000	1.045	0.880	1.099	0.989	0.078	0.019
	OVX	11	0.929	1.034	1.051	0.890	1.067	1.002	0.068	0.020
	ZOL	4	0.994	1.030	1.088	0.991	1.097	1.037	0.050	0.025
r2	Y1 CON	12	0.541	0.613	0.643	0.510	0.707	0.603	0.067	0.019
	OVX	13	0.524	0.598	0.631	0.481	0.660	0.578	0.063	0.017
	Y3 CON	16	0.530	0.578	0.628	0.507	0.662	0.581	0.057	0.014
	OVX	11	0.542	0.601	0.661	0.497	0.711	0.601	0.068	0.020
	ZOL	4	0.583	0.605	0.647	0.580	0.657	0.612	0.034	0.017
r3	Y1 CON	12	0.735	0.773	0.868	0.666	0.966	0.795	0.098	0.028
	OVX	13	0.704	0.774	0.823	0.684	0.870	0.772	0.068	0.019
	Y3 CON	16	0.727	0.842	0.894	0.638	0.933	0.813	0.104	0.026
	OVX	11	0.759	0.803	0.866	0.746	0.975	0.821	0.074	0.022
	ZOL	4	0.798	0.847	0.878	0.791	0.879	0.841	0.044	0.022
(b) Core	**µCT**	**n**	**25%**	**Med**	**75%**	**10%**	**90%**	**M**	**SD**	**SEM**
	Y1 CON	12	891.3	901.2	916.5	858.2	937.2	901.8	23.7	6.9
	OVX	13	872.0	897.4	910.0	825.2	940.6	891.1	35.8	9.9
	Y3 CON	16	896.4	905.4	933.1	863.4	942.6	910.0	27.0	6.7
	OVX	11	895.4	900.8	925.6	887.3	948.8	909.7	20.3	6.1
	ZOL	4	919.7	924.2	928.8	919.5	929.1	924.2	5.0	2.5

APPENDIX 6

Figure 6.5 data tables for µCT micro-architectural data (a) bone volume fraction BV / TV (b) trabecular number Tb. N (n.mm^{-1}) (c) trabecular thickness Tb. Th (mm) and (d) trabecular spacing Tb. Sp (mm).

(a) BV / TV	**n**	**25%**	**Med**	**75%**	**10%**	**90%**	**M**	**SD**	**SEM**
Y1 CON	12	0.25	0.30	0.36	0.16	0.41	0.30	0.08	0.02
OVX	13	0.21	0.26	0.32	0.15	0.37	0.26	0.07	0.02
Y3 CON	16	0.20	0.24	0.28	0.16	0.31	0.24	0.05	0.01
OVX	11	0.21	0.24	0.25	0.12	0.28	0.22	0.05	0.01
ZOL	4	0.23	0.28	0.29	0.22	0.30	0.27	0.04	0.02
(b) Tb. N	**n**	**25%**	**Med**	**75%**	**10%**	**90%**	**M**	**SD**	**SEM**
Y1 CON	12	1.38	1.61	1.78	1.12	2.16	1.61	0.32	0.09
OVX	13	1.24	1.59	1.93	1.21	2.26	1.62	0.38	0.10
Y3 CON	16	1.29	1.54	1.76	1.05	1.99	1.52	0.31	0.08
OVX	11	1.24	1.35	1.61	0.88	1.74	1.36	0.28	0.09
ZOL	4	1.31	1.56	1.82	1.25	1.88	1.56	0.27	0.13
(c) Tb. Th.	**n**	**25%**	**Med**	**75%**	**10%**	**90%**	**M**	**SD**	**SEM**
Y1 CON	12	0.18	0.20	0.23	0.16	0.27	0.21	0.04	0.01
OVX	13	0.16	0.18	0.22	0.15	0.22	0.19	0.03	0.01
Y3 CON	16	0.17	0.17	0.19	0.14	0.20	0.17	0.02	0.01
OVX	11	0.14	0.15	0.17	0.13	0.17	0.15	0.01	0.00
ZOL	4	0.17	0.17	0.17	0.17	0.17	0.17	0.00	0.00
(d) Tb. Sp.	**n**	**25%**	**Med**	**75%**	**10%**	**90%**	**M**	**SD**	**SEM**
Y1 CON	12	0.54	0.63	0.72	0.48	0.85	0.64	0.12	0.03
OVX	13	0.62	0.69	0.74	0.54	0.81	0.68	0.09	0.02
Y3 CON	16	0.63	0.68	0.78	0.55	0.90	0.71	0.12	0.03
OVX	11	0.65	0.69	0.74	0.60	1.03	0.72	0.13	0.04
ZOL	4	0.54	0.64	0.74	0.51	0.77	0.64	0.11	0.05

APPENDIX 6

Figure 6.7 data table for trabecular core compression tests to failure (a) ultimate compressive strength (MPa) (b) elastic modulus (MPa) and (c) energy to failure (kJ).

(a) UCS	**n**	**25%**	**Med**	**75%**	**10%**	**90%**	**M**	**SD**	**SEM**
Y1 CON	12	10.6	13.6	18.4	8.1	20.6	14.0	4.4	1.3
OVX	13	9.2	11.1	13.1	8.6	14.8	11.3	2.2	0.6
Y3 CON	16	8.3	12.1	14.3	7.1	17.3	11.8	3.4	0.8
OVX	11	6.6	8.9	10.9	2.9	14.1	8.8	3.5	1.1
ZOL	4	10.2	12.0	14.8	9.9	15.5	12.3	2.4	1.2
(b) *E*	**n**	**25%**	**Med**	**75%**	**10%**	**90%**	**M**	**SD**	**SEM**
Y1 CON	12	355.0	507.5	665.3	268.7	789.5	510.6	176.1	50.8
OVX	13	318.5	343.0	452.0	290.0	500.0	377.7	77.6	21.5
Y3 CON	16	460.3	602.5	703.0	426.5	806.7	603.9	145.1	36.3
OVX	11	342.0	428.0	561.0	199.0	711.2	431.7	159.2	48.0
ZOL	4	345.3	530.5	698.5	319.0	719.0	524.8	185.1	92.6
(c) EN	**n**	**25%**	**Med**	**75%**	**10%**	**90%**	**M**	**SD**	**SEM**
Y1 CON	12	47.8	356.5	1246.0	22.1	2003.0	690.8	743.8	214.7
OVX	13	508.0	674.0	785.5	248.6	841.2	621.0	201.7	56.0
Y3 CON	16	156.5	231.0	1083.0	107.7	1646.0	546.6	561.2	140.3
OVX	11	40.0	98.0	125.0	19.4	271.6	102.6	78.4	23.6
ZOL	4	195.3	354.0	613.3	153.0	689.0	387.5	223.7	111.9

APPENDIX 6

Figure 6.11 data tables for mechanical properties (UCS & E) of all trabecular cores, grouped CON/OVX and Y1/Y3 with data stratified by r2 aBMD (Low/Med/High).

(a) UCS (MPa)	**n**	**25%**	**Med**	**75%**	**10%**	**90%**	**M**	**SD**	**SEM**
CON Low	10	10.0	12.1	14.4	7.4	16.9	12.0	3.1	1.0
Med	9	9.0	12.8	14.3	6.6	14.8	11.7	3.0	1.0
High	9	9.2	17.3	19.7	8.1	20.6	14.7	5.3	1.8
OVX Low	8	8.5	9.2	10.6	3.9	14.3	9.3	2.9	1.0
Med	8	8.6	10.8	12.3	2.6	13.5	9.9	3.4	1.2
High	8	8.8	11.4	14.3	6.6	15.1	11.3	3.0	1.1
Y1 Low	8	9.2	10.3	13.9	8.7	14.4	11.2	2.3	0.8
Med	9	9.1	10.8	13.1	7.4	14.8	11.0	2.4	0.8
High	8	12.3	16.2	20.2	9.7	20.6	15.8	4.1	1.5
Y3 Low	9	7.9	11.0	13.4	3.9	17.2	10.8	3.9	1.3
Med	9	7.7	11.1	13.9	2.6	14.4	10.5	3.9	1.3
High	9	8.2	8.7	12.8	6.6	17.5	10.3	3.6	1.2
(b) *E* (MPa)	**n**	**25%**	**Med**	**75%**	**10%**	**90%**	**M**	**SD**	**SEM**
CON Low	10	451	623	690	263	936	592	194	61
Med	9	388	492	653	324	741	515	150	50
High	9	448	616	666	361	833	582	144	48
OVX Low	8	315	381	476	203	497	379	101	36
Med	8	294	357	420	198	561	363	107	38
High	8	350	427	561	302	744	465	143	51
Y1 Low	8	349	457	517	311	679	459	118	42
Med	9	303	343	366	245	492	344	68	23
High	8	351	540	672	302	833	534	183	65
Y3 Low	9	396	589	690	203	960	560	225	75
Med	9	412	561	653	198	741	514	170	57
High	9	426	467	630	409	744	528	121	40

APPENDIX 6

Figure 6.11 data tables for microarchitectural properties (BV/TV & Tb.N) of all cores, grouped CON/OVX and Y1/Y3 with data stratified by r2 aBMD (Low/Med/High).

(c) BV/TV (ratio)	**n**	**25%**	**Med**	**75%**	**10%**	**90%**	**M**	**SD**	**SEM**
CON Low	10	0.16	0.25	0.32	0.14	0.32	0.24	0.07	0.02
Med	9	0.22	0.27	0.29	0.20	0.31	0.26	0.04	0.01
High	9	0.24	0.28	0.37	0.20	0.43	0.30	0.07	0.02
OVX Low	8	0.20	0.23	0.27	0.15	0.35	0.24	0.06	0.02
Med	8	0.23	0.25	0.28	0.11	0.35	0.25	0.07	0.02
High	8	0.17	0.23	0.29	0.16	0.39	0.24	0.08	0.03
Y1 Low	8	0.21	0.28	0.32	0.15	0.35	0.27	0.07	0.02
Med	9	0.22	0.26	0.28	0.14	0.35	0.25	0.06	0.02
High	8	0.24	0.35	0.39	0.16	0.43	0.32	0.09	0.03
Y3 Low	9	0.18	0.21	0.26	0.16	0.32	0.22	0.05	0.02
Med	9	0.22	0.27	0.29	0.11	0.31	0.25	0.06	0.02
High	9	0.20	0.24	0.26	0.16	0.28	0.23	0.04	0.01
(d) Tb. N ($n.mm^{-1}$)	**n**	**25%**	**Med**	**75%**	**10%**	**90%**	**M**	**SD**	**SEM**
CON Low	10	1.08	1.39	1.99	1.00	2.20	1.49	0.44	0.14
Med	9	1.36	1.53	1.67	1.07	1.77	1.49	0.22	0.07
High	9	1.55	1.73	1.80	1.43	2.02	1.70	0.17	0.06
OVX Low	8	1.23	1.34	1.94	0.90	2.38	1.52	0.48	0.17
Med	8	1.23	1.42	1.61	0.87	1.84	1.40	0.30	0.11
High	8	1.37	1.59	1.73	1.21	2.08	1.58	0.27	0.09
Y1 Low	8	1.26	1.35	2.17	1.22	2.38	1.64	0.49	0.17
Med	9	1.36	1.59	1.66	1.05	1.84	1.51	0.24	0.08
High	8	1.56	1.71	1.96	1.21	2.08	1.71	0.28	0.10
Y3 Low	9	1.04	1.43	1.83	0.90	2.05	1.43	0.41	0.14
Med	9	1.16	1.49	1.61	0.87	1.77	1.39	0.29	0.10
High	9	1.39	1.54	1.74	1.24	1.80	1.54	0.19	0.06

APPENDIX 6

Figure 6.11 data tables for microarchitectural properties (Tb.Th & Tb.Sp) of all cores, grouped CON/OVX and Y1/Y3 with data stratified by r2 aBMD (Low/Med/High).

(e) Tb. Th (mm)	**n**	**25%**	**Med**	**75%**	**10%**	**90%**	**M**	**SD**	**SEM**
CON Low	10	0.15	0.17	0.20	0.12	0.20	0.17	0.03	0.01
Med	9	0.17	0.19	0.20	0.17	0.28	0.20	0.03	0.01
High	9	0.18	0.18	0.22	0.16	0.26	0.20	0.03	0.01
OVX Low	8	0.16	0.17	0.21	0.13	0.22	0.18	0.03	0.01
Med	8	0.15	0.16	0.19	0.14	0.22	0.17	0.03	0.01
High	8	0.14	0.16	0.18	0.14	0.22	0.16	0.03	0.01
Y1 Low	8	0.16	0.19	0.21	0.15	0.22	0.19	0.03	0.01
Med	9	0.18	0.20	0.22	0.15	0.28	0.20	0.04	0.01
High	8	0.17	0.18	0.23	0.15	0.26	0.20	0.04	0.01
Y3 Low	9	0.14	0.16	0.17	0.12	0.20	0.16	0.02	0.01
Med	9	0.15	0.17	0.18	0.14	0.20	0.17	0.02	0.01
High	9	0.14	0.17	0.18	0.14	0.20	0.17	0.02	0.01
(f) Tb. Sp (mm)	**n**	**25%**	**Med**	**75%**	**10%**	**90%**	**M**	**SD**	**SEM**
CON Low	10	0.58	0.66	0.87	0.48	0.98	0.70	0.17	0.05
Med	9	0.65	0.66	0.78	0.63	0.85	0.71	0.08	0.03
High	9	0.53	0.62	0.69	0.46	0.76	0.61	0.10	0.03
OVX Low	8	0.65	0.70	0.74	0.63	0.80	0.70	0.06	0.02
Med	8	0.65	0.71	0.79	0.59	1.09	0.75	0.15	0.05
High	8	0.60	0.67	0.73	0.51	0.77	0.66	0.09	0.03
Y1 Low	8	0.64	0.70	0.75	0.55	0.80	0.69	0.08	0.03
Med	9	0.62	0.72	0.79	0.58	0.89	0.71	0.10	0.03
High	8	0.51	0.57	0.65	0.46	0.69	0.57	0.08	0.03
Y3 Low	9	0.60	0.68	0.80	0.47	0.99	0.69	0.15	0.05
Med	9	0.65	0.68	0.80	0.63	1.09	0.74	0.15	0.05
High	9	0.68	0.71	0.77	0.60	0.79	0.71	0.06	0.02